Synthesis and Characterization of Well-Defined Heterobifunctional Polyethers for Coating of Magnetite and their Applications in Biomedicine and Magnetic Resonance Imaging

Philip Plaxico Huffstetler

Dissertation submitted to the Faculty of Virginia Polytechnic Institute and State University
in partial fulfillment of the requirements for the degree of

Doctor of Philosophy

In

Macromolecular Science and Engineering

Judy S. Riffle, Committee Chair
Richey M. Davis
Alan Esker
James E. McGrath
S. Richard Turner

September 15, 2009

Key words: contrast agents, MRI, magnetite, poly(ethylene oxide), poly(propylene oxide), diblock copolymers, heterobifunctional polyethers

Synthesis and Characterization of Well-Defined Heterobifunctional Polyethers for Coating of Magnetite and their Applications in Biomedicine and Magnetic Resonance Imaging

Philip Plaxico Huffstetler

Abstract

Well-defined heterobifunctional homopolyethers and amphiphilic block copolyethers containing a variety of functionalities were designed, synthesized, and characterized via GPC and ^{1}H NMR. These have included controlled molecular weight cholesterol-PEO-OH, mono- and trivinylsilyl-PEO-OH, monovinylsilyl-PEO-PPO-OH, monovinylsilyl-PEO-PPO-PEO-OH, maleimide-PEO-OH, stearyl alcohol-PEO-OH, propargyl alcohol-PEO-OH, trivinylsilyl-PPO-OH, trivinylsilyl-PPO-PEO-OH, and benzyl alcohol-initiated poly(allyl glycidyl ether)-OH. The focus of polymers utilized in this study involved the mono- and trivinylsilyl polyethers.

The vinylsilyl endgroups on these materials were functionalized with various bifunctional thiols through free radical addition of SH groups across the vinylsilyl double bonds. The resultant end-functional polyethers were adsorbed onto magnetite nanoparticles and the stabilities of the polymer-magnetite complexes were compared as a function of the type of anchoring moiety and the number of anchoring moieties per chain.

Anchoring chemistries investigated in this work included carboxylates, alkylammonium ions, and zwitterionic phosphonates. The anchor group-magnetite bond stability was investigated in water and phosphate buffered saline (PBS). Through these studies, the zwitterionic phosphonate group was shown to be a better anchoring group for magnetite than either carboxylate or ammonium ions. Tri-zwitterionic phosphonate anchor

groups provided stability of the complexes in PBS for a broad range of polymer loadings. Thus, investigations into the stability of polyether-magnetite complexes in PBS focused on hydrophilic zwitterionic phosphonate-PEO-OH and amphiphilic zwitterionic phosphonate-PPO-*b*-PEO-OH oligomer coatings on the surface of magnetite.

Superparamagnetic magnetite nanoparticles are of interest as potential contrast-enhancement agents for MRI imaging. Thus, transverse NMR relaxivities of these complexes were studied as a function of chemical composition and nanostructure size and compared to commercial contrast agents. The amphiphilic polyether-magnetite nanoparticles were shown to be stable in both aqueous media as well as physiological media and have much higher transverse relaxation values, r_2, than those of commercial contrast agents and other materials in the literature.

Acknowledgements

First and foremost, it has been a privilege and an honor working with Dr. Judy S. Riffle. Her ability as an advisor to guide her students while nurturing and focusing their creativity towards a specific goal is one of her greatest talents. She has also been there for her students as a caring person helping us along life's bumpy road. It has also been a pleasure working with Dr. Richey M. Davis as he has challenged me to look deeper towards the fundamentals and helped nurture scientific curiosity. Special thanks also goes out to Dr. Alan Esker, whose critical reviews helped mold my synthetic techniques into what they have become and for all the fun times on the golf course. I would also like to thank Dr. James E. McGrath and Dr. S. Richard Turner for listening and guiding me towards becoming a scientist.

Ph.D.'s, as many can attest too, are not a singular effort. There are many people that have influenced my development as a scientist and a person. These people include Dr. Jonathan D. Goff, Dr. Will C. Miles, John S. Boyd, Alfred Chen, Nikorn Pothayee, Dr. Shane Thompson, Timothy Vadala, and Dr. Yinnian Lin. A special thanks goes out to Dr. Jonathan Goff as he has taught me the ways of the Riffle group and brought me along his journey teaching me everything he knows. There were many days spent "discussing" a variety of topics and having fun being the devils advocate. I am forever grateful for our unending friendship and hope for nothing but the best for you in life's journey.

Collaborations are one of the most important tools in research today. Without these people the work could not have been done. They include Matt Carroll, Dr. William C. Miles, Dr. Robert Woodard, Dr. Tim St. Pierre, Michelle Gasko, Dr. Tatiana Bronich, and

Dr. Alexander Kabanov. Your insightful discussions have helped mold this work into what it is.

Support from colleagues and friends have been a quintessential part in obtaining a Ph.D. I want to deeply thank Dr. Jonathan Goff, Dr. Ane Turner Johnson, Dr. Chris and Jessica McGrady, Dr. Will and Munye Miles, John S. Boyd, Michael Heinzer, Adam Larkin, and Dean Masteropietro. We have had great times that are too numerous to list here and I hope that we can continue our friendships through the years.

I am most grateful to my family for everything. To Mom and Dad, you have raised me to believe that I can accomplish anything as long as I am willing to do the work. You instilled in me the ability to endure both the good and bad inherent in life's journey and to always be positive no matter what the situation. To my grandparents, Johnny and Eunice Huffstetler, there are not enough words in the English language to describe what you mean to me and for what you have done in my life. To my grandparents, Buddy and Annie Lou Goldsmith, your enduring love and teachings have helped mold me into the person that I am today and I thank you for being there. To my late grandparents, David and Helen Plaxico, time was taken from us, but the love and determination that you instilled into the family lives on. To my late great grandparents, Ray and Irene Goldsmith, your lives were examples to strive for the best and understand that family is important.

Lastly, I am thankful to the most important person in my life, my wife, Tiffany. You have given so much and I am thankful for all that you have done along our journey. I want you to know that I love you completely and look forward to all of life's adventures with you! I am so blessed to have a loving and caring wife like you.

Table of Contents

Abbreviations

3-HPMVS-3-hydroxypropyldimethylvinylsilane
3-HPTVS-3-hydroxypropyltrvinylsilane
AIBN-2,2'-azobis(methylpropionitrile)
BnO-benzyl alcohol
DMC-double metal catalyst
DMF-N,N'-dimethylformamide
EO-ethylene oxide
$Fe(acac)_3$-iron(III) acetylacetonate
GPC-gel permeation chromatography
HMPA-hexamethylphosphoramide
MWD-molecular weight distribution
MRI-Magnetic Resonance Imaging
PDI-polydispersity index
PEO-poly(ethylene oxide)
PO-propylene oxide
PPO-poly(propylene oxide)
R_2-Transverse Relaxation
THF-tetrahydrofuran

List of Figures

List of Tables

List of Schemes

1. Chapter 1: Dissertation Overview

A major goal in the design of magnetic resonance imaging contrast agents involves the synthesis and characterization of new polymeric materials that aid in the imaging of specific tissues and cells. The second chapter reviews the history and applications of small molecule and polymeric coatings on magnetite towards the development of negative contrast agents for magnetic resonance imaging.

The third chapter describes an improved synthetic method for preparing well-defined heterobifunctional polyethers via coordination polymerization. It includes an in-depth look into the development of zinc(II) hexacyanocobaltate as a coordination catalyst for the polymerization of a variety of epoxy monomers and with different initiator species. Insight into the proposed pathway of polymerization was also studied by investigating the effect of catalyst aging in the presence of the initiating species. A broad range of well-defined heterobifunctional polyethers and their characterization via ^{1}H NMR and GPC are described.

The fourth chapter describes the stability of magnetite-polyether complexes in water and in phosphate buffered saline (PBS) utilizing various anchoring chemistries including a carboxylate group, an alkylammonium group, and 1-3 zwitterionic phosphonate group(s). Functionalization of the polyethers with each group is described. Comparisons if the relative binding stabilities of the polymers on the magnetite as functions of the types and numbers of anchoring groups was probed via DLS and dialysis studies. Colloidal stabilities of the complexes in water and PBS were investigated in collaboration with Will Miles and Prof. Davis.

Chapter 5 builds on the principles discovered in the previous chapter involving the comparison of three anchor groups to one anchor group as well as the effect of molecular weight (in collaboration with Will Miles and Prof. Davis). The anchor groups studied were carboxylates, alkylammonium ions, and zwitterionic phosphonates. The stabilities of the magnetite complexes were investigated via DLS and dialysis over 24 hours and a polymer brush model was developed to explain differences in the behavior of each complex. Surface coverage of the magnetite by the anchor groups was determined to relate this parameter to colloidal stability.

Chapter 6 describes an investigation of NMR relaxivities of the polyether-magnetite nanoparticles that remained intact and colloidally stable due to their potential to serve as negative contrast agents for magnetic resonance imaging (MRI). A 3,400 g mol^{-1} tri-zwitterionic phosphonate-PEO-OH and two tri-zwitterionic-PPO-*b*-PEO-OH (3kPPO-5kPEO and 3kPPO-3kPEO) diblock copolymers were adsorbed onto magnetite nanoparticles to make a series of compositions. The stabilities of the binding moieties and their colloidal stabilities in PBS were determined via dialysis and dynamic light scattering studies. Transverse relaxation times were correlated to the intensity-weighted diameters of the polyether complexes. Comparison of these complexes to commercial materials showed much higher transverse relaxation values than the commercial analogues and also the commercial dextran-magnetite materials did not remain stably bound in PBS.

Chapter 7 describes an investigation of the colloidal properties of amphiphilic diblock copolyethers bound to magnetite through the tri-zwitterionic phosphonate anchor group. In collaboration with Will Miles, effects of molecular weight and polymer loading on the stability of the complexes in PBS were examined in detail. Comparisons of the

complex sizes over time obtained from DLS data for polymers bound through triammonium endgroups and zwitterionic phosphonates with similar molecular weights were made. Transverse magnetic relaxivities and cellular uptake data, obtained in collaboration with Matt Carroll and Michelle Gasko, are presented for the triammonium-bound complexes.

Chapter 8 describes the conclusions drawn from the previous chapters and proposed future work associated with this research.

Chapter 2: Magnetite Nanoparticles Coated with Small Molecules and Polymers and their Potential for Applications in Magnetic Resonance Imaging

2.1. Introduction

2.1.1 History and Background of Magnetic Nanoparticles

Magnetite nanoparticles are comprised of iron (II and III) and oxygen with the chemical formula Fe_3O_4 ($FeO{\cdot}Fe_2O_3$). Magnetite is one of many compounds in the iron oxide family and possesses magnetic characteristics such as ferrimagnetism. A list of iron oxides and their magnetic properties are provided in Table 2.1.1.1.[1, 2] Ferrimagnetism occurs when the magnetic moments of the atoms on different sub-lattices are opposed, as in anti-ferromagnetism.[1-5] However, in ferrimagnetic materials, the opposing moments are unequal and a spontaneous magnetization remains. Ferrimagnetic materials exhibit some features of ferromagnetic materials such as anisotropy, hysteresis, and spontaneous magnetization.[6] Anisotropy is induced by an external applied field, which aligns the magnetic dipoles producing a net magnetic dipole moment that promotes precession at a frequency controlled by the applied field. The net magnetization observed in ferrimagnetic materials is usually lower than in ferromagnetic materials due to anti-parallel spin arrangement in ferromagnetism. An illustration of different types of magnetism is shown in Figure 2.1.1.1.

Table 2.1.1.1 Iron oxyhydroxide and iron oxide species[2]

Mineral	Formula	Magnetic response
Goethite	α-FeOOH	Antiferromagnetic
Akaganéite	β-FeOOH	Antiferromagnetic
Lepidocrocite	γ-FeOOH	Antiferromagnetic
Feroxyhyte	δ′-FeOOH	Ferrimagnetic
Ferrihydrite	$Fe_5HO_8 \cdot 4H_2O$	Antiferromagnetic
Hematite	α- Fe_2O_3	Ferrimagnetic
Maghemite	γ- Fe_2O_3	Ferrimagnetic
Magnetite	Fe_3O_4	Ferrimagnetic

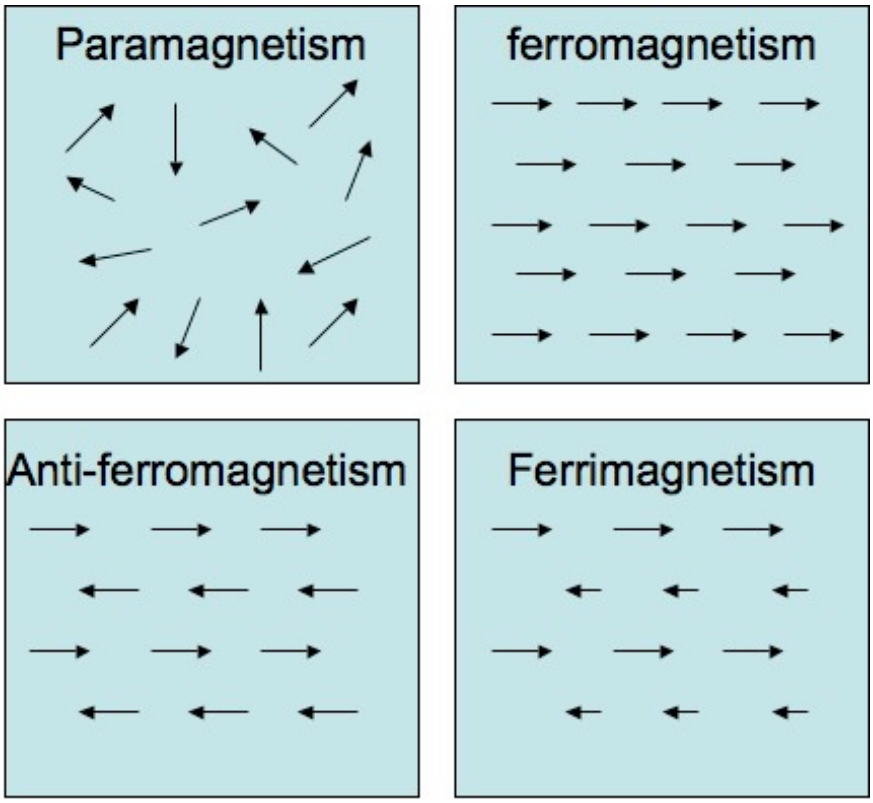

Figure 2.1.1.1 Arrangements of the dipoles in different types of magnetic materials[5]

Researchers have actively pursued magnetite and maghemite nanoparticles due to their stabilities against atmospheric oxidation that allows them to maintain their magnetic response over long times.[1, 2, 4, 7-12] Magnetite nanoparticles have a slightly higher magnetic

susceptibility than maghemite (see Table 2.1.1.2).[1, 2, 4, 7-12] However, magnetite has a low toxicity, LD_{50} ~ 400 mg/kg, as determined by *in vivo* injection in lab mice.[13]

Magnetite is a large source of iron ore and is made naturally when iron is oxidized in water. Interestingly, one natural occurrence exists off the coast of Western Australia on Rottnest Island where ponds containing many magnetotactic bacteria exist. Other natural occurrences of magnetite in nature involve migrating birds.[14] Magnetite in their brains is used as a magnetic compass to aid in migration while the tilt of the earth observed around seasons changes.[14]

Magnetite nanoparticles can be synthesized by various methods in a laboratory such as co-precipitation of iron salts,[1, 4, 7-11, 15] thermal decomposition of iron (III) organometallics in the presence of a reducing agent,[16] water-in-oil microemulsions,[17, 18] and in the presence of polymers or liposomes.[1, 4, 7, 10-12, 19-26] The properties of magnetite, for example ferrimagnetism, slow oxidation, low toxicity and a charged surface, give rise to the use of these materials in electronics and an abundance of biomedical applications.[1, 4, 7, 10-12, 19-26]

Table 2.1.1.2 Physical properties of magnetite and maghemite[2]

Compound	Crystal Lattice	Density (g/mL)	Magnetic Susceptibility (emu/g)	Cell Dimension (nm)
Magnetite	Cubic	5.26	90-98	0.839
Maghemite	Cubic or tetragonal	4.87	75-80	0.834

The charged surfaces of magnetite (Figure 2.1.1.2) allow for polymers and small molecules to adsorb onto nanoparticles of these materials and to stabilize colloidal dispersions of the nanoparticles in a given medium.[1, 4, 27] There are a vast array of polymers, small molecules and biological entities that have been investigated as coatings

for magnetite nanoparticles in aqueous media. An abbreviated list of these include oligosaccharide/polysaccharides,[8, 10] polyurethanes,[1] red blood cells,[7] oligonucleotides,[40] polyethers,[1, 4, 26] and liposomes.[36] These coatings allow for the stability and dispersibility of magnetite nanoparticles in aqueous media.[4, 7-12, 15, 19-26, 28-46] However, a very short list of polymeric materials aid in the stability of magnetite in physiological media mostly involving phosphonate functionality.[47]

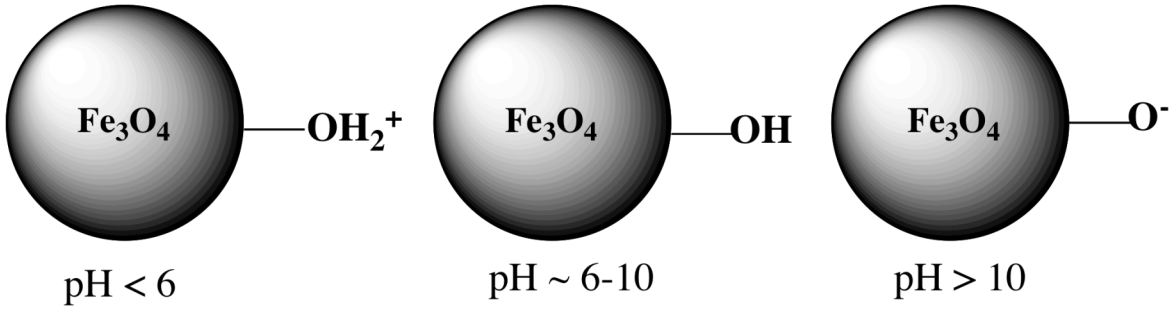

Figure 2.1.1.2. Surface charge of magnetite nanoparticles versus pH of media[1, 4, 27]

The mechanism by which functional groups adsorb onto magnetite consists of electrostatic adsorption of functional groups to the charged surfaces at specific pH's.[1, 4] Carboxylates, sulfates, phosphates and phosphonates are known to have binding affinities towards the surface of magnetite. These functional groups have been incorporated into many polymer and molecular systems in order to create coated nanoparticles independent of pH. An example of electrostatic adsorption onto the surface of magnetite is shown in Figure 2.1.1.3.[1, 4] Multiple polymeric and small molecule systems have been specifically synthesized to contain these functional groups.[47] Schwartz *et al.* has shown the functionalization of metal oxides with carboxylates and phosphonates yielding stable metal oxide nanoparticles for use in various biomedical applications such as cross coupling with

biomolecules.[47]

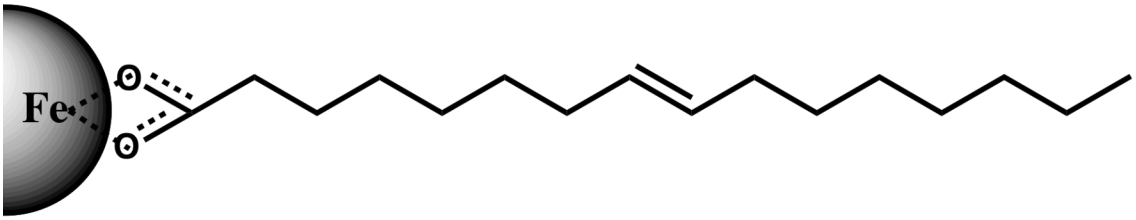

Figure 2.1.1.3. Stabilization of magnetite via electrostatic adsorption of the oleic acid carboxylate functionality

However, electrostatic stabilization is a pH sensitive method that is limited to specific pH ranges. This method of adsorption involves an ionic interaction between the surface of the nanoparticles and the stabilizer.[2, 15] The iso-electric point of magnetite has been reported in the literature as ~6.8.[1] This means an equal number of positive and negative charges are on the surface of the particle yielding a neutral surface, in turn potentially negating the use of electrostatic stabilization. There has been much research devoted to the use of electrostatic stabilization with multiple systems.[2, 4, 10, 12, 15, 21, 22, 25, 30-35, 48] Taboada *et al.* and Fauconnier *et al.* report the use of citric acid and gluconic acid for adsorption onto maghemite.[49] These particles were formed at a low pH, ~ 4, and the adsorption of the particles were determined by varying the pH. The researchers determined that citric acid and gluconic acid form stable complexes up to a pH of approximately eight.[49]

Coated nanoparticles have many advantageous properties. Many of these properties give rise to use in applications such as electronic devices.[4] The increase of memory storage in electronics is one of great interest as well as the optical, electrical, and transport applications of these nanoparticles. The application of interest for this review

involved the use of these nanoparticle systems in the medical realm. Potential applications consist of retinal detachment therapy, tumor treatment, cell separation, magnetic carriers for drugs, and the one of particular interest for this study is magnetic resonance imaging contrast agents.[4, 7, 9, 11, 19, 29, 50-52]

2.1.2 Magnetism

Magnetism is a phenomenon in which objects exert attractive or repulsive forces on other objects. Magnetic interactions are corrections to electric interactions where the magnetic energies and forces are expected to be smaller.[53-56] From this, all objects experience some magnetic response but for most the response is minimal. Magnetism is due to incomplete cancellation of electron spins that can be explained in at least two ways. The electron spin, which is equivalent to a circulating charge, does not balance out effectively in certain atoms.[1, 53-56] Due to the electron spin of ½, the net angular momentum cannot be zero unless electrons can pair their angular momentum.[1, 53-59] Also, the electron circulation around the nucleus of an atom resembles that of a current loop. The flow of charge in a current loop produces magnetic lines of force known as a dipole, shown in Figure 2.1.2.1. Thus magnetism arises from materials that contain these microscopic atomic currents and spins, as well as from currents provided by macroscopic current loops.

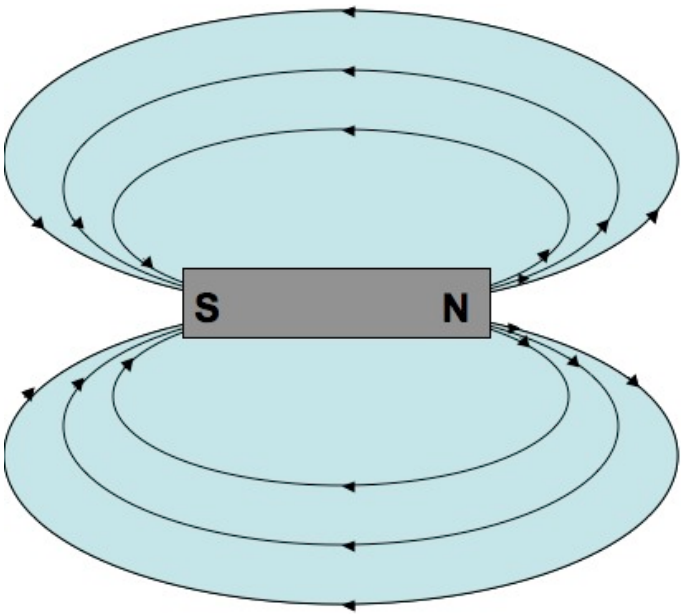

Figure 2.1.2.1. Magnetic field lines produced via a bar magnet[1]

2.2. Introduction to Magnetic Resonance Imaging and Principles

2.2.1. Introduction

Magnetic resonance imaging, commonly known as MRI, is a powerful non-invasive imaging technique that has transformed the medical world.[11] The technique has been utilized by physicians in both diagnosis and pre-surgical planning with limited risk to the patient.[54-56, 60-63] MRI aids neurologists and biological scientists in the discovery of anatomical and physiological abnormalities[11, 64-70] Unlike x-rays, MRI does not require exposure of the subject to ionizing radiation and hence is considered safe and provides more information than other imaging techniques.[11, 64-70]

MRI imaging is based on the phenomenon of nuclear magnetic resonance (NMR). Bloch and Purcell discovered this phenomenon in 1946 during their experiments of bulk materials and continued through the work of Proctor and Yu in the early 50's.[54, 68, 71, 72] During these experiments the researchers determined that certain atomic nuclei, when

placed in a static magnetic field, will assume one of two states; a higher energy level or a lower energy level. The energy difference between the two is linearly proportional to the strength of the applied magnetic field (Figure 2.2.1.1).[53, 54, 59-63, 68, 70-74] Figure 2.2.1.2 shows a depiction of this phenomenon when a magnetic field is applied to nuclei.

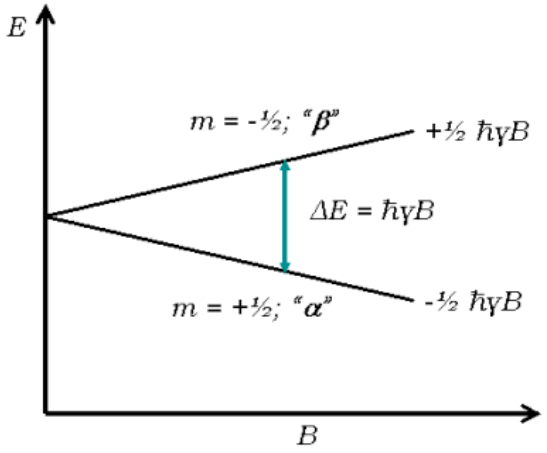

Figure 2.2.1.1. Splitting of the spin states of a nucleus upon application of a static magnetic field, ***B***.[53, 54, 59-63, 68, 70-74]

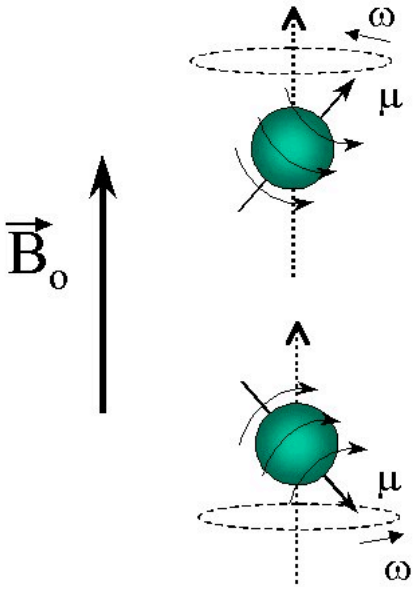

Figure 2.2.1.2. A representation of nuclei in the presence of a magnetic field, $\boldsymbol{B_o}$, with both orientations +1/2 and -1/2.[53, 54, 59-63, 68, 70-74]

In thermal equilibrium, the number of nuclei in the higher energy state is slightly less than the number of nuclei in the lower energy state.[53, 54, 56-63, 69, 70, 72-74] High energy nuclei can fall to the lower energy state through the emission of a photon with equal energy to that of the difference of the two states.[53, 54, 56-63, 69, 70, 72-74] Low energy nuclei can jump to the higher state by absorbing a photon to maintain equilibrium. When these nuclei are placed in a magnetic field, the lower energy state nuclei absorb photons and jump to the higher energy state, thus destroying the thermal equilibrium. When the external field is removed, the excess high-energy nuclei return to the lower energy state to re-establish the equilibrium. The re-balancing of the equilibrium emits a signal determined by the difference in energy states of the two nuclei and the decay rate of the signal depends on the molecular environment of the nuclei.[53, 54, 56, 57, 60, 61, 63, 70] The resulting signals can be analyzed to study the properties of the nuclei and their surrounding environments.[54, 55, 57, 66, 67, 75, 76]

Throughout the 50's and 60's, NMR, was primarily only used for spectroscopic analysis. In the early 70's Damadian and Lauterbur proposed using NMR for imaging.[57-59, 66] Lauterbur suggested that since the energy states of particular nuclei in an external field depend on the strength of the applied field, adjusting the magnetic field applied at each point could change the energy at every point in a material.[57-59, 66] As a result, the electromagnetic fields absorbed or emitted by the nuclei are also different from point to point. After these signals from the nuclei are collected, the frequency can be manipulated to yield spatial information of the nuclei.[57-59, 66] This general method provides the basic foundation for all NMR imaging, however the actual imaging techniques are much more

complicated. Since the pioneering work of Damadian and Lauterbur, the number of imaging techniques has grown substantially.[56-59, 66, 76]

The growth of this technique has lead to technological development of NMR images.[72] One major advance has been the invention of superconducting magnets. Superconducting magnets enable a much higher signal-to-noise ratio and better image resolution than previous permanent magnets. The use of computers have made this technique even more valuable through the ability to acquire and process a large amount of data in a short time.[54, 72] Computers also aided in elimination of distortion in images through complex RF pulse sequences. Advancements in RF coils have also improved image quality.[17, 54-57, 64, 66, 72, 76] With all of these advancements toward MRI, the need for better contrast in images is of current importance.

2.2.2. Relaxation of Materials in MRI

First, one must determine the effects of applying an external magnetic field to a proton. When a magnetic field is applied, the nuclei align in the parallel state or the anti-parallel state as shown previously in Figure 2.2.1.2. The parallel state is deemed when the proton aligns with the external magnetic field and the anti-parallel state is when the proton aligns opposite the external magnetic field.[17, 54-57, 64, 66, 72, 76]

Pulses of radiofrequency energy (RF pulses) allow one to observe behavior inherent in nuclei when the magnetic field is altered. The net magnetization is directly proportional to the magnetic moment of a proton, which allows for the assumption that magnetization, M, is similar to the magnetic moment, μ.[54-57, 60, 61, 63, 64, 66, 72, 76] When a molecule is placed in a magnetic field oriented in the z direction, a net magnetization in the z direction is developed. Through the RF pulse, the magnetization vector can be perturbed

from its equilibrium along the z-axis that is formed through application of the static field. This is accomplished through for example a '90^o pulse' or a '180^o pulse'. The direction of the field after applying the RF pulse can be predicted from equations 2.2.2.1 and 2.2.2.2 where γ is the gyromagnetic ratio and B_{eff} is the effective magnetic field strength.[53-57, 60, 61, 63, 64, 66, 72, 76, 77]

$$T_{90} = \pi / 2(\gamma B_{eff}) \qquad \textbf{Eq. 2.2.2.1}$$

$$T_{180} = \pi / (\gamma B_{eff}) \qquad \textbf{Eq. 2.2.2.2}$$

After a 90^o pulse the magnetization vector is aligned in the transverse plane, then the free induction decay (FID) resulting from relaxation of the magnetization is monitored.[53, 54] Canet[66] developed the Bloch[68] equations into

$$dM_{x,y} / dt = \gamma(\mathrm{M \times B})_{x,y} - (M_{x,y} / T_2) \qquad \textbf{Eq. 2.2.2.3}$$

$$dM_z / dt = \gamma(\mathrm{M \times B})_z + (M_o - M_z / T_1) \qquad \textbf{Eq. 2.2.2.4}$$

where T_2 and T_1 are the transverse and longitudinal relaxation times, respectively. M_0 is the equilibrium value of magnetization that lies in the z direction. What is observed is the return of the magnetization vector to its equilibrium state in both 90° and 180^o pulses.[53-57, 64-66, 68-70, 72, 74, 76] When a 90^o pulse is applied equation 2.2.2.3 can be rearranged and simplified into

$$M_{XY} = M_{XYo}\, exp\, (-t / T_2) \qquad \textbf{Eq. 2.2.2.5}$$

These equations govern the behavior observed experimentally when the molecule is pulsed in the presence of a magnetic field yielding exponential decay, as shown in Figure 2.2.2.1.

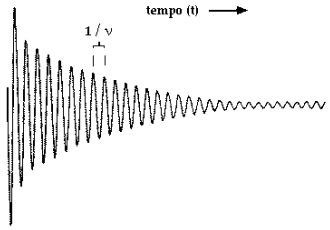

Figure 2.2.2.1. Typical FID exponential decay of an NMR signal[54]

In the case of a 180° pulse the first section of equation 2.2.2.4, $\gamma(\mathrm{M} \times \mathrm{B})_z$, is zero due to **B** lying in the z direction at all times so the equation simplifies to

$$dM_z / dt = (M_o - M_z / \mathrm{T}_1) \qquad \textbf{Eq. 2.2.2.6}$$

When the initial time value is zero, the equation can be given by

$$M_z(t) = M_0 [1 - \exp(-t / \mathrm{T}_1)] \qquad \textbf{Eq. 2.2.2.7}$$

From equations 2.2.2.5 and 2.2.2.7, the magnetization vector is shown returning to its equilibrium after specific RF pulses.[54, 66, 70]

2.2.3. Spin-Lattice or Longitudinal Relaxation (T_1)

When nuclei are in equilibrium, the net magnetization vector lies along the direction of the applied magnetic field B_o, shown in Figure 2.2.3.1. From the equations

discussed in the previous section the Z component of magnetization, M_z, is equal to that of the equilibrium magnetization, M_o.[54, 57, 60-63, 66, 70, 76] This M_z is known as the longitudinal magnetization.

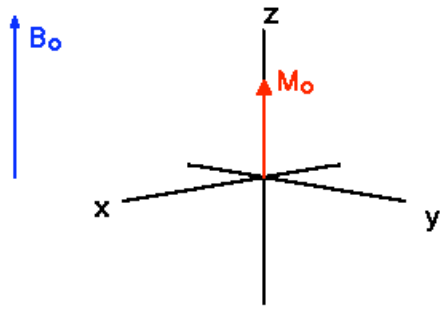

Figure 2.2.3.1 The equilibrium magnetization of the nuclei spins in an applied magnetic field, B_o.[70]

The net magnetization of nuclei can be altered by exposing the nuclei to an RF pulse equal to that of the energy difference of the spin states.[53-55, 60-63, 69, 70, 72, 74, 78] This saturates the spin system making $M_z = 0$, shown in Figure 2.2.3.2. The time constant that describes how M_z re-equilibrates to the origin is known as the spin-lattice or longitudinal relaxation time (T_1).[54-56] However, the T_1 measurement is not exactly how long the nuclei take to re-equilibrate but a measurement of the time it takes to reduce the difference between M_z and the equilibrium value by a factor of *e*. An example of this measurement is shown in Figure 2.2.3.3.[54-56, 70]

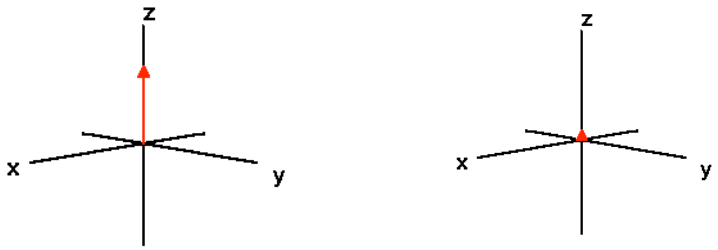

Figure 2.2.3.2 The suppression of the net magnetization vector via RF pulse[70]

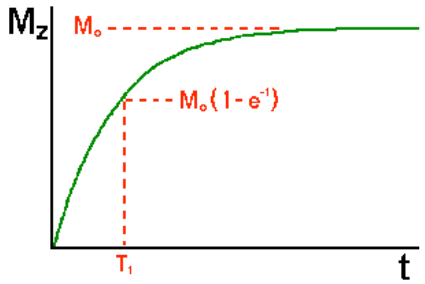

Figure 2.2.3.3. A graph of net magnetization suppression of the nuclei versus time shows the relaxation of the net magnetization.[70]

2.2.4. Transverse or Spin-Spin Relaxation (T_2)

Transverse or spin-spin relaxation is the measurement of the time required after the net magnetization is placed in the XY plane and the nuclei are allowed to decay or de-phase back to the Z-axis.[54, 56, 57, 64-66, 70, 76] The net magnetization de-phases because each nuclei experiences a slight difference in magnetic field and as time increases the phase difference in the sample increases. The net magnetization vector can be placed initially along the +Y or +X-axis, shown in Figure 2.2.4.1a, and the resulting vector is made up of many individual nuclei spins. Once the pulse is removed the nuclei begin to de-phase back to equilibrium, as shown in Figure 2.2.4.1b.[54, 56, 57, 64-66, 70, 76]

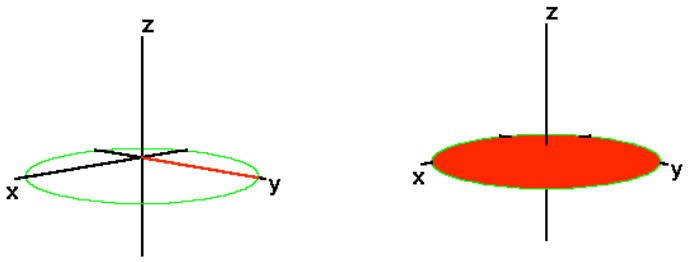

a b

Figure 2.2.4.1 A representative picture after a 90° pulse resulting in the alignment of the nuclei in the XY-plane(a) following de-phasing of the nuclei(b)[70]

The time constant that describes the return to equilibrium of the transverse magnetization, M_{xy}, is the spin-spin relaxation time, T_2. In comparison to T_1, T_2 is always less than or equal to T_1.[54-56, 70] The equations mentioned in the previous section, equation 1.9, allows for the determination of T_2. Figure 2.2.4.2 shows a representative T_2 curve and the time at which the spin-spin relaxation is taken is after decay by a factor of $1/e$.[54-56, 70]

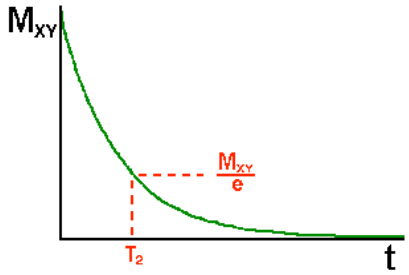

Figure 2.2.4.2 A graph of the transverse magnetization vs. time yielding the spin-spin relaxation after nuclei decay of $1/e$.[70]

2.2.5. Contrast in MRI via T_1 and T_2

The dependence of contrast in MRI is directly proportional to proton density, T_1 and T_2. Proton density variations among tissues are typically very close whereas the T_1

and T_2 relaxation times vary greatly in these tissues as can be accounted for in Table 2.2.5.1.[1, 53-57, 60, 63, 65, 66, 72, 76-78] These large variations in tissue allow for the determination of one tissue from another providing contrast in MRI.

Table 2.2.5.1 Relaxation times of various tissues at 1.5 Tesla[64]

Tissue	T_1 (ms)	T_2 (ms)
Gray Matter	920	101
White Matter	790	92
Cerebrospinal Fluid	2650	280
Kidney	650	58
Liver	490	43
Skeletal Muscle	870	47

When pulsed, tissues with different values of T_1 relax at different rates. Tissues with short T_1 values restore their longitudinal magnetization rapidly in comparison to tissues with long T_1.[54, 55, 60, 61, 63, 64] As a result, tissues with short T_1 are brighter in images and those with long T_1 are darker. In comparison to T_1, T_2 gives the opposite contrast. Variations in T_2 relaxation times in different tissues can be used to produce images with predominant T_2 contrast.[53-55, 60, 61, 63] These images are characterized by the bright appearance of tissues with long T_2 and dark appearance of tissues with short T_2.[53-55, 60, 61, 63] These phenomenon, T_1 and T_2, have allowed scientists to determine variations in tissues affording ways towards detection of disease.

2.3. Contrast Agents and Their Uses in MR Imaging

2.3.1. Introduction

Contrast agents are known to enhance MR imaging contrast by altering the T_1 and T_2 relaxation times of protons in the specific tissue. Contrast agents are frequently used in diagnostic MRI for determining physiological and anatomical conditions or to improve detection of abnormal cell growth. Unlike most contrast agents in medicine, these contrast agents indirectly affect the proton signal of the hydrogen nuclei.[54, 56] The most commonly used contrast agents significantly alter T_1 and T_2 relaxations times in tissue because of the dipole-dipole interactions with water protons.[53-55, 67] The theoretical model by Purcell[66, 68] on the changes in T_1 and T_2 caused by a contrast agent can be determined by

$$1/T_1 = 1/T_{1,0} + R_1 n_a \qquad \textbf{Eq. 2.3.1.1}$$

$$1/T_2 = 1/T_{2,0} + R_2 n_a \qquad \textbf{Eq. 2.3.1.2}$$

where the equations can be simplified to $1/T_1 = R_1$ and $1/T_2 = R_2$ in order to determine the relaxivity time, R_1 and R_2, of a contrast agent.[53-55, 67] The contrast of a specific agent is defined by the difference between T_1 and T_2. A contrast agent that alters the T_1 of a material is deemed a positive contrast agent and T_2 a negative contrast agent. For T_2 contrast agents, the greater the R_2/R_1 ratio the greater the effectiveness of the agent. Examples of positive contrast agents are gadolinium-based systems and negative contrast agents consist of metal oxide nanoparticles, most notably iron oxide nanoparticles.[53-57, 60-67, 76, 77]

2.3.2 Polymeric coatings for negative contrast agents

Many researchers have worked on coating magnetite nanoparticles with various polymer coatings in efforts to increase relaxivities. One particular coating that has received extensive attention is dextran. Jung *et al.* as well as Josephson *et al.* described various types of iron oxide nanoparticles coated with dextran and their resulting relaxivities.[11, 50, 79] Dextran, a complex branched polysaccharide, is coated onto the surface of magnetite to yield the commercial materials marketed as ferumoxide™ and ferumoxtran™ contrast agents.[11, 50, 79] Jung *et al.* also discussed the coating of iron oxide with siloxane with the trade name ferumoxsil™. The relaxivities of these materials along with the saturation magnetization at various fields are shown in Table 2.3.2.1. These values show relatively high T_2 relaxation times, with the highest being ferumoxide with an intensity average diameter of 225 nm. Ferumoxtran has the lowest relaxivity of the materials and also has the longest blood-half life, >200 minutes, and the smallest intensity average diameter of approximately 50 nm via DLS. The research by Jung *et al.* and Ferrucci *et al.* states that ferumoxide has a short blood-half life and is filtered out of the blood stream by macrophages into the liver and spleen.[9, 11] This effect in combination with high R_2 gives rise to ferumoxide being a good contrast agent for the detection of lesions and abnormalities in both the liver and spleen. Jung *et al.* also discovered that ferumoxide nanoparticles are not individual particles but aggregates through TEM analysis of the particles (reproduced in Figure 2.3.2.1).[11]

Table 2.3.2.1 Magnetization and relaxivity of various types of iron oxides and other contrast agents[11]

	Magnetization (emu/g Fe)			Relaxivity (mM Fe•s) $^{-1}$	
Sample	**1 kG**	**6 kG**	**50 kG**	**r_1**	**r_2**
Ferumoxides	37.7 ± 0.6	69.8 ± 1.2	93.6 ± 0.6	23.7 ± 1.2	107 ± 11
Ferumoxtran	53.6 ± 0.4	81.7 ± 0.6	94.8 ± 0.6	22.7 ± 0.2	53.1 ± 3.3
Ferumoxsil	49.4 ± 0.1	73.0 ± 0.1	91.1 ± 0.6	3.2 ± 0.9	72 ± 12
γ-Fe_2O_3	77.3 ± 0.8	107.8 ± 1.1	111.9 ± 0.6	0.1	37.7 ± 0.6
Magnetite	80.5 ± 0.3	122.7 ± 0.5	129.5 ± 0.6	-	-
$FeSO_4$• 7 H_2O	0.21	1.23	10.3	-	-
Fe(III)DTPA	-	-	-	0.73	0.85
GdDTPA	0.18	1.0	8.6	4.5	5.7

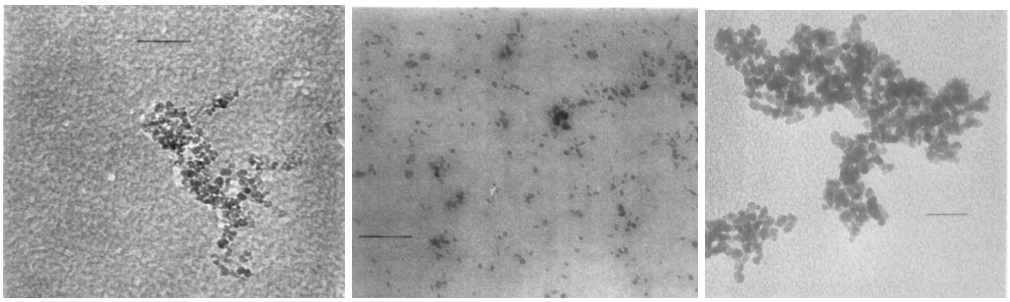

Figure 2.3.2.1 TEM micrographs of Ferumoxide (left), Ferumoxtran (center), and Ferumoxsil (right) taken at 400k-magnification (scale bar = 50 nm)[11]

The aggregation of Ferumoxide nanoparticles shown in the TEM may shed some light on the long T_2 value in comparison to the smaller particles of Ferumoxtran.[7, 8, 11, 29] Ferumoxsil, the [3-(2-amino-ethylamino)propyl]-trimethoxysilane adsorbed nanoparticle system, was shown to have good T_2 relaxation with an intensity-average diameter of 300 nm. Due to the silica coating on the surface of the nanoparticles, the drug can withstand the acidic conditions of the stomach.[19] Once the contrast agent has been ingested, the effect of the nanoparticles darken the stomach and intestines making imaging of other vital organs, such as the pancreas, in the mid-section easier.[11, 19, 37] Comparison of ferumoxide, ferumoxtran, and ferumoxsil with other contrast agents shows relatively high saturation

magnetizations and much greater relaxivities, specifically r_2. The paramagnetic iron(III) and gadolinium(III) systems have much lower r_2 values, making them unattractive towards the negative contrast regime.[11, 50] Hardy *et al.* investigated magnetic nanoparticles coated with a thin siloxane for use as a negative contrast agent.[2, 11, 29, 37] According to the researchers, enhanced proton relaxation, specifically r_2, using these nanoparticle systems is thought to involve the diffusion of water molecules between varying magnetic environments created by the nanoparticles.[2, 9, 11, 29, 37, 50, 79, 80] The diffusion of water molecules between the varying environments effectively reduces coherence of the magnetic moments of the protons leading to a decrease in the spin-spin relaxation time, hence a greater relaxivity.[9, 11, 27, 29, 50, 51] Many researchers have investigated various silica coatings for magnetite. Zhang *et al.* described the coating of magnetite nanoparticles with silica and the alkoxysilanes (3-aminopropyl)trimethoxysilane (APTMS) and [*N*-(2-aminoethyl)-3-aminopropyl]tri-methoxysilane (AEAPTMS).[37] The Si-OR bond allows the silanes to anchor to the surface of the magnetite. With such alkoxysilanes anchored to the surface, the functional end group can be utilized to attach multiple bio-molecules, polymers, and other specific molecules that have the ability to alter the transverse relaxation of protons.[15, 36, 37, 49]

Table 2.3.2.2. Transverse relaxation times of alkoxysilane and silica coated magnetite nanoparticles[37]

Coating	**R_2 (mM Fe^{-1} s^{-1})**
AEAPTMS	84.8
APTMS	134.4
Silica	339.8

The transverse relaxation of the coated magnetite nanoparticles, shown in Table 2.3.2.2, has a broad spectrum ranging from 85 $mM^{-1}s^{-1}$ for APTMS to 340 $mM^{-1}s^{-1}$ for that of silica.[37] The low transverse relaxations of APTMS and AEAPTMS are thought to be

due to the steric hindrance and added hydrophobicity which block the ability of water to interact with the surface of the magnetite.[29, 37, 50] The difference in transverse relaxation between APTMS and AEAPTMS could be due to the additional chain length, thus blocking or shielding the surface even more.[29, 37, 50]

Other coatings for magnetic nanoparticles include citrates. Taboada *et al.* investigated maghemite nanoparticles coated with citrate as potential candidates for MR imaging.[49] Comparison of citrate coated maghemite nanoparticles against maghemite suspended in water showed much higher relaxivities at both 20 MHz and 60 MHz, respectively.[49] The relaxivity measurements of maghemite-water and maghemite-citrate nanoparticles are shown in Tables 2.3.2.3 and 2.3.2.4, respectively.

Table 2.3.2.3. Relaxivites of Maghemite-water at 20 MHz (0.47 T) and 60 MHz (1.47 T) at basic pH (12.5) and 37 ^{o}C [49]

	r_1 (mM $^{-1}$s^{-1})	r_2 (mM $^{-1}$s^{-1})	r_2/r_1
20 MHz	20.81	28.61	1.38
60MHz	17.59	35.75	2.03

Table 2.3.2.4 Relaxivities of Maghemite-Citrate at 20 MHz (0.47 T) and 60 MHz (1.47 T) at neutral pH (7.4) and 37 ^{o}C [49]

	r_1 (mM $^{-1}$s^{-1})	r_2 (mM $^{-1}$s^{-1})	r_2/r_1
20 MHz	20.76	51.02	2.46
60MHz	14.50	66.90	4.61

The r_2/r_1 ratio of maghemite-water was determined to be 1.38, while the maghemite-citrate nanoparticles ratio was 2.46 at 20 MHz. While there was no increase in the r_1 of either system, the citrate coating showed an almost doubling of the r_2.[49] The relaxivity measurements of the maghemite-citrate are thought to have higher r_2 values due to

clustering of the maghemite-citrate particles.[49] The r_2/r_1 ratio could be directly proportional to the amount of clustering observed in the particles via dynamic light scattering.[8, 29, 49, 50, 81, 82] Furthermore, magnetite-coated citrate nanoparticles have been used to alter the transverse relaxation by loading the nanoparticles into red-blood cells.[7] The researchers were able to adjust the transverse relaxation of red-blood cells, shown in Figure 2.3.2.2, giving rise to MR imaging of small blood vessels for a number of medical applications.[7] The amount of magnetite is shown to play a significant role in the relaxation of a material.[7, 11, 29, 32, 50] As the percent magnetite is increased in the loading of red-blood cells, the darker the image region becomes, hence a increase in the transverse relaxation rate.

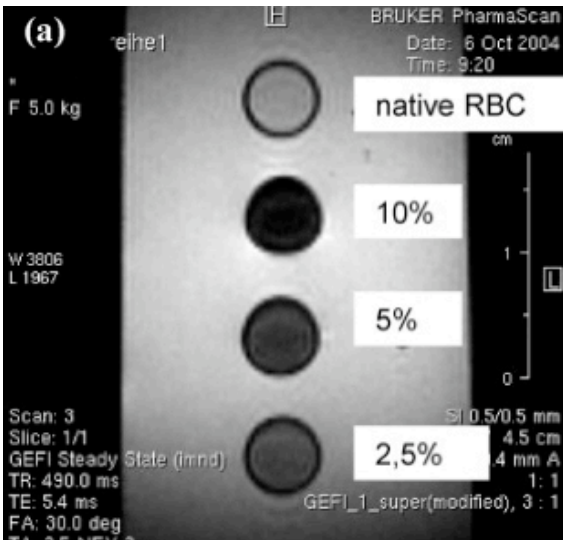

Figure 2.3.2.2. Transverse relaxation of various magnetite loaded red-blood cells[7]

Martina *et al.* investigated maghemite stabilized by phospholipids.[12] The resulting particles were coated with both egg-yolk-L-R-phosphatidylcholine (EPC) and 1,2-diacyl-SN-glycero-3-phosphoethanolamine-N-[methoxy(poly(ethylene glycol))-2000] (DSPE-PEG2000). One batch of particles involved 100% coating with EPC and the second batch

was coated with EPC:DSPE-PEG2000 (95:5 mol%) and for the PEGylated system the maghemite loading was differed to determine the effects of iron loading on relaxivity.[12] The researchers compared these materials to commercial endorem© and sinerem® agents. The transverse relaxivity, r_2, was much higher than the longitudinal relaxivity, r_1, showing the materials to have potential as T_2 contrast agents.[12, 24, 29] A list of the relaxivities obtained in this study is shown in Table 2.3.2.5.

Table 2.3.2.5 Experimental r_1 and r_2 values of magnetic-fluid liposomes in comparison to commercial materials[12]

System	Composition	r_1	r_2
Ferrofluid	Citrate-maghemite	36 ± 1	108 ± 5.4
Conventional MFL	EPC (100%)	10 ± 0.3	67 ± 3
PEG-ylated MLF	EPC:DSPE-PEG-$_{2000}$	18.6 ± 0.5	116 ± 5.8
Endorem	Dextran-maghemite	30	100
Sinerem	-	24	65

In comparison to commercial materials, the PEGylated systems show a higher r_2 than those of commercial materials as well as commercial magnetic ferrofluids.[12, 24, 29, 34-36] An increase in iron content has a direct correlation with the r_2 values.[9, 22, 35, 50] As the iron content of the particles was increased, the r_2 increased (Table 2.3.2.5). Comparison of the two coatings in this study showed a great effect on both r_1 and r_2. The addition of 5 mol% DSPE-PEG2000 nearly doubled the r_2. Others have hypothesized and experimented on the effects of hydrophilic polymers on the surface of iron oxide nanoparticles. The binding affinity of water with the PEG-polymer chain plays an integral role in the relaxivity.[2, 9, 22, 29, 35, 50, 62, 83, 84]

In conjunction to the work by Martina *et al.,* derivatives of DSPE-PEG2000 have also been investigated as coatings for magnetite nanoparticles. Tilborg *et al.* utilized a

maleimide terminated PEG2000-DSPE in conjunction with PEG2000-DSPE (5 mol%:95 mol%) to form phospholipid coated magnetite.[36] The maleimide end group was used as a tool to functionalize the surface of the nanoparticles with a biomolecule of interest. In this particular study, the maleimide end group was functionalized with annexin-A5-cysteine that can bind with apoptotic cells to manipulate the relaxivity of the cells. A diagram of the resulting superparamagnetic micelles is shown in Figure 2.3.2.3. Relaxivity measurements of the liposome-coated nanoparticles were acquired and compared to those of Ferumoxide and Ferumoxtran.[11, 36, 50] The results of the study are shown in Table 2.3.2.6.

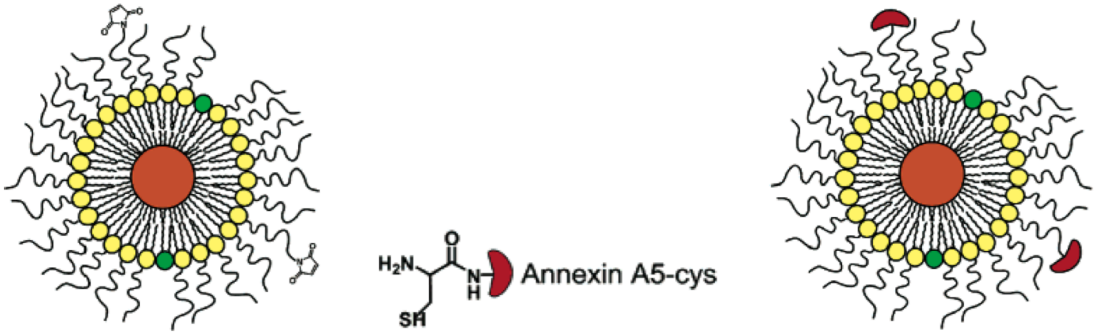

Figure 2.3.2.3. Synthesis of iron oxide nanoparticles stabilized with DSPE-PEG2000/DSPE-PEG2000-maleimide and functionalized with Anexxin-A5-cyteine[36]

Table 2.3.2.6 Relaxivities (mM^{-1} of Fe s^{-1}) of Superparamagnetic micelles and paramagneticliposomes for use in MR imaging[36]

	r_1 ($mM^{-1}s^{-1}$)	r_2 ($mM^{-1}s^{-1}$)	r_2/r_1
Superparamagnetic micelles	13.3	159.6	12.0
Paramagnetic liposomes	4.1	6.8	1.7

The superparamagnetic micelles had a much higher r_2 in comparison to other iron oxide nanoparticles with various coatings.[11, 12, 27, 29, 36, 50, 81] Comparison of relaxivity data to that of Martina *et al.* shows a much higher r_2. Tilborg *et al.* deemed this increase in

relaxivity to be due to use of 100% PEG instead of a mixture of DSPE:DSPE-PEG-2000 (95:5 mol%) lending to PEGs water affinity playing a role in the increase of r_2.[11, 12, 27, 29, 36, 50, 81]

Herceptin™, an anti-cancer therapy monoclonal antibody, has been investigated by Huh *et al.* as an MR imaging contrast agent for specific use in detection of breast cancer.[20] The researchers investigated the ability of the Herceptin™ coated magnetite nanoparticles to bind with a HER2/*neu* receptor site on the breast cancer cell line SK-BR-3. The particles were injected *in vivo* into rats with the specific tumor cells implanted into the rats. After injection of the nanoparticles, MRI was used to image the tumor to determine if the Herceptin™ bound with the tumor and reduced the transverse relaxation time of the tumor tissue.[12, 20, 24, 36] Figure 2.3.2.4 shows MR images obtained at pre-injection, immediate post-injection, one-hour after, 4-hours after, and 12-hours after injection. The tumor was shown via MR images to become dark and this continued to spread through the tumor as time increased.

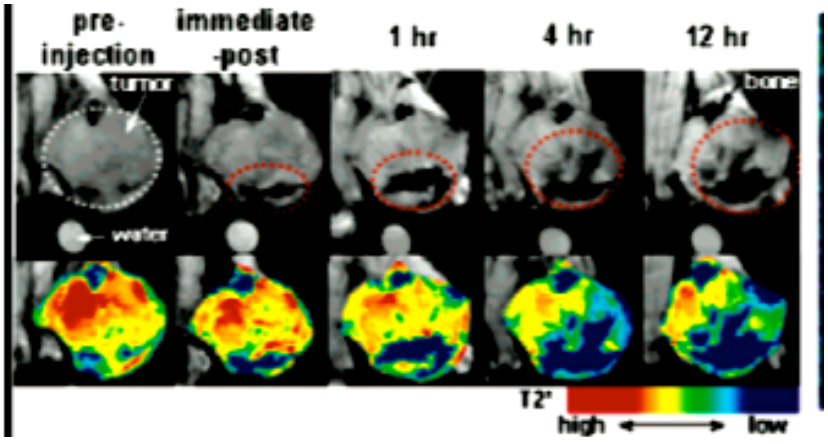

Figure 2.3.2.4 T_2-weighted MR images of implanted tumors at various times showing uptake of the particles by the tumor[20]

The transverse relaxation time of the tumor was shown to dramatically decrease, shown in Figure 2.3.2.4, making these materials potential site-specific negative contrast agents for the detection of breast cancer.[12, 20, 24, 36]

Hydrophobic-hydrophilic copolymers have been investigated for the coating of magnetite and their usefulness as T_2 contrast agents. Poly[3-(trimethoxysilyl)propyl methacrylate-*r*-poly(ethylene glycol) methyl ether methacrylate] (poly(TMSMA-*r*-PEGMA)) was used to coat magnetite, shown in Figure 2.3.2.5.[24]

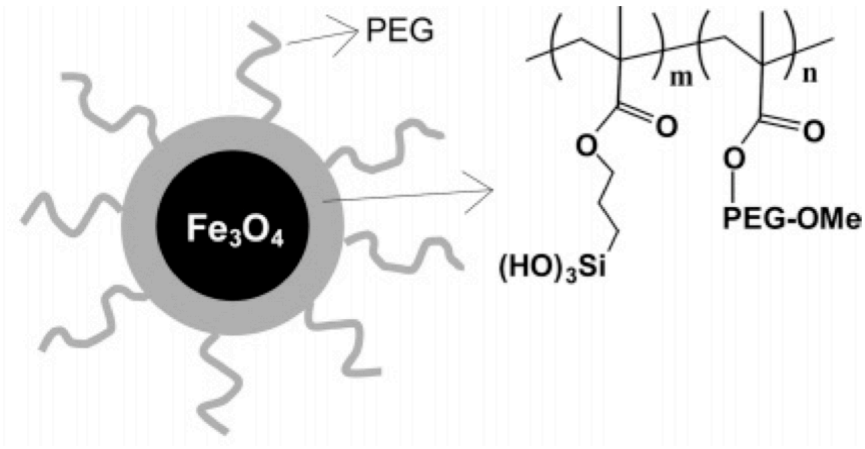

Figure 2.3.2.5 Diagram of poly(TMSMA-*r*-PEGMA) coating of magnetite forming stable magnetite nanoparticles[24]

Relaxation, r_2, of these nanoparticles was shown during the uptake into cancer cells, shown in Figure 2.3.2.6. After injection of the nanoparticles into the bloodstream the tumor, denoted by the white arrow, darken within one hour of injection. This shows that the nanoparticles are taken up by tumor cells through the decrease in r_2 of the tumor cells.[7, 12, 20, 24, 30]

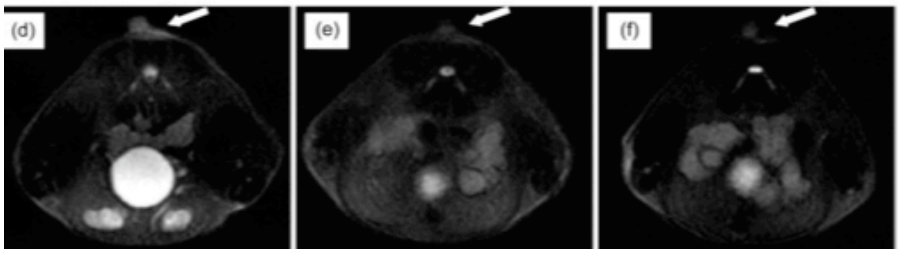

Figure 2.3.2.6 T_2-weighted images of pre-injection (left), 1 hour after injection (middle), and 4 hours after injection (right)[24]

The nanoparticles were compared to Ferridex I.V.® and shown to have longer circulation times within the bloodstream, which allows time for the nanoparticles to be taken up by tumors.[7, 8, 12, 20, 22-24, 26] Other researchers also investigated PEGylated systems such as poly(oligo(ethylene glycol) methacrylate-co-methacrylic acid). Coating and chemical structure of the block copolymer are shown in Figure 2.3.2.7.[26]

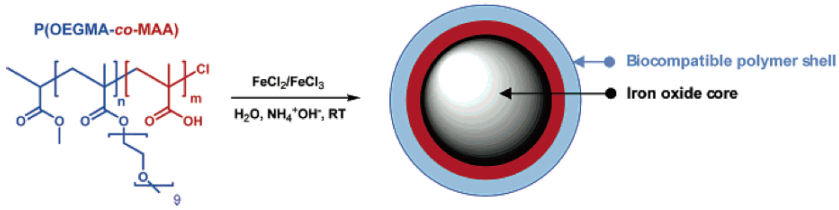

Figure 2.3.2.7. Coating of magnetite nanoparticles with P(OEGMA-co-MAA)[26]

The purpose of this coating was to aid in the development of a nanoparticle system that evaded the reticuloendothelial system (RES) and remained dispersed in the blood stream for long periods.[7, 21, 23, 26, 36-38, 49] T_2-weighted images suggested that the coating of the nanoparticles hindered aggregation, as the nanoparticles were not present in the spleen or liver for up to six hours after injection.[21,23,26, 36,49] Other methacrylate coatings for magnetite developed by Lee *et al.* utilized cross-linked networks that formed a so-called protective coating around magnetite.[25] Figure 2.3.2.8 shows the random copolymer used for coating and Figure 2.3.2.9 shows the surface modification of the coating with amines

and cy5.5 mono NHS ester.

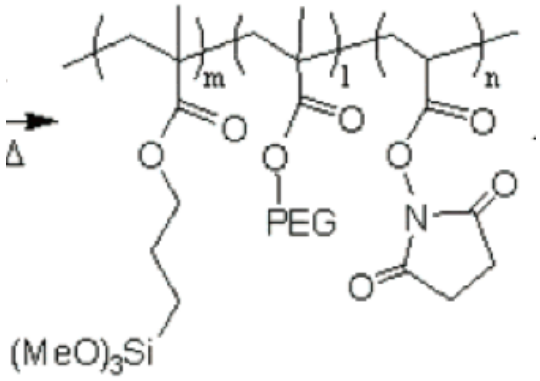

Figure 2.3.2.8 Poly(TMSMA-*r*-PEGMA-*r*-NAS) cross-linkable coating for magnetite nanoparticles[25]

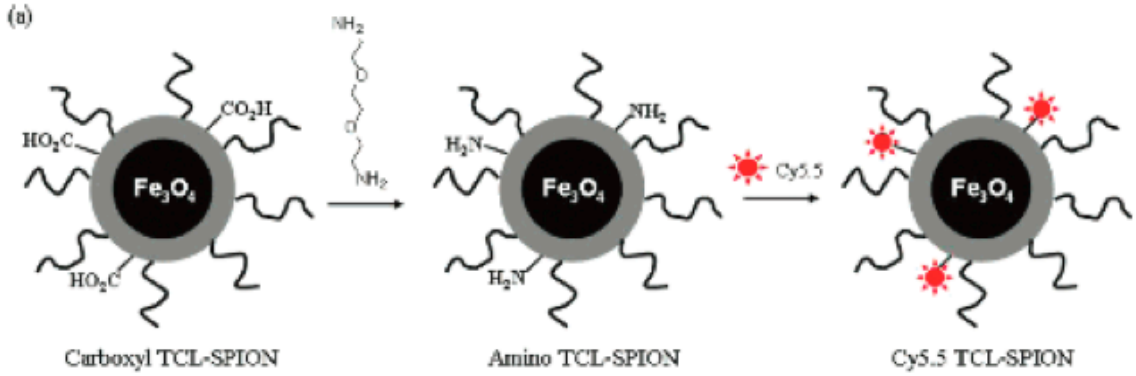

Figure 2.3.2.9 Modification of the polymeric surface with amines and Cy5.5 mono NHS ester[25]

The cy5.5 was used as a fluorescent marker and the amine could be used in the future for the attachment of site-specific molecules.[25] Cy5.5-TCL-nanoparticles were injected into mice and the transverse relaxation time was shown to decrease 3.5 hours after injection. The decrease in transverse relaxation time was also shown to be within the implanted tumor shown in Figure 2.3.2.10.[7, 24-26]

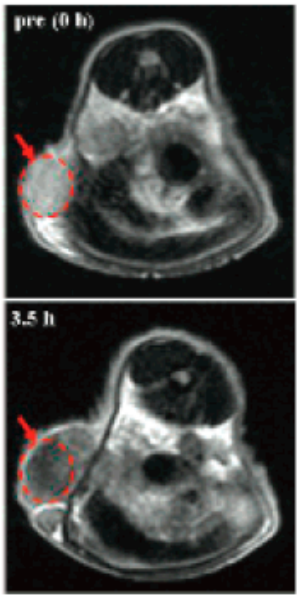

Figure 2.3.2.10 T_2 weighted images of pre-injected(top) and 3.5 hours after injection (bottom). The red dotted line indicates the tumor[25]

Aside from polymeric coatings, small molecules such as tetramethylammonium hydroxide have been used to coat magnetite nanoparticles. Shieh *et al.* described the synthesis of magnetite nanoparticles coated with tetramethylammonium hydroxide.[15] Synthesis of these nanoparticles yielded an amine surface on the magnetite through reduction of the quaternary amine on the surface with an organic acid.[15] The resulting amine surface was reacted with trypsin to determine the amount of amine on the surface of the magnetite.[15] The researchers discussed relaxivities, r_1 and r_2, of amine coated magnetite nanoparticles in aqueous media. These magnetite nanoparticles yielded an r_2 value of 44.56 s^{-1} mM^{-1} and an r_1 value of 6.77 s^{-1} mM^{-1}. Relaxivity measurements were much lower than those of commercial materials such as Resovist® (r_2 = 82 s^{-1} mM^{-1} and r_1 = 7.2 s^{-1} mM^{-1}).[11, 15, 29, 33, 48]

D-Mannose, a mono-saccharide, has also been investigated as a magnetite coating for

use in MR imaging. Horak *et al.* discussed the uses of D-mannose coated magnetite.[10] These nanoparticles were shown to have a high transverse relaxivity of 140 $mM^{-1}s^{-1}$ in differentiation to that of Endorem®, 127 $mM^{-1}s^{-1}$. Table 2.3.2.7 shows the transverse and longitudinal relaxivities of D-mannose coated magnetite and those values of Endorem, respectively. The higher relaxivities were proposed by the nanoparticles ability to undergo intracellular uptake by rat bone marrow stromal cells (rMSCs) where as Endorem was not as easily uptaken, yielding a much lower r_2 in labeled cells.[22-24, 26, 32, 52, 81]

Table 2.3.2.7 D-Mannose coated magnetite nanoparticles both in aqueous media and aqueous media

	Phantoms containing a suspension of pure contrast agent (s^{-1}/mm Fe)		Phantoms containing labeled cells (s^{-1}/million of cells/mL)	
	r_1	r_2	r_1	r_2
D-mannose-coated iron oxide nanoparticles	7.31 ± 0.11	140.4 ± 1.4	0.32 ± 0.04	12.1 ± 0.9
Endorem	19.8 ± 1.5	127 ± 9	0.18 ± 0.06	1.24 ± 0.15

2.4. Conclusions

Superparamagnetic iron oxide nanoparticles are shown to be efficient at reduction of the transverse relaxation time. These nanoparticles possess the ability to alter the transverse relaxation of water protons due to the local magnetic field that is created by the nanoparticle after magnetization. This ability to alter the transverse relaxation of surrounding protons gives rise for use in magnetic resonance imaging as negative contrast agents.

For biological and dispersive purposes, magnetite and maghemite nanoparticles have been coated with a variety of polymeric, bio-molecular, and small molecule coatings.

These coatings have a profound effect on the area at which the contrast is seen. Specific coatings can target abnormal cells leading to uptake of the particles into the abnormal cells for detection. Coatings that aggregate allow for the magnetic nanoparticles to accumulate in specific regions, i.e. the liver and spleen, for detection of abnormal tissue. This shows the usefulness of well-defined magnetic nanoparticles for site-specific reduction of the transverse relaxation for detection of many diseases.

2.5. References

1. Harris, L. A.; Polymer Stabilized Magnetite Nanoparticles and Poly(propylene oxide) Modified Styrene-Dimethacrylate Networks. PhD Dissertation, Virginia Polytechnic Institute and State University, Blacksburg, VA, 2002.

2. Cornell, R., Schertman, U., *The Iron Oxides: Structure, Properties, Reactions, Occurence and Uses*. VCH Publishers: Weinheim, 1996.

3. Aphesteguy, J. C., Jocobo, S.E., Composite of polyaniline containing iron oxides. *Physica B* **2004,** 354, 224-227.

4. Harris, L. A., Goff, J.D., Carmichael, A.Y., Riffle, J.S., Harburn, J.J., St. Pierre, T.G., Saunders, M., Magnetite Nanoparticle Dispersions Stabilized with Triblock Copolymers. *Chemist of Materials* **2003,** 15, 1367-1377.

5. Encyclopedia Britannica: Scientific American http://www.britannica.com. In.

6. Rosensweig, R. E., *Ferrohydrodynamics*. Cambridge University Press: Cambridge, 1985.

7. Brahler, M., Georgieva, R., Buske, N., Muller, A., Muller, S., Magnetite-Loaded Carrier Erythrocytes as Contrast Agents for Magnetic Resonance Imaging

. *Nano Letters* **2006,** 6, (11), 2505-2509.

8. Fahlvik, A., Schroder, U., Magnetic starch microspheres biodistribution and biotransformation. *Invest. Radiol.* **1990,** 25, 793-797.

9. Ferrucci, J., Stark, D., Iron-oxide enhanced MR imaging of the liver and spleen. *AJR* **1990,** 155, 943-950.

10. Horak, D., Babic, M., Jendelova, P., Herynek, V., D-Mannose-Modified Iron Oxide Nanoparticles for Stem Cell Labeling. *Biconjugate Chem* **2007,** 18, 635-644.

11. Jung, C., Jacobs, P., Physical and chemical properties of superparamagnetic iron oxide MR contrast agents: Ferumoxides, Ferumoxtran, Ferumoxsil. *Magnetic Resonance Imaging* **1995,** 13, 661-664.

12. Martina, M. S., Fortin, J., Menager, C., Clement, O., Barratt, G., Generation of Superparamagnetic Liposomes Revealed as Highly Efficient MRI Contrast Agents for in Vivo Imaging. *J. Am. Chem. Soc.* **2005,** 127, 10676-10685.

13. Iannoe, A., Magin, I., *Magn. Reson. Med.* **1991,** 22, 435.

14. http://www.wikipedia.com/magnetite. (February 2008),

15. Sheih, D. *e. a.*, Aqueous dispersions of magnetite nanoparticles with amonium surfaces for magnetic manipulations of biomolecules and MRI contrast agents. *Biomaterials* **2005,** 26, 7183-7191.

16. Pinna, N., Grancharov, S., Beato, P., Bonville, P., Antonietti, M., Niederberger, M, *Chem. Mater.* **2005,** 17, 3044.

17. Lee, K., Sorensen, C.M., Klablunde, K.J., *IEEE Transactions on Magnetics* **1992,** 28, 3180.

18. Dresco, P., Zaitsev, V., Gambino, R., Chu, J., *Langmuir* **1999,** 15, 1545.

19. Hahn, P., Gastrointentinal contrast agents. *AJR* **1991,** 156, 252-254.

20. Jun, Y. H., Y.; Choi, J.; Lee, J.; Song, H.; Kim, S.; Yoon, S.; Kim, K.; Shin, j.; Suh, J.; Cheon, J., Nanoscale Size Effecct of magnetic Nanocrystals and Their Utilization for Cancer Diagnosis via magnetic Resonance Imaging. *J. Am. Chem. Soc.* **2005,** 127, 5723-5733.

21. Kim, D. K., Mikhaylova, M., Zhang, Y., Muhammed, M., Protective Coating of Superparamagnetic Iron Oxide Nanoparticles. *Chemistry of Materials* **2003,** 15, (1617-1627).

22. Kim, D. K., Mikhaylova, M., Wang, F., Kehr, J., Starch-Coated Superparamagnetic Nanoparticles as MR Contrast Agents. *Chem. Mater.* **2003,** 15, 4343-4351.

23. Kohler, N., Sun, C., Wang, J., Methotrexate-Modified Superparamagnetic Nanoparticles and Their Intracellular Uptake into Human Cancer Cells. *Langmuir* **2005,** 21, 8858-8864.

24. Lee, H., Lee, E., Kim, D., Jang, N., Jeong, Y., Antibiofouling Polymer-Coated Superparamagnetic Iron Oxide Nanoparticles as Potential Magnetic Resonance Contrast Agents for in Vivo Cancer Imaging *J. Am. Chem. Soc.* **2006,** 128, 7383-7389.

25. Lee, H., Yu, M.K., Park, S., Moon, S., Min, J.J., Jeong, Y.Y., Thermally Cross-Linked Superparamagnetic Iron Oxide Nanoparticles: Synthesis and Application as a Dual Imaging Probe for Cancer in Vivo *J. Am. Chem. Soc.* **2007,** 129, 12739-12745.

26. Lutz, J., Stiller, S., Hoth, A., Kaufner, L., Pison, U., Cartier, R., One-Pot Synthesis of PEGylated Ultrasmall Iron-Oxide Nanoparticles and Their in Vivo Evaluation as Magnetic Resonance Imaging Contrast Agents *Biomacromolecules* **2006,** 7, 3132-3138.

27. Kroft, L. J. d. R., A. J. , *Magnetic Resonance Imaging* **1999,** 10, 395-403.

28. Glasel, J., Lee, K., On the interpretation of water NMR relaxation times in heterogeneous systems. *J. Am. Chem. Soc.* **1974,** 96, 970-978.

29. Hardy, P., Henkelman, R., Transverse relaxation enhancement caused by magnetic particulates. *Magnetic Resonance Imaging* **1989,** 7, 265-275.

30. Lee, J., Huh, Y., *et al.* , Artificially engineered magnetic nanoparticles for ultra-sensitive molecular imaging. *Nature Medicine* **2006,** 13, 95-99.

31. Marutani, E., Yamamoto, S., Ninjbadgar, T., Tsujii, Y., Fukuda, T., Takano, M., Surface-initiated atom transfer radical polymerization of methyl methacrylate on magnetite nanoparticles. *Polymer* **2004,** 45, (2231-2235).

32. Medonca, M., Lauterbur, P., , Ferromagnetic particles as contrast agents for magnetic resonance imaging of the liver and spleen. *Magn. Reson. Med.* **1986,** 3, 328-330.

33. Olsson, M., Persson, B., Salford, L., Schroder, U., Ferrormagnetic particles as contrast agents in T2 imaging. *Magnetic Resonance Imaging* **1986,** 4, (437-440).

34. Runge, V., Rijcken, T., Contrast-enhanced MR imaging of the liver. *J. MRI* **1994,** 4, 281-289.

35. Semelka, R., Helmberger,T., Contrast Agents for MR Imaging of the Liver. *Radiology* **2001,** 218, 27-38.

36. Tilborg, G., Mulder, W., Deckers, N., Storm, G., Annexin A5-Functionalized Bimodal Lipid-Based Contrast Agents for the Detection of Apoptosis. *Bioconjugate Chem* **2006,** 17, 741-749.

37. Zhang, C., Wangler, B., Morgenstern, B., Zentgraf, H., Eisenhut, M., Untenecker, H., Kruger,H. , Silica- and Alkoxysilane-Coated Ultrasmall Superparamagnetic Iron Oxide

Particles: A Promising Tool To Label Cells for Magnetic Resonance Imaging *Langmuir* **2006,** 23, 1427-1434.

38. Zhang, J., Xu, S., Kumacheva, E., Polymer Microgel: Reactors for Semiconductor, Metal, and Magnetic Nanoparticles. *J. Am. Chem. Soc.* **2003,** 126, 7908-7914.

39. Zheng, W., Gao, F., Gu, H., Magnetic polymer nanospheres with high and uniform magnetite content. *J. Magn. Magn. Mater.* **2005,** 288, 403-410.

40. Yeh, T., Zhang, W., Ildstad, S. T., and Ho, C. , Intracellular labeling of T-cells with superparamagnetic contrast agents. *Magn. Reson. Med.* **1993,** 30, 617-625.

41. Yeh, T., Zhang, W., Ildstad, S. T., and Ho, C. , Dynamic MRI tracking of rat T-cells labeled with superparamagnetic iron-oxide particles. *Magn. Reson. Med.* **1995,** 33, (200-208).

42. Shen, T., Weissleder, R., Papisov, M., Bogdanov, A. J., and Brady, T. J. , Monocrystalline iron oxide nanocompounds (MION): physicochemical properties. *Magn. Reson. Med.* **1993,** 29, 599-604.

43. Zhang, Y., Kohler, N, Zhang, M. , Surface modification of super- paramagnetic magnetite nanoparticles and their intracellular uptake. *Biomaterials* **2002,** 23, 1553-1561.

44. Cheng, F., Su, CH, Yang, YS, Yeh, CS, Tsai, CY, Wu, CL, Wu, MT, Shieh, DB. , Characterization of aqueous dispersions of Fe3O4 Nanoparticles and their biomedical applications. *Biomaterials* **2005,** 26, (729-738).

45. Chan, D., Kirpotin, DB, Bunn, PA. , Synthesis and evaluation of colloidal magnetic iron oxides for the site-specific radiofrequency- induced hyperthermia of cancer. *J. Magn. Magn. Mater.* **1993,** 122, 374-378.

46. Nitin, N., LaConte, L. E., Zurkiya, O., Hu, X., and Bao, G. , Functionalization and Peptide-Based Delivery of Magnetic Nano-particles As an Intracellular MRI Contrast Agent. *J. Biol. Inorg. Chem.* **2004,** 9, (706-712).

47. Schwartz, J., Trainia, C., Surface Modification of Y2O3 Nanoparticles. *Langmuir* **2007,** 23, 9158-9161.

48. Renshaw, R., Owen, C., McLaughlin, A., Ferromagnetic contrast agents: a new approach. *Magn. Reson. Med.* **1986,** 3, (217-225).

49. Taboada, E., Rodriguez, E., Roig, A., Oro, J., Muller, R., Relaxometric and Magnetic Characterization of Ultrasmall Iron Oxide Nanoparticles with High Magnetization. *Langmuir* **2007,** 23, 4583-4588.

50. Josephson, L., Lewis, J., Jacobs, P., Hahn, P., Stark, D., The effects of iron oxide on proton relaxivity. *Magnetic Resonance Imaging* **1988,** 6, 647-653.

51. Kuznetsov, A. A. F., V. I.; Alyautdin, R. N.; Torshina, N. L.; Kuznetsov, O. A. , *J. Magn. Magn. Mater.* **2001,** 225, 95-100.

52. Neuberger, T. S., B.; Hofmann, H.; Hofmann, M.; von Rechenberg, B. , *J. Magn. Magn. Mater.* **2005,** 293, 483-496.

53. Jin, J., *Electromagnetic Analysis and Design in magnetic Resonance Imaging*. CRC Press series in biomedical engineering: Boca Raton, FL, 1999.

54. Kuperman, V., *Magnetic Resonance Imaging: Physical Principle and Applications*. Academic Press: San Diego, CA, 2000.

55. Weishaupt, D., Kochli, V., Marincek, B., *How does MRI work?* 2nd ed.; Springer Verlag New York, 2006.

56. Liang, Z., Lauterbur, P.C., *Principles of Magnetic Resonance Imaging: A signal processing perspective*. IEEE Press: Piscataway, NJ, 2000.

57. Abragam, A., *Principles of Nuclear Magnetism*. Oxford University Press: New York, 1989.

58. Lauterbur, P. C., Image formation by inducel local interactions: Example employing nuclear magnetic resonance. *Nature* **1973,** 242, 190-191.

59. Lauterbur, P. C., Levin, D., Marr, R.B., Theory and simulation of NMR spectroscopic imaging and field plotting by projection reconstruction involving an intrinsic frequency dimension. *J. Magn. Reson.* **1984,** 59, 536-541.

60. Kean, D., Smith, M., *Magnetic Resonance Imaging: Principles and Applications*. William Heinemann Medical Books: Bedford Square, London, 1986.

61. Allison, W., *Fundamental Physics for Probing and Imaging*. Oxford University Press: New York, 2006.

62. *Frontiers in magnetic materials*. Springer Science: New York, 2005.

63. Horowitz, A. L., *MRI Physics for Radiologists*. 3rd ed.; Springer-Verlag: New York City, 1994.

64. *Magnetic Resonance Imaging: Method and Biologic Applications*. Humana Press: Totowa, NJ, 2006.

65. Harris, L. A.; Goff, J.; Carmichael, A.; Riffle, J.; Harburn, J.; St. Pierre, T.; Saunders, M., Polymer Stabilized Magnetite Nanoparticles and Poly(propylene oxide) Modified Styrene-Dimethacrylate Networks. *Chemistry of Materials* **2002,** 15, 1367-1377.

66. Canet, D., *Nuclear magnetic Resonance: Concepts and Methods*. John Wiley and Sons Inc.: New York, 1996.

67. NessAiver, M., *All You Really Need to Know about MRI Physics*. Simply Physics: Baltimore, MD, 1997.

68. Bloch, F., Hansen, W., Packard, M., Nuclear Induction. *Phys. Rev.* **1946,** 69, 127.

69. Bradley, W., Newton, T., Crooks, L., *Modern Neuroradiology Advanced Imaging Techniques*. Clavadel Press: San Anselmo, CA, 1983; Vol. 2.

70. Hornak, J. P. The Basics of MRI. http://www.cis.rit.edu/htbooks/mri

71. Magin, R. L. B., G.; Niesman, M. R.; Alameda, J. C., Jr.; Wright, S. M.; Swartz, H. M. , *Magn. Reson. Med.* **1991,** 20, 1-16.

72. Young, S., *Nuclear Magnetic Resonance Imaging: Basic Principles*. Raven Press: New York, 1984.

73. Boutry, S. L., S.; Vander Elst, L.; Muller, R. N. , *Contrast Med. Mol. Imaging* **2006,** 1.

74. Morris, P., *Nuclear Magnetic Resonance Imaging in medicine and Biology*. Oxford University Press: Oxford, 1986.

75. Bruce, I. J. T., J.; Todd, M.; Davies, M. J.; Borioni, E.; Sangregorio, C.; Sen, T. , *J. Magn. Magn. Mater.* **2004,** 284, 145.

76. Mattson, J., Simon, M., *The Pioneers of NMR and Magnetic Resonance in medicine*. Dean Books Co.: Jericho, NY, 1996.

77. *Experimental Methods in the Physical Sciences*. Academic Press Inc.: San Diego, CA, 2001; Vol. 36.

78. Sigal, R., *Magnetic Resonance Imaging: Basis for Interpretation*. Springer Verlag: New York, 1988.

79. Josephson, L. T., C. H.; Moore, A.; Weissleder, R. , *Bioconjungate Chem.* **1999,** 10, 186-191.

80. Johansson, L. O. B., A.; Ahlstro¨ m, H. K.; Ladd, D. L.; Fujii, D. K. , *Magnetic Resonance Imaging* **2001,** 13.

81. Gupta, A. G., M., *Biomaterials* **2005,** 26, (18).

82. Hamm, B. S., T.; Taupitz, M.; Maibauer, R.; Speidel, A.; Huppertz, A.; Frenzel, T.; Lawaczeck, R.; Wolf, K. J.; Lange, L. J. , *Magnetic Resonance Imaging* **1994,** 4, 659-668.

83. Brown, J. M., and Attardi, L. D. , The Role of Apoptosis in Cancer Development and Treatment Response. *Nat. Rev. Cancer* **2005,** 5, 231-237.

84. Ozaki, M., *Synthesis, Characterization, and Mechanisms of Growth*. Marcel Dekker: New York, 2000; Vol. 92.

Chapter 3: Novel Synthesis of Heterobifunctional Polyethers Via Double Metal Catalyzed Ring-Opening Polymerization

Philip P. Huffstetler,[1] Jonathan D. Goff,[1] John S. Boyd,[1] William C. Miles,[2] and Judy S. Riffle[2]

Department of Macromolecular Science and Engineering[1] and Department of Chemical Engineering[2] at Macromolecules and Interfaces Institute, Virginia Tech, Blacksburg, VA 24061

3.1 Abstract

Polymerizations of propylene oxide have been carried out by using double metal cyanide (DMC) catalysts based on $Zn_3[Co(CN)_6]_2$ systems. A series of poly(propylene oxide) homopolymers were synthesized using the DMC catalyst to determine if aging time plays a role in the molecular weight distribution of polymer system without the ability to constantly feed monomer. The study revealed that as the aging time was increased, the molecular weight distribution of the system decreased to 1.2 or less giving insight to the proposed coordination polymerization pathway. After determination of these parameters a variety of polyethers such as poly(propylene oxide), poly(ethylene oxide), and poly(allyl glycidyl ether) were synthesized. With this catalyst system, a variety of initiating species, such as cholesterol, 3-hydroxypropyldimethylvinylsilane, 3-hydroxypropyltrivinylsilane, N-(2-hydroxylethyl)maleimide, propargyl alcohol, and stearyl alcohol were investigated to create a novel set of polymeric materials. Post-functionalization chemistries were utilized to create polyether systems with carboxylic acid, ammonium, phosphate, and phosphonate functionalities.

3.2 Introduction

Poly(ethylene oxide) (PEO) is utilized extensively in the biomedical and pharmaceutical arena due to its physical properties such as aqueous and organic solubility, non-toxicity, and a sheathing ability against the reticuloendothelial system (RES) avoiding immunogenicity.[1-5] One of the most difficult problems faced in polyether synthesis is the process of post-functionalization to afford heterobifunctionality for specific applications.[2-17] Kabanov *et al.* reported the use of pluronics (HO-PEO-PPO-PEO-OH) of various molecular weights and compositions can be used for cell transfection or drug delivery vehicles.[18] The ability to afford heterobifunctional pluronics as well as other polyether homo- and copolymers have unlimited potential in biomedical applications.[2, 8, 11, 15, 18-20]

Polyethers are commonly synthesized by ring-opening polymerization initiated by an anionic initiator such as potassium hydroxide or an alkoxide.[1, 6, 9, 10, 12, 13, 15, 17, 21-23] This process is one of significance for most EO polymerizations, however for PO polymerizations the alkoxide species promotes side reactions leading to unsaturated chain ends.[15, 24, 25] Also, base catalyzed polymerizations using specific initiating species yield unwanted PEO oligomers. For these purposes, double metal cyanide (DMC) catalysts have been extensively investigated in order to avoid such side reactions in polyether polymerizations.[14, 15, 22, 26-29] Further investigation of DMC catalysts by Kim *et al.* reveal the kinetics of polyether polymerization as well as reaction conditions for a variety of DMC catalysts. However, these systems utilize a constant monomer feed system due to the nature of the catalyst and take a long time to polymerize taking away its economic advantage.[14, 15, 22, 26, 27, 30]

Herein, this paper describes the synthesis of a variety of well-defined heterobifunctional polyethers including poly(ethylene oxide) (PEO), poly(propylene oxide) (PPO), PEO-*b*-PPO diblock copolymers, poly(allyl glycidyl ether), and PEO-*b*-PPO-*b*-PEO triblock copolymers via DMC catalysis. These well-defined systems used a variety of initiating species such as 3-hydroxypropyldimethylvinylsilane, 3-hydroxypropyltrivinylsilane,[17] cholesterol, N-(2-hydroxyethyl)maleimide,[15] propargyl alcohol, and stearyl alcohol were used to yield specific functionality. An aging study was conducted to determine if introducing the DMC catalyst to the initiating species as a function of time would yield a more well-defined system. Characterization techniques, such as ^{1}H NMR and SEC, were used to determine the effect of aging the initiating species on molecular weight distributions (M_w/M_n) of the polymerizations.

3.3 Experimental

3.3.1 Materials

Tetrahydrofuran (THF, Optima Grade, EMD Chemicals, 99.5%) was refluxed over sodium metal with benzophenone until the solution reached a deep purple, fractionally distilled, and deoxygenated just prior to use. Acetone, allyl glycidyl ether (>99.5 %), azobisisobutyronitrile (AIBN), benzyl alcohol (>98%), ethylene oxide (EO, 99.5+%), diethylvinyl phosphonate (>99%), 2-ethanolamine (99%), furan (99%), mercaptoacetic acid (99%), 2-mercaptoethylamine hydrochloride, potassium (98%), propargyl alcohol (>99%), propylene oxide (PO, ≥99%), sodium iodide (>98%), triethylamine (98%), and 1.0 M vinyl magnesium bromide were purchased from Aldrich and used as received. Cholesterol (98%), and stearyl alcohol (>99%) were obtained from Alfa-Aesar and used as

received. 3-Chloropropyldimethylchlorosilane and 3-chloropropyltrichlorosilane (Gelest) were used as received. Chloroform, dichloromethane, diethyl ether, methanol, magnesium sulfate, and sodium bicarbonate (Fisher Scientific) were used as received. Ethanol (200 proof) was obtained from Decon Laboratories and used as received. Toluene (Fisher Scientific) was stirred over CaH_2, and fractionally distilled followed by deoxygenation with N_2 for 30 minutes prior to use. Naphthalene (Aldrich, 99%) was sublimed prior to use. Glacial acetic acid (Aldrich) was diluted with distilled THF to yield a 2.5 M solution. N,N-Dimethylformamide (DMF, EMD Chemicals) was dried over CaH_2, fractionally distilled under vacuum and stored under nitrogen at 25 °C. A double-metal catalyst, ($Zn_3[Co(CN)_6]_2$), graciously donated by Bayer was dried at room temperature for 24 h under vacuum and diluted with distilled THF to yield a 4.1 mg mL^{-1} dispersion.

3.3.2 Instrumentation

Spectroscopy analyses of the block copolymers were performed using a Varian Inova 400 NMR and a Varian Unity 400 NMR. Size exclusion chromatography (SEC) was conducted with an Alliance Waters 2690 Separations Module with a Viscotek T60A dual viscosity detector and laser refractometer equipped with a Waters HR 0.5 + HR 2 + HR 3 + HR 4 styragel column set at 30 °C. A Universal calibration was utilized to obtain absolute molecular weights.

3.3.3 Synthesis of 3-hydroxypropyldimethylvinylsilane and 3-hydroxypropyltrivinylsilane

3-HPMVS and 3-HPTVS were prepared utilizing a modified procedure originally developed by Vadala et al.[17, 19] The procedure described herein that was utilized to prepare 3-HPMVS can be applied to the synthesis of 3-HPTVS with appropriate substitution of the

trivinylsilane as the starting reagent. 3-Chloropropyldimethylchlorosilane (10.0 g, 0.06 mol) was syringed into a clean, flame-dried, two-neck, round-bottom flask equipped with a stir bar under a N_2 purge. The reaction flask was placed in an ice bath and cooled to 0 ºC. A 1.0 M solution of vinylmagnesium bromide (64.0 mL, 0.064 mol) in THF was slowly added to the flask over 30 min. The flask was allowed to warm to room temperature, and the mixture was stirred for 24 h. The reaction mixture was diluted with dichloromethane (100 mL), transferred to a separatory funnel and washed with a saturated aqueous ammonium chloride solution (150 mL), then the organic layer was further washed with aqueous sodium chloride (3 X 150 mL). Magnesium sulfate was added to the organic layer to remove any residual water, followed by vacuum filtration. Dichloromethane was removed under vacuum and the product was distilled at 100 ºC, 0.8 Torr, yielding 3-chloropropyldimethylvinylsilane (8.91 g, 0.55 mol, 94% yield) (3-CPMVS). ^{1}H NMR was used to confirm the quantitative addition of vinyl groups.

3-CPMVS (8.91 g, 0.55 mol) was placed in a 250-mL round-bottom flask equipped with a stir bar and condenser. In a separate round-bottom flask, sodium iodide (16.4 g, 0.11 mol) was dissolved in acetone (60 mL) and the solution was syringed into the flask. The mixture was heated at 56 ºC for 24 h. Acetone was removed under vacuum and the product was dissolved in dichloromethane (100 mL) and vacuum filtered to remove the salt by-products. Dichloromethane was removed under vacuum and the product was distilled at 100 ºC, 0.8 Torr, yielding 3-iodopropyldimethylvinylsilane (3-IPMVS, 13.4 g, 0.05 mol). ^{1}H NMR confirmed the expected structure.

3-IPMVS (13.4 g, 0.05 mol) was placed in a 250-mL round-bottom flask equipped with a stir bar and condenser. DMF (20 mL) was added to the reaction flask followed by

sodium bicarbonate (8.8 g, 0.10 mol) and DI water (5 mL). The mixture was heated to 100 ^{o}C for 24 h and conversion of the alkyl iodide to an alcohol was monitored via ^{1}H NMR. The reaction mixture was transferred to a separatory funnel and washed 3X with DI water to remove the excess sodium bicarbonate and DMF. The product was fractionally distilled at 90 ^{o}C, 0.8 Torr, yielding 3-hydroxypropyldimethylvinylsilane (3-HPMVS, 7.4 g, 0.048 mol, 95% yield). ^{1}H NMR confirmed the expected chemical structure.

3.3.4 Synthesis of 3a, 4,7,7a-tetrahydro-4,7-epoxyisobenzofuran-1,3-dione

Maleic anhydride (40.0 g, 0.41 mol) was added to a flame-dried 500-mL roundbottom flask under a nitrogen atmosphere that was equipped with a magnetic stir bar, and suspended in toluene (200 mL). Furan (30 mL, 0.41 mol) was added to the reaction flask via syringe and allowed to stir at room temperature. After 24 h, the white crystals were collected via vacuum filtration and washed with diethyl ether (3 x 50 mL).

3.3.5 Synthesis of 4,7-Epoxyisobenzofuran-1,3-dione-4,7-Epoxy-1H-isoindole- 1,3(2H)-dione

4,7,7a-Tetrahydro-4,7-epoxyisobenzofuran-1,3-dione (15.05 g, 90.5 mmol) was added under a nitrogen atmosphere to a flame-dried, three neck, 250-mL roundbottom flask equipped with a reflux condenser and a magnetic stir bar. Ethanolamine (5.53 g, 90.5 mmol) dissolved in methanol (30 mL) was quickly added to the reaction flask and the solution was stirred for 30 min at room temperature, then refluxed for 24 h. The reaction mixture was cooled to room temperature and the product crystallized from solution. The reaction mixture was stored at 4 ^{o}C overnight. The crystals were collected via vacuum filtration and washed with methanol (3 x 20 mL).

3.3.6 Synthesis of N-(2-Hydroxyethyl)maleimide

7-Epoxyisobenzofuran-1,3-dione-4,7-epoxy-1H-isoindole-1,3(2H)-dione (5.44 g, 26.0 mmol) and toluene (50 mL) were added under a nitrogen atmosphere to a three neck, 250-mL, roundbottom flask equipped with a Dean Stark trap and a magnetic stir bar. The reaction mixture was heated to reflux and stirred for 6 h. Toluene (10 mL) was removed from the Dean Stark trap and allowed to refill. The reaction mixture was hot filtered and the product crystallized from solution upon cooling. The crystals were collected via vacuum filtration.

3.3.7 Synthesis of monovinylsilyl- and trivinylsilyl-PEO-OH

An exemplary procedure for the polymerization of a 2,000 g mol^{-1} dimethylvinylsilyl-PEO-OH is provided. Preparation of trivinylsilyl-PEO-OH can achieved by using 3-HPTVS as the initiating species. 3-HPMVS (0.69 g, 5.0 mmol) was syringed into a clean, flame-dried roundbottom flask followed by syringing 5 mL of THF and ARCOL 3 catalyst solution (0.48 mL, 2.0 mg). The resulting initiator mixture was stirred for 26 hours. A 300-mL, high-pressure Series 4561 Parr reactor was utilized for the polymerizations. EO (10.0 g, 0.23 mol) was distilled from a lecture bottle into the pressure reactor cooled with an isopropanol-dry ice bath followed by 30 psi of ultra high purity nitrogen. The initiator solution was added to the Parr reactor via syringe and heated to 105 ^{o}C. A maximum pressure of 150 psi was noted followed by a temperature spike of 26 ^{o}C and a gradual pressure decrease of 75 psi over 40 minutes. Once an equilibrium pressure was achieved the reactor was cooled to room temperature and its contents were diluted

with ~200 mL of chloroform. The resulting solution was filtered through celite to remove the catalyst followed by precipitation of the polymer into cold diethyl ether and dried under vacuum at room temperature. This reaction yielded 9.47 g of dimethylvinylsilyl-PEO-OH and ^{1}H NMR gave an M_n of 1,990 g mol^{-1} and SEC yielded an M_n of 1,910 g mol^{-1} with a MWD of 1.11.

3.3.8 Synthesis of trivinylsilyl-PPO-OH

An exemplary procedure for the polymerization of a 3,000 g mol^{-1} propylene oxide utilizing 3-hydroxypropyltrivinylsilane is as follows. 3-HPTVS (1.12 g, 6.7 mmol) was syringed into a clean, flame-dried roundbottom flask followed by THF (5 mL) and ARCOL 3 catalyst solution (0.72 mL, 3.0 mg). The mixture was aged for 20 hours via stirring. Propylene oxide (PO) (20 g, 0.34 mol) was syringed into a 300-mL, high-pressure Series 4561 Parr reactor filled with 30 psi of ultra high purity nitrogen. The initiator mixture was syringed into the reactor and heated to 105 ^{o}C and a maximum pressure of 170 psi was noted. An increase in temperature (47 ^{o}C) and pressure decrease (100 psi) was noted. The reaction was cooled to room temperature and diluted with chloroform (250 mL). The polymer solution was filtered through celite in order to remove the catalyst followed by roto-evaporation of the chloroform. The resulting polymer was dried at 60 ^{o}C under vacuum for 24 hrs. ^{1}H NMR analysis revealed an M_n of 3,010 g mol^{-1} and SEC results gave an M_n of 3,100 g mol^{-1} with a MWD of 1.09.

3.3.9 Synthesis of benzyl alcohol initiated poly(allyl glycidyl ether) (BnO-PAGE-OH)

An exemplary procedure for the polymerization of a 3,000 g mol^{-1} Benzyl alcohol-PAGE-OH is provided. Benzyl alcohol (0.37 g, 3.3 mmol) was syringed into a clean, flame-dried roundbottom flask followed by syringing 5 mL of THF and ARCOL 3 catalyst solution (0.48 mL, 2.0 mg). The resulting initiator mixture was stirred for 24 hours. A 300-mL, high-pressure Series 4561 Parr reactor filled with 30 psi of nitrogen was utilized for the polymerization. Allyl glycidyl ether (10.0 g, 0.09 mol) was added to the Parr reactor via syringe. The initiator solution was added to the Parr reactor via syringe and heated to 105 ^{o}C. A maximum pressure of 163 psi was noted followed by a temperature spike of 34 ^{o}C and a gradual pressure decrease of 91 psi over 52 minutes. Once an equilibrium pressure was achieved the reactor was cooled to room temperature and its contents were diluted with ~200 mL of chloroform. The resulting solution was filtered through celite to remove the catalyst followed by solvent removal via roto-evaporation. The polymer was dried under vacuum at 60 ^{o}C for 24 hrs. This reaction yielded 9.21 g of benzyl alcohol-PAGE-OH and ^{1}H NMR gave an M_n of 2,850 g mol^{-1} and SEC yielded an M_n of 3,110 g mol^{-1} with a MWD of 1.21.

3.3.10 Synthesis of Maleimide-PEO-OH

A procedure for the preparation of a 5,000 g mol^{-1} N-(2-hydroxyethyl)maleimide initiated poly(ethylene oxide) is given. N-(2-hydroxyethyl)maleimide (0.28 g, 2.0 mmol) was placed in a 50 mL clean, flame-dried roundbottom flask equipped with a stirbar and purged with nitrogen for 30 minutes. THF (5 mL) was charged to the roundbottom followed by an ARCOL 3 catalyst solution (0.48 mL, 2.0 mg) and the initiator solution

was stirred for 27 hours. Ethylene oxide (EO) (10.0 g, 0.23 mol) was distilled from a lecture bottle into a 300-mL, high-pressure Series 4561 Parr reactor cooled with an isopropanol-dry ice bath (-30 ^{o}C). The initiator solution was added to the reactor via syringe. The resulting mixture was heated to 105 ^{o}C while stirring at which a pressure of 162 psi was noted. A noticeable increase in temperature (45 ^{o}C) and decrease in pressure (90 psi) was observed when polymerization occurred and continued heating for 1 hour after noted behavior. The reaction was cooled to room temperature and diluted with chloroform (250 mL). Celite was used to filter the catalyst from the reaction and the polyether was concentrated and precipitated into cold diethyl ether (500 mL). The polymer was dried under vacuum at room temperature for 24 hours yielding 8.91 g of Maleimide-PEO-OH. ^{1}H NMR analysis revealed an M_n of 5,050 and SEC yielded an M_n of 5,440 with a MWD of 1.24.

3.3.11 Synthesis of propargyl alcohol-initiated PEO-OH

An exlempary procedure for the preparation of a 2,500 g mol^{-1} propargyl alcohol initiated poly(ethylene oxide) (PA-PEO) is provided. Freshly distilled propargyl alcohol (0.23 g, 4.0 mmol) was syringed into a clean, flame-dried 50 mL roundbottom flask followed by the addition of THF (5 mL) and ARCOL 3 catalyst solution (0.5 mL, 2.1 mg) and stirred for 24 hours. Ethylene oxide (EO) (10.0 g, 0.23 mol) was distilled from a lecture bottle into a 300-mL, high-pressure Series 4561 Parr reactor cooled with an isopropanol-dry ice bath (-30 ^{o}C). The initiator solution was added to the reactor via syringe. The resulting mixture was heated to 105 ^{o}C while stirring at which a pressure of 150 psi was noted. A noticeable increase in temperature (42 ^{o}C) and decrease in pressure

(80 psi) was observed when polymerization occurred and continued heating for 1 hour after noted behavior. The reaction was cooled to room temperature and diluted with chloroform (250 mL). Celite was used to filter the catalyst from the reaction and the polyether was concentrated and precipitated into cold diethyl ether (500 mL). The polymer was dried under vacuum at room temperature for 24 hours yielding 9.49 g of PA-PEO-OH. ^{1}H NMR analysis revealed an M_n of 2,450 and SEC yielded an M_n of 2,240 with a MWD of 1.07.

3.3.12 Synthesis of stearyl alcohol-initiated PEO-OH

An exlempary procedure for the preparation of a 6,000 g mol^{-1} stearyl alcohol initiated poly(ethylene oxide) (SA-PEO) is provided. Stearyl alcohol (0.55 g, 2.0 mmol) was placed in a 50 mL roundbottom flask equipped with a stirbar and dried under vacuum at 50^{o}C for 24 hours. The compound was dissolved in THF (2 mL) and a zinc(II) cobalt(III) hexacyanoate ($Zn_3[Co(CN)_6]_2$ (1.56 mg, 0.37 mL) solution was syringed into the flask and stirred for 22 hours. Ethylene oxide (EO) (10.0 g, 0.23 mol) was distilled from a lecture bottle into a 300-mL, high-pressure Series 4561 Parr reactor cooled with an isopropanol-dry ice bath (-30 ^{o}C), The initiator solution was added to the reactor via syringe. The resulting mixture was heated to 105 ^{o}C while stirring at which a pressure of 150 psi was noted. A noticeable increase in temperature (42 ^{o}C) and decrease in pressure (120 psi) was observed when polymerization occurred and continued heating for 1 hour after noted behavior. The reaction was cooled to room temperature and diluted with chloroform (250 mL). Celite was used to filter the catalyst from the reaction and the polyether was concentrated and precipitated into cold diethyl ether (500 mL). The polymer

was dried under vacuum at room temperature for 24 hours yielding 9.1 g of SA-PEO. ^{1}H NMR analysis revealed an M_n of 6,050 and SEC yielded an M_n of 6,300 with a MWD of 1.11.

3.3.13 Synthesis of Cholesterol-PEO-OH

An exlempary procedure for the preparation of a 6,000 g mol^{-1} cholesterol initiated poly(ethylene oxide) (Chol-PEO-OH) is provided. Cholesterol (0.64 g, 1.7 mmol) was placed in a 50 mL roundbottom flask equipped with a stirbar and dried under vacuum at 50 ^{o}C for 24 hours. The compound was dissolved in THF (5 mL) and an ARCOL 3 catalyst solution ($Zn_3[Co(CN)_6]_2$, 1.56 mg, 0.37 mL) was syringed into the flask and stirred for 22 hours. Ethylene oxide (EO) (10.0 g, 0.23 mol) was distilled from a lecture bottle into a 300-mL, high-pressure Series 4561 Parr reactor cooled with an isopropanol-dry ice bath (-30 ^{o}C). The initiator solution was added to the reactor via syringe. The resulting mixture was heated to 105 ^{o}C while stirring at which a pressure of 160 psi was noted. A noticeable increase in temperature (37 ^{o}C) and decrease in pressure (90 psi) was observed when polymerization occurred and continued heating for 1 hour after noted behavior. The reaction was cooled to room temperature and diluted with chloroform (250 mL). Celite was used to filter the catalyst from the reaction and the polyether was concentrated and precipitated into cold diethyl ether (500 mL). The polymer was dried under vacuum at room temperature for 24 hours yielding 9.61 g of Chol-PEO-OH. ^{1}H NMR analysis revealed an M_n of 5,900 and SEC yielded an M_n of 6,300 with a MWD of 1.11.

3.3.14 Synthesis of monovinylsilyl-PEO-b-PPO-OH diblock copolymer

An exlempary procedure for the addition of a 3,500 g mol^{-1} poly(propylene oxide) (PPO) block to a 2,000 g mol^{-1} dimethylvinylsilyl-PEO-OH is provided. A 2,000 g mol^{-1} dimethylvinylsilyl-PEO-OH (5.0 g, 2.5 mmol) homopolymer was added to a 100 mL roundbottom flask and dried under vacuum at 60 ^{o}C for 24 hours. The polymer flask was purged with nitrogen followed by the addition of 10 mL of THF and ARCOL 3 catalyst solution (0.72 mL, 3.0 mg) and stirred for 23.5 hours. PO (8.75 g, 0.15 mol) was added via syringe to a clean 300-mL, high-pressure Series 4561 Parr reactor filled with ultra high purity nitrogen. The macroinitiator solution was added via syringe to the Parr reactor and heated to 105 ^{o}C at which a maximum pressure of 172 psi was noted. A noticeable increase in temperature was seen (45 ^{o}C) and a pressure drop (100 psi) was observed over a 55 min period at which an equilibrium pressure was reached (~70 psi). The reactor was cooled to room temperature and its contents diluted with chloroform (200 mL). Celite was used to filter the catalyst out of the solution and the solvent was removed via roto-evaporation. The block copolymer was dried under vacuum at 60 ^{o}C for 24 hours yielding 13.1 g. ^{1}H NMR revealed the addition of the PPO block with an M_n of 3,500 g mol^{-1} and SEC noted a total molecular weight of 5,600 g mol^{-1} with a MWD of 1.07.

3.3.15 Synthesis of well-defined heterobifunctional asymmetric pluronics (monovinylsilyl-PEO-b-PPO-b-PEO-OH)

An exlempary procedure for the addition of a 1,500 g mol^{-1} PEO to a 5,500 g mol^{-1} monovinylsilyl-PEO-PPO-OH yielding an asymmetric pluronic is given. EO (2.8 g, 0.06 mol) was distilled from a lecture bottle into the pressure reactor cooled with an isopropanol-dry ice bath. THF (5 mL) was added to the reactor via syringe. A potassium

naphthalide solution was prepared by charging naphthalene (14.1 g, 0.11 mol) into a 250-mL, flame-dried, round-bottom flask equipped with a glass stir bar. Dry THF (100 mL) was syringed into the flask to dissolve the naphthalene. Potassium metal (3.96 g, 0.10 mol) was added to the solution followed by a N_2 purge for 30 min. The solution was stirred overnight and titrated with 1 N HCl to determine the molarity of the potassium naphthalide solution, which was shown to be 0.95 M. Monovinylsilyl-PEO-PPO-OH (M_n = 5,500 g mol^{-1}, 10.0 g, 1.8 mmol) was placed in a 100 mL roundbottom and dried under vacuum at 60 ^oC for 24 hours followed by a 30 minute nitrogen purge at room temperature. THF (10 mL) was added to dissolve the polymer followed by addition of a potassium naphthalide solution (1.72 mL, 1.7 mmol). The resulting macroinitiator solution was added to the reactor via syringe and stirred for 36 hours at room temperature. The polymerization was terminated by adding acetic acid (0.7 mL of a 2.5 M solution in THF, 1.75 mmol) to the pressure reactor via syringe. The pressure reactor was purged with N_2 for 1 h, then opened and its contents were transferred to a 250-mL round-bottom flask. The solvent was removed under vacuum at room temperature, and the product was dissolved in 200 mL of dichloromethane. The product was washed twice with DI water (2 X 100 mL). The solution was removed via roto-evaporation followed by drying the polymer under vacuum at 60 ^oC for 24 hrs yielding 12.1 g. ^1H NMR revealed the addition of 1,480 g mol^{-1} PEO block and SEC yielded a total M_n of 7,010 g mol^{-1} with a MWD of 1.06.

3.3.16 Carboxylate functionalization of mono- and trivinylsilyl-polyethers via ene-thiol chemistries

An representative procedure for adding a carboxylic acid group via ene-thiol free radical chemistry across a vinylsilyl endgroup is provided for an 2,000 g mol^{-1} dimethylvinylsilyl-PEO-OH. Dimethylvinylsilyl-PEO-OH (1.0 g, 0.5 mmol) was charged to a 100-mL round-bottom flask equipped with a stir bar and dissolved in 2 mL of deoxygenated toluene. Mercaptoacetic acid (63.0 mg, 0.60 mmol) was syringed into the reaction flask followed by the addition of AIBN (9.2 mg, 0.06 mmol) dissolved in 0.5 mL of toluene. The mixture was deoxygenated for 10 min by sparging with N_2, then reacted at 80 ºC for 24 h. The reaction mixture was dissolved in 200 mL of dichloromethane, then transferred to a separatory funnel and washed with DI water 3X to remove the excess mercaptoacetic acid. The dichloromethane was removed via rotary evaporation and the resulting polymer was precipitated into cold diethyl ether. The polymer was dried at room temperature under vacuum for 24 h yielding 0.94 g of carboxylic acid-functionalized PEO-OH.

3.3.17 Ammonium functionalization of mono- and trivinylsilyl-polyethers via ene-thiol chemistries

Heterobifunctional polyethers with a terminal ammonium group (ammonium-PEO-OH) were obtained via ene-thiol addition of mercaptoethylamine hydrochloride across the vinylsilane. In a characteristic procedure, a 2,000 g mol^{-1} dimethylvinylsilyl-PEO-OH (2 g, 1.0 mmol), mercaptoethylamine hydrochloride (138.9 mg, 1.2 mmol), and AIBN (20 mg, 0.12 mmol) were dissolved in deoxygenated DMF (5 mL) in a 100-mL round-bottom flask equipped with a stir bar. The reaction was conducted at 70 °C for 24 h with stirring,

then the reaction mixture was cooled to room temperature. DI water (100 mL) was added to the flask, and the mixture was transferred to a separatory funnel. Dichloromethane (200 mL) was added to the separatory funnel to extract the alkylammonium-functionalized polyether from the water layer. The dichloromethane layer was washed with a 1 N solution of sodium bicarbonate (3X), followed by 3 washes with DI water. The dichloromethane solution was concentrated under vacuum, and the ammonium-PEO-OH oligomer was precipitated into cold diethyl ether and dried at 25 °C under vacuum for 12 h yielding 1.9 g of product (95% yield).

3.3.18 Phosphonate functionalization via Michael addition

A representative procedure for the addition of phosphonate via Michael addition is given. A characteristic procedure for adding a phosphonate group to an 8,300 g mol^{-} ammonium-PEO-OH is provided. An ammonium-PEO-OH oligomer (1.0 g, 0.12 mmol) was charged to a clean, flame-dried, 100-mL, round-bottom flask equipped with a stir bar, and dissolved in ethanol (9 mL). TEA (0.20 mL, 0.14 mmol) was added to the reaction, followed by diethyl vinyl phosphonate (0.26 mL, 0.14 mmol). The reaction was carried out at 70 ^{o}C for 24 h. The reaction mixture was diluted with DI water to obtain a 75:25 water:ethanol composition and placed in a 1,000 g mol^{-1} MWCO cellulose acetate dialysis bag and dialyzed against 4 L of DI water for 24 h to remove excess diethyl vinyl phosphonate. The contents of the dialysis bag were transferred to a 100-mL round-bottom flask and lyophilized, yielding 0.91 g of diethyl phosphonate-functionalized PEO-OH.

3.3.19 De-esterification of diethylphosphonate yielding zwitterionic phosphonate-PEO-OH

The given procedure for the de-esterification of phosphonate is representative for multiple polymer samples. Phosphonic acid-PEO-OH was prepared from diethyl phosphonate-PEO-OH using a hydrolysis procedure adapted from Caplan et al.[31] In a representative procedure, an 8,300 g mol^{-1} diethyl phosphonate-PEO-OH (0.80 g, 0.10 mmol) was charged to a clean, 100-mL round-bottom flask equipped with a stir bar and dissolved in 5 mL of dichloromethane. Trimethylsilyl bromide (0.032 mL, 0.24 mmol) was syringed into the reaction flask and stirred at room temperature for 24 h. Methanol (0.01 mL, 0.24 mmol) was added and stirred for 2 h to cleave the trimethylsilyl groups. Dichloromethane (50 mL) was added, and the mixture was washed 3X with DI water (100 mL each) in a separatory funnel. The dichloromethane layer was concentrated, then the oligomer was precipitated by pouring the mixture into cold diethyl ether. The polymer was vacuum-dried at 25 ^{o}C for 24 h yielding 0.77 g of phosphonic acid-PEO-OH.

3.4 Results and Discussion

A major goal in the design of polymeric biomaterials deals with controlling the interactions of biomacromolecules and cells with biomaterial surfaces.[3, 8, 15, 20, 30] The potential of well-defined heterobifunctional polyethers for biomedical applications involve the use of said materials in polymer-drug and polymer-protein conjugates, cell transfection, micellular drug delivery agents, polyplexes, and stabilizers for iron oxide nanoparticles for magnetic resonance contrast agents.[1, 3-5, 8-12, 15, 19, 30] The addition of polyethers to biological systems such as lipoproteins and hydrophobic drugs has emerged as the easiest way to solubilize such compounds in physiological media as well as incorporate a stealth

sheath against the RES system avoiding immunogenicity.[1-6, 9-11, 15-17, 20] The goal of this research was to determine an efficient way to initiate polyether growth off of a variety of biomolecules of interest with low molecular weight distributions ($M_w/M_n < 1.1$).

3.4.1 Aging studies determining the polydispersity of PPO

An aging study was conducted by aging the initiator of choice with the ARCOL 3 catalyst for specific periods of time to determine the effect on molecular weight control and distribution. 3-HPTVS was utilized as the initiating species for this experiment and the molar ratio of initiator to monomer was used to control the molecular weight, which was constantly targeted at 3,000 g mol^{-1}. The amount of catalyst was kept constant at 100 ppm based on total weight of solute and solvent in order to maintain a specific rate of polymerization. ARCOL 3 catalyst ($Zn_3[Co(CN)_6]_2$) was aged for a periods of 15 minutes, 17.5 hours, 20.1 hours, and 24 hours, respectively (Figure 3.4.1.1, Table 3.4.1.1). Aging the initiating species with the initiator of choice for specific times plays an integral role in lowering the molecular weight distribution as well as the monomodality of the polymer. This data shows that aging the catalyst and initating species together allows for the primary alcohol to insert itself into the catalyst particle. Once the catalyst was activated, the amount of initiator complexed in the catalyst began the ring-opening polymerization of the propylene oxide. Comparison of the SEC data gives foresight into the ability to show the amount of initiator that was not complexed into the catalyst particles. The complexed initiator begins the polymerization process first followed by the interaction of the free initiator with the activated catalyst. The difference in these times of polymerization broadens the molecular weight distribution of the polymer based on the free initiator

present. Comparison of this aging technique to the commercial polymerzation utilizing this catalyst gives some insight into the mechanism.

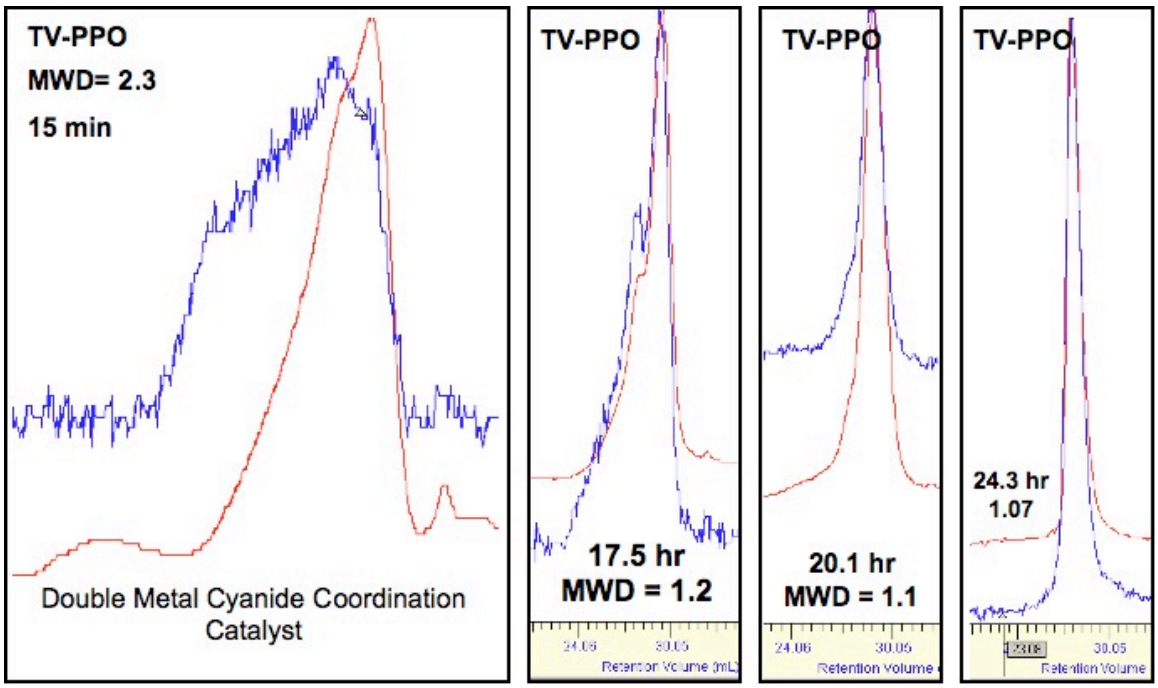

Figure 3.4.1.1. SEC analysis of trivinylsilyl-PPO-OH oligomers at specific aging times

Table 3.4.1.1. Characterization of trivinylsilyl-PPO-OH at various aging times

Targeted Molecular Weight	Aging Time (hr)	M_n (g mol^{-1})		MWD
		^{1}H NMR	SEC	
Trivinylsilyl-3,000 g mol^{-1}	0.25	3,610	3,900	2.30
Trivinylsilyl-3,000 g mol^{-1}	17.5	3,300	3,220	1.21
Trivinylsilyl-3,000 g mol^{-1}	20.1	3,100	3,390	1.10
Trivinylsilyl-3,000 g mol^{-1}	24.3	2,900	3,050	1.07

Commercial polymerization of propylene oxide involves adding a small amount of monomer with the initiating species and the double metal catalyst followed by activating the catalyst. When a pressure drop is observed, a monomer feed unit is used in order to pump monomer into the reactor keeping the polymerization rate constant. Comparison of the commercial technique to the aging technique discussed above indicates that the initiating species seems to be coordinating with the zinc as shown in Figure 3.4.1.2.

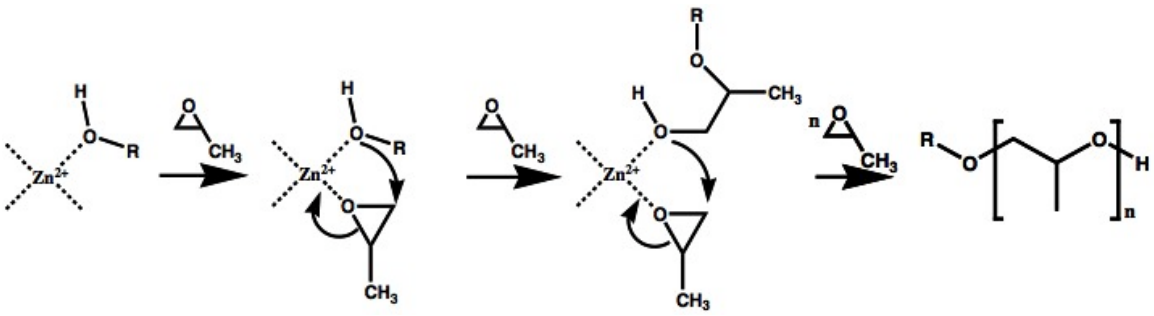

Figure 3.4.1.2. Proposed pathway of ARCOL 3 catalyst ring opening polymerization

As the monomer comes in contact with the catalyst particles, the oxygen of the propylene oxide coordinates with the zinc allowing for the oxygen of the initiating species to attack the methylene carbon ring-opening the monomer. The coordinated oxygen from the added monomer unit has a negative charge in which the electrons then abstract the proton from the protonated initiator oxygen yielding a propylene oxide unit added to the alcohol. This process is repeated rapidly due to the temperature increase noted in the polymerization, which is a by-product of the energy dissociated by the ring opening of the epoxide species.

Narrowing of the molecular weight distribution as a function of aging gives insight into the pathway at which the coordination catalyst works. Aging the catalyst with the alcohol initiator seems to open more zinc sites for propagation. The aging process appears to coordinate the alcohol to the maximum amount zinc available, making the alcohol ready to undergo monomer insertion.[22, 26, 32] Interpretation of the SEC data (Figure 1, Table 1) indicate that the alcohol and propagating species exchange so fast on the zinc coordination sites relative to the rate of propagation that all the alcohols seem to undergo chain homologation at the same rate.[32] As the aging time is decreased only a partial amount of zinc sites have alcohol bound thus lowering the rate of exchange close to that of the rate of propagation broadening the molecular weight distribution.[32]

The use of the double metal catalyst is an important discovery in the polymerization of propylene oxide when compared to that of base catalyzed propylene oxide. When using base in the ring-opening polymerization of PO, the generated secondary alkoxide can abstract hydrogen from the pendant methyl group of PO generating a primary allyl-alkoxide (Scheme 3.4.1.1). The formation of this primary allyl-alkoxide yields unwanted unsaturation as well as lowering the target molecular weight and broadening of the molecular weight distribution.

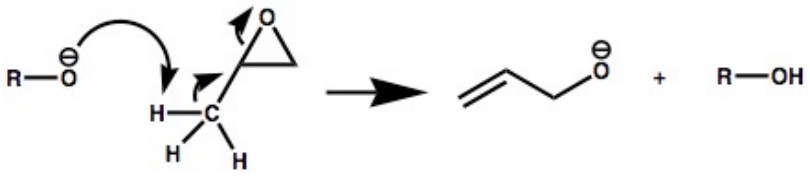

Scheme 3.4.1.1. Mechanism of anionic ring-opening polymerization side product of propylene oxide via base catalysis

3.4.2 Synthesis of PEO and PPO heterobifunctional oligomers utilizing the ARCOL 3 catalyst

In order to create a polymer with heterobifunctionality one must begin with an initiator capable of post polymerization functionalization or begin with an initiating species with only one hydroxyl group. 3-HPMVS or 3-HPTVS was utilized for this purpose due to the ability to add a variety of functional groups post polymerzation. 3-HPMVS or 3-HPTVS was aged with 100 ppm catalyst, based on total weight, for 24 hours or more to insure a narrow molecular weight distribution (Scheme 3.4.2.1).

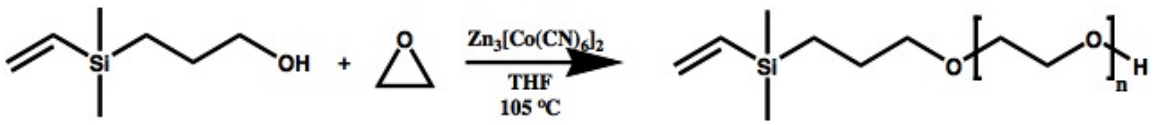

Scheme 3.4.2.1. Synthesis of dimethylvinylsilyl-PEO-OH oligomer via ARCOL 3 coordination polymerization

Dimethylvinylsilyl-PEO-OH oligomer with targeted molecular weights of 2,000 and 5,000 g mol^{-1} were synthesized (Scheme 3.4.2.1) and the materials were characterized using ^{1}H NMR and SEC (Table 3.4.2.1). Also, a series of trivinylsilyl-PEO-OH oligomers with targeted molecular weights of 1,500-, 2,000-, 3,500-, and 5,000 g mol^{-1} were synthesized and characterized by ^{1}H NMR and SEC (Table 3.4.2.1). Figure 3.4.2.1 shows a representative ^{1}H NMR spectrum of a dimethylvinylsilyl-PEO-OH oligomer. The number average molecular weight (M_n) was determined by comparing the integral ratios of the resonances corresponding to the methylene groups in the initiator (labeled C and D) to the repeat unit of ethylene oxide labeled F. SEC analysis revealed symmetric monomodal peaks with molecular weight distributions of 1.2 or less for both the dimethylvinylsilyl- and trivinylsilyl-PEO-OH oligomers. Good agreement in molecular weight was given by both methods of analysis.

Table 3.4.2.1. Characterization of dimethylvinylsilyl- and trivinylsilyl-PEO-OH oligomers

Targeted Molecular Weight	M_n (g mol^{-1})		MWD
	^{1}H NMR	SEC	
Monovinylsilyl-2,000 g mol^{-1}	1,990	1,920	1.11
Monovinylsilyl-5,000 g mol^{-1}	5,010	5,200	1.07
Trivinylsilyl-1,500 g mol^{-1}	1,600	1,540	1.18
Trivinylsilyl-2,000 g mol^{-1}	2,100	1,910	1.09
Trivinylsilyl-3,500 g mol^{-1}	3,430	3,400	1.06
Trivinylsilyl-5,000 g mol^{-1}	4,800	4,970	1.05

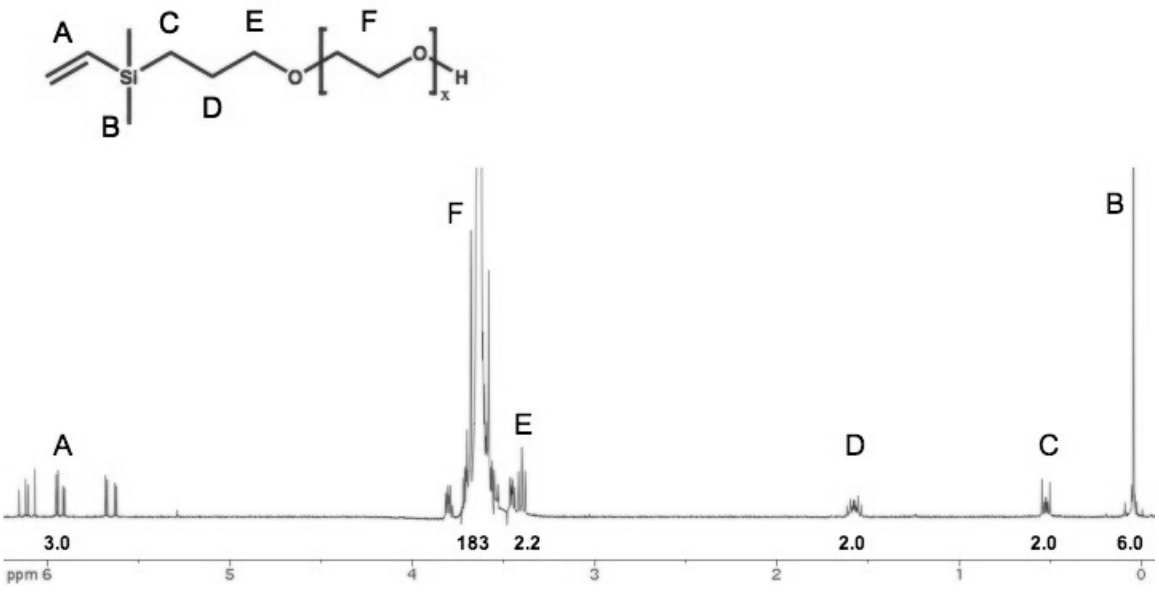

Figure 3.4.2.1. ^{1}H NMR of a 2,000 g mol^{-1} dimethylvinylsilyl-PEO-OH oligomer via coordination polymerization

3.4.3 Synthesis of poly(propylene oxide) via ARCOL 3 catalyst polymerization using a macroinitiator

Dimethylvinylsilyl-PEO-*b*-PPO-OH oligomers were synthesized by using the aforementioned 2,000 and 3,500 g mol^{-1} dimethylvinylsilyl-PEO-OH oligomer as the initiating species (Scheme 3.4.3.1). The macroinitiators were aged for 24 hours to insure coordination of the hydroxyl group to the catalyst yielding a low molecular weight distribution.

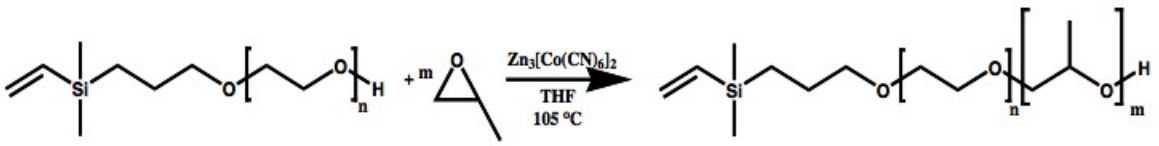

Scheme 3.4.3.1. Utilization of a macroinitiator for the polymerization of PPO via ARCOL 3 catalyst polymerization

Figure 3.4.3.1 shows a representative ^{1}H NMR spectrum of a dimethylvinylsilyl-PEO-*b*-PPO-OH oligomer. The number average molecular weight was determined by

comparing the integral ratios of the resonances corresponding to the methylene groups in the intiator, labeled C and D to the pendant methyl group in the repeat unit of propylene oxide (peak G). Determination of the M_n of the PEO block can be found by subtracting the integral ratio corresponding to G from the backbone protons, peaks E and F, of the ethylene oxide and propylene oxide repeat units to ensure maintenance of the PEO chains. SEC of the diblock copolymers confirm the M_n attained by ^{1}H NMR revealing symmetric monomodal peaks with molecular weight distributions of less than 1.1 (Table 3.4.3.1).

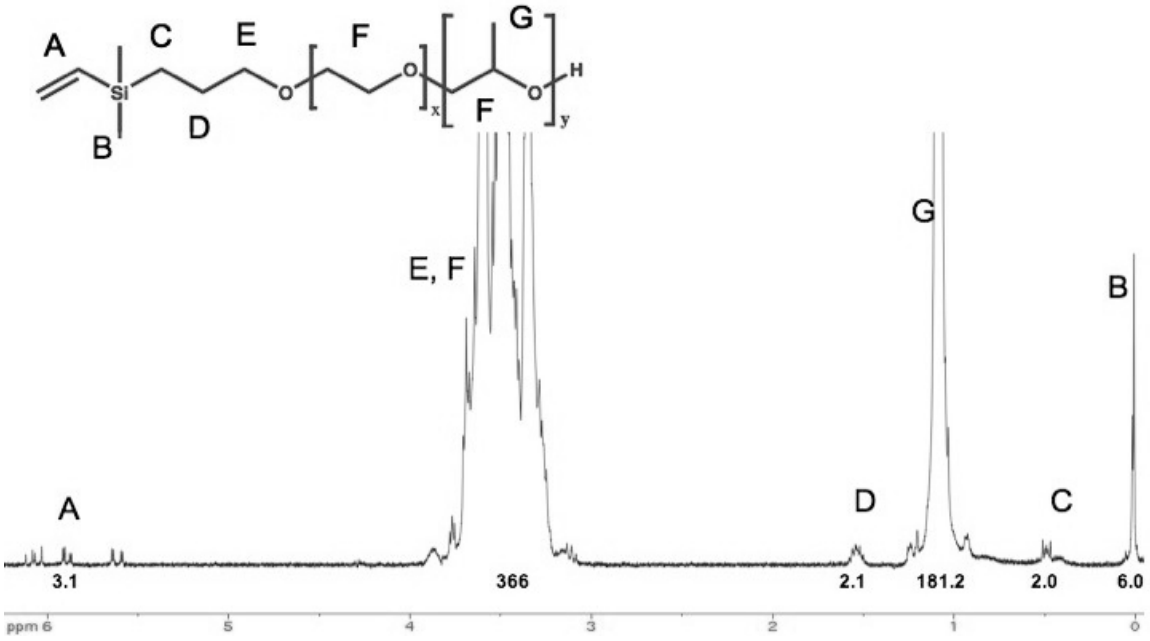

Figure 3.4.3.1. ^{1}H NMR of dimethylvinylsilyl-PEO-PPO-OH oligomer via ARCOL 3 catalyst coordination polymerization

Table 3.4.3.1. Molecular weight characterization of dimethylvinylsilyl-PEO-*b*-PPO-OH

Targeted Molecular Weight	M_n (g mol^{-1})		MWD*
	^{1}H NMR	SEC	
Monovinylsilyl-2kPEO-3.5kPPO	5,460	5,600	1.07
Monovinylsilyl-3.5kPEO-3.5kPPO	7,090	7,000	1.07

The ability to polymerize a second polyether block off of an existing polymer gives rise to quickly create a vast library of hetero-bifunctional amphiphilic block copolymers. This polymerization technique can be utilized to alter the amphiphilicity for specific applications such as cell transfection and attachment of hydrophobic drugs. Through this study, the ability to add block lengths sequentially can be utilized by addition of EO followed by PO to form well-defined systems.

3.4.4 Synthesis of poly(allyl glycidyl ether) (BnO-PAGE) via ARCOL 3 coordination polymerization

With the ability to polymerize polyethers without introduction of an alkoxide affords the use of many epoxy monomers that were previously unpolymerizable. One such epoxy monomer is allyl glycidyl ether, which yields a pendant vinyl group upon ring-opening the monomer. The given polymer was initiated with benzyl alcohol that was aged for 24 hours with ARCOL 3 catalyst. The molar amount of initiator to monomer was carefully controlled to target specific molecular weights. The monomer was introduced to the initiator catalyst solution and heated to activate the polymerization (Scheme 3.4.4.1).

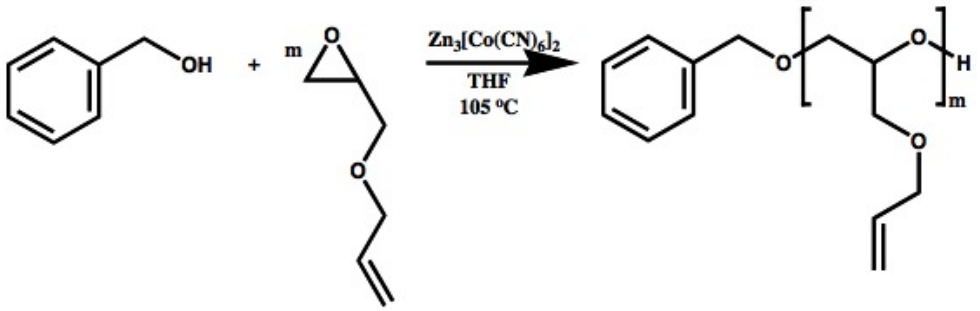

Scheme 3.4.4.1. Synthesis of poly(allyl glycidyl ether) via ARCOL 3 coordination polymerization

Benzyl alcohol-poly(allyl glycidyl ether) with a targeted molecular weight of 3,000 g mol^{-1} was characterized by ^{1}H NMR and SEC, respectively. Figure 3.4.4.1 yields the ^{1}H NMR of the polyether oligomer. The M_n was calculated by comparing the integral ratios of the methylene group in the initiator, peak B, to the vinyl protons, peak F and G, as well as the methylene and methyne protons in the backbone of the polymer (peaks C, D, and E). Through this calculation the M_n was determined to be 2,850 g mol^{-1}. SEC yielded a symmetric monomodal peak with a M_n of 3,110 g mol^{-1} with a molecular weight distribution of 1.21.

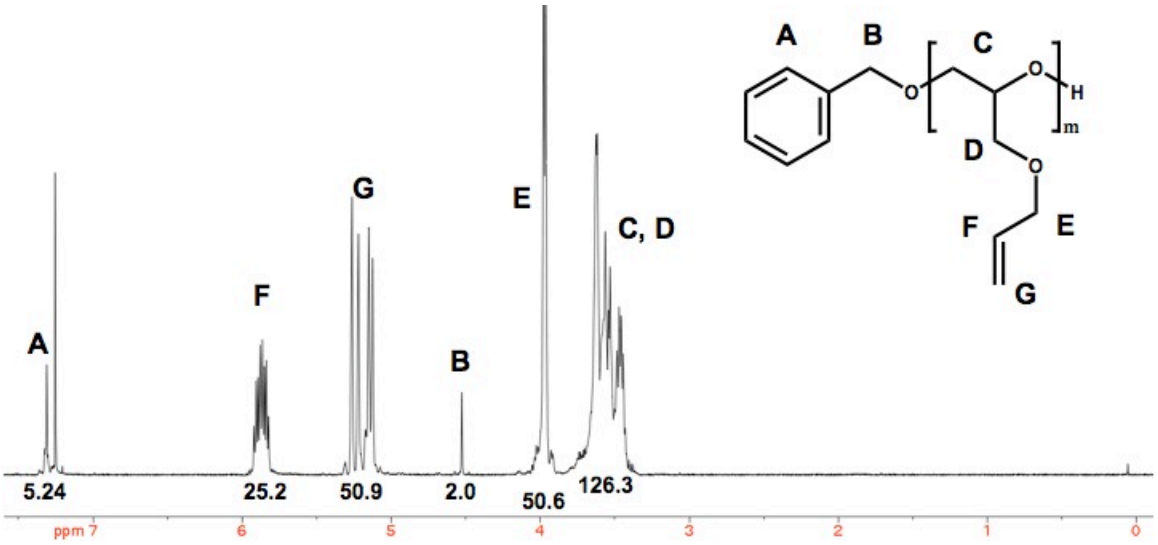

Figure 3.4.4.1. ^{1}H NMR of BnO-PAGE-OH polymerized via ARCOL 3 coordination polymerization

Through a series of post-functional chemistries, this polymer can yield a variety of pendant functional groups for the binding of specific drugs or proteins for a vast array of biomedical applications.

*3.4.5 Synthesis of well-defined heterobifunctional pluronics (monovinylsilyl-PEO-b-*PPO-*b-PEO-OH)*

Dimethylvinylsilyl-PEO-*b*-PPO-OH was used as a versatile macroinitiator for the living anionic polymerization of EO to produce a well-defined hetero-bifunctional amphiphilic oligomer with the ability to post-functionalize with various chemistries. Potassium naphthalide was introduced to the dimethylvinylsilyl-PEO-*b*-PPO-OH oligomer forming an alkoxide for initiating EO. The number of moles of the macroinitiator relative to EO controlled the molecular weight. A small deficiency of naphthalide to macroinitiator ensured that the alkoxide was formed and not residual naphthalide. The remaining alcohol chains transferred with the growing PEO chains throughout the polymerization and the reaction was terminated with acetic acid prior to opening to avoid any unwanted oxidative side reactions (Scheme 3.4.5.1).

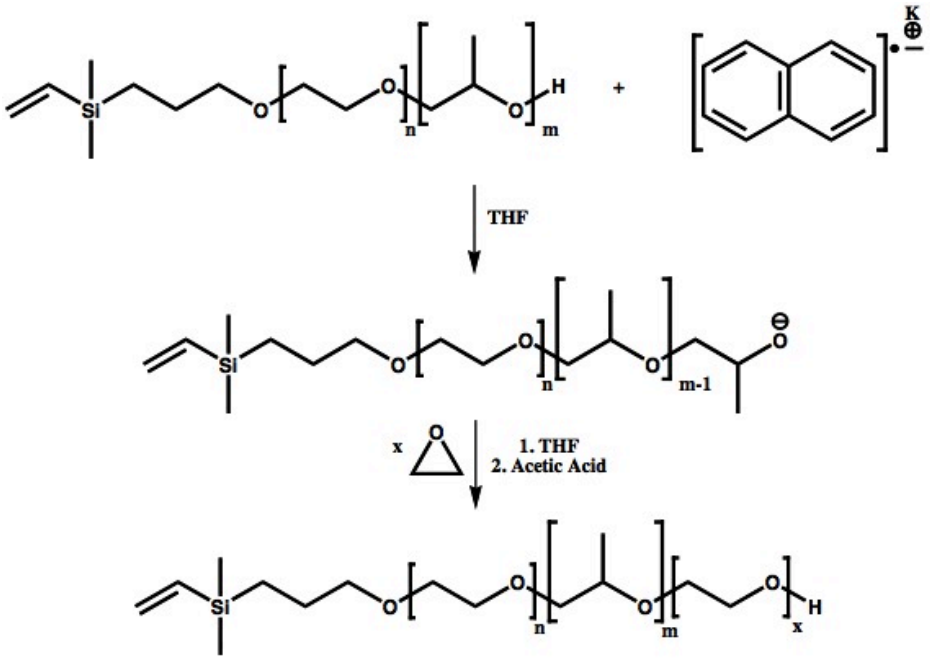

Scheme 3.4.5.1. Synthesis of dimethylvinylsilyl-PEO-*b*-PPO-*b*-PEO-OH via living anionic ring-opening polymerization

Figure 3.4.5.1 shows the ^{1}H NMR spectrum of the dimethylvinylsilyl-PEO-*b*-PPO-*b*-PEO-OH oligomer. The M_n of the additional PEO block was determined by comparing the integral ratios of the resonances corresponding to the methylene group, peak C, to the backbone peak, labeled F. The original number of protons associated with the macroinitiator (Figure 4, peak F) were subtracted from peak F yielding the molecular weight of the third PEO block.

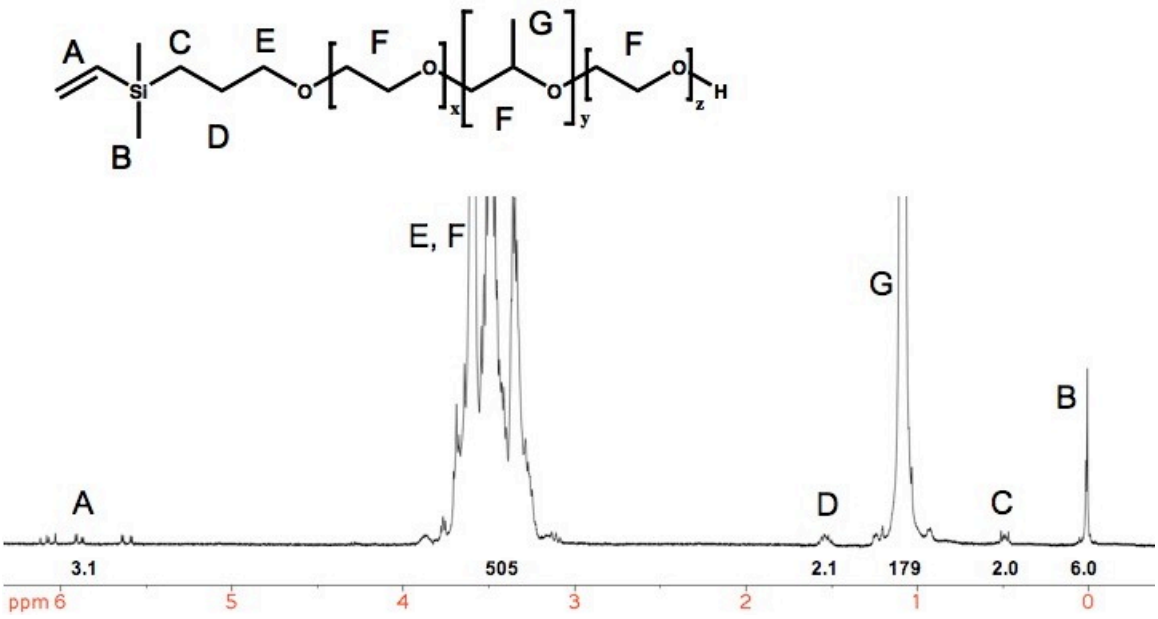

Figure 3.4.5.1. ^{1}H NMR of dimethylvinylsilyl-2kPEO-3.5kPPO-1.5kPEO-OH oligomer

SEC of each step of the dimethylvinylsilyl-PEO-*b*-PPO-*b*-PEO-OH oligomer is shown in Figure 3.4.5.2. Each SEC yielded symmetric monomodal peaks with molecular weight distributions of 1.1 or less. Taking a closer look at the SEC data reveals addition of each block via coordination polymerization and base catalyzed polymerization techniques, respectively.

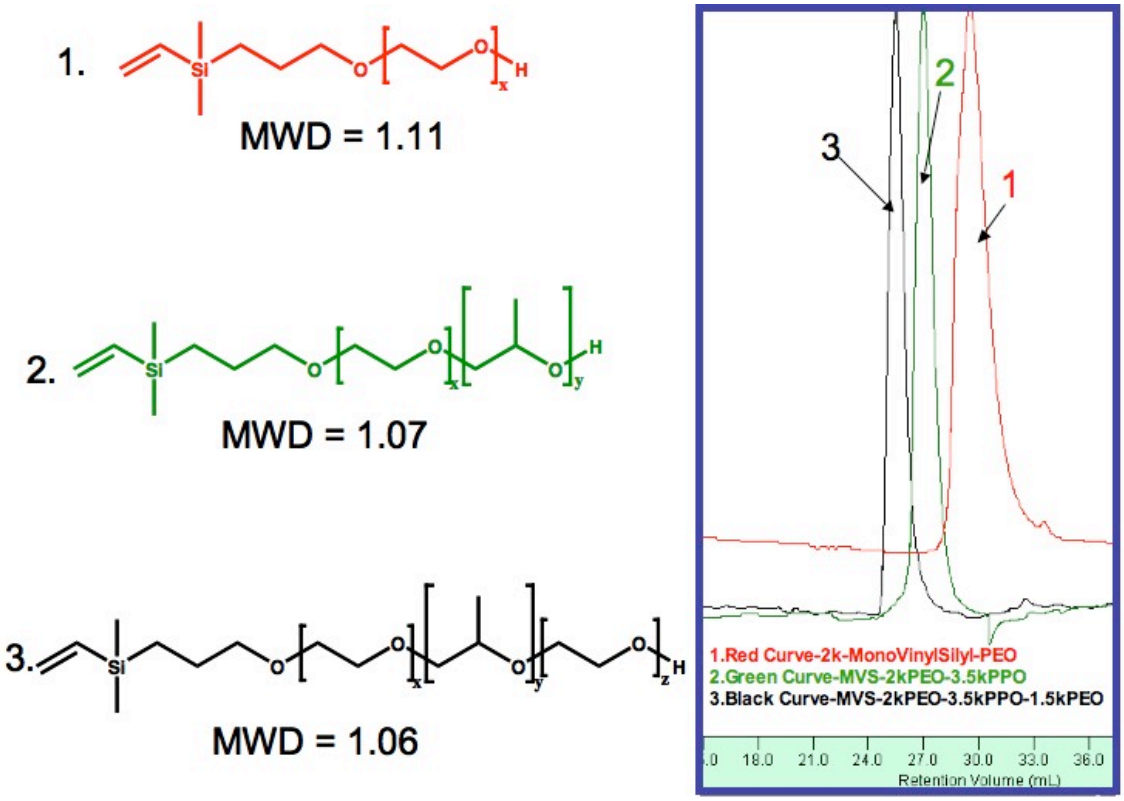

Figure 3.4.5.2. Overlay of SEC traces revealing well-defined hetero-bifunctional pluronics via combination of ARCOL 3 coordination polymerizations and anionic ring-opening polymerization

3.4.6 Synthesis of other novel well-defined heterobifunctional polyethers

A series of other well-defined heterobifunctional polyethers have been synthesized by the use of the double metal catalyst (Table 3.4.6.1). The coordination polymerization opens up a variety of new initiating speices with one alcohol group that could potentially important to the development of new bioconjugates as well as other biomedical applications.

Table 3.4.6.1. Characterization of a variety of novel PEO systems by use of the coordination polymerization technique

Targeted Molecular Weight	M_n (g mol^{-1})		MWD
	^{1}H NMR	SEC	
Cholesterol-PEO-2,500 g mol^{-1}	2,500	2,670	1.18
Cholesterol-PEO-6,000 g mol^{-1}	6,050	6,300	1.11
Maleimide-PEO-5,000 g mol^{-1}	5,050	5,440	1.24
Propargyl alcohol-PEO-2,500 g mol^{-1}	2,450	2,240	1.07
Stearyl alcohol-PEO-5,000 g mol^{-1}	6,050	6,300	1.11

Each initiating species was aged with the coordinating catalyst for at least 24 hours prior to introduction of EO monomer and the polymerizations were carried out at 105 ^{o}C. Characterization of by ^{1}H NMR and SEC revealed targeted molecular weights with low molecular weight distributions were achieved. The ability to polymerize EO with these monomers was not possible with base catalysis for a variety of reasons. In the case of propargyl alcohol, the introduction of base deprotonates both the alcohol and the alkyne proton, creating a di-initiator and yielding a bimodal polymer distribution. N-(2-hydroxyethyl)maleimide has similar problems when introduced to a base in which the maleimide group ring opens loosing its functionality. Cholesterol-PEO-OH was also difficult to polymerize via base due to the gelation of the initiator upon addition of the base solution. The synthetic scheme of cholesterol initated PEO is shown in Scheme 3.4.6.1.

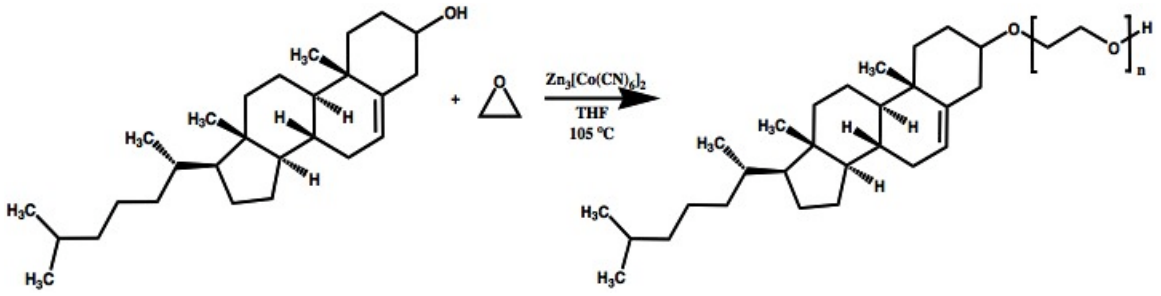

Scheme 3.4.6.1. Polymerization of cholesterol-PEO-OH oligomer via coordination polymerization

^{1}H NMR characterization of the cholesterol initiated PEO is shown in Figure 3.4.6.1 below. The M_n was calculated by comparing the integral ratios of the vinyl proton of the cholesterol, peak A, to the backbone protons of the EO repeat units (peak B).

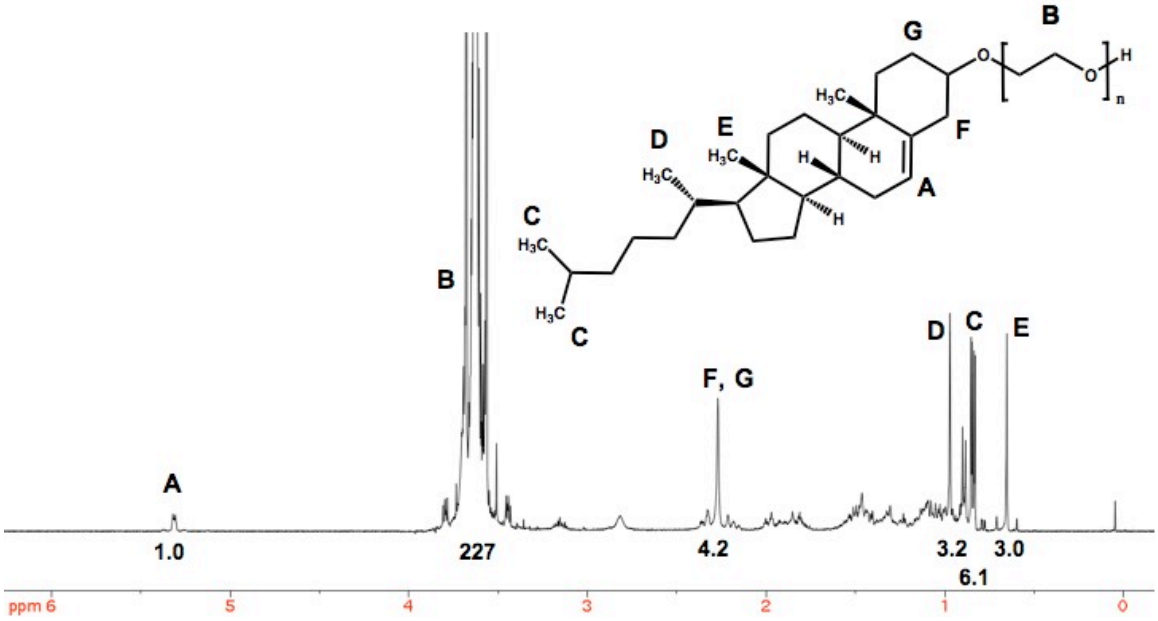

Figure 3.4.6.1. ^{1}H NMR of cholesterol-PEO-OH oligomer via coordination polymerization

3.4.7 Carboxylate, ammonium, and phosphonate functionalization of dimethylvinylsilyl- and trivinylsilyl-PEO-OH oligomers

Ene-thiol additions were utilized to introduce carboxylate and ammonium endgroups onto the polyethers (Scheme 3.4.7.1). The vinylsilyl functionality is unusual among vinyl groups in that it does not polymerize readily by free radical reactions, and thus it is seemingly an ideal substrate for ene-thiol functionalization reactions because polymerization does not compete. Nevertheless, excesses of the thiol relative to vinylsilane were utilized for these reactions to ensure quantitative addition.

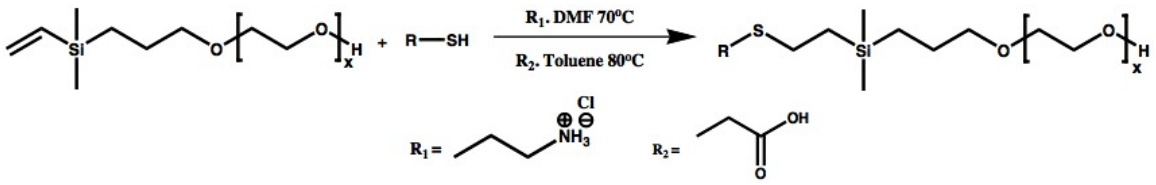

Scheme 3.4.7.1. Ene-thiol chemistries of affording carboxyilic acid and ammonium functionality

Addition of mercaptoacetic acid to dimethylvinylsilyl-PEO-OH was monitored by ^{1}H NMR. Complete disappearance of the vinyl group at ~6 ppm indicated stoichiometric conversion to a carboxylic acid-PEO-OH (Figure 3.4.7.1A). Additionally, appearances of the methylene peaks labeled 1-3 in the spectrum indicated addition of mercaptoacetic acid. Comparison of the resonance integrals corresponding to the methylene peaks of the thiol (1-3) to the methylene peak labeled 5 confirmed quantitative addition across the vinylsilane endgroups.

^{1}H NMR was also utilized to monitor ene-thiol addition of 2-mercaptoethylamine hydrochloride onto the vinylsilane endgroups of dimethylvinylsilyl-PEO-OH and trivinylsilyl-PEO-OH by observing the complete disappearance of the vinyl groups and appearances of methylene peaks labeled 1-4 in the spectra (Figure 3.4.7.1B). Comparison of integrations confirmed quantitative functionalization with ammonium groups to form ammonium-PEO-OH or ammonium$_3$-PEO-OH. The same ene-thiol chemistries were utilized in the addition of amine to the well-defined heterobifunctional pluronic as well (Figure 3.4.7.2).

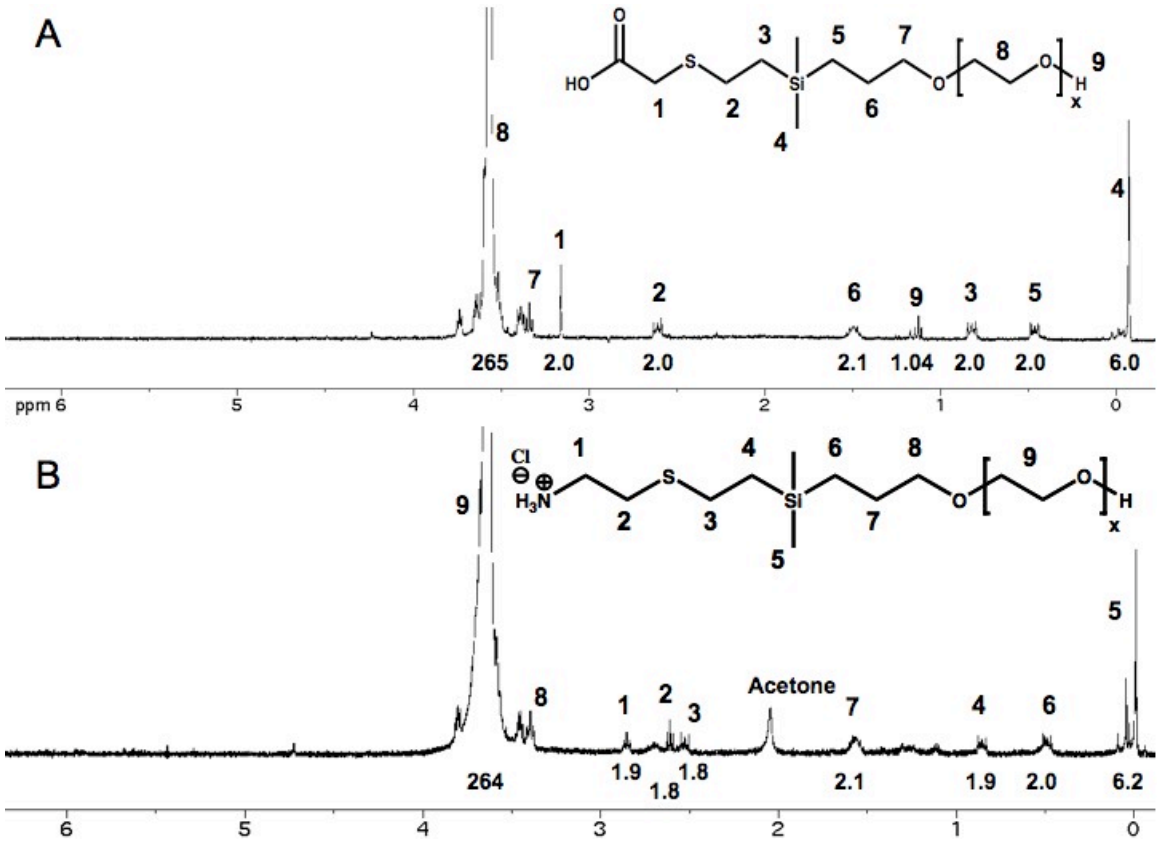

Figure 3.4.7.1. ^{1}H NMR of ene-thiol additions of (A) mercaptoacetic acid and (B) 2-mercaptoethylamine hydrochloride to a dimethylvinylsilyl-PEO-OH oligomer

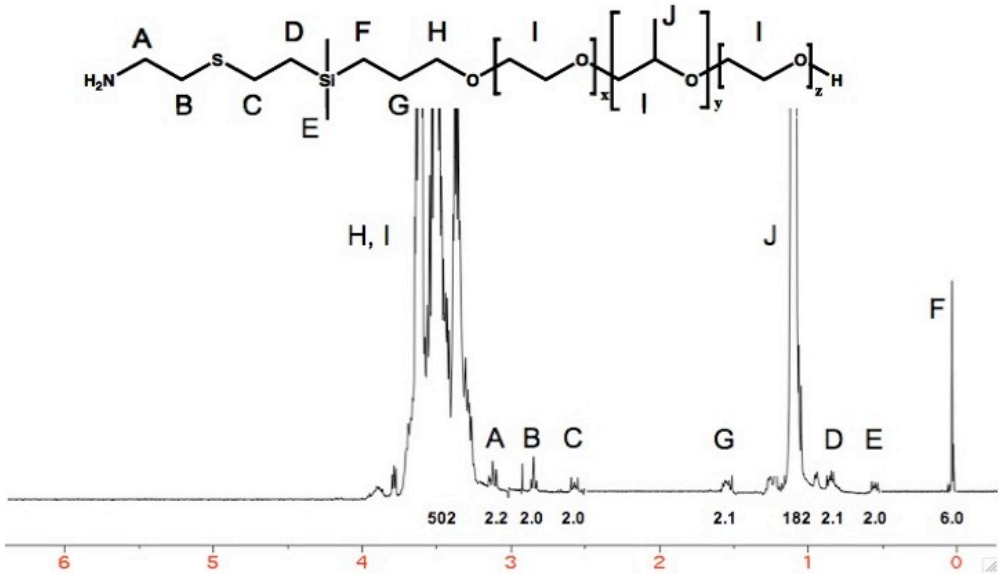

Figure 3.4.7.2. ^{1}H NMR of ammonium addition via ene-thiol chemistries yielding NH_2-PEO-*b*-PPO-*b*-PEO-OH oligomers

The ammonium-functional PEO oligomers were used as precursors to form the zwitterionic phosphonate-functional polyethers. The ammonium endgroups were first reacted with triethylamine to afford the corresponding free amines. A slight molar excess of triethylamine was added to maintain basic reaction conditions, aiding in nucleophilic addition to diethyl vinyl phosphonate. Diethyl vinyl phosphonate was added to the amine group(s) via Michael addition, yielding diethylphosphonate-PEO-OH (Scheme 3.4.7.2) or diethylphosphonate$_3$-PEO-OH.

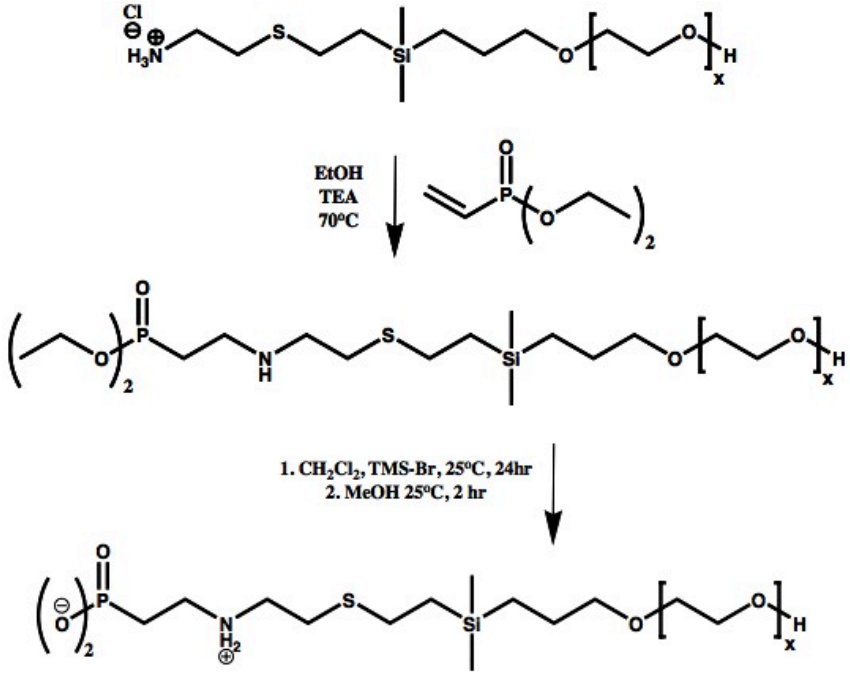

Scheme 3.4.7.2. Michael addition of amine-PEO-OH to diethyl vinyl phosphonate and de-esterification to remove the ethyl groups yielding zwitterionic phosphonate-PEO-OH

Figure 3.4.7.3A shows the ^{1}H NMR of a representative diethylphosphonate-PEO-OH oligomer. Two methylene peaks corresponding to the converted vinyl group of the phosphonate reactant are observed as peaks 3 and 4 in the spectrum of the product. Quantitative addition to diethyl vinyl phosphonate was determined by comparing the

integrations of peaks 1-4 to the integration of the methylene peak labeled 10. The ethyl phosphonate groups were cleaved using bromotrimethylsilane (TMS-Br).[31] Reacting with TMS-Br yielded an intermediate bis-trimethylsilyl ester with an alkyl halide by-product. In the methanolysis step of the reaction, the alcohol cleaved the silyl ester, yielding phosphonic acid (Scheme 3.4.7.2). A zwitterionic endgroup was afforded in the phosphonate-PEO-OH product (or in the corresponding phosphonate$_3$-PEO-OH) at a pH less than 10, due to the negative charge of the phosphonate and the protonated secondary amine. ^{1}H NMR spectra confirmed that deprotection of the diethylphosphonate-PEO-OH oligomers was complete as shown in Figure 3.4.7.3B. In addition to the disappearance of the ethyl resonances in the spectrum, there was an upfield shift (~1.6 ppm) of the methylene group adjacent to the phosphorus atom.

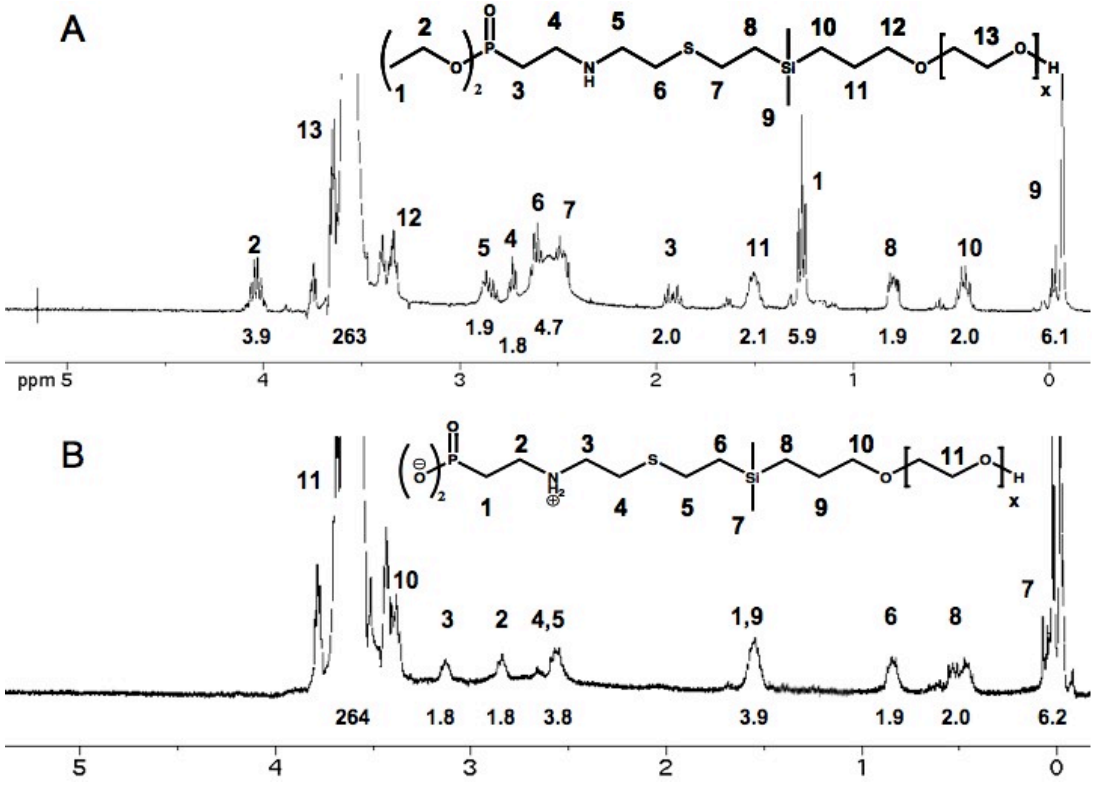

Figure 3.4.7.3. ^{1}H NMR revealing (A) phosphonate addition followed by (B) de-esterification yielding a zwitterionic phosphonate-PEO-OH oligomer.

3.5 Conclusions

A novel synthetic method for the polymerization of PEO via coordination catalysis was shown to yield well-defined systems with molecular weight distributions of 1.2 or less. Various initiating species were utilized in the polymerization process affording heterobifunctional PEOs, PEO-*b*-PPOs, and PEO-*b*-PPO-*b*-PEOs. Specific post-functionalization chemistries, such as ene-thiol additions and Michael additions, were used to give specific functionality towards these polyether systems.

Aging studies of the coordination catalyst revealed insight into the pathway in which monomer units are added. SEC data indirectly suggested that aging the initiating species activated most of the zinc sites for propagation yielding a faster rate of exchange of alcohols on the zinc compared to the rate of propagation, thus narrowing the molecular weight distribution.

3.6 Acknowledgements

The authors are grateful for the financial support from NSF under contract DMR-0805179.

3.7 References

1. Harris, L. Goff, J.; Carmichael, A.; Riffle, J.; Harburn, J.; St. Pierre, T.; Saunders, M., Magnetite nanoparticle Dispersions Stabilized with Triblock Copolymers. *Chemistry of Materials* **2003,** 15, 1367-1377.

2. Holmberg, K.; Malmsten, M.; Brink, C., Grafting with hydrophilic polymer chains to prepare protein-resistant surfaces. *Colloids Surfaces A: Physicochem. Eng. Aspects* **1997,** 123-124, 3168-3174.

3. Kingshott, P.; Bagge-Ravn, D.; Gadegaard, N.; Gram, L., Covalent Attachment of Poly(ethylene glycol) to Surfaces, Critical for Reducing Bacterial Adhesion. *Langmuir* **2003,** 19, 6912-6921.

4. Li, C.; Yang, D.; Milas, L.; Hunter, N.; Kim, E.; Wallace, S., Synthesis and evaluation of water soluble polyethylene glycol-paclitaxel conjugate prodrug. *Anticancer Drugs* **1996,** 7, 642-650.

5. Mai-ngam, K., Comblike poly(ethylene oxide)/hydrophobic C6 branched chitosan surfactant polymers as anti-infection surface modifying agents. *Colloids and Surfaces B: Biointerfaces* **2006,** 49, 117-125.

6. Allen, T.; Hansen, C.; Kao, G.; Zalipsky, S., A new strategy for attachment of antibodies to sterically stabilized liposomes resulting in efficient targeting to cancer cells. *Biochimica et Biophysica Acta* **1995,** 1237, 99-108.

7. Bailey, F.; Eds, Alkylene Oxides and Their Polymers. *Marcel Dekker: New York* **1991**.

8. Chen, H.; Sheardown, H.; Brook, M., Immobilization of heparin on a silicone surface through a heterobifunctional PEG spacer. *Biomaterials* **2005,** 26, 7418-7424.

9. Choi, S.; Park, T., PEGylations of G-CSF using cleavable oligo-lactic acid linkage. *Journal of Controlled Release* **2003,** 89, 271-284.

10. Diamente, P.; Veggel, F., Bioconjugation of Ln3+-Doped LaF3 Nanoparticles to Avidin. *Langmuir* **2006,** 22, 1782-1788.

11. Duncan, R.; Satchi-Fainaro, R., Polymer Therapeutics: Polymers as Drugs, Drug and Protein Conjugates and Gene Delivery Systems: Past, Present and Future Opportunities. *Advanced Polymer Science* **2006,** 192, 1-8.

12. Griffith, L., Polymeric Biomaterials. *Acra Materialia* **2000,** 48, 263-277.

13. Huang, Y.; Chen, G.; Chin, J., *Journal of Polymer Science* **2002,** 20.

14. Robertson, N.; Dallinger, G.; Lobkovsky, E.; Lee, S.; Coates, G., Two-dimensional double metal cyanide commplexes: highly active catalysts for the homopolymerization of propylene oxide and copolymerization of propylene oxide and carbon dioxide. *Dalton Trans.* **2006**, 5390-5395.

15. Thompson, M.; Vadala, T.; Vadala, M.; Lin, Y.; Riffle, J., Synthesis and applications of heterobifunctinal poly(ethylene oxide) oligomers. *Polymer* **2008,** 49, 345-373.

16. Woodle, M., Controlling liposome blood clearance by surface-grafted polymers. *Advanced Drug Delivery Reviews* **1998,** 32, 139-152.

17. Vadala, M.; Thompson, M.; Ashworth, M.; Lin, Y.; Vadala, T.; Ragheb, R.; Riffle, J., *Biomacromolecules* **2008,** 9, 1035-1043.

18. Kabanov, A.; Bronich, T.; Kabanov, V.; Yu, K.; Eisenberg, A., *Advances in Genetics* **2005,** 53, 231-261.

19. Huffstetler, P. Miles, W.; Goff, J.; Reinholz, C.; Carroll, M.; Woodward, R.; St. Pierre, T.; Davis, R.; Riffle, J. S., *Polymer Preprints* **2008,** 49, (2), 1103-1104.

20. Safavy, A.; Khazaeli, M.; Buchsbaum, D.; Bonner, J., Paclitaxel Derivatives for Targeted Therapy of Cancer: Toward the Development of Smart Taxanes. *Journal of Medical Chemistry* **1999,** 42, 4919-4924.

21. Huang, Y.; Wang, Y., *Journal of Polymer Science: Part A: Polymer Chemistry* **2002,** 40.

22. Kim, I.; Ha, C., Ring-Opening Polymerizations of Propylene Oxide by Double Metal Cyanide Catalysts Prepared with ZnX2 (X = F, Cl, Br, or I). *Journal of Polymer Science: Part A: Polymer Chemistry* **2005,** 43, 4393-4404.

23. Sarbu, T.; Beckman, E., *Nature* **2000**, 405, 165-168.

24. Rexin, O., Anionic Ring-Opening Polymerization of Propylene Oxide in the Presence of Phosphonium Catalysts. *Journal of Polymer Sciencce: Part A: Polymer Chemistry* **2002,** 40, 864-873.

25. Yin, X., *Coord. Chem. Rev.* **1999,** 181, 27-59.

26. Kim, I.; Ha, C.; Yang, C.; Park, I., Polymerization of propylene oxide by using double metal cyanide catalysts and the application to polyurethane elastomer. *Polymer* **2003,** 44, 3417-3428.

27. Kuyper, J.; Pogany, G. (Shell Oil Co.), *U.S. Pat., 4826953, 4826952, 4826887* **1989**.

28. Leitner, W., *Coord. Chem. Rev.* **1996,** 153, 257-284.

29. Milgrom, J., (General Tire & Rubber) *U.S. Pat., 3404109* **1968**.

30. Chen, S.; Fang, Z.; Qi, G., *Polymer* **2004,** 45, 6519-6524.

31. Caplan, N.; Hayes, D.; Blackburn, G., *The Royal Society of Chemistry* **2000,** 1, 421-437.

32. Huheey, J.; Keiter, R., *Inorganic Chemistry: Principles of Structure and Reactivity*. 4th ed.; HarperCollins College Publishers: New York, NY, 1993.

Chapter 4: Novel Phosphonate-functional Poly(ethylene oxide)-Magnetite Nanoparticles form Stable Colloidal Dispersions in Phosphate Buffered Saline

P. P. Huffstetler,[1,2] J. D. Goff,[1,2] W. C. Miles,[1,3] N. Pothayee,[1,2] C. M. Reinholz,[1,2] S. Ball,[1] R. M. Davis[1,3] and J. S. Riffle[1,2]

[1]Macromolecules and Interfaces Institute, [2]Department of Chemistry, and [3]Department of Chemical Engineering, Virginia Tech, Blacksburg, Virginia 24061, USA

4.1 Abstract

Many studies have concerned the colloidal stability of magnetite nanoparticles coated with poly(ethylene oxide) (PEO), but their long-term stability when such complexes are exposed to physiological media is still not well understood. This paper describes effects of different functional anchor groups, including one carboxylate, one ammonium, one phosphonate zwitterion, and three phosphonate zwitterions, on the structural stabilities of PEO-magnetite nanoparticle complexes in water and phosphate buffered saline (PBS). While PEO oligomers bound to the magnetite through any of these functional groups remain stably bound in water, only the complexes with polymers bound through the zwitterionic phosphonates were stable in PBS. The stabilities of the PEO-magnetite complexes with these phosphonate zwitterions in PBS allowed for investigating colloidal properties of their dispersions as functions of the number of phosphonates per chain and the chain densities and molecular weights. In contrast to all of the other complexes studied, PEO-magnetite nanoparticles bound through three phosphonate zwitterions on one end of the PEO exhibited no significant change in size for over 24 hours even when they

were dispersed in PBS. The colloidal properties of all of these dispersions are discussed in light of their compositions and structures.

4.2 Introduction

Magnetite nanoparticles coated with biocompatible macromolecules have been of great interest due to a wide range of potential biomedical applications including drug delivery, treatment of detached retinas, cell separations and contrast enhancement agents for MRI.[1-6] PEO has been one of the most widely used coatings for magnetite nanoparticles due to its low cytotoxicity, ability to mask foreign substrates from the immune system, and FDA approval for *in vivo* applications.[1, 7, 8] Despite the prevalence of PEO as a coating for magnetite, there is a need to improve upon the binding efficacy of the polymer to the magnetite surface so that the materials will remain intact in physiological media.[9-11]

Functional anchor groups on polymers can aid in their adsorption to the surface of magnetite. Polymeric magnetite dispersion stabilizers containing carboxylate and alkylammonium anchor groups have been previously reported.[8, 11-17] Over the past few decades, significant effort has been devoted to the surface modification of magnetite with PEO-containing polymers to improve their biocompatibility, resist protein adsorption and increase their circulation time within the body.[1, 7, 18, 19] Previous work by others has shown the capacity to coat magnetite nanoparticles with polymers containing pendant carboxylate groups, as well as with carboxylate, alkylammonium, or methoxysilane termini.[8, 20-27] Investigations of the colloidal stabilities of magnetite and maghemite nanoparticles having organic coatings have been conducted in water and in saline (e.g., sodium chloride).[12-16, 20]

Stabilities of these complexes in water and saline were adequate, but the issue of their stabilities in media simulating physiological conditions that contain phosphate salts has not been adequately addressed.

This paper describes the synthesis of PEO oligomers containing functional anchor groups at one end (one carboxylate, one ammonium, one phosphonate zwitterion, three phosphonate zwitterions) and their adsorption onto magnetite nanoparticles. Relationships between the chemical nature of the anchor group(s) and the capacity to remain firmly bound to the magnetite, as well as the colloidal dispersion stabilities of the PEO-magnetite complexes, were studied in water and in PBS. Additionally, the influence of PEO molecular weight on colloidal properties of the PEO-magnetite complexes with similar polymer loadings has been investigated.

4.3 Experimental

4.3.1 Materials

Azobisisobutyronitrile (AIBN), benzyl alcohol (>98%), diethyl ether, diethyl vinyl phosphonate (97%), ethylene oxide (EO, 99.5+%), hexanes (HPLC grade), iron (III) acetylacetonate ($Fe(acac)_3$), mercaptoacetic acid (97+%), oleic acid (90%, technical grade), sodium iodide (99%), triethylamine (TEA, 99.5%), and 1.0 M vinylmagnesium bromide in THF were purchased from Aldrich and used as received. Tetrahydrofuran (THF, Optima Grade, EMD Science, 99.5%) was refluxed over sodium metal with benzophenone until the solution reached a deep purple, fractionally distilled, and deoxygenated just prior to use. Glacial acetic acid (EMD Science) was diluted with THF yielding a 2.0 M acetic acid solution. Naphthalene (Aldrich) was sublimed prior to use. Bromotrimethylsilane (TMS-Bromide, 97%) and mecaptoethylamine hydrochloride were purchased from Alfa Aesar

and used as received. Ethanol (Decon Laboratories Inc.) was used as received. Methanol (HPLC grade), chloroform (HPLC grade), *N,N*-dimethylformamide (DMF, Optima Grade), dichloromethane (HPLC grade), sodium bicarbonate, ammonium chloride, sodium chloride, and acetone (HPLC grade) were purchased from Fisher Scientific and used as received. 3-Chloropropyldimethylchlorosilane and 3-chloropropyltrichlorosilane were purchased from Gelest and used as received. Dialysis tubing (25,000 g mol^{-1} MWCO and 1,000 g mol^{-1} MWCO) was obtained from Spectra/Por. Phosphate buffered saline 10X (PBS) was obtained from Lonza and diluted to appropriate concentrations.

4.3.2 Synthesis of 3-hydroxypropyldimethylvinylsilane (3-HPMVS) and 3-hydroxypropyltrivinylsilane (3-HPTVS)

3-HPMVS and 3-HPTVS were prepared utilizing a modified procedure originally developed by Vadala et al.[11, 17] The procedure described herein that was utilized to prepare 3-HPMVS can be applied to the synthesis of 3-HPTVS with appropriate substitution of the trivinylsilane as the starting reagent. 3-Chloropropyldimethylchlorosilane (10.0 g, 0.06 mol) was syringed into a clean, flame-dried, two-neck, round-bottom flask equipped with a stir bar under a N_2 purge. The reaction flask was placed in an ice bath and cooled to 0 ^{o}C. A 1.0 M solution of vinylmagnesium bromide (64.0 mL, 0.064 mol) in THF was slowly added to the flask over 30 min. The flask was allowed to warm to room temperature, and the mixture was stirred for 24 h. The reaction mixture was diluted with dichloromethane (100 mL), transferred to a separatory funnel and washed with a saturated aqueous ammonium chloride solution (150 mL), then the organic layer was further washed with aqueous sodium chloride (3 X 150 mL). Magnesium sulfate was added to the organic layer to remove any residual water, followed by vacuum filtration. Dichloromethane was

removed under vacuum and the product was distilled at 100 ^{o}C, 0.8 Torr, yielding 3-chloropropyldimethylvinylsilane (8.91 g, 0.55 mol, 94% yield) (3-CPMVS). ^{1}H NMR was used to confirm the quantitative addition of vinyl groups.

3-CPMVS (8.91 g, 0.55 mol) was placed in a 250-mL round-bottom flask equipped with a stir bar and condenser. In a separate round-bottom flask, sodium iodide (16.4 g, 0.11 mol) was dissolved in acetone (60 mL) and the solution was syringed into the flask. The mixture was heated at 56 ^{o}C for 24 h. Acetone was removed under vacuum and the product was dissolved in dichloromethane (100 mL) and vacuum filtered to remove the salt by-products. Dichloromethane was removed under vacuum and the product was distilled at 100 ^{o}C, 0.8 Torr, yielding 3-iodopropyldimethylvinylsilane (3-IPMVS, 13.4 g, 0.05 mol). ^{1}H NMR confirmed the expected structure.

3-IPMVS (13.4 g, 0.05 mol) was placed in a 250-mL round-bottom flask equipped with a stir bar and condenser. DMF (20 mL) was added to the reaction flask followed by sodium bicarbonate (8.8 g, 0.10 mol) and DI water (5 mL). The mixture was heated to 100 ^{o}C for 24 h and conversion of the alkyl iodide to an alcohol was monitored via ^{1}H NMR. The reaction mixture was transferred to a separatory funnel and washed 3X with DI water to remove the excess sodium bicarbonate and DMF. The product was fractionally distilled at 90 ^{o}C, 0.8 Torr, yielding 3-hydroxypropyldimethylvinylsilane (3-HPMVS, 7.4 g, 0.048 mol, 95% yield). ^{1}H NMR confirmed the expected chemical structure.

4.3.3 Synthesis of dimethylvinylsilyl-functional PEO-OH (dimethylvinylsilyl-PEO-OH)

A representative procedure for synthesizing a dimethylvinylsilyl-PEO-OH is provided. An 8,300 g mol^{-1} M_n PEO oligomer was initiated with 3-HPMVS. A 300-mL, high-pressure Series 4561 Parr reactor was utilized for the polymerizations. EO (10.0 g,

0.23 mol) was distilled from a lecture bottle into the pressure reactor cooled with an isopropanol-dry ice bath. THF (5 mL) was added to the reactor via syringe. A potassium naphthalide solution was prepared by charging naphthalene (14.1 g, 0.11 mol) into a 250-mL, flame-dried, round-bottom flask equipped with a glass stir bar. Dry THF (100 mL) was syringed into the flask to dissolve the naphthalene. Potassium metal (3.96 g, 0.10 mol) was added to the solution followed by a N_2 purge for 30 min. The solution was stirred overnight and titrated with 1 N HCl to determine the molarity of the potassium naphthalide solution, which was shown to be 0.95 M. An initiator solution consisting of 3-HPMVS (0.19 g, 1.29 mmol), THF (5 mL) and potassium naphthalide (1.26 mL of a 0.95 M solution in THF, 1.20 mmol) was prepared in a separate flame-dried, 100-mL, round-bottom flask. The initiator solution was added to the stirring reaction mixture via syringe. The cooling bath was removed, and the reaction mixture was allowed to reach room temperature and maintained for 24 h. The polymerization was terminated by adding acetic acid (0.66 mL of a 2.5 M solution in THF, 1.65 mmol) to the pressure reactor via syringe. The pressure reactor was purged with N_2 for 1 h, then opened and its contents were transferred to a 250-mL round-bottom flask. The solvent was removed under vacuum at room temperature, and the product was dissolved in 200 mL of dichloromethane. The product was washed twice with DI water (2 X 100 mL). The solution was concentrated under vacuum at room temperature and precipitated in cold diethyl ether.

4.3.4 Synthesis of trivinylsilyl-functional PEO-OH (trivinylsilyl-PEO-OH)

An exemplary procedure for synthesizing a trivinylsilyl-PEO-OH oligomer is provided. A 9,100 g mol^{-1} M_n PEO oligomer was initiated with 3-HPTVS in a 300-mL, high-pressure Series 4561 Parr reactor. EO (10.0 g, 0.23 mol) was distilled from a lecture

bottle into the pressure reactor cooled with an isopropanol-dry ice bath (-30 ^{o}C), followed by addition of THF (5 mL) via syringe. A potassium naphthalide solution was prepared by charging naphthalene (14.1 g, 0.11 mol) into a 250-mL, flame-dried, round-bottom flask equipped with a glass stir bar. Distilled THF (100 mL) was syringed into the flask to dissolve the naphthalene. Potassium metal (3.96 g, 0.10 mol) was added to the solution followed by a N_2 purge for 30 min. The solution was stirred overnight and titrated with 1 N HCl to determine the molarity of the potassium naphthalide solution, which was shown to be 0.97 M. An initiator solution consisting of 3-HPTVS (0.19 g, 1.12 mmol), THF (5 mL) and potassium naphthalide (1.03 mL of a 0.97 M solution in THF, 1.0 mmol) was prepared in a separate flame-dried, 100-mL, round-bottom flask. The initiator solution was added to the stirring pressure reactor mixture via syringe. The dry-ice/isopropanol bath was removed, and the reaction mixture was allowed to reach room temperature and maintained for 24 h. The polymerization was terminated by adding acetic acid (0.66 mL of a 2.5 M solution in THF, 1.65 mmol) to the pressure reactor via syringe. The pressure reactor was purged with N_2 for 1 h, then opened and its contents were transferred to a 250-mL round-bottom flask. The solvent was removed under vacuum at room temperature, and the product was dissolved in 200 mL of dichloromethane and washed twice with DI water (2 X 100 mL). The solution was concentrated under vacuum at room temperature and precipitated in cold diethyl ether.

4.3.5 Functionalization of dimethylvinylsilyl-PEO-OH with carboxylic acid groups

An exemplary procedure for adding a carboxylic acid group via ene-thiol free radical chemistry across the vinylsilyl endgroup is provided for an 8,300 g mol^{-1} dimethylvinylsilyl-PEO-OH. Dimethylvinylsilyl-PEO-OH (1.0 g, 0.12 mmol) was

charged to a 100-mL round-bottom flask equipped with a stir bar and dissolved in 2 mL of deoxygenated toluene. Mercaptoacetic acid (37.0 mg, 0.36 mmol) was syringed into the reaction flask followed by the addition of AIBN (9.2 mg, 0.06 mmol) dissolved in 0.5 mL of toluene. The mixture was deoxygenated for 10 min by sparging with N_2, then reacted at 80 ^{o}C for 24 h. The reaction mixture was dissolved in 200 mL of dichloromethane, then transferred to a separatory funnel and washed with DI water 3X to remove the excess mercaptoacetic acid. The dichloromethane was removed via rotary evaporation and the resulting polymer was precipitated into cold diethyl ether. The polymer was dried at room temperature under vacuum for 24 h yielding 0.94 g of carboxylic acid-functionalized PEO.

4.3.6 Functionalization of dimethylvinylsilyl-PEO-OH or trivinylsilyl-PEO-OH with ammonium group(s)

Heterobifunctional polyethers with a terminal ammonium group (ammonium-PEO-OH) were obtained via ene-thiol addition of mercaptoethylamine hydrochloride across the vinylsilane. In a characteristic procedure, an 8,300 g mol^{-1} dimethylvinylsilyl-PEO-OH (2 g, 0.24 mmol), mercaptoethylamine hydrochloride (45.2 mg, 0.4 mmol), and AIBN (20 mg, 0.12 mmol) were dissolved in deoxygenated DMF (5 mL) in a 100-mL round-bottom flask equipped with a stir bar. The reaction was conducted at 70 °C for 24 h with stirring, then the reaction mixture was cooled to room temperature. DI water (100 mL) was added to the flask, and the mixture was transferred to a separatory funnel. Dichloromethane (200 mL) was added to the separatory funnel to extract the alkylammonium-functionalized polyether from the water layer. The dichloromethane layer was washed with a 1 N solution of sodium bicarbonate (3X), followed by 3 washes with DI water. The dichloromethane solution was concentrated under vacuum, and the ammonium-PEO-OH

oligomer was precipitated into cold diethyl ether and dried at 25 °C under vacuum for 12 h yielding 1.9 g of product (95% yield).

A PEO oligomer with three ammonium groups on one end (ammonium$_3$-PEO-OH) was prepared by a similar procedure using trivinylsilyl-PEO-OH as the starting substrate, and the same molar ratios of reagents to equivalents of vinyl groups as described above.

4.3.7 Michael addition of ammonium-PEO-OH or ammonium$_3$-PEO-OH onto diethyl vinyl phosphonate

A characteristic procedure for adding a phosphonate group to an 8,300 g mol^{-} ammonium-PEO-OH is provided. An ammonium-PEO-OH oligomer (1.0 g, 0.12 mmol) was charged to a clean, flame-dried, 100-mL, round-bottom flask equipped with a stir bar, and dissolved in ethanol (9 mL). TEA (0.20 mL, 0.14 mmol) was added to the reaction, followed by diethyl vinyl phosphonate (0.26 mL, 0.14 mmol). The reaction was carried out at 70 ^{o}C for 24 h. The reaction mixture was diluted with DI water to obtain a 75:25 water:ethanol composition and placed in a 1,000 g mol^{-1} MWCO cellulose acetate dialysis bag and dialyzed against 4 L of DI water for 24 h to remove excess diethyl vinyl phosphonate. The contents of the dialysis bag were transferred to a 100-mL round-bottom flask and lyophilized, yielding 0.91 g of diethyl phosphonate-functionalized PEO.

A PEO oligomer with three phosphonate groups on one end (phosphonate$_3$-PEO-OH) was prepared by a similar procedure using ammonium$_3$-PEO-OH as the starting substrate, and the same molar ratios of reagents to equivalents of ammonium groups as described above.

4.3.8 Hydrolysis of diethylphosphonate-PEO-OH (or diethylphosphonate$_3$-PEO-OH) yielding phosphonic acid-PEO-OH (or phosphonic acid$_3$-PEO-OH)

Phosphonic acid-PEO-OH was prepared from diethyl phosphonate-PEO-OH using a hydrolysis procedure adapted from Caplan et al.[28] In a representative procedure, an 8,300 g mol^{-1} diethyl phosphonate-PEO-OH (0.80 g, 0.10 mmol) was charged to a clean, 100-mL round-bottom flask equipped with a stir bar and dissolved in 5 mL of dichloromethane. Trimethylsilyl bromide (0.032 mL, 0.24 mmol) was syringed into the reaction flask and stirred at room temperature for 24 h. Methanol (0.01 mL, 0.24 mmol) was added and stirred for 2 h to cleave the trimethylsilyl groups. Dichloromethane (50 mL) was added, and the mixture was washed 3X with DI water (100 mL each) in a separatory funnel. The dichloromethane layer was concentrated, then the oligomer was precipitated by pouring the mixture into cold diethyl ether. The polymer was vacuum-dried at 25 ^{o}C for 24 h yielding 0.77 g of phosphonic acid-PEO-OH.

A PEO oligomer with three phosphonate groups on one end (phosphonate$_3$-PEO-OH) was prepared by a similar procedure using diethylphosphonate$_3$-PEO-OH as the starting substrate, and the same molar ratios of reagents to equivalents of phosphonate groups as described above.

4.3.9 Magnetite synthesis via reduction of Fe(acac)$_3$

Magnetite nanoparticles were synthesized using a reduction method adapted from Pinna et al.[29] Fe (III) acetylacetonate (2.14 g, 8.4 mmol) and benzyl alcohol (45 mL, 0.43 mol) were charged to a 250-mL, three-neck, round-bottom flask equipped with a water condenser and placed in a Belmont metal bath with an overhead stirrer with both thermostatic (+/- 1 ^{o}C) and revolution per minute control. The solution was sparged with

N_2 for 1 h. While stirring under N_2, the solution was heated at 100 °C for 4 h, then the temperature was increased to 205 °C at a rate of ~25 °C h^{-1}. Following 24 h at 205 ˚C, the reaction was cooled to room temperature, then the magnetite particles were collected with a magnet and the benzyl alcohol was decanted. The magnetite nanoparticles were washed 3X with acetone (100 mL each), then were dispersed in chloroform (20 mL) containing oleic acid (0.3 g). The solvent was removed under vacuum at room temperature, and the oleic acid-stabilized magnetite nanoparticles were washed 3X with acetone (100 mL each). The particles were dried under vacuum for 24 h at 25 ˚C. The composition of the particles obtained from thermogravimetric analysis (TGA) was 5% organic residue to 95% magnetite.

4.3.10 Adsorption of functional polyether stabilizers onto magnetite nanoparticles

A representative method for preparing a targeted composition of 70:30 wt:wt polyether:magnetite complex is provided. Oleic acid-stabilized magnetite nanoparticles (50.0 mg) prepared as described above were dispersed in chloroform (10 mL) and charged to a 50-mL round-bottom flask. A functional PEO (117.0 mg) was dissolved in chloroform (10 mL) and added to the dispersion. The pH of each solution and the resulting mixture were approximately neutral. The reaction mixture was sonicated in a VWR 75T sonicator for 16 h under N_2, and then the nanoparticles were precipitated in hexanes (300 mL). A magnet was utilized to collect the magnetite nanoparticles and free oleic acid was decanted with the supernatant. The complexes were dispersed in DI water (20 mL) using sonication for 30-60 s. The complexes were dialyzed against DI water (4 L) for 24 h using 25,000 g mol^{-1} MWCO dialysis bags.

4.3.11 Characterization

^{1}H NMR spectral analyses of compounds were performed using a Varian Unity 400 NMR or a Varian Inova 400 NMR operating at 399.97 MHz.

An Alliance Waters 2690 Separations Module with a Viscotek T60A dual viscosity detector and laser refractometer equipped with a Waters HR 0.5 + HR 2 + HR 3 + HR 4 styragel column set was used for size exclusion chromatography (SEC) analyses. SEC data were collected in chloroform at 30 °C. Data were analyzed utilizing a Universal calibration made with polystyrene standards to obtain absolute molecular weights.

TGA was used to determine the polymer loading for each complex. TGA measurements were carried out on the PEO-magnetite nanoparticles using a TA Instruments TGA Q500 to determine the fraction of each complex that was comprised of polymer. Freeze-dried samples were first held at 110 ºC for 10 min to drive off any excess moisture. The samples (10-15 mg) were then equilibrated at 100 ºC and the temperature was ramped at 10 °C min^{-1} to a maximum of 700 ºC in a nitrogen atmosphere. The mass remaining was recorded throughout the experiment. The mass remaining at 700 °C was taken as the fraction of magnetite in the complexes. The experiments were conducted in triplicate.

DLS measurements were conducted with a Malvern Zetasizer NanoZS particle analyzer (Malvern Instruments Ltd, Malvern, UK) at a wavelength of 633 nm from a 4.0 mW, solid-state He-Ne laser at a scattering angle of 173° and at 25 ± 0.1 ˚C. Intensity, volume and number average diameters were calculated with the Zetasizer Nano 4.2 software utilizing an algorithm, based upon Mie theory, that transforms time-varying intensities to particle diameters.[30] For DLS analysis, the dialyzed complexes dispersed in

DI water were diluted to ~0.05 mg mL^{-1} and filtered through a Whatman Anotop, 100-nm, alumina filter directly into a polystyrene cuvette. This corresponds to a volume fraction of 1.3×10^{-5} to 2.2×10^{-5} depending on the polymer loading on the magnetite. In experiments where PBS was added, 0.1 mL of 10X PBS was mixed with 0.9 mL of the 0.05 mg mL^{-1} complex solution, then the solution was filtered through a 100-nm alumina filter into a clean polystyrene cuvette. Each sample was analyzed immediately following filtration and re-measured every 30 min over 24 h.

A 7T MPMS Squid magnetometer (Quantum Design) was used to determine magnetic properties. Hysteresis loops were generated for the magnetite nanoparticles at 300K and 5K. Fe concentration of the magnetite was determined chemically by acid digestion followed by ICP-AES analysis. These concentrations were in good agreement with TGA values.

4.4 Results and Discussion

One primary issue regarding the structures of polymer-magnetite nanostructures for biomedical applications is the colloidal stability of dispersions of such complexes in physiological media.[9, 10, 21] The aim of this study has been to compare the binding efficacies of PEO oligomers with different functional anchoring groups to magnetite, particularly in the presence of phosphate salts found in physiological media. PEO oligomers with one terminal carboxylate, ammonium or a phosphonate zwitterion, and with three phosphonate zwitterions (all on one end of the PEO) were adsorbed onto magnetite nanoparticles, and the stabilities of the complexes were compared. Knowledge of which binding groups remained stably bound to the magnetite in water and in PBS then allowed us to examine the colloidal properties of the stable nanoparticles in dispersions in

light of the molecular weights and chain densities of the bound oligomers on the magnetite surfaces.

4.4.1 Synthesis of PEO oligomers with different functional endgroups for binding to magnetite

3-HPMVS was used as a versatile initiator for living anionic polymerizations of EO to produce heterobifunctional oligomers that could be post-functionalized with the different chemical groups to adsorb onto the magnetite nanoparticles (Scheme 4.4.1.1).[17, 25]

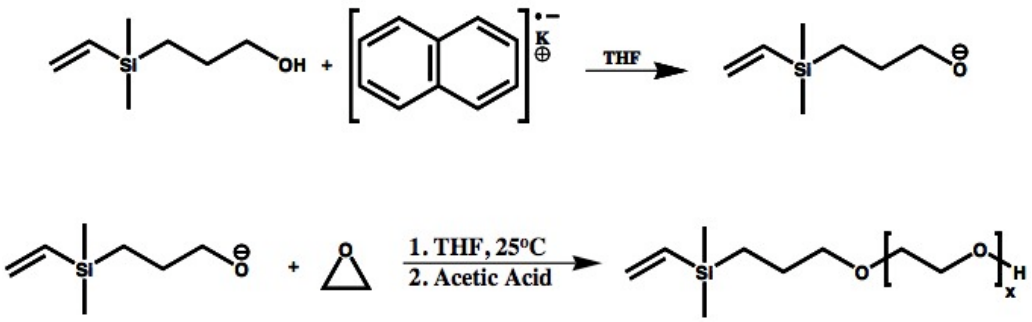

Scheme 4.4.1.1. Synthesis of dimethylvinylsilyl-PEO-OH via living anionic polymerization

This approach allowed for utilizing the same oligomer for comparing dispersion properties with the only difference being the functional anchor groups. A variation of this approach using 3-HPTVS as the initiator was also investigated to prepare phosphonic acid$_3$-PEO-OH oligomers, so that the dispersion properties could be compared with nanoparticles having different surface densities of functional binding groups. Potassium naphthalide was reacted with 3-HPMVS or 3-HPTVS to form an alkoxide for initiating EO, and the number of moles of the alcohol initiator relative to EO controlled the molecular weight. A small deficiency of the naphthalide relative to alcohol ensured that only the alkoxide (and not residual naphthalide) initiated the chains, and the remaining

alcohol chains transferred with the growing PEO chains throughout the reaction. It is noteworthy that these polymerizations were terminated with acetic acid prior to opening the reaction vessel to avoid any unwanted oxidative side reactions.

Dimethylvinylsilyl-PEO-OH oligomers with targeted molecular weights of approximately 3,000 and 8,000 g mol^{-1} were prepared and the materials were characterized using ^{1}H NMR and SEC (Table 4.4.1.1).

Table 4.4.1.1. Molecular weights of dimethylvinylsilyl-PEO-OH and trivinylsilyl-PEO-OH oligomers

Targeted Molecular Weight	M_n (g mol^{-1})		PDI*
	^{1}H NMR	SEC	
Monovinylsilyl-3,000 g mol^{-1}	2,900	3,100	1.09
Monovinylsilyl-8,000 g mol^{-1}	8,300	7,900	1.05
Trivinylsilyl-3,000 g mol^{-1}	3,400	3,400	1.04
Trivinylsilyl-9,000 g mol^{-1}	9,100	9,500	1.09

*PDI = Polydispersity Index

Figure 4.4.1.1 shows a representative NMR spectrum of a dimethylvinylsilyl-PEO-OH oligomer.

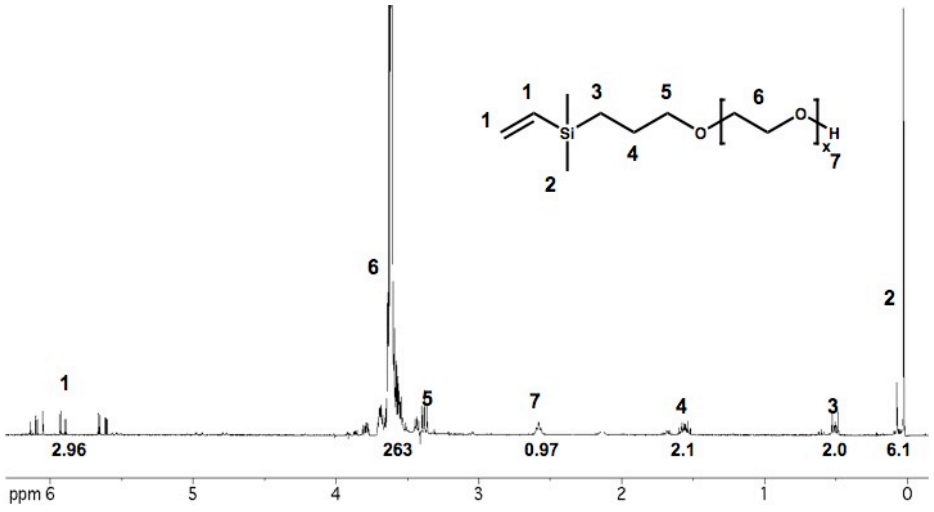

Figure 4.4.1.1. ^{1}H NMR of a 2,900 g mol^{-1} dimethylvinylsilyl-PEO-OH oligomer

Number average molecular weight was determined by comparing the integral ratios of the resonances corresponding to the methylene groups in the initiator (labeled 3 and 4) to the repeat unit of ethylene oxide labeled 6.

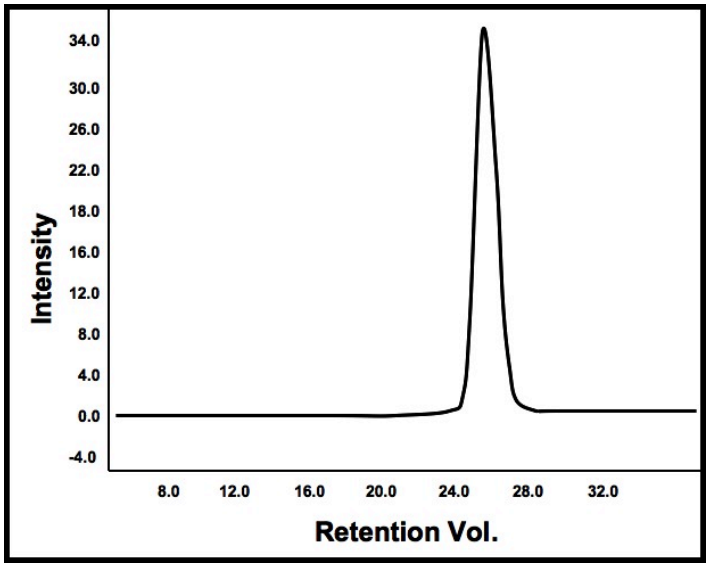

Figure 4.4.1.2. SEC chromatogram of a dimethylvinylsilyl-PEO-OH oligomer showing a M_n of 7,900 g mol^{-1} and a molecular weight distribution of 1.05

SEC of the dimethylvinylsilyl-functional polyethers revealed symmetric monomodal peaks with molecular weight distributions of less than 1.1, which are indicative of living anionic polymerizations (Figure 4.4.1.2). Good molecular weight agreement was found between both methods of analysis.

Ene-thiol additions were utilized to introduce carboxylate and ammonium endgroups onto the polyethers (Scheme 4.4.1.2).

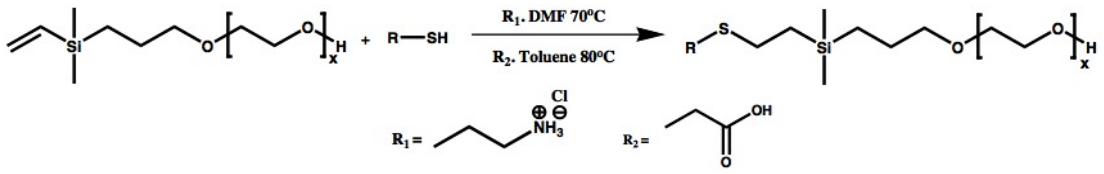

Scheme 4.4.1.2. Ene-thiol additions of 2-mercaptoethylamine hydrochloride (R_1) and mercaptoacetic acid (R_2) to dimethylvinylsilyl-PEO-OH

The vinylsilyl functionality is unusual among vinyl groups in that it does not polymerize readily by free radical reactions, and thus it is seemingly an ideal substrate for ene-thiol functionalization reactions because polymerization does not compete. Nevertheless, excesses of the thiol relative to vinylsilane were utilized for these reactions to ensure quantitative addition.

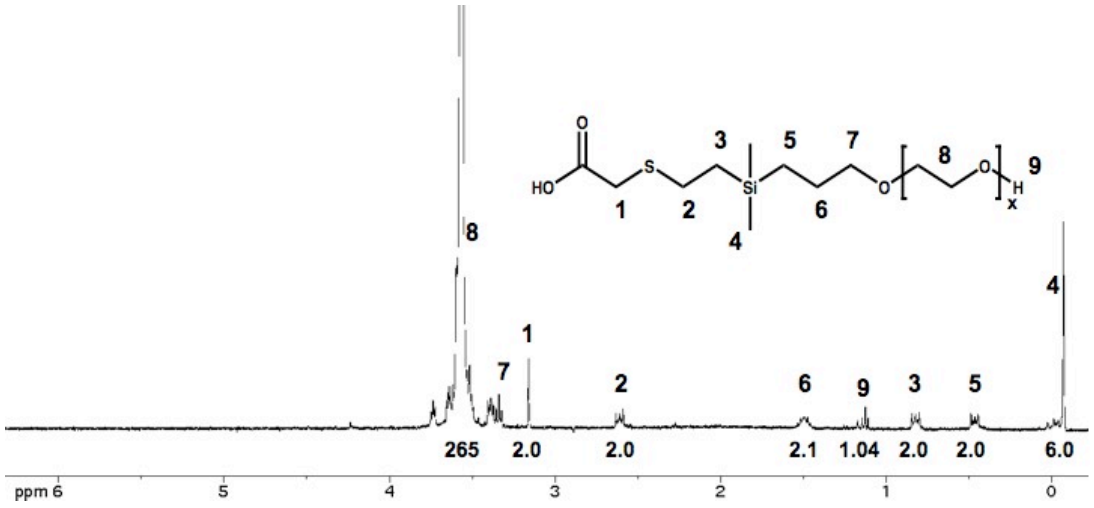

Figure 4.4.1.3. Ene-thiol addition of mercaptoacetic acid to a 2,900 g mol^{-1} polyether yielding a carboxylic acid-functionalized PEO (HOOC-PEO-OH)

Addition of mercaptoacetic acid to dimethylvinylsilyl-PEO-OH was monitored by ^{1}H NMR. Complete disappearance of the vinyl group at ~6 ppm indicated stoichiometric conversion to a carboxylic acid-PEO-OH (Figure 4.4.1.3). Additionally, appearances of the methylene peaks labeled 1-3 in the spectrum indicated addition of mercaptoacetic acid.

Comparison of the resonance integrals corresponding to the methylene peaks of the thiol (1-3) to the methylene peak labeled 5 confirmed quantitative addition across the vinylsilane endgroups.

^{1}H NMR was also utilized to monitor ene-thiol addition of 2-mercaptoethylamine hydrochloride onto the vinylsilane endgroups of dimethylvinylsilyl-PEO-OH and trivinylsilyl-PEO-OH by observing the complete disappearance of the vinyl groups and appearances of methylene peaks labeled 1-4 in the spectra (Figure 4.4.1.4). Comparison of integrations confirmed quantitative functionalization with ammonium groups to form ammonium-PEO-OH or ammonium$_3$-PEO-OH.

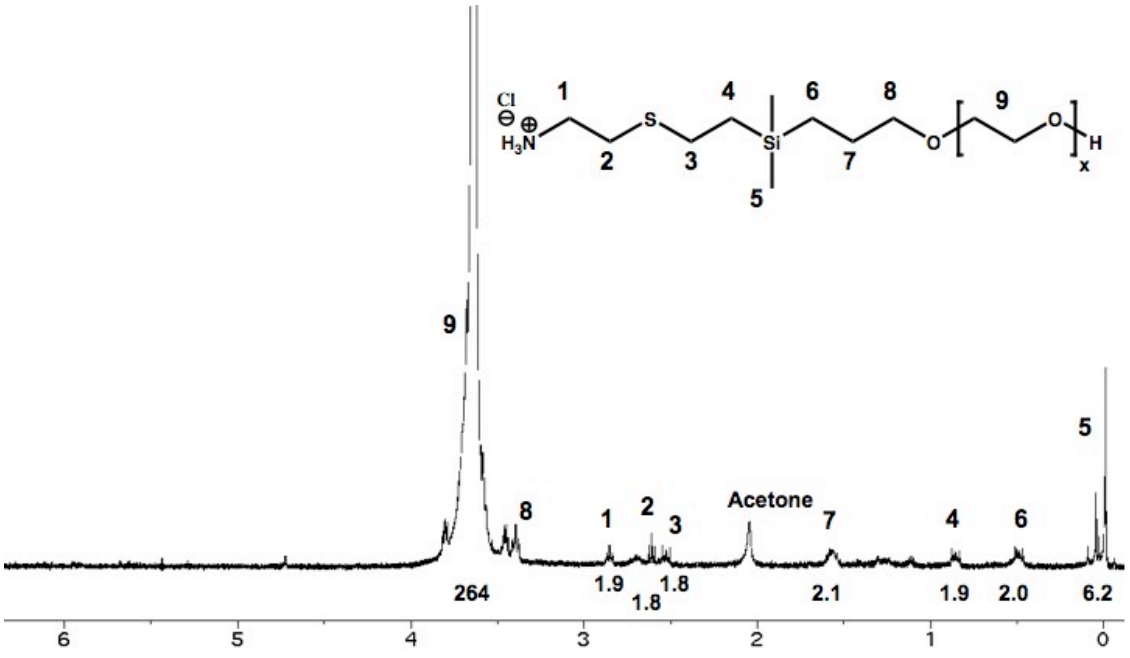

Figure 4.4.1.4. Ene-thiol addition of mercaptoethylamine hydrochloride to a 2,900 g mol^{-1} dimethylvinylsilyl-PEO-OH to produce ammonium-PEO-OH

The ammonium-functional PEO oligomers were used as precursors to form the zwitterionic phosphonate-functional polyethers. The ammonium endgroups were first reacted with triethylamine to afford the corresponding free amines. A slight molar excess

of triethylamine was added to maintain basic reaction conditions, aiding in nucleophilic addition to diethyl vinyl phosphonate. Diethyl vinyl phosphonate was added to the amine group(s) via Michael addition, yielding diethylphosphonate-PEO-OH (Scheme 4.4.1.3) or diethylphosphonate$_3$-PEO-OH utilizing a procedure adapted from the literature.[31]

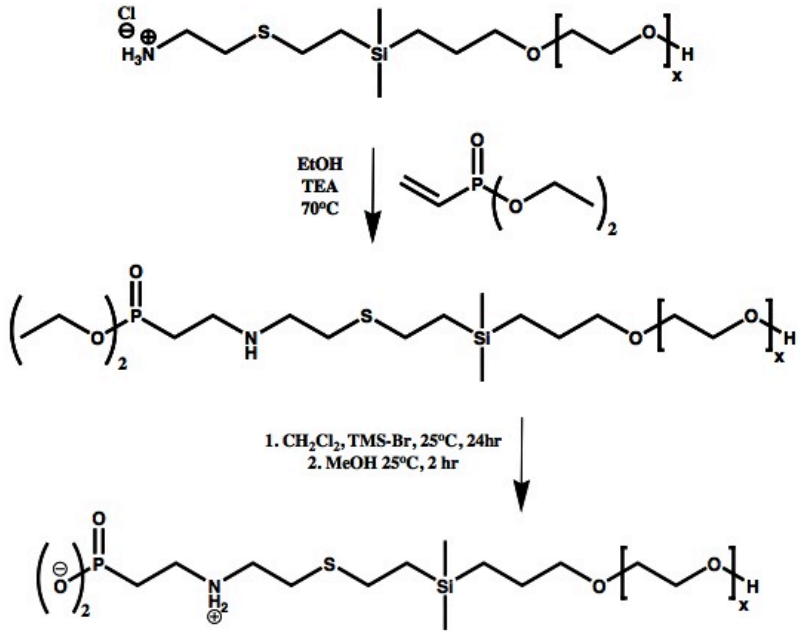

Scheme 4.4.1.3. Michael addition of amine-PEO-OH to diethyl vinyl phosphonate and de-esterification to remove the ethyl groups yielding zwitterionic phosphonate-PEO-OH

Figure 4.4.1.5 shows the ^{1}H NMR of a representative diethylphosphonate-PEO-OH oligomer. Two methylene peaks corresponding to the converted vinyl group of the phosphonate reactant are observed as peaks 3 and 4 in the spectrum of the product. Quantitative addition to diethyl vinyl phosphonate was determined by comparing the integrations of peaks 1-4 to the integration of the methylene peak labeled 10.

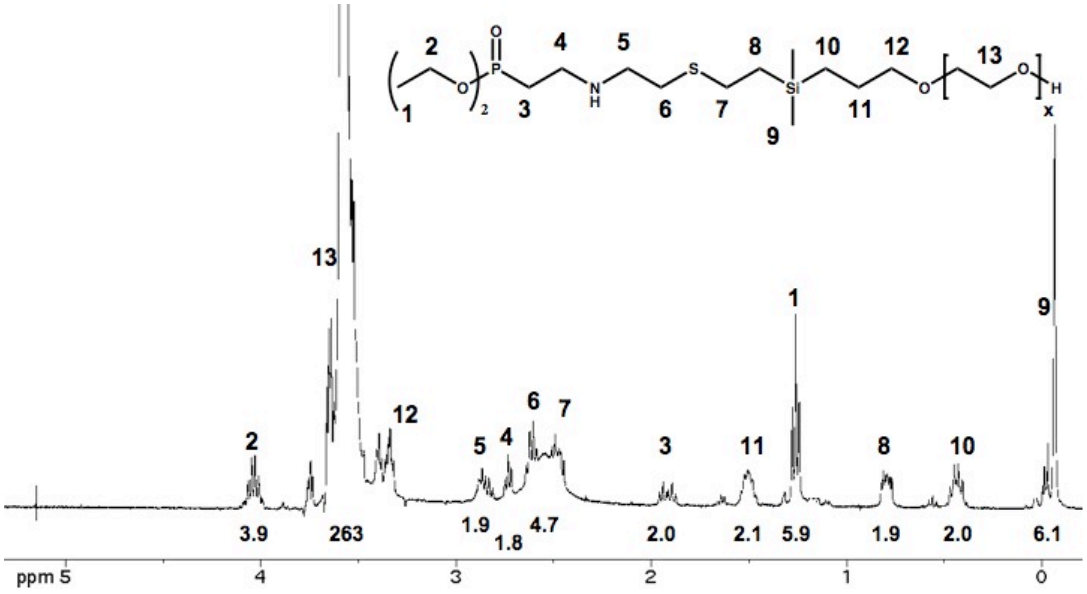

Figure 4.4.1.5. ^{1}H NMR of a 2,900 g mol^{-1} diethylphosphonate-PEO-OH

For binding to magnetite, the ethyl phosphonate groups were cleaved using bromotrimethylsilane (TMS-Br).[28] Reaction with TMS-Br yielded an intermediate bis-trimethylsilyl ester with an alkyl halide by-product. In the methanolysis step of the reaction, the alcohol cleaved the silyl ester, yielding phosphonic acid (Scheme 4.4.1.3). A zwitterionic endgroup was afforded in the phosphonate-PEO-OH product (or in the corresponding phosphonate$_3$-PEO-OH) at a pH less than 10, due to the negative charge of the phosphonate and the protonated secondary amine. ^{1}H NMR spectra confirmed that deprotection of the diethylphosphonate-PEO-OH oligomers was complete (Figure 4.4.1.6). In addition to the disappearance of the ethyl resonances in the spectrum, there was an upfield shift (~1.6 ppm) of the methylene group adjacent to the phosphorus atom.

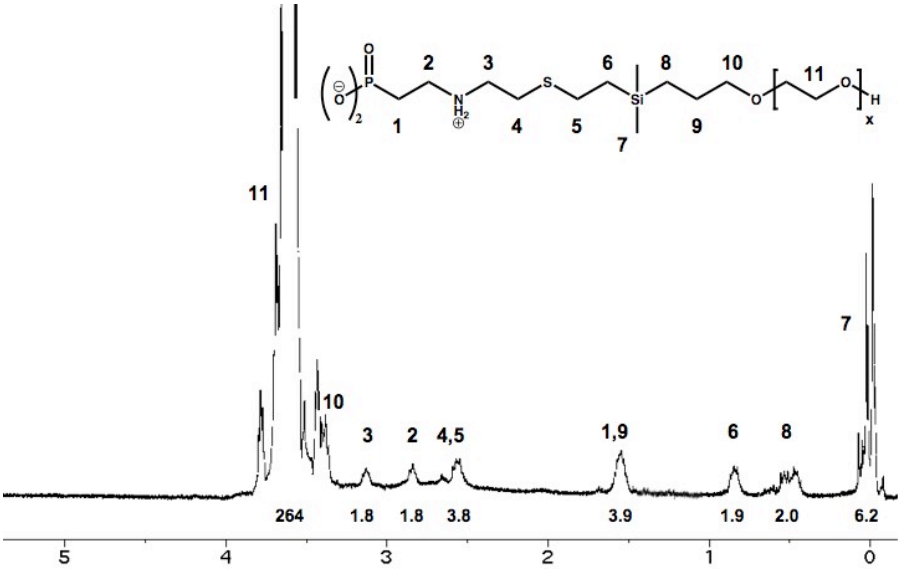

Figure 4.4.1.6. ^{1}H NMR of a 2,900 g mol^{-1} zwitterionic phosphonate-PEO-OH

4.4.2 Formation of PEO-magnetite complexes via adsorption of the functional PEO oligomers onto the surfaces of magnetite nanoparticle

PEO-magnetite complexes with similar polymer loadings were formed with the two sets of different molecular weight PEO oligomers, then the complexes were dialyzed against water to remove any unbound PEO (Figure 4.4.2.1).

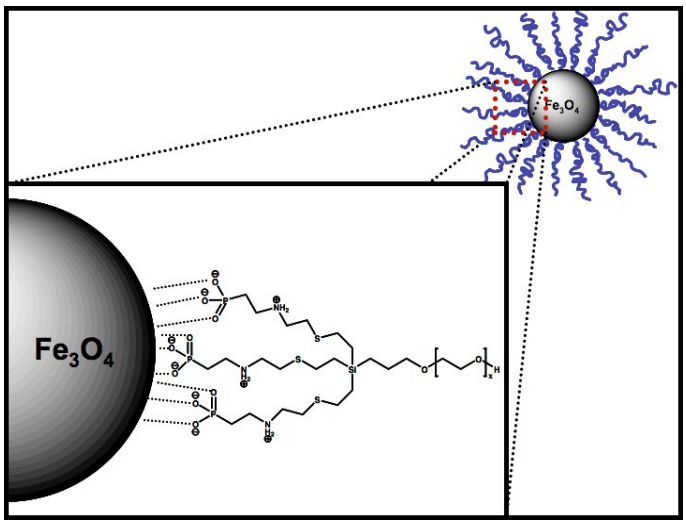

Figure 4.4.2.1. Depiction of a tri-zwitterionic phosphonate-PEO-OH binding to the surface of a magnetite nanoparticle

Table 4.4.2.1 shows the polymer loadings in the complexes determined by TGA after dialysis and the number weighted average diameters in water as measured by dynamic light scattering (DLS).

Table 4.4.2.1. Compositions of the PEO-magnetite nanoparticle complexes

PEO Molecular Weight (g mol^{-1})	Anchor Group(s)	Initial Polymer Loading after Dialysis against H_2O (Wt %)	D_n (nm)	Polymer Loading after Dialysis against PBS (Wt %)
2,900	Mono-Carboxylate	64.7 ± 0.9	19.9	40.7 ± 1.4
8,300	Mono-Carboxylate	68.4 ± 1.6	24.5	45.3 ± 1.4
2,900	Mono-Ammonium	66.8 ± 0.8	26.8	41.0 ± 0.7
8,300	Mono-Ammonium	77.1 ± 0.9	31.7	42.6 ± 0.7
2,900	Mono-Zwitterionic Phosphonate	63.3 ± 0.4	26.2	65.1 ± 1.4
8,300	Mono-Zwitterionic Phosphonate	70.2 ± 0.7	39.6	67.7 ± 0.7
3,400	Tri-Zwitterionic Phosphonate	69.0 ± 0.6	27.6	68.8 ± 0.4
9,100	Tri-Zwitterionic Phosphonate	70.5 ± 0.8	34.2	69.2 ± 0.8

The compositions of the PEO-magnetite complexes were in close agreement with the targeted 30 wt% magnetite:70 wt% polyether composition. The PEO-magnetite complexes with the ammonium and zwitterionic phosphonate anchor groups had approximately the same number weighted average diameters, while the complexes with the carboxylate anchor groups were significantly smaller. The size of the magnetite nanoparticle core was measured via TEM with an average diameter of 8.1 ± 2.9 nm (Figure 4.4.2.2).

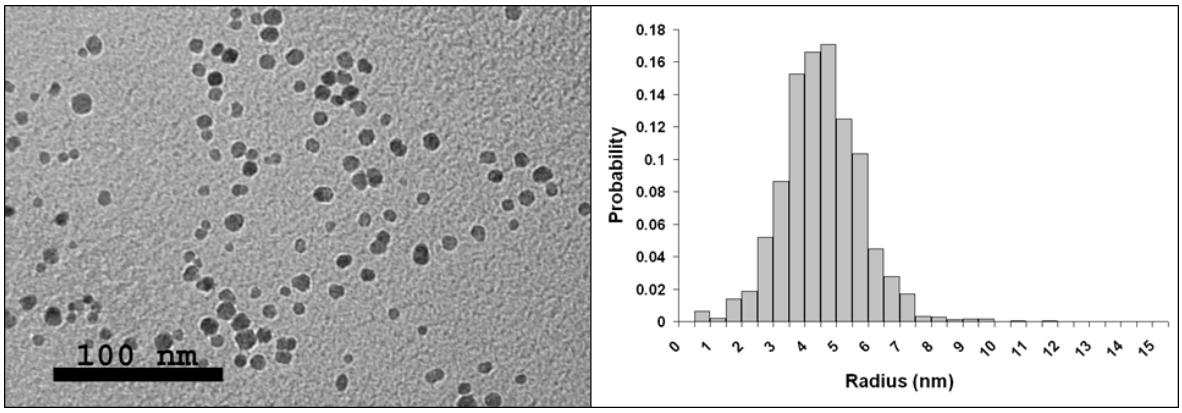

Figure 4.4.2.2. TEM of the magnetite nanoparticles (A) and a histogram of the particle size distribution (B).

The magnetic properties of the magnetite nanoparticles were characterized via superconducting quantum interference device analyses. Hysteresis loops revealed superparamagnetic behavior and a saturation magnetization of 80 emu g^{-1} of magnetite.

4.4.3 Determination of the efficacies of various anchor groups for magnetite nanoparticles in PBS

Binding of the polymers to the magnetite surfaces in PBS were studied to compare the stabilities of these complexes in a medium simulating physiological conditions. Dispersions of the complexes were dialyzed against PBS for 24 hours to measure any polymer desorption that might be caused by displacement by salts in the medium. The complexes were subsequently dialyzed against water for an additional 24 hours to remove any desorbed polymer and salts. TGA was used to determine the polymer loadings of the complexes before and after this process to investigate anchor group efficacies in the presence of phosphate salts in the medium (Table 4.4.2.1). Desorption of the polymer from the magnetite surface in PBS was indicated by a decrease in polymer loading. Large decreases in polymer loadings (~25 wt%) were observed for the complexes bound through carboxylate or ammonium anchor groups. In addition, significant sedimentation of these

complexes was observed during the PBS dialysis step, further substantiating instability in PBS. In contrast, no loss in polymer loading was observed for the complexes containing mono-zwitterionic phosphonate anchor groups or tri-zwitterionic phosphonate anchor groups after PBS dialysis. These complexes also did not exhibit sedimentation in the PBS during the 24 hours. Based on this study, it was reasoned that PEO-magnetite nanoparticles with the zwitterionic phosphonate anchor groups would likely have superior stability in physiological media in comparison to ammonium or carboxylate groups.

4.4.4 Investigation of colloidal stabilities of the PEO-magnetite nanoparticle dispersions in water and PBS using DLS

Colloidal stabilities of the PEO-magnetite complexes against flocculation in DI water and PBS were examined using DLS by measuring the nanoparticle diameters every 30 minutes for 24 hours. Figure 4.4.4.1 shows the diameters of the complexes containing the PEO oligomers with the mono-ammonium anchor group.

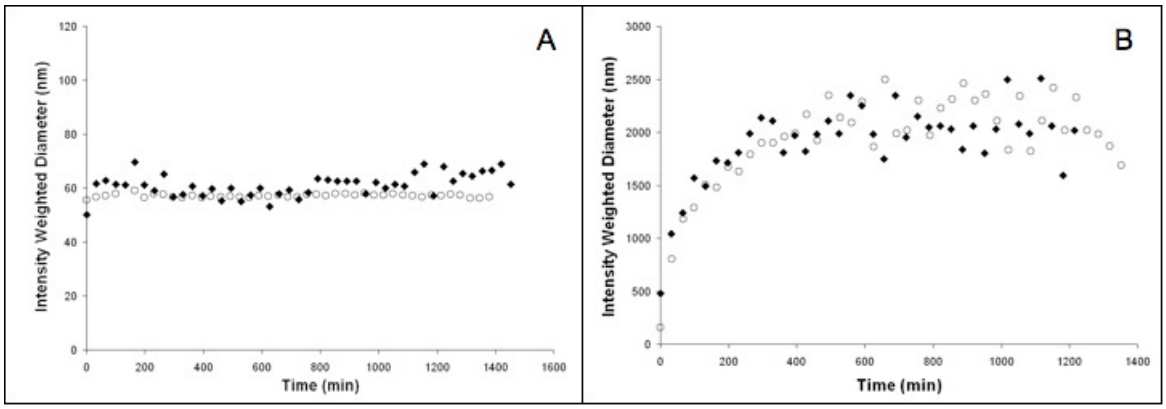

Figure 4.4.4.1. Intensity weighted diameters from DLS of the 2,900 (open circles) and 8,300 g mol^{-1} (black diamonds) ammonium-PEO-magnetite complexes in DI water (A) and PBS (B) over 24 hours

Intensity weighted diameters are reported due to their sensitivity to the presence of aggregates (since they scale with radii to the 6^{th} power), so that any agglomeration with

time is magnified. Consistent with the desorption data, sizes of the ammonium-PEO-magnetite complexes did not change significantly over 24 hours in water, while large increases in the diameters were observed for the complexes in PBS. Moreover, sediment was visually observed for the ammonium-PEO-magnetite complexes in PBS. Based on the calculation for the terminal velocity of a sphere (eq. 4.4.4.1) in solution, a magnetite complex should settle to the bottom of the DLS cuvette (traverse a distance of 1 cm) when an aggregate diameter of ~400-700 nm is reached.[19]

$$U = \frac{2}{9}\frac{r^2 g\left(\rho_{mag} - \rho_{solvent}\right)}{\mu_{solvent}} \qquad (4.4.4.1)$$

Here, U is the terminal velocity of the particle, g is the gravitational constant, r is the particle radius, ρ_{mag} is the density of the magnetite complex (2.28 g cm^{-3}), $\rho_{solvent}$ is the density of the solvent, and $\mu_{solvent}$ is the viscosity of the solvent at 25 ºC. Thus, after ~200 minutes in PBS the ammonium-PEO-magnetite complexes were likely on the verge of sedimentation and the sizes measured by DLS do not represent complexes that were at equilibrium in terms of size.

Magnetic characterization data shows that the magnetite nanoparticles display superparamagnetic behavior. The maximum potential energy of magnetic dipoles aligned with an applied magnetic field can be estimated by equation 4.4.4.2.[32]

$$V_M = \frac{8\pi\mu_o a^3 M^2}{9\left(\frac{h}{a} + 2\right)^3} \qquad (4.4.4.2)$$

Here, a is the particle radius, M is the magnetization, μ_o is the magnetite permeability in vacuum (1.26×10^{-6} Tm/A), and h is the surface-to-surface separation of two

particles.(reference) With the application of the Earth's magnetic field (0.3 – 0.6 Gauss), any dipole-dipole interaction is significantly smaller than the van der Waal's interactions of the actual particle ($V_{vdW}/kT = 0.4$, h = 5 nm) , even at particle sizes of 1000 nm ($V_M/kT = 2 \times 10^{-7}$, h = 5 nm) where the particles are settling out of suspension. Thus, van der Waal's forces would dominate and cause flocculation before any magnetic dipole-dipole interaction would become significant. Figure 4.4.4.2 compares the diameters of the complexes containing the carboxylate anchor groups in DI water (A) and PBS (B and C).

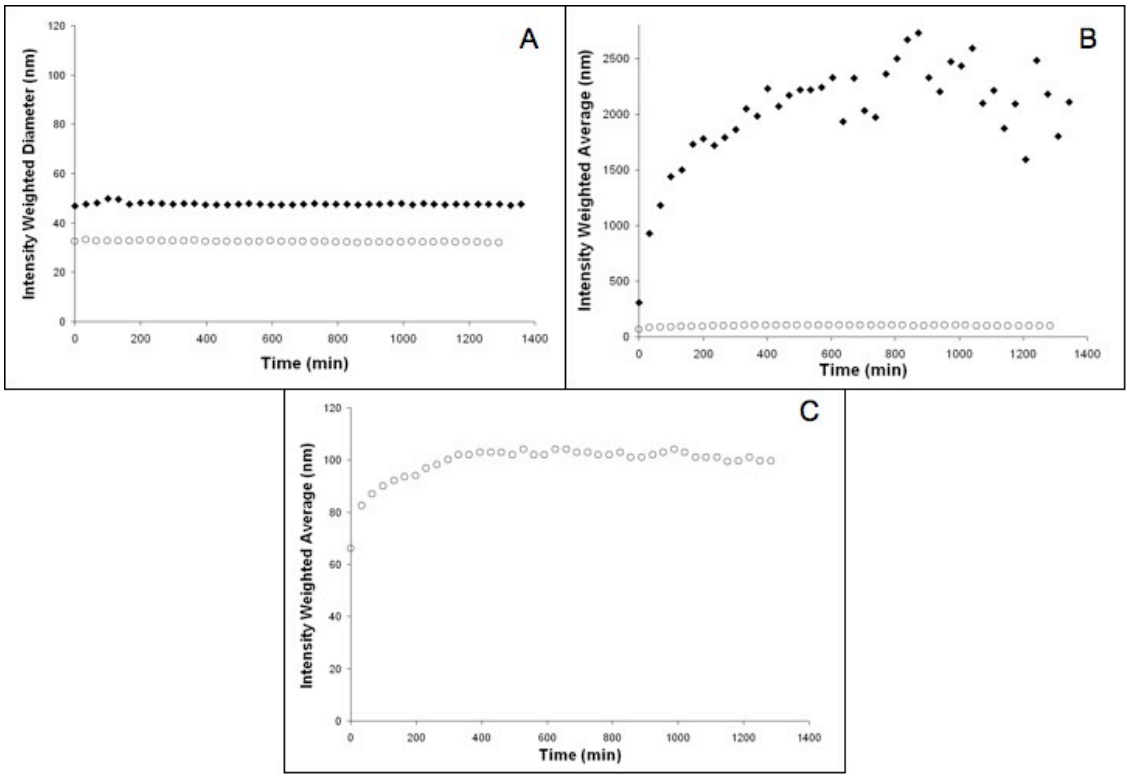

Figure 4.4.4.2. DLS intensity weighted diameters of the 2,900 (open circles) and 8,300 g mol^{-1} (black diamonds) of carboxylate-PEO-magnetite complexes in DI water (A) and PBS (B) over 24 hours. A magnified plot of the 2,900 g mol^{-1} carboxylate-PEO-magnetite complex in PBS is shown in (C).

These complexes did not increase in intensity average diameter in DI water over time. However, flocculation was observed for the 8,300 g mol^{-1} carboxylate-PEO-

magnetite complex in PBS over time, and the complexes with the 2,900 g mol^{-1} PEO aggregated to ~100 nm in intensity weighted diameter with an equilibrium diameter reached after ~5 hours. Thus, even with polymer desorption, the PEO molecular weight affects the behavior of these complexes in PBS. A possible explanation for this difference is the number of polymer chains anchored to the magnetite nanoparticle surfaces in the two cases. Each complex has approximately the same polymer loading (~65 wt %), resulting in more total chains for the 2,900 g mol^{-1} complexes (~3.0 chains nm^{-2}) relative to the 8,300 g mol^{-1} complexes (~1.1 chains nm^{-2}). DLS data presented in Table 4.4.2.1 also shows that the complexes with carboxylate anchor groups have significantly smaller number weighted average diameters than their ammonium counterparts. The smaller diameters of the complexes with the carboxylate anchor groups reflect a higher local density of polymer near the magnetite surface. As reflected in Figure 4.4.4.2, the complexes with carboxylate anchor groups also flocculate less rapidly in PBS relative to the complexes with ammonium anchors. This can be partially attributed to the higher polymer density.

The relative colloidal stability of dispersions of these complexes with ammonium or carboxylate endgroups in DI water versus PBS is consistent with the absence of polymer desorption in water and significant desorption in PBS. Based on previous work, it appears that phosphate salts from the PBS can displace these polymer anchor groups.[9] This reduces steric repulsion and promotes flocculation of the nanoparticles due to pair-pair van der Waal's interactions. Figure 4.4.4.3 illustrates adsorption of phosphate salts on the magnetite surface.

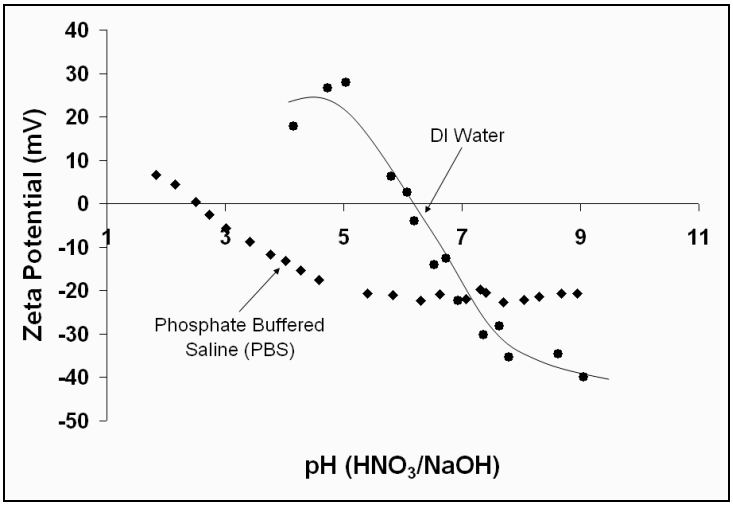

Figure 4.4.4.3. Zeta potentials indicate the charge characteristics of magnetite nanoparticle surfaces in DI water versus PBS.

In PBS, the magnetite nanoparticles cross the line of zero charge at ~pH 2.5, and this closely corresponds to the lowest pK_a of phosphonic acid. This suggests that phosphate salts from the PBS adsorb on the magnetite surfaces. Figure 4.4.4.4 shows intensity-weighted diameters of complexes bound through the mono-zwitterionic phosphonate anchor groups in DI water (A) and PBS (B), where polymer desorption does not occur in either medium.

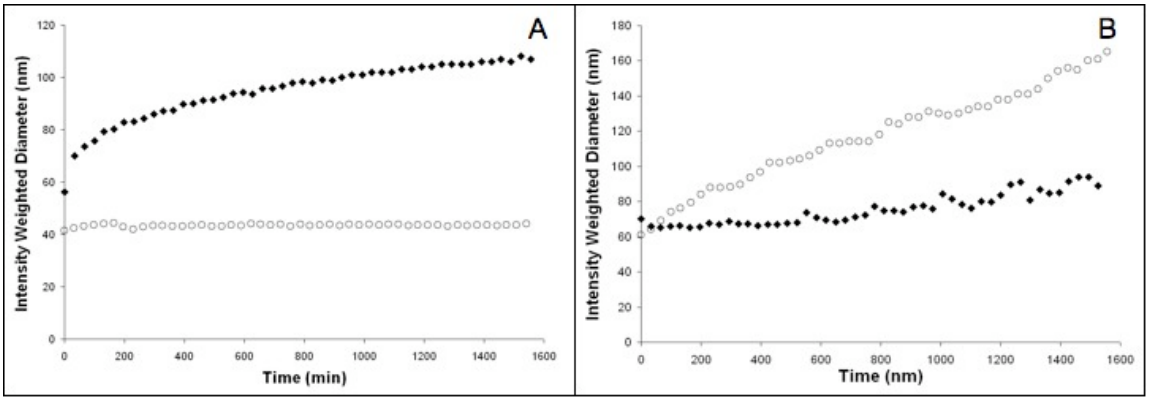

Figure 4.4.4.4. DLS intensity weighted diameters of the 2,900 (open circles) and 8,300 g mol^{-1} (black diamonds) mono-zwitterionic phosphonate-PEO-magnetite complexes in DI water (A) and PBS (B) over 24 hours

While the sizes of some of these nanoparticles remained constant over time, some of them increased in size over time in both media, even without polymer desorption. The hydrodynamic sizes in PBS, however, remained significantly smaller than the analogous materials containing the carboxylate or ammonium anchors, and this result was deemed promising. While the dialysis data in Table 4.4.2.1 indicates that the polymer does not desorb, the aggregation behavior observed in PBS does seem to indicate some desorption from the magnetite surface, particularly since there is no aggregation in sodium chloride. This indicates that there may be small-scale desorption of the polymer accompanied by an attraction between phosphonate anchors of one complex with the exposed magnetite of neighboring complex.

Figure 4.4.4.5 compares intensity-weighted diameters of the complexes containing the PEO with one phosphonate zwitterion anchor group over time in DI water and a 0.17 M NaCl solution (same ionic strength as the PBS).

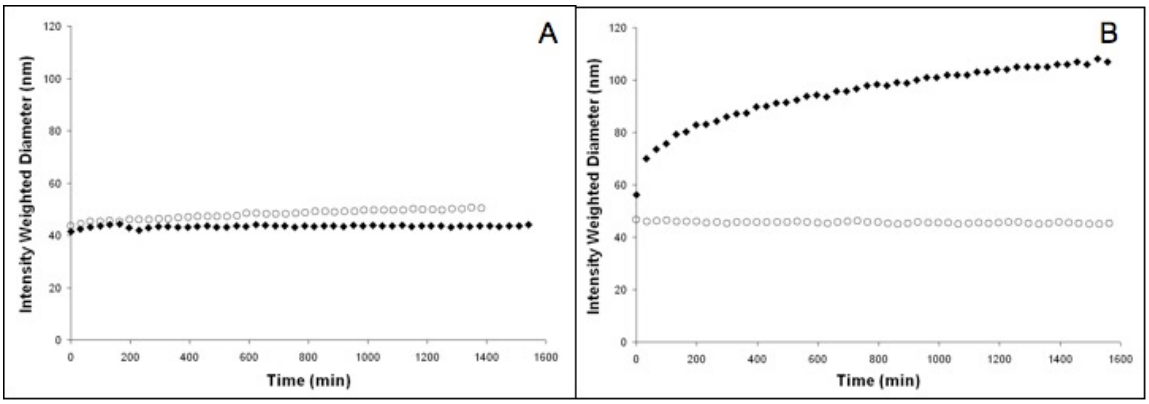

Figure 4.4.4.5. DLS intensity weighted diameters of (A) the 2,900 g mol^{-1} mono-zwitterionic phosphonate-PEO-magnetite complex in DI water (black diamonds) and 0.17 M NaCl (open circles), and (B) the 8,300 g mol^{-1} mono-zwitterionic phosphonate-PEO-magnetite complex in DI water (black diamonds) and 0.17 M NaCl (open circles)

No difference in size was observed for the complex with the 2,900 g mol^{-1} PEO in

the salt solution, and better stability was observed for the 8,300 g mol^{-1} complex in the salt solution. This indicates that it is not the ionic strength of the PBS that induces flocculation in these cases. The slight aggregation of the complex with the 8,300 g mol^{-1} PEO in DI water appears to be due to attractive electrostatic forces that are screened when the complex is in 0.17 M NaCl. The reduction in Debye length with sodium chloride appears to reduce the electrostatic attraction. Additionally, the stability of the 2,900 g mol^{-1} complex in DI water indicates that a denser polymer brush layer also prevents aggregation.

Based on the data discussed above, PEO-magnetite complexes containing one zwitterionic phosphonate anchor group showed significant improvement over the other anchor groups, but long-term colloidal stability was still not achieved. To address this issue, three phosphonate zwitterions, all on one end of the PEO oligomers, were investigated as anchor groups to probe any effect of cooperative binding and/or of each chain having a larger "footprint" on the magnetite surface. Figure 4.4.4.6 shows the intensity-weighted diameters of PEO-magnetite complexes bound through tri-zwitterionic phosphonates in (A) DI water and (B) PBS.

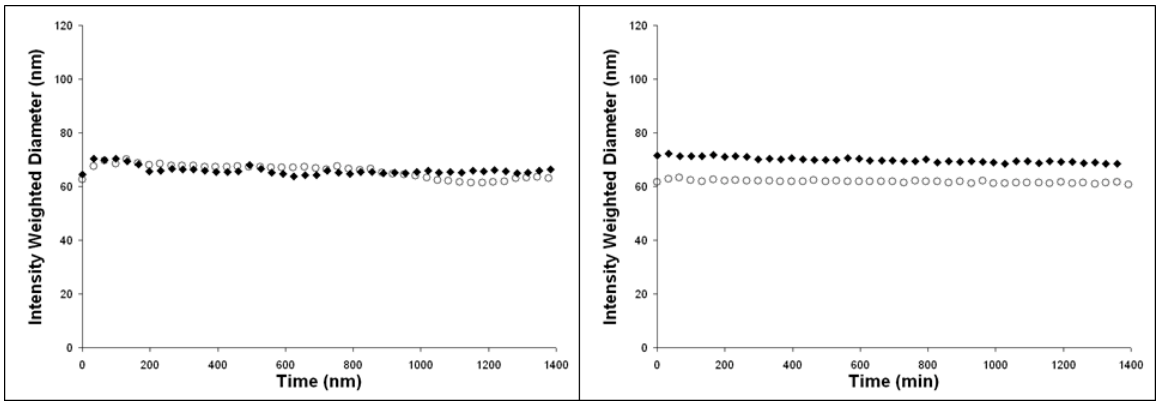

Figure 4.4.4.6. Intensity weighted diameters of the 3,400 (open circles) and 9,100 g mol^{-1} (black diamonds) tri-zwitterionic phosphonate-PEO-magnetite complexes in DI water (A) and PBS (B) over 24 hours

Long-term colloidal size stability was observed for the 3,400 g mol^{-1} and 9,100 g mol^{-1} tri-zwitterionic phosphonate PEO-magnetite complexes in both media. Thus, at similar polymer loadings, three phosphonate anchor groups on the polymer chain end yielded complexes that did not undergo polymer desorption and they did not aggregate over 24 hours in PBS.

A plausible hypothesis involving the size stability of the zwitterionic phosphonate$_3$-PEO-magnetite complexes in PBS can be primarily attributed to high magnetite nanoparticle surface coverage. McDermott et al. performed quartz crystal microbalance experiments on octadecylphosphonate adsorbed onto SiO_2 in THF (a good solvent) and determined the footprint of the phosphonate group to be 18.5 Å.[26] Assuming this applies to our system, for a magnetite sphere with a radius of 4.0 nm there is 145 nm^2 of available surface area, or enough space for 734 zwitterionic phosphonate groups to adsorb. We can calculate the total number of chains per particle for each complex and then calculate how much of the available surface area is taken up by each chain depending on whether there is one or three zwitterionic phosphonate anchor groups. The 2,900 and 8,300 g mol^{-1} mono-zwitterionic phosphonate complexes and the 3,400 and 9,100 g mol^{-1} tri-zwitterionic phosphonate complexes have 83%, 36%, >100%, and >100% surface coverage, respectively. Thus, the complex with the most available magnetite surface area also shows aggregation in DI water. At constant polymer loading, decreasing the PEO molecular weight increases the total number of chains and anchor groups and eliminates this aggregation in DI water. Moreover, by increasing the number of anchor groups three-fold, the predicted surface coverage increases substantially, as do the stabilities of the complexes in both DI water and PBS. This shows that by increasing the total number of

anchor groups, either through reduction of molecular weight (more chains nm^{-2}) or by increasing the number of anchor groups per chain (tri-zwitterionic phosphonate anchor group), the colloidal stability of these materials can be controlled in PBS.

Aggregation observed in DI water for complexes with the 8,300 g mol^{-1} mono-zwitterionic phosphonate anchor group was likely due to an interaction between the magnetite of one complex and the anchor groups of another complex. Were this aggregation due to an interaction between anchor groups of different complexes, we would expect to see more aggregation with an increase in the number of anchor groups. However, we see no aggregation of the tri-zwitterionic phosphonate complexes in DI water, indicating that the critical variable is not an interaction between anchor groups, but rather the availability of the magnetite surface.

4.5 Conclusions

It has been shown that the phosphonate zwitterion endgroups remain stably bound to the magnetite in either water or PBS, while the carboxylate and ammonium endgroups allow the polymers to desorb in PBS. The colloidal instabilities of the carboxylate and ammonium complexes are attributed to polymer desorption from the surface of the magnetite nanoparticles in the presence of phosphate salts.[9]

PEO-magnetite complexes with phosphonate zwitterions remained stably bound in PBS allowed us to consider colloidal size stabilities in light of the density of chains, molecular weights of the bound chains and the predicted surface coverage (i.e., the possible footprint of a trifunctional vs. monofunctional zwitterionic phosphonate chain). The improved colloidal size stability of complexes with the tri-zwitterionic phosphonate anchor groups is likely due to an increase in surface coverage associated with the multiple

anchor groups. For a given polymer loading, the availability of the magnetite surface can also be reduced by shortening the polymer molecular weight, which increases the total number of adsorbed chains.

TGA data confirmed that neither of the novel mono-zwitterionic phosphonate or the tri-zwitterionic phosphonate-anchored polyethers desorbed from the magnetite surface upon exposure to PBS. Coupled with no measurable aggregation of the tri-zwitterionic phosphonate polyether-magnetite complexes in PBS, these seem to be the best-suited complexes for applications that occur in physiological conditions.

4.6 References

1 T. N. Bronich, H.; Eisenberg, A.; Kabanov, A., *Journal of the American Chemical Society* **122:**8339-8343 (2000).

2 C. J. Jung, P., *Magnetic Resonance Imaging* **13:**661-674 (1995).

3 O. T. Mefford, M. R. J. Carroll, M. L. Vadala, J. D. Goff, R. Mejia-Ariza, M. Saunders, R. C. Woodward, T. G. S. Pierre, R. M. Davis and J. S. Riffle, *Chemistry of Materials* **20:**2184-2191 (2008).

4 O. T. Mefford, M. L. Vadala, J. D. Goff, M. R. J. Carroll, R. Mejia-Ariza, B. L. Caba, T. G. S. Pierre, R. C. Woodward, R. M. Davis and J. S. Riffle, *Langmuir* **24:**5060-5069 (2008).

5 A. S. Thunemann, D.; Kaufner, L.; Pison, U.; Mohwald, H., *Langmuir* **22:**(2006).

6 K. S. Wilson, J. D. Goff, J. S. Riffle, L. A. Harris and T. G. St Pierre, *Polymers for Advanced Technologies* **16:**200-211 (2005).

7 A. B. Kabanov, T.; Kabanov, V.; Yu, K.; Eisenberg, A., *Advancers in Genetics* **53:**231-261 (2005).

8 L. A. Harris, J. D. Goff, A. Y. Carmichael, J. S. Riffle, J. J. Harburn, T. G. St. Pierre and M. Saunders, *Chemistry of Materials* **15:**1367-1377 (2003).

9 W. C. Miles, J. D. Goff, P. P. Huffstetler, C. M. Reinholz, N. Pothayee, B. L. Caba, J. S. Boyd, R. M. Davis and J. S. Riffle, *Langmuir* (2008).

10 P. H. Alexandridis, T., *Colloid Surfaces A* **96:**1-46 (1995).

11 P. P. Huffstetler, W. C. Miles and J. D. Goff, et al. , *Polymer Preprints* **49:**1103-1104 (2008).

12 S. R. O. Avelino, F. M. L.; Oliveira, A. C.; Morais, P. C., *Journal of Non-Crystalline Solids* **352:**3692-3696 (2006).

13 E. R. S. J. Cintra, J. L.; Socolovsky, L. M.; Buske, N.; Bakuzis, A. F., *Journal of Magnetism and Magnetic Materials* **320:**351-353 (2008).

14 P. P. B. Gravina, A. F.; Neto, K. S.; Azevedo, R. B.; Morais, P. C., *Journal of Magnetism and Magnetic Materials* **289:**448-451 (2005).

15 F. M. L. A. Oliveira, S. R.; Eloi, M. T. A.; Gravina, P. P.; Neto, K. S.; Lima, E. C. D.; Morais, P. C., *Journal of Non-Crystalline Solids* **352:**3689-3691 (2006).

16 F. M. L. C. Oliveira, A. P.; Figueiredo, L. C.; Neto, K. S.; Morais, P. C., *Journal of Applied Physics* **105:**33906-33909 (2009).

17 M. L. Vadala, M. S. Thompson, M. A. Ashworth, Y. Lin, T. P. Vadala, R. Ragheb and J. S. Riffle, *Biomacromolecules* **9:**1035-1043 (2008).

18 J. Andrade, Hlady, V., Jeon, S., *Advanced Chem Ser* **248:**51-59 (1996).

19 W. M. Deen, *Analysis of Transport Phenomena (Topics in Chemical Engineering)*, Oxford University Press (1998).

20 J. Y. C. Park, E. S.; Baek, M. J.; Lee, G. H., *Materials Letters* **63:**379-381 (2009).

21 Q. A. Zhang, M. S. Thompson, A. Y. Carmichael-Baranauskas, B. L. Caba, M. A. Zalich, Y. N. Lin, O. T. Mefford, R. M. Davis and J. S. Riffle, *Langmuir* **23:**6927-6936 (2007).

22 D. Bica, Vekas, L., Avdeev, M., Marinica, O., Socolluc, V., Balasolu, M., Garamus, M., *Journal of Magnetism and Magnetic Materials* **311:**17-21 (2007).

23 G. Storm, Belloit, S., Daemen, T., Lasic, D., *Advanced Drug Delivery Rev* **17:**31-48 (1995).

24 M. A. M. Tapan K. Jain, Sanjeeb K. Sahoo, Diandra L. Leslie-Pelecky, and Vinod labhaseOxidetwar, *Molecular Pharmaceutics* **2:**194-205 (2005).

25 M. S. Thompson, T. P. Vadala, M. L. Vadala, Y. Lin and J. S. Riffle, *Polymer* **49:**345-373 (2008).

26 A. F. Thunemann, D. Schutt, L. Kaufner, U. Pison and H. Mohwald, *Langmuir* **22:**2351-2357 (2006).

27 Y. Zhang, Kohler, N., Zhang, M., *Biomaterials* **23:**1553-1561 (2002).

28 N. P. Caplan, C.; Hayes, D.; Blackburn, M., *The Royal Society of Chemistry* **1:**421-437 (2000).

29 Y. Sun, B. Wang, C. Hui, H. P. Wang and J. M. Jiang, *Journal of Macromolecular Science Part B-Physics* **45:**653-658 (2006).

30 B. B. Yellen, Z. G. Forbes, D. S. Halverson, G. Fridman, K. A. Barbee, M. Chorny, R. Levy and G. Friedman, *Journal of Magnetism and Magnetic Materials* **293:**647-654 (2005).

31 M. Jones Jr., *Organic Chemistry*, W. W. Norton and Company (2000).

32 R. E. Rosensweig, *Ferrohydrodynamics*, Cambridge Univ. Press, UK (1985).

Chapter 5: The Design of Stable, Well-Defined Polyether-Magnetite Complexes In Aqueous Media: Effect of Anchor Group, Molecular Weight, and Magnetite Loading

P. P. Huffstetler,[1,2] W. C. Miles,[1,3] J. D. Goff,[1,2] S. Ball,[1] R. M. Davis[1,3] and J. S. Riffle[1,2]

[1]Macromolecules and Interfaces Institute, [2]Department of Chemistry, and [3]Department of Chemical Engineering, Virginia Tech, Blacksburg, Virginia 24061, USA

5.1 Abstract

Colloidal stability of polymer-stabilized nanoparticles in physiological media is critical for the use of nanomaterials in therapeutics. The presence of electrolytes, particularly phosphate, in physiological media presents complications to colloidal stability not found with particles suspended in deionized water. As such, this research looks at three different types of anchor groups consisting of a carboxylate group, an ammonium group, and a zwitterionic phosphonate group for the attachment of poly(ethylene oxide) (PEO) to magnetite nanoparticles. Three critical variables were examined: the number of anchor groups, the PEO molecular weight, and the magnetite loading of each complex. Stability of each of these complexes was examined in water and phosphate buffered saline (PBS) which allowed for observation of differences between the two aqueous media. This also allowed conclusions to be drawn about reasons for differences in the stabilities of different complexes. Information found showed that the zwitterionic phosphonate anchor group is considerably more effective than either the carboxylate or ammonium anchor groups in phosphate buffered saline. This is due to the strong interaction between the phosphonate group and the magnetite, as evidenced by the magnetite's affinity for

phosphate through zeta potential measurements, and the aggregation of monophosphonate-anchored complexes in DI water. Because of this aggregation in DI water, it was found that a triphosphonate anchor group is necessary for colloidal stability for greater than 24 hours in PBS. Additionally, this was true for both short and long PEO brushes and at varying magnetite loadings, which should allow for the design of materials with very specific functionality.

5.2 Introduction

Research into magnetite nanoparticles has been of great interest due to a wide range of potential biomedical applications including drug delivery, treatment of detached retinas, cell separations and contrast enhancement agents for MRI.[1-6] Biocompatible macromolecules, such as poly(ethylene oxide) (PEO) has been one of the most widely used coatings for magnetite nanoparticles because it is FDA approved for in vivo applications and its ability to prevent protein adsorption and subsequent phagocytosis. [1, 7, 8] Despite the prevalence of PEO as a coating for various nanomaterials, the binding efficiency of the PEO to the surface must be improved to ensure colloidal stability of the materials being sterically stabilized by the polymer brush.[9-11]

Functional anchor groups on polymers can aid in their adsorption to the surface of magnetite. However, these same anchor groups can be susceptible to desorption with the addition of phosphate salts commonly found in biological systems. Polymeric magnetite dispersion stabilizers containing carboxylate, alkylammonium, and phosphonate zwitterion anchor groups have been previously reported.[8, 12-14] Significant effort has been devoted to the surface adsorption of PEO-containing polymer onto the magnetite surface to improve biocompatibility, and increase circulation time.[1, 7, 15, 16] Previous work by others has shown

the adsorption of polymers to magnetite nanoparticles using pendant carboxylate groups, as well as with carboxylate, alkylammonium, or methoxysilane termini.[8, 17-23] Much of this work has examined stability in saline solutions, but the robustness of these anchor groups in solutions containing phosphate salts remains a concern.[24-26] Previously, fundamental understanding of the effects of anchor group, molecular weight, and polymer loading on colloidal stability has been difficult to deconvolve. This has made designing stable, effective complexes a challenge with significant guesswork. However, development of models to describe both the complex size and stability have recently been developed which can be applied to these systems.[4, 11, 27]

This paper describes the colloidal stability of PEO-magnetite complexes where the PEO oligomers contain functional anchor groups at one end (one and three carboxylate(s), one and three ammonium(s), one and three phosphonate zwitterion(s)) to aid adsorption onto the magnetite. Relationships between the type of anchor group, number of anchor groups, polymer molecular weight, and magnetite loading on the capacity of the polymer to remain firmly bound to the magnetite, and thus remain colloidally stable, were studied in water and in PBS. Through comparisons of stability in these two media, reasons for their stability (or instability) can be explored. Previous work has shown that stability in PBS can be achieved with specific tailoring of polymer molecular weight and magnetite loading.[11, 14] However, through the development of the triphosphonate zwitterion anchor group, we have developed PEO-magnetite complexes that are stable for over 24 hours in PBS regardless of molecular weight or magnetite loading. This allows the design of materials with a polymer stabilizer for a particular application, rather than to ensure stability in a given aqueous media.

5.3 Experimental

5.3.1 Materials

Azobisisobutyronitrile (AIBN), benzyl alcohol (>98%), diethyl ether, diethyl vinyl phosphonate (97%), ethylene oxide (EO, 99.5+%), hexanes (HPLC grade), iron (III) acetylacetonate ($Fe(acac)_3$), mercaptoacetic acid (97+%), oleic acid (90%, technical grade), sodium iodide (99%), triethylamine (TEA, 99.5%), and 1.0 M vinylmagnesium bromide in THF were purchased from Aldrich and used as received. Tetrahydrofuran (THF, Optima Grade, EMD Science, 99.5%) was refluxed over sodium metal with benzophenone until the solution reached a deep purple, fractionally distilled, and deoxygenated just prior to use. Glacial acetic acid (EMD Science) was diluted with THF yielding a 2.0 M acetic acid solution. Naphthalene (Aldrich) was sublimed prior to use. Bromotrimethylsilane (TMS-Bromide, 97%) and mecaptoethylamine hydrochloride were purchased from Alfa Aesar and used as received. Ethanol (Decon Laboratories Inc.) was used as received. Methanol (HPLC grade), chloroform (HPLC grade), N,N'-dimethylformamide (DMF, Optima Grade), dichloromethane (HPLC grade), sodium bicarbonate, ammonium chloride, sodium chloride, and acetone (HPLC grade) were purchased from Fisher Scientific and used as received. 3-Chloropropyldimethylchlorosilane and 3-chloropropyltrichlorosilane was purchased from Gelest and used as received. Dialysis tubing (25,000 g mol^{-1} MWCO and 1,000 g mol^{-1} MWCO) was obtained from Spectra/Por. Phosphate buffered saline 10X (PBS) was obtained from Lonza and diluted to appropriate concentrations.

5.3.2 Synthesis of 3-hydroxypropyldimethylvinylsilane (3-HPMVS) and 3-hydroxypropyltrivinylsilane (3-HPTVS)

3-HPMVS and 3-HPTVS were prepared utilizing a modified procedure originally developed by Vadala et al.[11,12] The procedure described herein that was utilized to prepare 3-HPMVS can be applied to the synthesis of 3-HPTVS with appropriate substitution of the trivinylsilane as the starting reagent. 3-Chloropropyldimethylchlorosilane (10.0 g, 0.06 mol) was syringed into a clean, flame-dried, two-neck, round-bottom flask equipped with a stir bar under a N_2 purge. The reaction flask was placed in an ice bath and cooled to 0 ºC. A 1.0 M solution of vinylmagnesium bromide (64.0 mL, 0.064 mol) in THF was slowly added to the flask over 30 min. The flask was allowed to warm to room temperature, and the mixture was stirred for 24 h. The reaction mixture was diluted with dichloromethane (100 mL), transferred to a separatory funnel and washed with a saturated aqueous ammonium chloride solution (150 mL), then the organic layer was further washed with aqueous sodium chloride (3 X 150 mL). Magnesium sulfate was added to the organic layer to remove any residual water, followed by vacuum filtration. Dichloromethane was removed under vacuum and the product was distilled at 100 ºC, 0.8 Torr, yielding 3-chloropropyldimethylvinylsilane (8.91 g, 0.055 mol, 94% yield) (3-CPMVS). ^{1}H NMR was used to confirm the quantitative addition of vinyl groups.

3-CPMVS (8.91 g, 0.055 mol) was placed in a 250-mL round-bottom flask equipped with a stir bar and condenser. In a separate round-bottom flask, sodium iodide (16.4 g, 0.11 mol) was dissolved in acetone (60 mL) and the solution was syringed into the flask. The mixture was heated at 56 ºC for 24 h. Acetone was removed under vacuum and the product was dissolved in dichloromethane (100 mL) and vacuum filtered to remove the salt by-products. Dichloromethane was removed under vacuum and the

product was distilled at 100 °C, 0.8 Torr, yielding 3-iodopropyldimethylvinylsilane (3-IPMVS, 13.4 g, 0.05 mol). ^{1}H NMR confirmed the expected structure.

3-IPMVS (13.4 g, 0.05 mol) was placed in a 250-mL round-bottom flask equipped with a stir bar and condenser. DMF (20 mL) was added to the reaction flask followed by sodium bicarbonate (8.8 g, 0.10 mol) and DI water (5 mL). The mixture was heated to 100 °C for 24 h and conversion of the alkyl iodide to an alcohol was monitored via ^{1}H NMR. The reaction mixture was transferred to a separatory funnel and washed 3X with DI water to remove the excess sodium bicarbonate and DMF. The product was fractionally distilled at 90 °C, 0.8 Torr, yielding 3-hydroxypropyldimethylvinylsilane (3-HPMVS, 7.4 g, 0.048 mol, 95% yield). ^{1}H NMR confirmed the expected chemical structure.

5.3.3 Sythesis of dimethylvinylsilyl-PEO-OH oligomers

A representative procedure for synthesizing a dimethylvinylsilyl-PEO-OH is provided. An 8,300 g mol^{-1} M_n PEO oligomer was initiated with 3-HPMVS. A 300-mL, high-pressure Series 4561 Parr reactor was utilized for the polymerizations. EO (10.0 g, 0.23 mol) was distilled from a lecture bottle into the pressure reactor cooled with an isopropanol-dry ice bath. THF (5 mL) was added to the reactor via syringe. A potassium naphthalide solution was prepared by charging naphthalene (14.1 g, 0.11 mol) into a 250-mL, flame-dried, round-bottom flask equipped with a glass stir bar. Dry THF (100 mL) was syringed into the flask to dissolve the naphthalene. Potassium metal (3.96 g, 0.10 mol) was added to the solution followed by a N_2 purge for 30 min. The solution was stirred overnight and titrated with 1 N HCl to determine the molarity of the potassium naphthalide solution, which was shown to be 0.95 M. An initiator solution consisting of 3-HPMVS (0.19 g, 1.29 mmol), THF (5 mL) and potassium naphthalide (1.26 mL of a 0.95

M solution in THF, 1.20 mmol) was prepared in a separate flame-dried, 100-mL, round-bottom flask. The initiator solution was added to the stirring reaction mixture via syringe. The cooling bath was removed, and the reaction mixture was allowed to reach room temperature and maintained for 24 h. The polymerization was terminated by adding acetic acid (0.66 mL of a 2.5 M solution in THF, 1.65 mmol) to the pressure reactor via syringe. The pressure reactor was purged with N_2 for 1 h, then opened and its contents were transferred to a 250-mL round-bottom flask. The solvent was removed under vacuum at room temperature, and the product was dissolved in 200 mL of dichloromethane. The product was washed twice with DI water (2 X 100 mL). The solution was concentrated under vacuum at room temperature and precipitated in cold diethyl ether.

5.3.4 Synthesis of trivinylsilyl-PEO-OH oligomers

A characteristic procedure for the synthesis of a 9,100 g mol^{-1} trivinylsilyl-PEO-OH is provided. EO (10.0 g, 0.23 mol) was distilled from a lecture bottle into a 300-mL, high-pressure Series 4561 Parr reactor cooled with an isopropanol-dry ice bath (-30 ^{o}C), followed by addition of THF (5 mL) via syringe. A potassium naphthalide solution was prepared by charging naphthalene (14.1 g, 0.11 mol) into a 250-mL, flame-dried, round-bottom flask equipped with a glass stir bar. Distilled THF (100 mL) was syringed into the flask dissolving the naphthalene. Potassium metal (3.96 g, 0.10 mol) was added to the solution followed by a N_2 purge for 30 min. The solution was stirred overnight and titrated with 1 N HCl to determine the molarity of the solution, which was shown to be 0.97 M. In a separate flame-dried 100 mL roundbottom flask, 3-HPTVS (0.19 g, 1.12 mmol) and THF (5 mL) were added via syringe followed by the addition of a potassium naphthalide solution (1.03 mL, 1.0 mmol) creating an alkoxide initiator solution. The initiator solution

was added to the stirring pressure reactor mixture via syringe. The dry-ice/isopropanol bath was removed, and the reaction mixture was allowed to reach room temperature and maintained for 24 h. The polymerization was terminated by adding an acetic acid solution (0.66 mL 1.65 mmol) to the pressure reactor via syringe. The pressure reactor was purged with N_2 for 1 h, then opened and its contents were transferred to a 250-mL round-bottom flask. The solvent was removed under vacuum at room temperature, and the product was dissolved in 200 mL of dichloromethane and washed twice with DI water (2 X 100 mL). The solution was concentrated under vacuum at room temperature and precipitated in cold diethyl ether yielding 9.6 g of trivinylsilyl-PEO-OH.

5.3.5 Functionalization of trivinylsilyl-PEO-OH with mercaptoacetic acid

An exemplary procedure for addition of carboxylic acid groups via ene-thiol free radical chemistry across the vinylsilyl endgroups is provided for a 9,100 g mol^{-1} trivinylsilyl-PEO-OH. Trivinylsilyl-PEO-OH (1.0 g, 0.11 mmol) was charged to a 100-mL roundbottom flask equipped with a stir bar and dissolved in 2 mL of deoxygenated toluene. Mercaptoacetic acid (45.5 mg, 0.49 mmol) was syringed into the reaction flask followed by the addition of AIBN (10.0 mg, 0.06 mmol) dissolved in 0.5 mL of toluene. The mixture was deoxygenated for 10 min by sparging with N_2, then heated at 80 ^oC for 24 h. The reaction mixture was dissolved in 200 mL of dichloromethane, then transferred to a separatory funnel and washed with DI water 3X to remove the excess mercaptoacetic acid. Dichloromethane was removed via roto-evaporation and the resulting polymer was precipitated into cold diethyl ether. The polymer was dried at room temperature under vacuum for 24 h yielding 0.97 g of tricarboxylic acid-functionalized PEO.

5.3.6 Functionalization of trivinylsilyl-PEO-OH with 2-mercaptoethylamine hydrochloride

Heterobifunctional polyethers with a three-ammonium groups (triammonium-PEO-OH) were obtained via the ene-thiol addition of 2-mercaptoethylamine hydrochloride across the vinylsilane groups. A characteristic procedure for a 9,100 g mol^{-1} trivinylsilyl-PEO-OH is provided. Trivinylsilyl-PEO-OH (2 g, 0.22 mmol), mercaptoethylamine hydrochloride (46.1 mg, 0.4 mmol), and AIBN (21 mg, 0.12 mmol) were dissolved in deoxygenated DMF (5 mL) in a 100-mL roundbottom flask equipped with a stir bar. The reaction was heated at 80 °C for 24 h, then the reaction mixture was cooled to room temperature. DI water (100 mL) was added to the flask, and the mixture was transferred to a separatory funnel. Dichloromethane (200 mL) was added to the separatory funnel to extract the triammonium-functionalized polyether from the aqueous layer. The dichloromethane layer was washed with a 1 N solution of sodium bicarbonate (3X), followed by 3 washes with DI water. The dichloromethane solution was concentrated under vacuum, and the triammonium-PEO-OH oligomer was precipitated into cold diethyl ether and dried at 25 °C under vacuum for 12 h yielding 1.91 g of product (95% yield).

5.3.7 Michael addition of diethyl vinyl phosphonate to triammonium-PEO-OH

A characteristic procedure for addition of diethyl phosphonate groups to a 9,100 g mol^{-} triammonium-PEO-OH is provided. Triammonium-PEO-OH (1.0 g, 0.11 mmol) was charged to a clean, flame-dried, 100-mL roundbottom flask equipped with a stir bar and dissolved in ethanol (5 mL). TEA (0.20 mL, 0.14 mmol) was added to the reaction, followed by addition of diethyl vinyl phosphonate (0.26 mL, 0.14 mmol). The reaction was carried out at 70 ^{o}C for 24 h. The reaction mixture was diluted with DI water to obtain

a 75:25 water:ethanol composition and placed in a 1,000 g mol^{-1} MWCO cellulose acetate dialysis bag and dialyzed for 24 h to remove excess diethyl vinyl phosphonate. The contents of the dialysis bag were transferred to a 100-mL roundbottom flask and lyophilized, yielding 0.94 g of tri(diethyl phosphonate)-functionalized PEO.

5.3.8 De-esterification of tri(diethyl phosphonate)-PEO-OH yielding tri(phosphonic acid)-PEO-OH

Tri(phosphonic acid)-PEO-OH was prepared from tri(diethyl phosphonate)-PEO-OH using a hydrolysis procedure adapted from Caplan et al. In a representative procedure, a 9,100 g mol^{-1} tri(diethyl phosphonate)-PEO-OH (0.90 g, 0.10 mmol) was charged to a clean, 100-mL roundbottom flask equipped with a stir bar and dissolved with 5 mL of dichloromethane. Trimethylsilyl bromide (0.082 mL, 0.62 mmol) was syringed into the reaction flask and stirred at room temperature for 24 h. Methanol (0.03 mL, 0.62 mmol) was added and stirred for 2 h to cleave the trimethylsilyl groups. Dichloromethane (50 mL) was added to the mixture and washed 3X with DI water (100 mL each) in a separatory funnel. The organic layer was concentrated and precipitated by pouring the mixture into cold diethyl ether. The polymer was dried at 25 ^{o}C under vacuum for 24 h yielding 0.81 g of tri(phosphonic acid)-PEO-OH.

5.3.9 Magnetite synthesis via high temperature reduction of $Fe(acac)_3$

Magnetite nanoparticles were synthesized using a reduction method adapted from Pinna et al. Iron(III) acetylacetonate (4.28 g, 16.8 mmol) and benzyl alcohol (90 mL, 0.86 mol) were charged to a 250-mL, three-necked roundbottom flask equipped with a water condenser and placed in a Belmont metal bath with an overhead stirrer with both thermostatic (+/- 1 ^{o}C) and revolution per minute control. The solution was sparged with

N_2 for 1 h to remove any oxygen present in the system. While stirring under N_2, the solution was heated at 100 °C for 4 h, then the temperature was increased to 205 °C at a rate of ~25 °C h^{-1}. After 24 h at 205 ˚C, the reaction was cooled to room temperature and the magnetite nanoparticles were collected with a magnet and the benzyl alcohol was decanted. The magnetite nanoparticles were washed 3X with acetone (100 mL each), followed by dispersion in chloroform (40 mL) containing oleic acid (0.6 g). The solvent was removed under vacuum at room temperature and the oleic acid-stabilized magnetite nanoparticles were washed 3X with acetone (100 mL). The particles were dried under vacuum for 24 h at 25 ˚C and the composition of the particles obtained from thermogravimetric analysis (TGA) was 5% organic residue to 95% magnetite.

5.3.10 Adsorption of trifunctional polyether stabilizers onto magnetite nanoparticles

A representative method for preparing a targeted composition of 70:30 wt:wt polyether:magnetite complex is provided. Oleic acid-stabilized magnetite nanoparticles (50.0 mg) prepared as described above were dispersed in chloroform (10 mL) and charged to a 50-mL roundbottom flask. A trifunctional polyether (117.0 mg) was dissolved in chloroform (10 mL) and added to the dispersion. The pH of each solution and the resulting mixture were approximately neutral. The reaction mixture was sonicated in a VWR 75T sonicator for 16 h under N_2 followed by precipitation into hexanes (300 mL). A magnet was utilized to collect the magnetite nanoparticles and the displaced oleic acid was decanted with the hexanes. The complexes were dried under nitrogen for 30 min and dispersed in DI water (50 mL) using sonication for 30-60 s. The complexes were dialyzed against DI water (4 L) for 24 h using 25,000 g mol^{-1} MWCO dialysis bags.

5.3.11 Characterization

^{1}H NMR spectral analyses of compounds were performed using a Varian Inova 400 NMR or a Varian Unity 400 NMR operating at 399.97 MHz. Size exclusion chromatography (SEC) was performed using an Alliance Waters 2690 Separations Module with a Viscotek T60A dual viscosity detector and laser refractometer equipped with a Waters HR 0.5 + HR 2 + HR 3 + HR 4 styragel column set. SEC data were collected in chloroform at 30 °C. Data were analyzed utilizing a Universal calibration made with polystyrene standards to obtain absolute molecular weights.

Thermogravimetric analysis (TGA) was used to determine the polymer loading for each complex. TGA measurements were carried out on the PEO-magnetite nanoparticles using a TA Instruments TGA Q500 to determine the fraction of each complex that was comprised of polymer. Each sample was first held at 120ºC for 10 min to drive off any excess moisture. The sample (10-15 mg) was then equilibrated at 100ºC and the temperature was ramped at 10°C min^{-1} to a maximum of 700ºC in a nitrogen atmosphere. The mass remaining was recorded throughout the experiment. The mass remaining at 700°C was used to calculate the fraction of magnetite in the complexes. The experiments were conducted in triplicate.

Dynamic Light Scattering (DLS) measurements were conducted with a Malvern Zetasizer NanoZS particle analyzer (Malvern Instruments Ltd, Malvern, UK) at a wavelength of 633 nm from a 4.0 mW, solid-state He-Ne laser at a scattering angle of 173° and at 25 ± 0.1 ˚C. Number average diameters were calculated with the Zetasizer Nano 4.2 software utilizing an algorithm, based upon Mie theory, that transforms time-varying intensities to particle diameters.[29] For DLS analysis, the polymer-magnetite complexes

were received dispersed in DI water and were diluted to ~0.05 mg mL^{-1} and filtered through a Whatman Anotop, 100-nm, alumina filter directly into a polystyrene cuvette. This corresponds to a volume fraction of 1.3×10^{-5} to 2.2×10^{-5} depending on the polymer loading on the magnetite. In experiments where the complex was exposed to PBS, 0.15 mL of 10X PBS was mixed with 1.35 mL of the 0.05 mg mL^{-1} complex solution, then the solution was filtered through either a 100 or 1000-nm filter into a clean polystyrene cuvette. Each sample was analyzed immediately following filtration and re-measured every 30 min over 24 h.

Transmission electron microscopy (TEM) was conducted using a Philips EM-420 field-emission-gun transmission electron microscope. Samples of the polymer-magnetite complexes were suspended in water with probe sonication and cast onto amorphous carbon-coated copper grids. Images were acquired at a magnification of 96 kx at a voltage of 100 kV, corresponding to a resolution of 3.7 pixels nm^{-1}. At least 2000 particles taken from five separate images were used for image analysis. Particle distribution analyses were performed using Reindeer Graphics' Fovea Pro 4 plug-in for Adobe Photoshop 7.0.

A 7T MPMS Squid magnetometer (Quantum Design) was used to determine magnetic properties. Hysteresis loops were generated for the magnetite nanoparticles at 300K and 5K. Fe concentration of the magnetite was determined chemically by acid digestion followed by ICP-AES analysis. These concentrations were in good agreement with TGA values.

5.3.12 Density distribution model to predict sizes of the polyether-magnetite nanoparticle complexes

Modeling of the polyether-magnetite complexes to predict their sizes was performed using methods developed by Mefford, Zhang, and Miles[3, 4, 17, 30] The particles were imaged with TEM and image analysis was performed on the magnetite cores to obtain a particle size distribution. This distribution was then fit with a Weibull probability distribution (*P(a)*) as shown in Equation 1 where *a* is the particle radius and *b* and *c* are the Weibull shape and scale parameters, respectively.

$$P(a) = \frac{c}{b}\left(\frac{a}{b}\right)^{c-1} \exp\left[-\left(\frac{a}{b}\right)^{c}\right] \qquad (1)$$

The average surface area of the magnetite could then be calculated and by combining the average surface area with the average polymer loading per mass of complex (from TGA), the average number of chains per magnetite surface area, α, could be determined.

$$\alpha = \frac{(1 - W_{mag}) N_{Av} \rho_{mag}}{3 M_n W_{mag}} \frac{\int_0^\infty a^3 P(a) dr}{\int_0^\infty a^2 P(a) dr} \qquad (2)$$

Here, ϱ_{mag} is the density of magnetite (5.21 g cm^{-3}),[31] W_{mag} is the weight fraction of the complex that is magnetite (from TGA), N_{Av} is Avogadro's number, and M_n is the PEO number average molecular weight. Through application of a modified version of the Vagberg density distribution model,[3, 4, 30, 32] the average number of chains and the radius of the PEO-magnetite complexes was calculated as

$$f(a) = 4\pi a^2 \alpha \qquad (3)$$

$$R_m(a) = \left(\frac{8 N_k f(a)^{\frac{1-\nu}{2\nu}} L_k^{1/\nu}}{4^{1/\nu} 3\nu} + a^{1/\nu} \right)^{\nu} \qquad (4)$$

where N_k is the number of Kuhn segments, L_k is the Kuhn length (0.6 nm)[31], υ is the Flory exponent (0.583 for PEO in water at 25 °C),[33] and *f(a)* is the number of chains per particle.

Comparison to DLS measurements were made by calculating the number average diameter D_n from the combination of the Weibull probability size distribution fit and the density distribution model.

$$D_n = 2\int_0^{\infty} R_m(a) P(a) da \qquad (5)$$

The focus was on the number weighted average, both from a modeling and a light scattering perspective because the number weighted average is the least sensitive to aggregation. Compared to the intensity weighted average size, significantly more aggregation must occur before the number average will change significantly. Thus, comparison of a calculated number average to an experimental average from light scattering allows determination of considerable aggregation.

The brush model can also be used to calculate the pair-pair potential for polymer-particle complexes of the same size as previously described by our group.[4, 30] The calculation of these potentials is described in equations 6 through 9.

$$V_{Total} = V_{vdW} + V_M + V_{ES} + V_S \tag{6}$$

$$V_{ES} = 2\pi a\varepsilon\varepsilon_o\psi_o^2 \ln(\left(1 + e^{-\kappa(r-2a)}\right) \tag{7}$$

$$V_{vdW} = -\frac{1}{6}A_{eff}\left(\frac{2a^2}{r^2-4a^2} + \frac{2a^2}{r^2} + \ln\left(\frac{r^2-4a^2}{r^2}\right)\right) \tag{8}$$

$$V_S = \frac{5}{18}kTf(a)^{3/2}\left\{\begin{array}{ll} -\ln\left(\frac{r}{\sigma} + \frac{1}{1+\frac{\sqrt{f(a)}}{2}}\right); & r \le \sigma \\ \frac{1}{1+\frac{\sqrt{f(a)}}{2}}\left(\frac{\sigma}{r}\right)\exp\left(-\frac{\sqrt{f(a)}}{2\sigma}(r-\sigma)\right); & r > \sigma \end{array}\right\} \tag{9}$$

V_{Total} is the total potential energy, V_{vdW} is the attractive potential due to van der Waal's interactions, V_M is the attractive potential produced by an applied magnetic field, V_{ES} is the repulsive potential due to electrostatic interactions, and V_S is the repulsive potential due to steric repulsion of the polymer brushes. All calculations and measurements are performed without an applied magnetic field, and so V_M is negligible.[14] Here, ε is the dielectric constant of the solvent, ε_o is the permittivity of free space, ψ_o is the surface potential, $\varkappa$ is the inverse Debye length, r is the center-to-center separation, and *a* is the particle radius, h is the surface-to-surface separation of two particles[34], r is the center-to-center separation distance of two particles, A_{eff} is the effective retarded Hamaker constant calculated according to previous work [4, 11]

For the case of a densely adsorbed brush layer, the steric contribution to the interaction potential may be described by equation 9, where r is the center-to-center separation, f(a) is the number of chains per particle, and σ/2 is the distance from the center of the core to the center of the outermost blob layer, and σ is defined as $1.3R_{g,}$ the radius of gyration of the ensemble.[35, 36] Thus, determination of the onset of a sharp increase in the steric potential is determined by the R_g, which is calculated as done previously.[4, 11] By summing these potential energy terms (van der Waals, electrostatic, and steric) in equation 6, a pair-pair potential energy diagram can be constructed to determine the effect of a magnetic field on the separation of these materials as a function of molecular weight.

Finally, the calculation of V_{Total} allows for the determination of the stability ratio and the half-life for doublet formation using equations 10 and 11, respectively, where μ is the solvent viscosity, Φ is the volume fraction of particles in solution, and $\bar{a}$ is the average particle radius.[37, 38]

$$W = 2\bar{a}\int_{2\bar{a}}^{\infty} \frac{e^{\frac{V_{Total}}{kT}}}{r^2} dr \qquad (10)$$

$$t_{1/2} = \frac{\bar{a}^3 \pi \mu W}{\phi kT} \qquad (11)$$

The classical expression for W does not account for polydispersity and only concerns pair interactions for particles of like sizes. We account for the size distribution by computing ā (4.0 nm) from the Weibull distribution (equation 1). The half-life for doublet formation provides a basis to compare complexes with different molecular weights and polymer loadings.

5.4 Results and Discussion

The aim of this study was to compare the stability of different PEO-magnetite complexes by varying the type of functional anchor used, the number of functional anchors used, the polymer molecular weight, and the magnetite loading of each complex. This was done in both DI water and PBS, which while not a perfect biological analog, does contain phosphate salts commonly found in physiological media while still allowing the use of light scattering as a characterization tool.

5.4.1 Synthesis of PEO oligomers with different functional endgroups for binding to magnetite

3-HPMVS and 3-HPTVS were used as versatile initiators for the living anionic polymerization of EO yielding heterobifunctional oligomers useful for post-functionalization with specific chemical groups for the adsorbtion onto magnetite nanoparticles. A characteristic synthesis of trivinylsilyl-PEO-OH is shown in Scheme 5.4.1.1. This approach allowed for utilization of the same oligomer for comparing dispersion properties while only changing the type and number of functional anchor groups. Functionalization of these oligomers with carboxylic acid, ammonium, and zwitterionic phosphonates have previously been reported by Goff *et al*. Potassium naphthalide was reacted with 3-HPMVS or 3-HPTVS to form an alkoxide for initiating EO, and the number of moles of the alcohol initiator relative to EO controlled the molecular weight. A slight deficiency of naphthalide relative to alcohol ensured the alkoxide and not residual naphthalide initiated the polymer chains, while the residual alcohols transferred with the propagating PEO chains. These anionic ring-opening

polymerizations were terminated with acetic acid in order to avoid any unwanted oxidative side reactions.

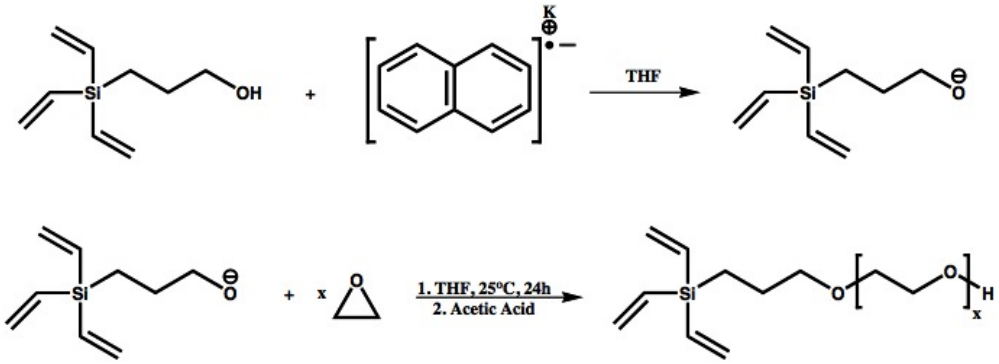

Scheme 5.4.1.1. Synthesis of trivinylsilyl-PEO-OH via anionic ring-opening polymerization

Both Dimethylvinylsilyl-PEO-OH and trivinylsilyl-PEO-OH oligomers with molecular weights ranging from 3,000 g mol^{-1} to 9,000 g mol^{-1} were prepared and characterized utilizing SEC and `H NMR as shown in Table 5.4.1.1.

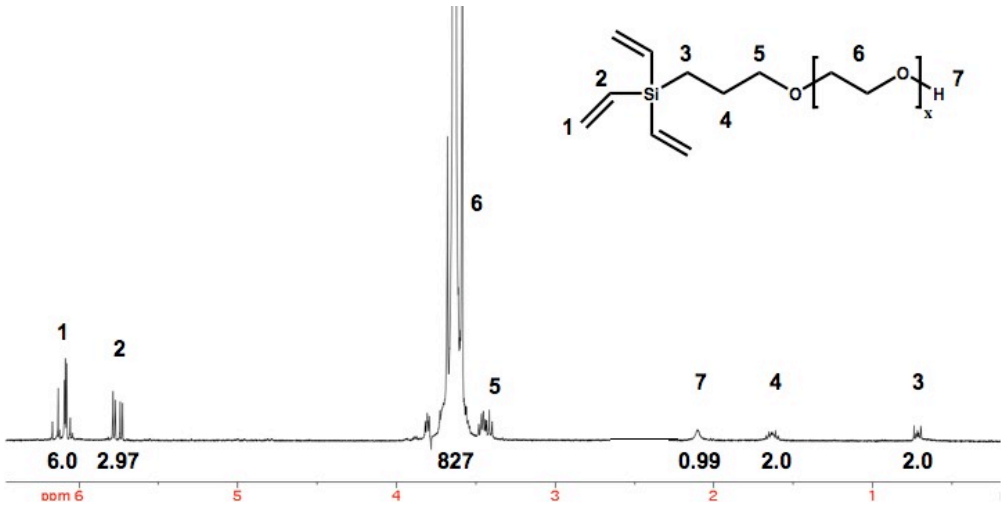

Figure 5.4.1.1. ^{1}H NMR of a 9,100 g mol^{-1} trivinylsilyl-PEO-OH oligomer

Figure 5.4.1.1 shows the ^{1}H NMR spectrum of a 9,100 g mol^{-1} trivinylsilyl-PEO-OH oligomer. Molecular weight of the oligomer was determined by comparing the integral ratios of the methylene protons in the initiator (peak 3) to the backbone protons of the EO repeat units (peak 6).

Table 5.4.1.1. Molecular weights of dimethylvinylsilyl- and trivinylsilyl-PEO-OH oligomers

Targeted Molecular Weight	M_n (g mol^{-1})		MWD
	^{1}H NMR	SEC	
Monovinylsilyl-3,000 g mol^{-1}	2,900	3,100	1.09
Monovinylsilyl-8,000 g mol^{-1}	8,300	7,900	1.05
Trivinylsilyl-3,000 g mol^{-1}	3,400	3,400	1.04
Trivinylsilyl-9,000 g mol^{-1}	9,100	9,500	1.09

As previously reported, ene-thiol free-radical additions were used to introduce both carboxylic acid and ammonium functionality for both the dimethylvinylsilyl-PEO-OH and trivinylsilyl-PEO-OH oligomers.[14] The vinylsilyl group was used because it does not readily polymerize via free-radical chemistries. As previously reported, ene-thiol free-radical additions were used to introduce both carboxylic acid and ammonium functionality for both the dimethylvinylsilyl-PEO-OH and trivinylsilyl-PEO-OH oligomers (Scheme 5.4.1.2). The vinylsilyl group was used because it does not readily polymerize via free-radical chemistries.

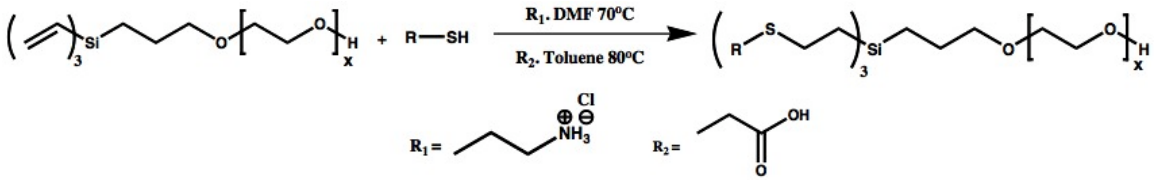

Scheme 5.4.1.2. Ene-thiol addition chemistries affording both ammonium and carboxylic acid functionalities

Addition of mercaptoacetic acid and 2-mercaptoethylamine hydrochloride were monitored via $^{-1}$H NMR through the disappearance of the vinyls between 5.8 and 6.2 ppm as previously reported(Figure 5.4.1.2A and B). In order to show quantative conversion of the vinyl groups the integral ratios of the methylene protons of the silyl initiator were compared to those of the converted vinyl protons and the added mercaptan of choice. Comparison of the integrations confirmed quantative functionalization.

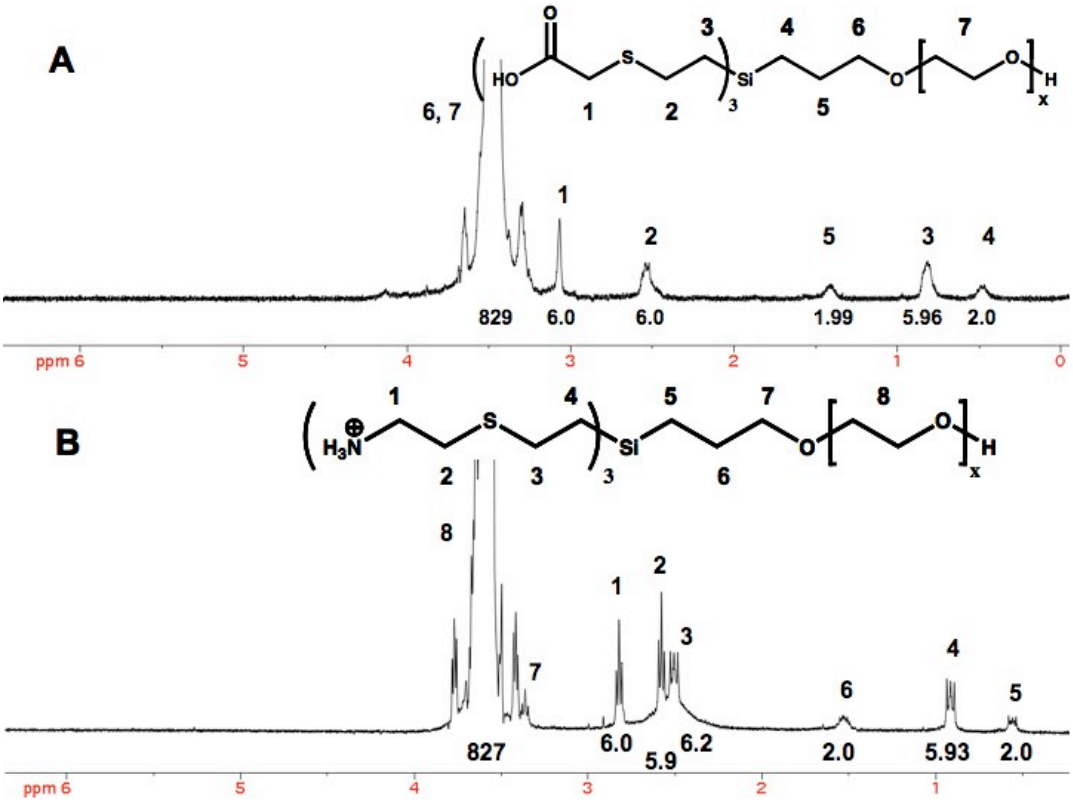

Figure 5.4.1.2. ^{1}H NMR of (A) mercaptoacetic acid addition to a 9,100 g mol^{-1} trivinylsilyl-PEO-OH and (B) 2-mercaptoethylamine hydrochloride addition to a 9,100 g mol^{-1} trivinylsilyl-PEO-OH

The ammonium and triammonium-functionalized PEO oligomers were utilized as precursors towards the formation of zwitterionic phosphonate PEO-OH. The ammonium polyethers were neutralized by addition of triethylamine affording free amines followed by the introduction of diethyl vinyl phosphonate. Diethyl vinyl phosphonate was added to the

amine group(s) through the Michael addition. The ethyl groups of both diethyl phosphonate-PEO-OH and tri(diethyl phosphonate)-PEO-OH oligomers were cleaved via addition of bromotrimethylsilane (TMS-Br). The methylsilyl ester was cleaved via methanolysis yielding phosphonic acid functionality (Scheme 5.4.1.3). A zwitterionic functional group was afforded at a pH of less than 10, due to the negative charge of the phosphonate and the protonated secondary amine.

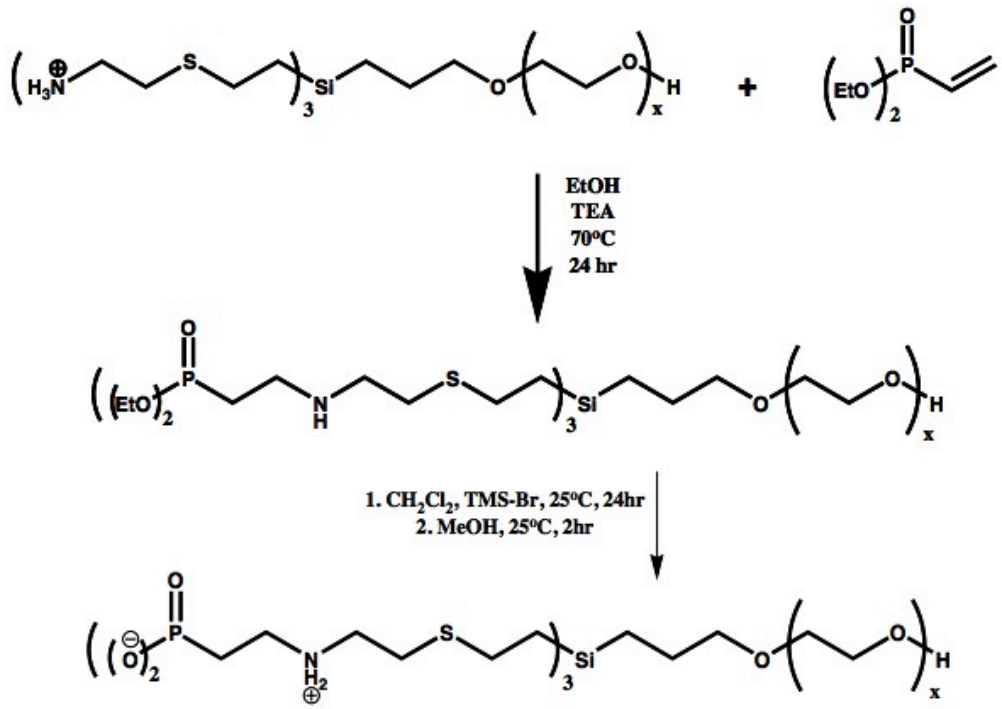

Scheme 5.4.1.3. Michael addition of diethyl vinyl phosphonate followed by de-esterification of ethyl groups yielding a zwitterionic phosphonate-PEO-OH

^{1}H NMR spectra of the representative tri(diethylphosphonate)-PEO-OH oligomer is shown in Figure 5.4.1.3A. The methylene peaks of the converted vinyl group of the diethyl vinyl phosphonate reactant were observed as peaks 3 and 4 with the peak located at approximately 2 ppm corresponds the the methylene adjacent to the phosphorus atom. Quantitative addition of diethyl vinyl phosphonate to the amines was determined by comparing the integral ratios of peaks 1-4 to the ratio of the methylene silyl peak labeled 9.

In order to effectively bind to the surface of magnetite the ethyl groups were cleaved as discussed above followed by ^{1}H NMR characterization (Figure 5.4.1.3B). In addition to the disappearance of the methyl and methylene protons, an upshift (~1.6 ppm) of the methylene adjacent to the phosphorous atom was noted.

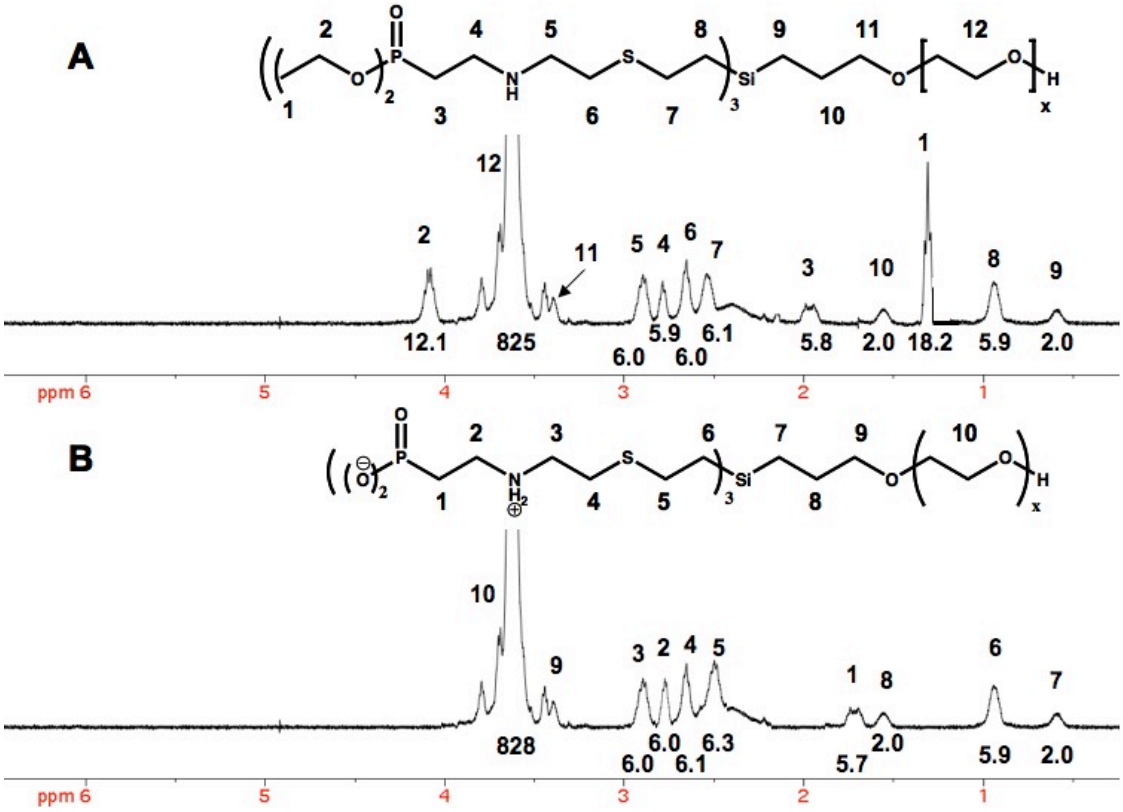

Figure 5.4.1.3. ^{1}H NMR of (A) addition of diethyl vinyl phosphonate to a 9,100 g mol^{-1} triammonium-PEO-OH followed by (B) de-esterification of a 9,100 g mol^{-1} tri(diethylphosphonate)-PEO-OH yielding tri-zwitterionic phosphonate-PEO-OH

5.4.2 Formation of PEO-magnetite complexes via adsorption of the functional PEO oligomers onto the surfaces of magnetite nanoparticles

PEO-magnetite complexes were formed with the four sets of varying molecular weight PEO oligomers, after which the complexes were dialyzed against water to remove any unbound PEO. The compositions of the PEO-magnetite complexes were in close

agreement with the targeted magnetite:polyether composition as measured by TGA. Figure 5.4.2.1 shows a representative TEM image of the polyether-magnetite complex, which indicates a well-defined particle size distribution of 7.7 nm ± 2.3 nm.

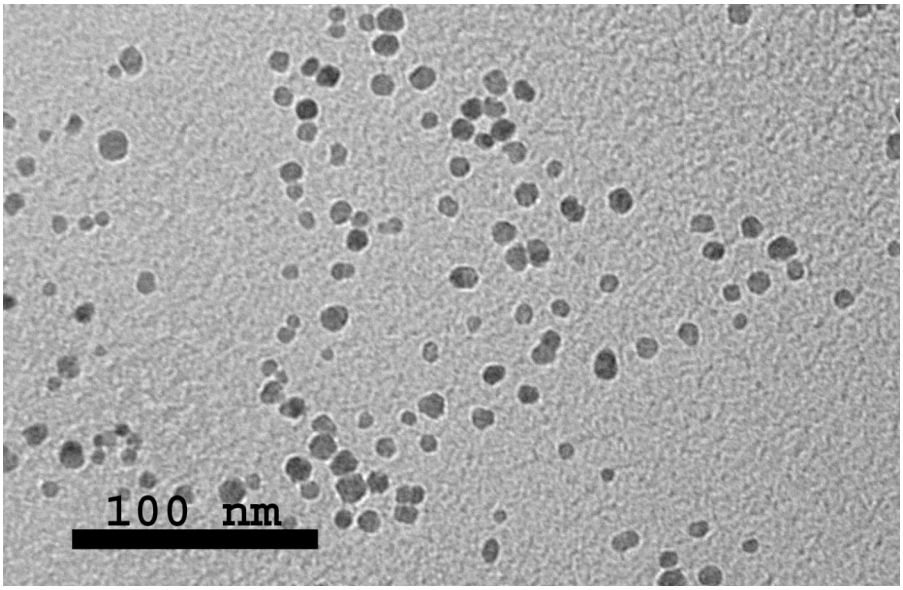

Figure 5.4.2.1. A representative TEM image of polyether-magnetite complexes indicate a well-defined particle distribution.

The magnetic properties of the magnetite nanoparticles were characterized via superconducting quantum interference device analyses. Hysteresis loops revealed superparamagnetic behavior and a saturation magnetization of 80 emu g^{-1} for the magnetite nanoparticles. This compares with reported saturated magnetization of 82 emu g^{-1} for bulk magnetite.[39]

5.4.3 Colloidal Stability of Polyether-Magnetite Complexes in Deionized Water

Before examination of the stability of these materials under physiological conditions, characterization of their colloidal stability in deionized (DI) water was needed

to understand the complexities associated with varying molecular weights and polymer loadings. Figure 5.4.3.1 shows DLS over time for two different PEO molecular weights for the monoammonium and monocarboxylic acid anchor groups with approximately 30% magnetite loading.

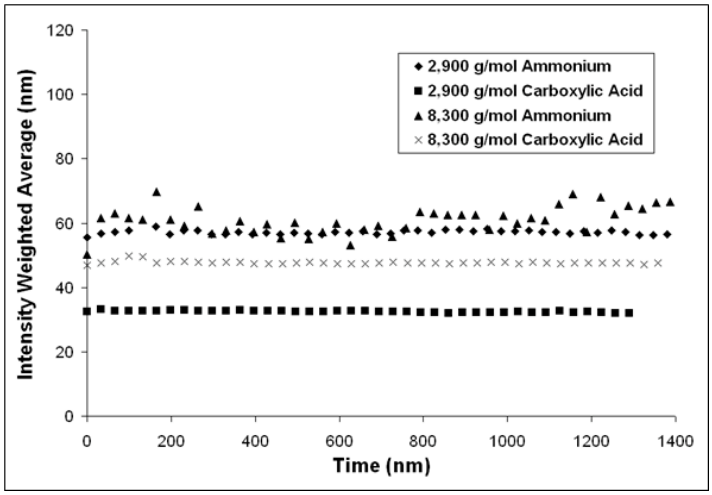

Figure 5.4.3.1. All monoammonium- and monocarboxylic acid-anchored complexes were stable for 24 hours in DI water (approximately 30% magnetite loading for each).

Similar stabilities were observed for the triammonium and tricarboxylic acid anchor groups for two similar PEO molecular weights. However, the stability of the monophosphonate anchor groups in DI water was considerably different, as shown in Figure 5.4.3.2.

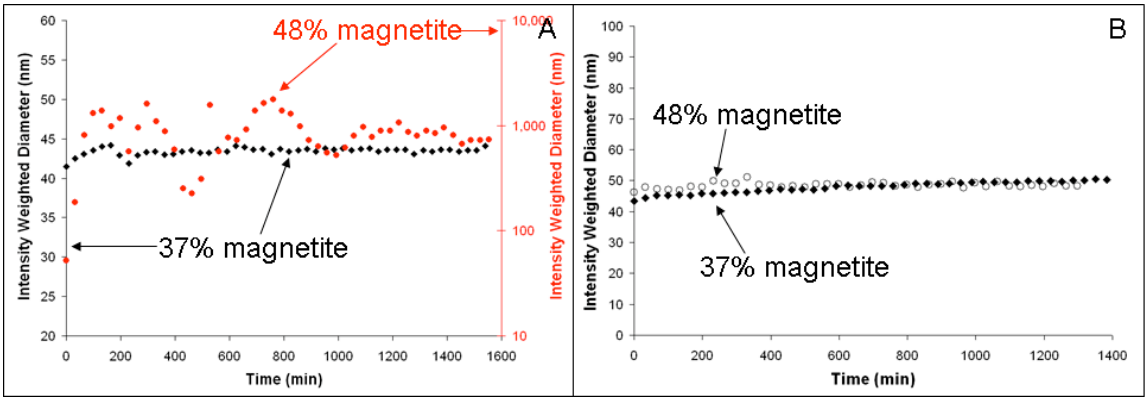

Figure 5.4.3.2. Intensity weighted diameters (D_I) of the 2,900 g mol^{-1} Mono-phosphonate-PEO-OH complexes in DI water (A) and 0.17 M sodium chloride (B).

There was no appreciable aggregation for the monophosphonate-anchored 2,900 g mol^{-1} complex with 37 wt % magnetite loading and the measured particle size was very close to that predicted for a dispersed primary particle using the Density Distribution model. However, there was significant aggregation of the complex once the magnetite loading was increased to 48 wt % (A). This behavior is very different than the ammonium and carboxylic acid anchor groups. These results indicate that the phosphonate anchor group may contribute to the onset of this aggregation. Through addition of sodium chloride (0.17 M), the aggregation was eliminated, showing that the aggregation appears to be due to electrostatic interactions (Figure 5.4.3.2B).

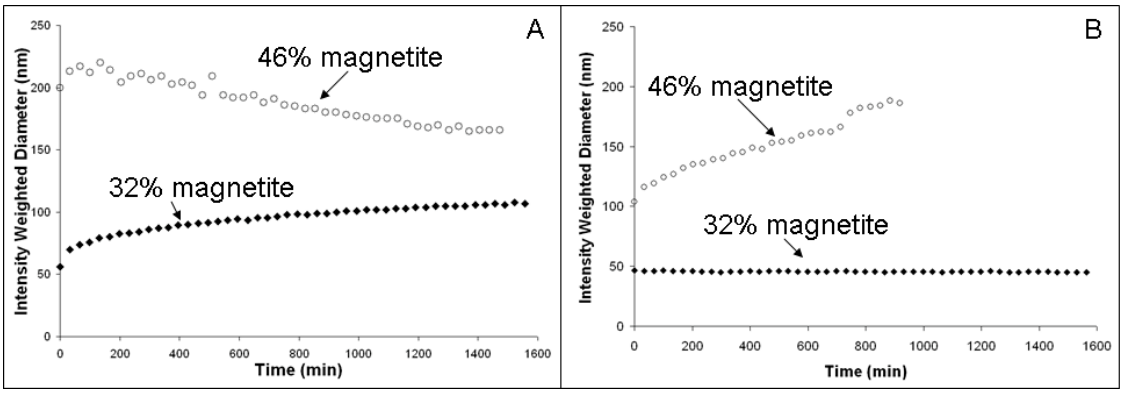

Figure 5.4.3.3. Aggregation of the monophosphonate-anchored 8,300 g mol^{-1} PEO complexes occurred in DI water (A). This aggregation was hindered with the addition of 0.17 M sodium chloride (B).

Similar behavior was observed for the monophosphonate-anchored 8,300 g mol^{-1} PEO complexes, as shown in Figure 5.4.3.3. Aggregation was observed in DI water for both the 32 wt % and 46 wt % magnetite loadings (A). In contrast to the 2,900 g mol^{-1} complexes, the 46% magnetite loading for the 8,300 g mol^{-1} complex could not be completely dispersed in the water, as indicated by its initial size of approximately 200 nm. This indicates the presence of a secondary potential energy minimum deep enough to prevent reduction of the complex to its primary size, even with extensive sonication. There was no appreciable growth of the complex size over time, but much of the sample was captured in the filter prior to measurement and there was visible sedimentation upon completion of the experiment. For the 32% magnetite loading, the particle size is initially very close to that of a dispersed primary particle but then increases with time, indicating flocculation into a shallower secondary minimum than was the case for the 46% loading.

In Figure 5.4.3.3(B), addition of 0.17 M sodium chloride eliminated all aggregation for the complex with 32 wt % magnetite loading. The aggregation could not be completely eliminated for the complex with 46 wt % magnetite loading. However, sonication of the

complex did reduce the particle size below that obtainable in water, which confirms that the flocculation observed in DI water is due to a secondary minimum and that the minimum can be reduced with the addition of salt. This indicates an electrostatic interaction and because this is not observed with any of the other anchor groups, it must be due to the zwitterionic phosphonate group.

The length scale at which this electrostatic interaction is significant can be estimated using extended DLVO theory. The Debye length for each complex should be approximately 30 nm (assuming an ionic strength of 10^{-4} M) and the electrostatic potential decays exponentially from the charged surface. Measurement of the zeta potential to quantify this electrostatic potential is not useful because currently there is no model to account for the zwitterionic nature of the anchor group, it is an average measurement which would always result in a negative potential, and it would not be a representative measurement due to the shifting of the shear plane due to the polymer brush. However, it is useful to compare the length scale of the steric repulsive potential with that of electrostatic interactions. Figure 5.4.3.4 shows the steric potentials as a function of surface to surface separation for two 8,300 g mol^{-1} complexes with 32% and 46% magnetite loadings.

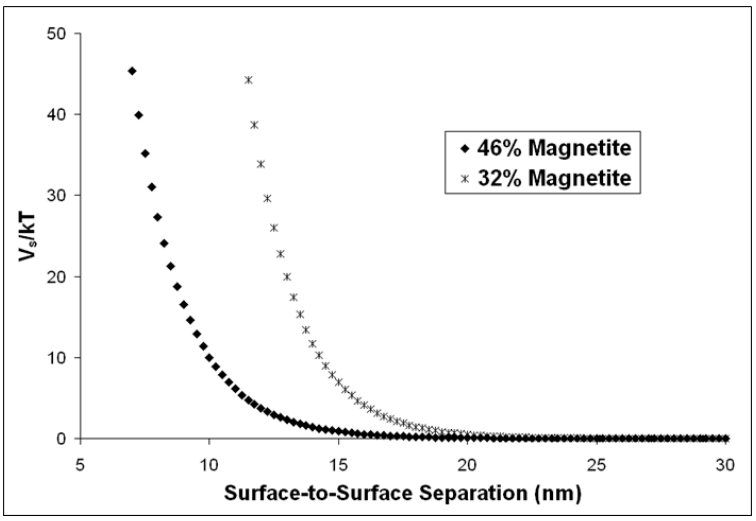

Figure 5.4.3.4. Plots of the steric potential as a function of surface to surface separation for the 8,300 g mol^{-1} complex with 32% and 47% magnetite loadings.

The 32% magnetite loading provides the longer-range steric repulsion, beginning to dominate (> 10kT) at a separation distance of 14 nm compared to 10 nm for the complex with 46% magnetite loading. However, a large enough secondary potential energy minimum is created by the electrostatic interaction caused by the phosphonate anchor group to prevent the sample with 46% magnetite from being resuspended as a single particle system. In this case, the electrostatic interaction must increase significantly enough to produce the large secondary minimum between 10-14 nm to explain the observed behavior.

Extended DLVO theory also explains the behavior observed for the 2,900 g mol^{-1} complex with 48% magnetite loading (Figure 5.4.3.3A). If the onset of strong electrostatic interaction is indeed between 10-14 nm, then significantly more flocculation would be expected for smaller molecular weight stabilizers due to smaller repulsive steric potentials (Figure 5.4.3.5).

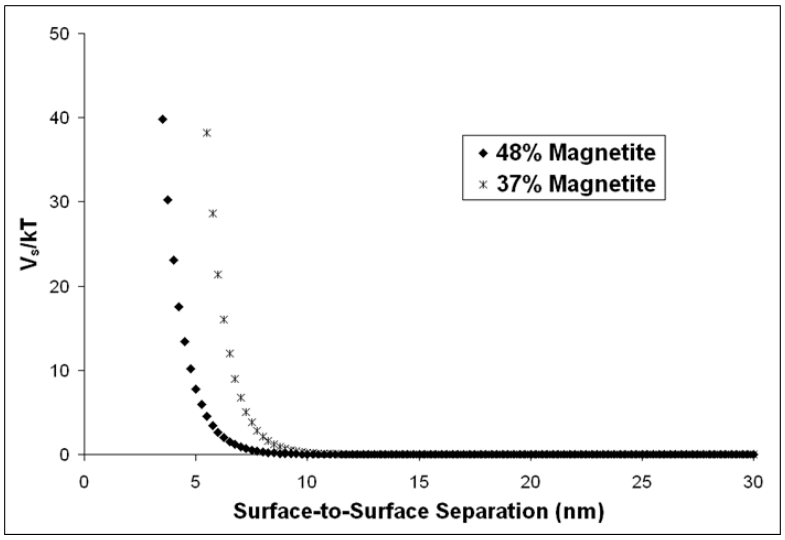

Figure 5.4.3.5. Steric potentials for the 2,900 g mol^{-1} complexes with 37 and 48% magnetite loadings.

However, if this were a complete explanation then both complexes should flocculate in water and not just the complex with 48% magnetite loading. The only real difference between the complexes is that the lower magnetite loading has a denser polymer brush. It is possible that this polymer brush is dense enough to appreciably screen out any electrostatic interaction and prevent flocculation in DI water. This increased stability may also indicate that the electrostatic interaction is between the phosphonate anchor group of one complex and the magnetite of a neighboring complex.

The nature of the electrostatic interaction was examined through the use of triphosphonate anchor groups, which provided more magnetite surface coverage without increasing the polymer chain density compared to the monophosphonate counterparts. Also, an increase in the number of anchor groups would increase the electrostatic interaction were it due to an interaction between anchor groups of neighboring complexes. Stability of these complexes for two different triphosphonate-anchored PEO molecular weights (3,400 g mol^{-1} (A) and 9,100 g mol^{-1} (B)) are shown in Figure 5.4.3.6.

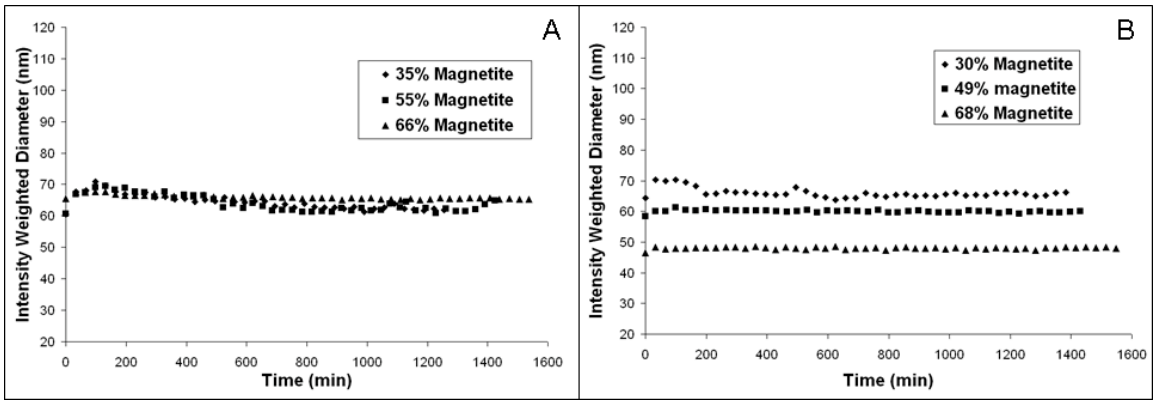

Figure 5.4.3.6. Intensity weighted diameters (D_I) of (A) 3,400 g mol^{-1} and (B) 9,100 g mol^{-1} PEO complexes with triphosphonate anchors in DI water over 24 hrs.

No aggregation was observed for any of the triphosphonate-anchored 3,400 or 9,100 g mol^{-1} PEO complexes in DI water, regardless of the magnetite loading of the complex. Addition of two more anchor groups per chain eliminated the aggregation observed for the monophosphonate-anchored complexes. This suggested that the aggregation was not due to attraction between anchor groups of different complexes but rather due to attraction of magnetite of one complex to an anchor group of another complex. This required an estimate of the fraction of the magnetite particle surface covered by the anchor groups.

To determine the magnetite surface coverage, a method was needed to quantify the surface area occupied by a particular anchor group. The program ChemBio3D Ultra 11.0 was used to determine the average bond length for a specific anchor group (1.7 Å for a P-O bond in a phosphonate anchor group and 1.1 Å for an ammonium anchor group). This value was then used as the radius of a sphere representing the anchor group located at the magnetite nanoparticle surface as shown in Figure 5.4.3.7.

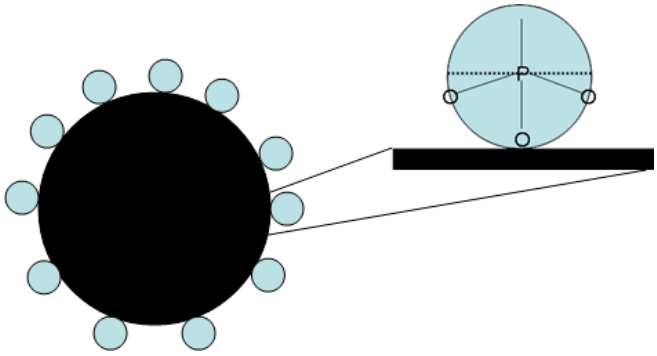

Figure 5.4.3.7. Visualization of the area occupied by the phosphonate anchor group in contact with the magnetite surface.

Assuming only the lower half of the sphere can contact the magnetite surface, the surface area occupied by a particular anchor group was taken to be the surface area of the hemisphere. For a monophosphonate, this model yields a molecular footprint of 18.2 $Å^2$. This approximation compares well with the literature, where McDermott *et al.* used QCM-D to calculate the molecular footprint of a phosphonate group attached to an alkyl chain to be 18.5 $Å^2$. The model yields a much smaller molecular footprint for the monoammonium group of 7.6 $Å^2$.

Table 5.4.3.1 illustrates the surface coverage based on a surface area of 122 $m^2\ g^{-1}$ for the magnetite particle distribution and a molecular footprint of 18.2 $Å^2$. The number of available anchors was determined through the calculation of polymer chains using equations 1 through 3 and then multiplied by three for the triphosphonate-anchored complexes.

Table 5.4.3.1. Percent surface coverage calculated based on the surface area occupied by the phosphonate anchor group.

Anchor Group	Molecular Weight (g/mol)	% Magnetite	Number of Anchors	% Surface Coverage	Stable in DI Water?
Monophosphonate	2,900	37	648	96%	Yes
	2,900	48	381	57%	No
	2,900	67	163	24%	No
	8,300	32	283	42%	No
	8,300	46	133	20%	No
	8,300	71	57	8%	No
Triphosphonate	3,400	31	2166	322%	Yes
	3,400	55	975	145%	Yes
	3,400	66	417	62%	Yes
	9,100	30	849	126%	Yes
	9,100	49	363	54%	Yes
	9,100	68	156	23%	Yes

For the monophosphonate-anchored complexes, the only sample that exhibited 24-hour stability in DI water was the 2,900 g mol^{-1} complex with 37% magnetite loading. This sample had 96% surface coverage according to the calculation while the next closest complex had a surface coverage of 57%. Thus, it appears that the stability observed in Figure 5.4.3.2A of the 2,900 g mol^{-1} complex with 37% magnetite loading in DI water was due to a decrease in the magnitude of the electrostatic interaction because very little magnetite was available to neighboring anchor groups. Also, none of the 8,300 g mol^{-1} complexes have complete coverage and both show some flocculation in DI water (Figure 5.4.3.3A). The relative amounts of flocculation observed have already been explained using extended DLVO theory. Stability of these materials in DI water is quite complex, with the existence of an interaction potential due to the attraction of the phosphonate anchor group to the magnetite surface coupled with a repulsive steric interaction potential that stabilizes the complexes.

As illustrated in Table 5.4.3.1, the complexes made with triphosphonate anchors show no aggregation over 24 hours in DI water. They also show much higher surface coverages, including complexes where the estimated area occupied by the anchor groups exceeds the surface area of the magnetite. However, at higher magnetite loadings, i.e. the 9,100 g mol^{-1} complex with 68% magnetite loading, the surface coverage becomes relatively small but no aggregation occurs. This phenomenon may be due to interactions between phosphonate anchors that would cause them to spread out over the magnetite surface and thus increase the footprint of the triphosphonate anchor. Thus, for the complexes made with triphosphonate anchors, the effective % surface coverage of magnetite available for interaction with other complexes might be significantly smaller than that calculated in Table 5.4.3.1. This may account for the increased stability of these complexes, even at high magnetite loadings.

5.4.4 Colloidal Stability of Polyether-Magnetite Complexes in Phosphate Buffered Saline

Previous work has shown that colloidal stability in DI water is no guarantee that these polyether-magnetite complexes will be stable in more complex solutions, such as phosphate buffered saline (PBS). Desorption of these polyethers with the introduction of phosphate salts into solution has been a significant barrier to the development of these materials.[11, 14] Through the incorporation of an amphiphilic diblock copolymer with finely-tuned polymer molecular weights and magnetite loadings, this desorption could be hindered.[11] Additionally, recent development of the phosphonate anchor group has allowed for increased stability of these materials.[14] However, previous work has also indicated that a reduction in polymer loading can significantly decrease the stability of a complex in PBS.[11] The ability to tailor a polymer-magnetite complex size may be critical

to possible biological targeting, and the size of a complex is directly related to its polymer loading.[11, 27] Thus, it is critical to determine the efficacy of a particular anchor group over a range of magnetite loadings.

Figure 5.4.4.1 shows zeta potential measurements made of the magnetite nanoparticles at different pH in two different buffers: PBS and sodium phosphate.

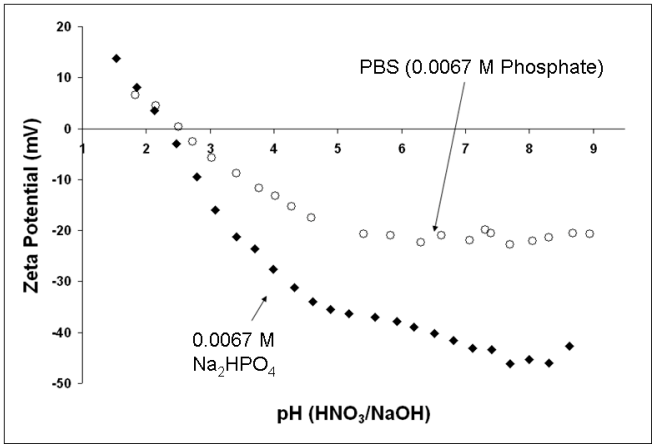

Figure 5.4.4.1. Zeta potential measurements indicate that phosphate is a potential determining ion for magnetite.

The molarity of the sodium phosphate was adjusted to the same molarity of phosphate in PBS and the pH was adjusted with indifferent electrolytes. The isoelectric point of the magnetite in water was measured at 6.1. A shift was noted in the charging behavior of the magnetite with the addition of either PBS or sodium phosphate. The isoelectric point for these solutions is around 2.5, which is near the lowest pK_a of phosphate and it appears that phosphate is a potential determining ion that adsorbs strongly to the magnetite surface. This change in charging behavior is observed even after a polymer stabilizer is added to the magnetite surface, and desorption of the polymer is due

to competitive adsorption between the phosphate in solution and the polyether anchor block.

One way to measure the stability of these materials in PBS is to measure the rate of aggregation over time with DLS. This allows the comparison across different types of anchor groups and different magnetite loadings. A comparison of anchor group stability in PBS is shown in Table 5.4.4.1.

Table 5.4.4.1. Rate of aggregation over 24 hours for complexes made with indicated anchor groups at 25°C in PBS.

Anchor Group	Molecular Weight (g/mol)	% Magnetite	Chains/nm^2	Slope in PBS (nm/hr)
Monocarboxylate	2,900	35	3.0	18.5
Tricarboxylate	3,400	30	3.4	17.7
Monocarboxylate	8,300	32	1.3	1604
Tricarboxylate	9,100	34	1.0	36.4
Monoammonium	2,900	33	3.3	999
Triammonium	3,400	31	3.2	227
Monammonium	8,300	21	2.3	3598
Triammonium	9,100	36	1.0	2.1
Monophosphonate	2,900	38	2.8	3.5
Triphosphonate	3,400	31	3.2	0.0
Monophosphonate	8,300	32	1.3	1.1
Triphosphonate	9,100	30	1.3	0.0

Three pieces of information can be drawn from Table 3. The first piece shows three anchor groups provide much better stability than one anchor group. This indicates a competitive adsorption of the phosphate salts can trigger anchor group desorption. Hence, the removal of more anchor groups should require more time, slowing the aggregation process. Secondly, the stability of the complexes made with carboxylate anchor groups was much better than those made with ammonium groups for one anchor group, but, for complexes made with three anchor groups, stability depended on PEO molecular weight. Finally, the phosphonate anchor groups are better than either the ammonium or carboxylate anchor groups, regardless of whether one or three anchor groups were used. The increased

stability of the monocarboxylate anchor groups appears to be due to a specific interaction between the carboxylic acid and the PEO. This behavior was inferred by comparing the predicted number average diameters from the density distribution model to DLS measurements as shown in Table 5.4.4.2.

Table 5.4.4.2. For mono-anchor complexes, comparison of predicted number average diameters to experimental diameters measured by DLS indicates a specific interaction for the carboxylic acid-functionalized PEO complexes.

Anchor Group	Molecular Weight (g/mol)	Magnetite Loading (%)	DLS D_n (nm)	Model D_n (nm)	% Difference
Carboxylate	2,900	35	20	29	43%
Ammonium	2,900	33	27	29	8%
Phosphonate	2,900	38	26	28	6%
Carboxylate	8,300	32	25	42	71%
Ammonium	8,300	23	44	46	4%
Phosphonate	8,300	32	40*	43	8%

*Initial measurement used due to flocculation in DI water

Previous studies have shown agreement between the density distribution model and DLS measurements to within 8% for both polyether-magnetite and polydimethylsiloxane-magnetite complexes.[11, 27] This level of agreement was observed in the present work for both the monoammonium and monophosphonate anchor groups. However, for the monocarboxylate anchor groups, the measured diameter was significantly smaller than the predicted model diameter. It appears that something about the carboxylate anchor group reduces the extension of the PEO brush away from the magnetite surface for both long and short PEO molecular weights. Table 5.4.4.1 indicates that shorter, denser brushes provide better stability against desorption of polymer from the magnetite surface. The interaction between the carboxylate anchor group and the PEO provides a denser brush than other anchor groups. This may be a significant reason for the better stability in PBS for the

carboxylate anchor group compared to the ammonium group for the same molecular weight.

The aggregation behavior for complexes made with the tricarboxylate and triammonium anchor groups are very different and show a striking dependence on anchor type and PEO molecular weight as shown in Figure 5.4.4.2.

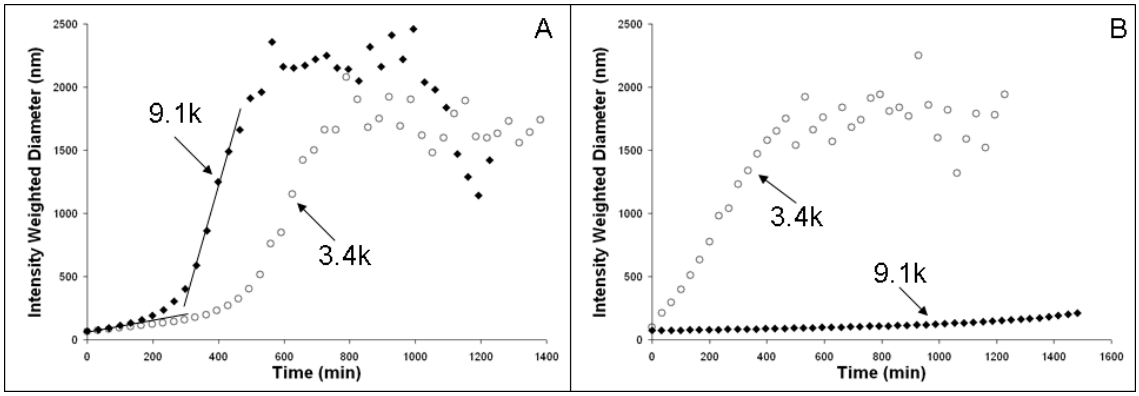

Figure 5.4.4.2. Aggregation for the complexes made with tricarboxylate anchor groups (A) indicates two distinct desorption mechanisms compared to the ammonium anchor groups (B).

For the tricarboxylate anchor groups, there are two distinct desorption steps whereas, for the triammonium anchor groups, there is one distinct slope. This provides further evidence of an interaction between the carboxylic acid group and the PEO brush. The three anchor groups initially provide significantly better resistance to desorption. However, after some polymer is removed, there is acceleration in aggregation rate, possibly due to an increased desorption rate caused by the anchor groups attached to a PEO chain interacting with a neighboring PEO chain and aiding in its desorption from the magnetite surface.

Another interesting aspect of Figure 5.4.4.2 was the relative stability of the triammonium-anchored complexes. For all of the other complexes, shorter and denser polymer brushes provide better colloidal stability in PBS. The reasoning was that when both complexes are at a magnetite loading of 30 wt %, there are more total chains of a smaller molecular weight species and thus, diffusion of phosphate to the surface is hindered. For the triammonium-anchored complexes, the 9,100 g mol^{-1} complex exhibits far greater stability than its 3,400 g mol^{-1} counterpart. Again, this anomalous behavior appears to be due to magnetite surface coverage by the anchor groups. In this case, the 3,400 g mol^{-1} triammonium complex with 31% magnetite loading has a surface coverage above 100%, as illustrated in Table 5.4.4.3.

Table 5.4.4.3. Surface coverage calculations for the ammonium anchor group explain stability behavior in PBS.

Anchor Group	Molecular Weight (g/mol)	% Magnetite	Number of Anchors	% Surface Coverage	Slope in PBS (nm/hr)
Monoammonium	2,900	33	773	48%	999
	8,300	23	445	28%	3598
Triammonium	3,400	31	2166	135%	227
	3,400	48	1056	66%	47
	9,100	36	648	40%	2.1

The ammonium anchor is significantly smaller than the phosphonate anchor (7.6 $Å^2$ vs. 18.2 $Å^2$), meaning there is significantly less surface coverage for these anchors by comparison. However, there are more anchors than available magnetite surface area for the 3,400 g mol^{-1} triammonium complex. This leads to free anchor groups that are not attached to the magnetite surface, which weakens the interaction between the polymer chain and the magnetite surface compared to the 9,100 g mol^{-1} complexes. We would then expect to observe a decrease in aggregation rate in PBS as the magnetite loading is

increased for the 3,400 g mol^{-1} complex. This behavior was indeed observed as the rate of aggregation in PBS was reduced from 227 to 47 nm h^{-1} when the magnetite loading was increased from 31 wt % to 48 wt %. This is the opposite to the behavior observed for triammonium-anchored complexes with a 7,200 g mol^{-1} stabilizer reported previously.[11] This confirms that the surface coverage is an important design parameter and also validates the method being used to at least qualitatively calculate the surface coverage for these anchor groups. To our knowledge, this correlation of particle stability with surface coverage by anchor groups has not been previously reported.

From the results for complexes with mono-anchor groups shown in Table 5.4.4.1, the complexes made with the zwitterionic phosphonate anchors exhibited less aggregation in PBS than did those made with ammonium or carboxylate chemistries. In order to overcome this problem, a tri-zwitterionic phosphonate was examined at various polymer loadings and molecular weights as shown in Table 5.4.4.4.

Table 5.4.4.4. Triphosphonate-anchored complexes show no appreciable aggregation in PBS over 24 hours.

Anchor Group	Molecular Weight (g/mol)	% Magnetite	Chains/nm^2	Slope in PBS (nm/hr)
Triphosphonate	3,400	35	2.7	0.0
Triphosphonate	3,400	36	2.6	0.0
Triphosphonate	3,400	42	2.0	0.0
Triphosphonate	3,400	45	1.8	0.0
Triphosphonate	3,400	55	1.2	0.0
Triphosphonate	3,400	56	1.1	0.0
Triphosphonate	3,400	66	0.6	0.0
Triphosphonate	9,100	30	1.3	0.0
Triphosphonate	9,100	49	0.5	0.0
Triphosphonate	9,100	68	0.2	0.0

No appreciable aggregation was observed for any of the tri-zwitterionic phosphonate-anchored complexes over 24 hours in PBS at various polymer loadings. The stability of these complexes is further supported by dialysis experiments, where each sample was

suspended in DI water, dialyzed against water for 24 hours, against PBS for 24 hours, and then against DI water again for 48 hours and the polymer desorption was measured using TGA.[14]

The amount of polymer desorption that occurs after the PBS dialysis is shown in Table 5.4.4.5. Significant desorption was observed for the monocarboxylate, tricarboxylate, monoammonium, and triammonium anchor groups after exposure to PBS. However, significant desorption was not observed for either the monophosphonate or triphosphonate anchor groups. Thus it appears that the aggregation measured over time by DLS combined with the dialysis data in Table 5.4.4.5 are effective ways to characterize the colloidal stability of the anchor groups used to attach the PEO to the magnetite nanoparticle.

Table 5.4.4.5. Polymer desorption can be quantified through dialysis against PBS.

PEO Molecular Weight ($g\ mol^{-1}$)	Anchor Group	Initial Polymer Loading after Dialysis against H_2O (Wt %)	Polymer Loading after Dialysis against PBS (Wt %)
2,900	Monocarboxylate	64.7 ± 0.9	40.7 ± 1.4
8,300	Monocarboxylate	68.4 ± 1.6	45.3 ± 1.4
2,900	Monoammonium	66.8 ± 0.8	41.0 ± 0.7
8,300	Monoammonium	77.1 ± 0.9	42.6 ± 0.7
2,900	Monophosphonate	63.3 ± 0.4	65.1 ± 1.4
8,300	Monophosphonate	70.2 ± 0.7	67.7 ± 0.7
3,400	Tricarboxylate	70.3 ± 0.7	25.0 ± 1.2
9,100	Tricarboxylate	66.2 ± 0.7	27.6 ± 1.4
3,400	Triammonium	69.3 ± 0.8	44.0 ± 0.8
9,100	Triammonium	64.2 ± 0.3	47.4 ± 0.8
3,400	Triphosphonate	69.0 ± 0.6	68.8 ± 0.4
3,400	Triphosphonate	34.5 ± 0.9	35.4 ± 0.5
3,400	Triphosphonate	57.6 ± 0.4	57.9 ± 0.3
3,400	Triphosphonate	55.0 ± 0.9	54.7 ± 0.8
3,400	Triphosphonate	44.0 ± 0.6	44.8 ± 0.5
3,400	Triphosphonate	45.3 ± 0.8	44.7 ± 0.1
9,100	Triphosphonate	32.3 ± 0.7	32.8 ± 0.7
9,100	Triphosphonate	70.5 ± 0.8	69.2 ± 0.8

5.5 Conclusions

Colloidal stability in DI water and PBS is a necessary first step towards the design of polyether-magnetite complexes for biomedical applications. As such, designing anchor groups that effectively adhere the polyethers to the magnetite surface is an essential part of obtaining colloidal stability in various aqueous media. Additionally, having a strong interaction between the anchor group and the magnetite allows for a reduction in the polymer loading necessary for sterically stabilizing the complex, which may allow for the maximization of the magnetite's magnetic properties for imaging or other applications.

Both mono- and tri-functional polyethers were synthesized with anchor groups containing carboxylic acid, ammonium, and zwitterionic phosphonate functionalities. These polyethers were attached to magnetite nanoparticles through these anchor groups and the stabilities of the polyether-magnetite complexes were measured in both DI water and PBS. All the complexes were stable in DI water for greater than 24 hours except for the monophosphonate-anchored complexes. These showed considerable aggregation, particularly as the magnetite loading was increased, indicating a specific interparticle interaction between the phosphonate anchor group of one complex and the magnetite of another. This aggregation was eliminated with the use of a triphosphonate anchor group, indicating that the critical parameter dictating aggregation is the magnetite surface that is occupied by the anchor group.

Both the carboxylate and ammonium anchor groups showed considerable aggregation in PBS due to polymer desorption. The amount of desorbed polymer was determined through TGA measurements made before and after dialysis of the complex

against PBS. Aggregation of the complexes was significantly reduced with the use of tri-functional anchors rather than mono-functional anchors. The phosphonate anchor groups showed significantly less aggregation than their carboxylate and ammonium counterparts, and the aggregation could be completely eliminated through use of a triphosphonate anchor group, regardless of the magnetite loading. This is a significant advance from previous work, which requires specific control of both molecular weight and magnetite loading to inhibit flocculation. Additionally, the triphosphonate complexes showed no significant polymer loss after dialysis against PBS, indicating that these complexes are indeed stable in PBS. The increased stability of these complexes is attributable to the large interaction energy between the magnetite and phosphonate, which is observed in the adsorption of phosphate to the magnetite surface through zeta potential measurements, and the aggregation of monophosphonate-anchored complexes due to an attraction between the phosphonate groups of one complex with magnetite of another.

Calculations of surface coverage were carried out using a simple method to estimate the size of an individual anchor group. Values obtained from this method were in good agreement with literature values for a phosphonate group. The surface coverage calculations were validated qualitatively through measurement of stability of monophosphonate-anchored complexes in DI water. Extrapolation of this method to ammonium groups was confirmed through stability measurements made in PBS. To our knowledge, this is a novel approach to exploring colloidal stability and the effect of anchor groups on that stability and might be applied to other polymer-particle systems.

Polyether-magnetite complexes have been synthesized and characterized showing long-term (24 hour) stability in both DI water and PBS. Additionally, these complexes are

made with a well-defined magnetite particle size distribution and a brush structure that is well-described by the density distribution model, allowing for fairly precise (within 8%) control of the average particle size. This should allow for the rapid development of biocompatible polyether-magnetite nanoparticles with properties specifically tailored for a desired application.

5.6 References

1 T. N. Bronich, H.; Eisenberg, A.; Kabanov, A., *Journal of the American Chemical Society* **122:**8339-8343 (2000).

2 C. J. Jung, P., *Magnetic Resonance Imaging* **13:**661-674 (1995).

3 O. T. Mefford, M. R. J. Carroll, M. L. Vadala, J. D. Goff, R. Mejia-Ariza, M. Saunders, R. C. Woodward, T. G. S. Pierre, R. M. Davis and J. S. Riffle, *Chemistry of Materials* **20:**2184-2191 (2008).

4 O. T. Mefford, M. L. Vadala, J. D. Goff, M. R. J. Carroll, R. Mejia-Ariza, B. L. Caba, T. G. S. Pierre, R. C. Woodward, R. M. Davis and J. S. Riffle, *Langmuir* **24:**5060-5069 (2008).

5 A. S. Thunemann, D.; Kaufner, L.; Pison, U.; Mohwald, H., *Langmuir* **22:**(2006).

6 K. S. Wilson, J. D. Goff, J. S. Riffle, L. A. Harris and T. G. St Pierre, *Polymers for Advanced Technologies* **16:**200-211 (2005).

7 Kabanov, A.; Bronich, T.; Kabanov, V.; Yu, K.; Eisenberg, A., *Advances in Genetics* **53:**231-261 (2005).

8 L. A. Harris, J. D. Goff, A. Y. Carmichael, J. S. Riffle, J. J. Harburn, T. G. St. Pierre and M. Saunders, *Chemistry of Materials* **15:**1367-1377 (2003).

9 P. Alexandridis and T. A. Hatton, *Colloids and Surfaces a-Physicochemical and Engineering Aspects* **96:**1-46 (1995).

10 P. P. Huffstetler, W. C. Miles, J. D. Goff, C. M. Reinholz, M. R. J. Carroll, R. C. Woodward, T. G. St. Pierre, R. M. Davis and J. S. Riffle, *Polymer Preprint* **49:**1103-1104 (2008).

11 W. C. Miles, J. D. Goff, P. P. Huffstetler, C. M. Reinholz, N. Pothayee, B. L. Caba, J. S. Boyd, R. A. Davis and J. S. Riffle, *Langmuir* **25:**803-813 (2009).

12 M. L. Vadala, M. S. Thompson, M. A. Ashworth, Y. Lin, T. P. Vadala, R. Ragheb and J. S. Riffle, *Biomacromolecules* **9:**1035-1043 (2008).

13 P. P. Huffstetler, W. C. Miles and J. D. Goff, et al. , *Polymer Preprints* **49:**1103-1104 (2008).

14 J. D. Goff, P. P. Huffstetler, W. C. Miles, N. Pothayee, C. M. Reinholz, S. Ball, R. M. Davis and J. S. Riffle, *Chemistry of Materials* **Accepted:**(2009).

15 J. Andrade, Hlady, V., Jeon, S., *Advanced Chem Ser* **248:**51-59 (1996).

16 W. M. Deen, *Analysis of Transport Phenomena (Topics in Chemical Engineering)*, Oxford University Press (1998).

17 Q. A. Zhang, M. S. Thompson, A. Y. Carmichael-Baranauskas, B. L. Caba, M. A. Zalich, Y. N. Lin, O. T. Mefford, R. M. Davis and J. S. Riffle, *Langmuir* **23:**6927-6936 (2007).

18 D. Bica, Vekas, L., Avdeev, M., Marinica, O., Socolluc, V., Balasolu, M., Garamus, M., *Journal of Magnetism and Magnetic Materials* **311:**17-21 (2007).

19 G. Storm, Belloit, S., Daemen, T., Lasic, D., *Advanced Drug Delivery Rev* **17:**31-48 (1995).

20 M. A. M. Tapan K. Jain, Sanjeeb K. Sahoo, Diandra L. Leslie-Pelecky, and Vinod labhaseOxidetwar, *Molecular Pharmaceutics* **2:**194-205 (2005).

21 M. S. Thompson, T. P. Vadala, M. L. Vadala, Y. Lin and J. S. Riffle, *Polymer* **49:**345-373 (2008).

22 A. F. Thunemann, D. Schutt, L. Kaufner, U. Pison and H. Mohwald, *Langmuir* **22:**2351-2357 (2006).

23 Y. Zhang, Kohler, N., Zhang, M., *Biomaterials* **23:**1553-1561 (2002).

24 J. Y. Park, E. S. Choi, M. J. Baek and G. H. Lee, *Materials Letters* **63:**379-381 (2009).

25 M. Chanana, S. Jahn, R. Georgieva, J. F. Lutz, H. Baumler and D. Y. Wang, *Chemistry of Materials* **21:**1906-1914 (2009).

26 E. R. Cintra, J. L. Santos, L. M. Socolovsky, N. Buske and A. F. Bakuzis, Field-induced flocculation on biocompatible magnetic colloids, in *8th Latin American Workshop on Magnetism, Magnetic Materials and Their Applications*, Rio de Janeiro, BRAZIL, pp. E351-E353 (2007).

27 W. C. Miles, J. D. Goff, P. P. Huffstetler, O. T. Mefford, J. S. Riffle and R. M. Davis, *Polymer* **Submitted:**(2009).

28 N. P. Caplan, D. Hayes and M. Blacksburn, *The Royal Society of Chemistry* **1:**421-437 (2000).

29 B. B. Yellen, Z. G. Forbes, D. S. Halverson, G. Fridman, K. A. Barbee, M. Chorny, R. Levy and G. Friedman, *Journal of Magnetism and Magnetic Materials* **293:**647-654 (2005).

30 W. C. Miles, J. D. Goff, P. P. Huffstetler, C. M. Reinholz, N. Pothayee, B. L. Caba, J. S. Boyd, R. M. Davis and J. S. Riffle, *Langmuir* **25:**803-813 (2009).

31 CRC Handbook of Chemistry and Physics. CRC Press, Boca Raton, FL (2006-2007).

32 L. J. M. Vagberg, K. A. Cogan and A. P. Gast, *Macromolecules* **24:**1670-1677 (1991).

33 S. L. Nolan, R. J. Phillips, P. M. Cotts and S. R. Dungan, *Journal of Colloid and Interface Science* **191:**291-302 (1997).

34 R. C. Plaza, J. de Vicente, S. Gomez-Lopera and A. V. Delgado, *Journal of Colloid and Interface Science* **242:**306-313 (2001).

35 A. Jusufi, M. Watzlawek and H. Lowen, *Macromolecules* **32:**4470-4473 (1999).

36 C. N. Likos, *Soft Matter* **2:**478-498 (2006).

37 P. Hiemenz and R. Rajagopalan, *Principles of Colloid and Surface Chemistry*, Marcel Dekker, Inc., New York (1997).

38 W. Russel, *The Phase Behavior and Dynamics of Colloidal Dispersions*, Princeton University, Department of Chemical Engineering (2001).

39 P. Guardia, B. Batlle-Brugal, A. G. Roca, O. Iglesias, M. P. Morales, C. J. Serna, A. Labarta and X. Batlle, Surfactant effects in magnetite nanoparticles of controlled size, in *Joint European Magnetic Symposia (JEMS 06)*, San Sebastian, SPAIN, pp. E756-E759 (2006).

Chapter 6: The Design of Amphiphilic Polyether-Magnetite Complexes for Enhancement of MRI Contrast and Cell Entry

Philip P. Huffstetler,[1,2] William C. Miles,[1,3] Jonathan D. Goff,[1,2] Christian M. Reinholz,[1,2] Matthew R.J. Carroll,[5] Michelle Gasko,[4] Tania Bronich,[4] Alexander Kabanov,[4] Robert C. Woodward,[5] Tim G. St. Pierre,[5] Richey M. Davis[1] and J. S. Riffle[2]

[1]Macromolecules and Interfaces Institute, [2]Department of Chemistry, [3]Department of Chemical Engineering, Virginia Tech, Blacksburg, Virginia 24061, USA, and [5]School of Physics, The University of Western Australia, Crawley, WA 6009, Australia

6.1 Abstract

Magnetite particles have many uses in biological systems including as contrast agents for MRI, drug delivery, hyperthermia treatments, and many more. Amphiphilic polyethers have shown promise as agents for drug delivery because of their ability to traverse cell membranes. This study is an effort to combine the advantages of both systems by adsorbing an amphiphilic stabilizer—consisting of poly(ethylene oxide)-b-poly(propylene oxide) diblock copolymers with varying molecular weights—to magnetite nanoparticles. The aim is to understand how to determine the optimum molecular weights for maximum relaxivity while still being able to infiltrate the cell. These results provide preliminary data to suggest that a hydrophobic interaction between the amphiphilic polyethers is present and that it may be the reason for increases in cellular uptake and relaxivity. Modeling of these complexes using a polymer brush model should provide a tool to allow for further understanding of these mechanisms.

6.2 Introduction

Superparamagnetic iron oxide nanoparticles (SPION) coated with biocompatible macromolecules have been of great interest due to a wide range of potential biomedical

applications including drug delivery, treatment of detached retinas, cell separations and contrast enhancement agents for MRI, where they have been studied intensely as T_2 contrast agents.[1-13] These SPIONs have been used for different tissues, including examining the liver, spleen, brain and many others.[10, 12-14] However, designing the complexes for controlled cellular uptake has continued to be a major hurdle.

PEO has been one of the most widely used coatings for magnetite nanoparticles due to its low cytotoxicity, ability to mask foreign substrates from the immune system, and FDA approval for *in vivo* applications.[1, 15, 16] Amphiphilic block copolymers (particularly Pluronics®) have shown potential for applications in drug delivery for multi-drug resistant cancer cells.[17-19] Through careful selection of the molecular weights of the blocks, the hydrophobic to hydrophilic ratio can be controlled, as can cellular uptake.[17-19] Small Angle X-Ray Scattering (SAXS) has been used to probe the interaction between a lipid bilayer mimicking a cell membrane and a Pluronic® triblock copolymer. These studies indicated that by carefully selecting the molecular weight of the hydrophobic copolymer (poly(propylene oxide) (PPO)), insertion of the Pluronic® into the cell membrane can be achieved.[20]

The approach of this work has been to combine the two systems, using magnetite to enhance contrast and an amphiphilic diblock copolymer to facilitate cell uptake. Poly(propylene oxide)-*b*-poly(ethylene oxide) (PPO-*b*-PEO) diblock copolymers were synthesized using an anionic living polymerization, allowing for precise control of molecular weight and the molecular weight distribution. The effect of polymer molecular weight and magnetite loading was explored by comparing the sizes of the complexes measured by dynamic light scattering (DLS) to calculated sizes for dispersed primary

particles from a polymer brush model developed by Vagberg, et al.[21] and further adapted to polymer-particle systems by Mefford, Miles, Huffstetler, and Goff et al.[3, 4, 22-25] The difference between the DLS measurements and the model provide a measure of the extent of aggregation of the particles which helps to explain significant relaxation measurements and cellular uptake measurements. This provides a tool to both design materials and to elucidate the mechanism by which increases in relaxivity and cellular uptake are achieved.

6.3 Experimental

6.3.1 Materials

Azobisisobutyronitrile (AIBN), benzyl alcohol (>98%), diethyl ether, diethyl vinyl phosphonate (97%), ethylene oxide (EO, 99.5+%), propylene oxide (>99%), hexanes (HPLC grade), iron (III) acetylacetonate ($Fe(acac)_3$), mercaptoacetic acid (97+%), oleic acid (90%, technical grade), sodium iodide (99%), triethylamine (TEA, 99.5%), and 1.0 M vinylmagnesium bromide in THF were purchased from Aldrich and used as received. d_6-Propylene oxide (99.8% deuterated) was obtained from polymer source and distilled just prior to use. Tetrahydrofuran (THF, Optima Grade, EMD Science, 99.5%) was refluxed over sodium metal with benzophenone until the solution reached a deep purple, fractionally distilled, and deoxygenated just prior to use. Glacial acetic acid (EMD Science) was diluted with THF yielding a 2.0 M acetic acid solution. Naphthalene (Aldrich) was sublimed prior to use. Bromotrimethylsilane (TMS-Bromide, 97%) and mecaptoethylamine hydrochloride were purchased from Alfa Aesar and used as received. Ethanol (Decon Laboratories Inc.) was used as received. Methanol (HPLC grade), chloroform (HPLC grade), N,N'-dimethylformamide (DMF, Optima Grade),

dichloromethane (HPLC grade), sodium bicarbonate, ammonium chloride, sodium chloride, and acetone (HPLC grade) were purchased from Fisher Scientific and used as received. 3-Chloropropyldimethylchlorosilane and 3-chloropropyltrichlorosilane was purchased from Gelest and used as received. Dialysis tubing (25,000 g mol^{-1} MWCO and 1,000 g mol^{-1} MWCO) was obtained from Spectra/Por. Phosphate buffered saline 10X (PBS) was obtained from Lonza and diluted to appropriate concentrations.

6.3.2 Synthesis of Polyether Stabilizers

A representative procedure for the synthesis of a deuterated-PPO-*b*-hydrogenated-PEO copolymer is provided. A 6,500 g mol^{-1} (48:52 EO:PO wt%) was initiated with 3-hydroxypropyltrivinylsilane (3-HPTVS). 3-HPTVS was synthesized using an adapted procedure by Vadala *et al.* PO (5 g, 0.087 mol) was syringed into a 300-mL pressure reactor with 5 mL of distilled THF. An initiator solution consisting of 3-HPTVS (0.25 g, 1.5 mmol), THF (5 mL), and ARCOL 3 catalyst (0.36 mL, 1.5 mg) was prepared in a separate round-bottom flask and vortexed for 15 min. The initiator solution was added to the pressure reactor via syringe. The reaction was heated to 105 ^{o}C, and the polymerization was conducted until a decrease in pressure was no longer observed (~2.5 h). The reactor was cooled and purged with nitrogen and the polymer was transferred to a round-bottom flask. The solvent was removed under vacuum and the polymer was dried under vacuum overnight at room temperature yielding trivinylsilyl-DPPO-OH. ^{1}H NMR revealed no molecular weight information and SEC revealed an M_n of 3,100 g mol^{-1} with a molecular weight distribution of 1.3.

Naphthalene (14.1 g, 0.11 mol) was sublimed and transferred to a 250-mL round-bottom flask and dissolved in THF (100 mL). Potassium metal (3.91 g, 0.10 mol) was

added to the resulting naphthalene solution and stirred overnight and titrated against 1.0 N HCl with bromophenol blue as the indicator to yield a 1.0 M potassium naphthalide solution. The trivinylsilyl initiated, hydroxy terminated DPPO (5 g, 1.6 mmol) was anionically initiated with a potassium naphthalide solution (0.9 mL) with THF (5 mL) in a 50-mL round-bottom flask. The mixture was added to a stirring 300-mL pressure reactor that was cooled with an isopropanol-dry ice bath, and that contained EO (5 g, 0.11 mol) and THF (10 mL). The reactor was allowed to warm to room temperature and stirred overnight. A stoichiometric amount of acetic acid was added to the reaction via syringe to terminate the reaction prior to its exposure to oxygen. The block copolymer was precipitated into cold ethyl ether and dried under vacuum at room temperature overnight yielding 9.1 g of polymer. ^{1}H NMR revealed an M_n of 6,500 g mol^{-1} (3,100 PPO and 3,400 PEO) and SEC showed an M_n of 6,300 g mol^{-1} with a molecular weight distribution of 1.2.

6.3.3 Functionalization of trivinylsilyl(PPO-b-PEO) and trivinylsilyl(PEO)

The vinylsilane terminus of the amphiphilic diblock copolymer or homopolymer was functionalized via an ene-thiol addition of cysteamine hydrochloride. Tri-vinylsilyl-DPPO-*b*-PEO-OH (2 g, 0.31 mmol) was dissolved in deoxygenated DMF (3 mL) at 60 ^{o}C in a 50-mL round-bottom flask. In a separate flask, cysteamine hydrochloride (137 mg, 1.3 mmol) was dissolved in DMF (1 mL) and added to the polymer. AIBN (26 mg, 0.15 mmol) was dissolved in DMF (0.5 mL) and added to the reaction and the mixture was deoxygenated for 20 min with N_2. The mixture was heated to 70 ^{o}C for 24 h. The mixture was dissolved in water (200 mL) and the block copolymer was extracted into methylene chloride (200 mL) to separate it from the excess cysteamine hydrochloride. The methylene

chloride layer was removed and more methylene chloride (200 mL) was added to further extract the polymer. This extraction was repeated 3x to ensure that the polymer was completely extracted from the water and the excess cysteamine hydrochloride was removed. The methylene chloride was removed via roto-evaporation and the polymer was again extracted from water with methylene chloride. The triammonium-PPO-*b*-PEO-OH polymer was dried at 50 ^{o}C under vacuum.

The triammonium-functionalized species were further utilized to add the phosphonate moiety as described in previous chapters.

6.3.4 Synthesis and Stabilization of Magnetite Nanoparticles with Trifunctional-(PPO-b-PEO)

Magnetite nanoparticles were synthesized using a thermal decomposition method adapted from Pinna *et al.*[12] A procedure for preparing a 33 wt% magnetite-copolymer complex is provided. Fe(III) acetylacetonate (2.14 g) was added to benzyl alcohol (45 mL) in a 250-mL three-neck round-bottom flask equipped with a stirring rod and water condenser. The mixture was sparged with N_2 for 1 h. The solution was stirred and heated to 100 ^{o}C and the temperature was increased to 205 ^{o}C over 4 h, and held at 205 ^{o}C for 24 h. The mixture was cooled to room temperature, centrifuged and the supernatant was discarded. The resulting particles were washed with acetone 3x, collected with a magnet and dried under N_2 for 1 h. The particles were diluted with chloroform (25 mL) and oleic acid (0.3 mL) was added to disperse the particles. Magnetite nanoparticles stabilized with oleic acid (50 mg) were dispersed in chloroform (10 mL) in a 50-mL round-bottom flask. Triamino-PPO-*b*-PEO-OH (100 mg) dissolved in chloroform (10 mL) was pipetted into the magnetite solution and sonicated for 16 h. The resulting magnetite-copolymer complex

solution was precipitated into hexanes (300 mL) to remove free oleic acid and the particles were collected with a magnet. The complexes were dried under N_2 at 25 °C, dispersed in DI water and dialyzed against water with a 25,000 g mol^{-1}-cut-off cellulose acetate dialysis bag, then the dispersion was lyophilized to concentrate the sample.

6.3.5 Characterization

^{1}H NMR spectral analyses of compounds were performed using a Varian Inova 400 NMR or a Varian Unity 400 NMR operating at 399.97 MHz. Size exclusion chromatography (SEC) was performed using an Alliance Waters 2690 Separations Module with a Viscotek T60A dual viscosity detector and laser refractometer equipped with a Waters HR 0.5 + HR 2 + HR 3 + HR 4 styragel column set. SEC data were collected in chloroform at 30 °C. Data were analyzed utilizing a Universal calibration made with polystyrene standards to obtain absolute molecular weights.

TGA was used to determine the polymer loading for each complex. TGA measurements were carried out on the PEO-magnetite nanoparticles using a TA Instruments TGA Q500 to determine the fraction of each complex that was comprised of polymer. Each sample was first held at 120 ºC for 10 min to drive off any excess moisture. The sample (10-15 mg) was then equilibrated at 100 ºC and the temperature was ramped at 10 °C min^{-1} to a maximum of 700 ºC in a nitrogen atmosphere. The mass remaining was recorded throughout the experiment. The mass remaining at 700 °C was taken as the fraction of magnetite in the complexes. The experiments were conducted in triplicate.

DLS measurements were conducted with a Malvern Zetasizer NanoZS particle analyzer (Malvern Instruments Ltd, Malvern, UK) at a wavelength of 633 nm from a 4.0 mW, solid-state He-Ne laser at a scattering angle of 173° and at 25 ± 0.1 ˚C. Number

average diameters (D_n) were calculated with the Zetasizer Nano 4.2 software utilizing an algorithm, based upon Mie theory, that transforms time-varying intensities to particle diameters.[26] For DLS analysis, the polymer-magnetite complexes were received dispersed in DI water and were diluted to ~0.05 mg mL^{-1} and filtered through a Whatman Anotop, 100-nm, alumina filter directly into a polystyrene cuvette. This corresponds to a volume fraction of 1.3×10^{-5} to 2.2×10^{-5} depending on the polymer loading on the magnetite. In experiments where the complex was exposed to PBS, 0.15 mL of 10X PBS was mixed with 1.35 mL of the 0.05 mg mL^{-1} complex solution, then the solution was filtered through either a 100 or 1000-nm filter into a clean polystyrene cuvette. Each sample was analyzed immediately following filtration and re-measured every 30 min over 24 h.

Relaxometry measurements were performed using a Bruker mq-60 minispec NMR Analyzer. Samples were diluted to specific concentrations between 0.01 and 0.0001 wt%. Each sample (0.4 mL) was transferred to a 7.5-mm glass NMR tube and sealed with parafilm. The sample tubes were placed in an aluminum block enclosed in a water bath at 37.5 °C for 30 min prior to relaxometry measurements. A Carl-Purcell-Meiboom-Gill (CPMG) spin echo sequence of 1000 echoes (echo spacing, TE, of 2 ms), and a repetition time of 15 s, was used to measure T_2.

6.3.6 Application of a brush model to the polyether-magnetite complexes

The incorporation of a non-solvated PPO shell surrounding the magnetite core was implemented to describe the brush behavior as shown in Figure 6.3.6.1.

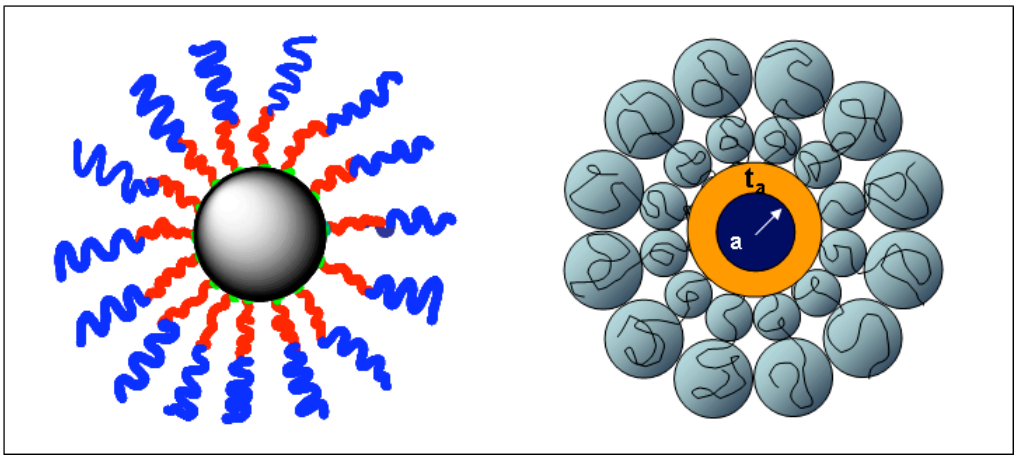

Figure 6.3.6.1. Cartoon depiction of a magnetite core, non-solvated PPO layer, and an extended PEO brush in concentric blobs extending out from the PPO surface.

The equivalent radii were graphed versus the probability of their occurrence and this histogram was fit with a Weibull probability distribution as shown in equation 6.3.6.1.

$$P(a) = \frac{c}{b}\left(\frac{a}{b}\right)^{c-1} \exp\left[\left(\frac{a}{b}\right)^{c}\right] \qquad (6.3.6.1)$$

Here, c is the Weibull scale parameter, b is the Weibull shape parameter, and a is the particle radius. The Weibull distribution has the advantage that it flexible. If b = 1, then P(a) reduces to an exponential distribution. If b = 3.4, P(a) reduces to a Gaussian distribution.

Hydrodynamic radii (R_m) of the magnetite-polymer complexes were calculated by the method of Mefford, et al.[3, 4] TEM image analysis data was first fitted with a Weibull probability distribution to calculate an average specific surface area of the magnetite

particles. Combining average surface area with the average polymer loading per mass of the complex (from TGA) leads to an average number of chains per magnetite surface area, α, as shown in Equation 6.3.6.2.[3]

$$\alpha = \frac{(1 - W_{mag}) N_{Av} \rho_{mag}}{3 M W_{Total} W_{mag}} \frac{\int_0^\infty a^3 P(a) da}{\int_0^\infty a^2 P(a) da} \qquad (6.3.6.2)$$

Here, ρ_{mag} is the density of magnetite (5.21 g cm^{-3}),[27] W_{mag} is the weight fraction of the complex that is magnetite, and MW_{Total} is the polymer number average molecular weight. The integral must be taken at this point to sum up the effect of the particle size distribution. This is because the measurement of the polymer mass via TGA is inherently an average measurement of the entire distribution. The assumption is made that each magnetite particle has the same ratio of magnetite to polymer, and so the average of the distribution must be taken at this juncture.

Using a modification of Vagberg's density distribution model,[21] we calculate the number of chains per particle, f(a), and the complex radius $R_m(a)$—the radius of the particle plus its attached brush –as

$$f(a) = 4\pi a^2 \alpha \qquad (6.3.6.3)$$

$$R_m(a) = \left(\frac{8 N_k f(a)^{\frac{1-\nu}{2\nu}}}{4^{1/\nu} 3\nu} L_k^{1/\nu} + a^{1/\nu} \right)^\nu \qquad (6.3.6.4)$$

where N_k is the number of statistical segments in the polymer brush chain, υ is the Flory exponent of the brush in the solvent, L_k is the length of a statistical segment, and a is the particle radius.

For complexes with an amphiphilic diblock copolymer, the hydrophobic layer was assumed to be a nonsolvated, hydrophobic shell surrounding the magnetite core and the brush was modeled as concentric blobs extending out from the surface of the PPO layer. To account for the hydrophobic layer, the model was adapted to include a new effective core size, which is the radius of the magnetite core obtained from the Weibull distribution plus the thickness of the hydrophobic anchor layer (t_a) (equation 6.3.6.5).

$$t_a = \left(\left(\frac{\rho_{mag} a^3 \left(1 - W_{mag}\right)}{W_{mag} MW_{anchor} \rho_{anchor} MW_{Total}} \right) + a^3 \right)^{1/3} - a \qquad (6.3.6.5)$$

Here, ρ_{anchor} is the density of the hydrophobic anchor layer, MW_{anchor} is the anchor layer number average molecular weight, and MW_{Total} is the total polymer number average molecular weight. Thus, the predicted hydrodynamic radius of the complex as a function of magnetite particle radius can be described by equation 6.3.6.6.

$$R_m(a) = \left(\frac{8 N_k f(a)^{\frac{1-\nu}{2\nu}}}{4^{1/\nu} 3\nu} L_k^{1/\nu} + (a + t_a)^{1/\nu} \right)^{\nu} \qquad (6.3.6.6)$$

This function along with the Weibull distribution function for the magnetite particle radius is used to determine radial distribution averages for comparison with DLS experimental data. Each average weights particles of various diameters differently and thus gives an

estimate of the homogeneity of the particle systems. The number average diameter, D_n, of the magnetite complex can be calculated as

$$D_n = 2\int_0^\infty R_m(a)P(a)da \qquad (6.3.6.7)$$

The volume average diameter, D_v, of the magnetite complex can be calculated as

$$D_v = 2\frac{\int_0^\infty R_m(a)^4 P(a)da}{\int_0^\infty R_m(a)^3 P(a)da} \qquad (6.3.6.8)$$

Using a method by Mefford, et al. and assuming the particles are in the Rayleigh scattering regime,[3] the intensity average diameter, D_i, for the magnetite complex was calculated as

$$D_i = 2\frac{\int_0^\infty R_m(a)^6 P(a)da}{\int_0^\infty R_m(a)^5 P(a)da} \qquad (6.3.6.9)$$

6.4 Results and Discussion

6.4.1Modeling and Stability in DI Water

Polyether-magnetite complexes were synthesized with varying molecular weights and both tri-zwitterionic phosphonate and triammonium functional anchor groups. ^{1}H NMR and SEC data for the diblock copolymers are shown in Table 6.4.1.1.

Table 6.4.1.1. ^{1}H NMR and SEC data for the amphiphilic diblock copolymers.

Polymer	M_n (g mol^{-1})			Molecular Weight Distribution
	^{1}H NMR of PPO	^{1}H NMR of PEO	GPC	
3.3kPPO-*b*-2.6kPEO-OH, Triammonium	3,300	2,600	5,400	1.3
3.3kPPO-*b*-4.8kPEO-OH, Triammonium	3,300	4,800	7,900	1.3
3kPPO-3kPEO-OH, Triphosphonate	3,000	2,900	6,100	1.1
3kPPO-5kPEO-OH, Triphosphonate	3,000	5,000	8,300	1.1

Molecular weights were targeted so that the effect of each anchor group could also be compared. For the magnetite complexes stabilized with polymers with triammonium anchors, referred to hereafter as the triammonium complexes, hydrodynamic diameters measured by dynamic light scattering (DLS) were compared to model predictions from the polymer brush model (Table 6.4.1.2).

Table 6.4.1.2. Comparison of DLS size measurements made in DI water at 25^{o}C to model predictions for the triammonium complexes.

Anchor Group	PPO Molecular Weight (g/mol)	PEO Molecular Weight (g/mol)	Magnetite Loading (%)	DLS D_n (nm)	Model D_n (nm)	% Difference
Triammonium	3,300	2,600	35	30.6	25.2	18%
Triammonium	3,300	2,600	34	31.4	25.5	19%
Triammonium	3,300	2,600	39	31.7	24.2	24%
Triammonium	3,300	2,600	41	27.5	23.4	15%
Triammonium	3,300	2,600	48	26.8	22.3	17%
Triammonium	3,300	2,600	50	28.4	21.9	23%
Triammonium	3,300	4,800	32	23.5	31.9	36%
Triammonium	3,300	4,800	41	26.4	29.3	11%
Triammonium	3,300	4,800	51	31.1	26.9	14%

For the 3.3kPPO-*b*-4.8kPEO-OH complexes, the DLS particle size increased with increasing magnetite loading. Aggregation appears to be occurring for the 3.3kPPO-*b*-4.8kPEO-OH complex as the magnetite loading is increased due to a reduction in the steric repulsion. However, for the 3.3kPPO-*b*-2.6kPEO-OH complexes, the particle size was essentially constant over all magnetite loadings. This may indicate an interaction between

PPO layers of neighboring complexes that prevents complete dispersion of the complex with an increased polymer loading. While there is significant deviation between the model and the DLS measurements for both complexes, the deviation was less for the 3kPPO-*b*-4.8kPEO-OH complexes for the two highest magnetite loadings. Similar trends were observed for the tri-zwitterionic phosphonate-anchored complexes (Table 6.4.1.3). For the 3kPPO-*b*-5kPEO-OH complexes, the values of D_n increased with the magnetite loading while no such trend was observed for the 3kPPO-*b*-3kPEO-OH complexes. At low magnetite loadings - 30-40% for the 3kPPO-*b*-3kPEO-OH complexes and 30% for the 3kPPO-*b*-5kPEO-OH complexes - these complexes match the brush model considerably better than did their ammonium counterparts. The model significantly underpredicts values of D_n in Table 6.4.1.2 for the triammonium complexes at low magnetite loadings. Since the model assumes that the PPO layer is nonsolvated, it may be that the PPO layer in the triammonium complexes is more solvated compared to the PPO layer in the triphosphonate complexes. This hypothesis is consistent with the results of small angle neutron scattering (SANS) experiments discussed below. It is worth noting that results from Chapters 4 and 5 show that the zwitterionic phosphonate anchor group introduces an interparticle electrostatic attraction while the triammonium anchor group does not. It is possible that triammonium anchor group also affects the solvation of the PPO layer in the diblock complexes in some way. The issue of solvation will be addressed in a later section.

Table 6.4.1.3. Comparison of DLS size measurements made in DI water at 25°C to model predictions for the tri-zwitterionic phosphonate anchored complexes.

Anchor Group	PPO Molecular Weight (g/mol)	PEO Molecular Weight (g/mol)	Magnetite Loading (%)*	DLS D_n (nm)	Model D_n (nm)	% Difference
Triphosphonate	3,000	2,900	35	27.6	28.0	1%
Triphosphonate	3,000	2,900	39	27.8	28.0	1%
Triphosphonate	3,000	2,900	41	26.2	25.3	3%
Triphosphonate	3,000	2,900	42	26.6	25.3	5%
Triphosphonate	3,000	2,900	55	27.2	23.1	15%
Triphosphonate	3,000	2,900	60	27.1	23.1	15%
Triphosphonate	3,000	5,000	36	35.3	31.4	11%
Triphosphonate	3,000	5,000	37	36.2	31.1	14%
Triphosphonate	3,000	5,000	41	40.3	30.0	26%
Triphosphonate	3,000	5,000	43	37.7	29.4	22%
Triphosphonate	3,000	5,000	47	42.3	28.4	33%
Triphosphonate	3,000	5,000	53	42.9	27.0	37%

*TGA measurements pending for the 3kPPO-*b*-3kPEO-OH complexes (values shown are targeted values)

Again, the size of the 3kPPO-*b*-3kPEO-OH complexes does not change with magnetite loading. It seems highly unlikely that the sizes would be constant for both the ammonium and tri-zwitterionic phosphonate complexes with the smaller PEO molecular weight just due to a reduction in steric repulsion. Indeed, for the 3kPPO-*b*-5kPEO-OH complexes, a significant increase in size is noted with an increase in magnetite loading. It may be that the PPO layers for the 3kPPO-*b*-3kPEO-OH complexes are interacting, generating a consistent particle size.

6.4.2. Colloidal Stability of diblock copolymer complexes

The use of these complexes in biological systems requires that they be stable when exposed to biological environments, particularly those with phosphate salts. Complexes made with the diblocks triammonium 3.3kPPO-b-2.6kPEO-OH and triphosphonate 3kPPO-b-3kPEO-OH (from Tables 6.4.1.2 and 6.4.1.3) show no increase in size over 24 hours in DI water. The molecular weights compared here are roughly the same. However, in PBS, the triammonium anchored complexes showed time-dependent aggregation as the magnetite loading was increased (Figure 6.4.2.1 A).

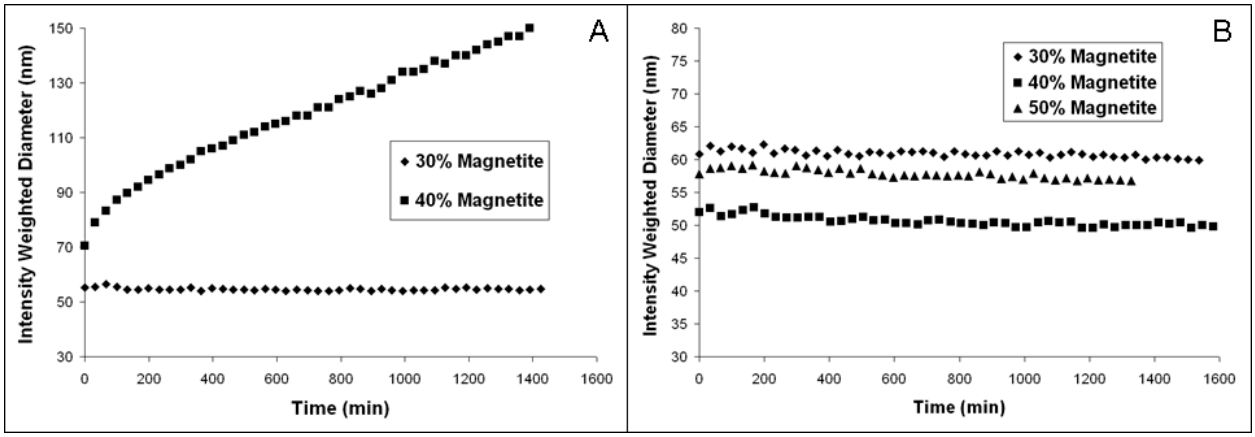

Figure 6.4.2.1. DLS of the triammonium 3.3kPPO-b-2.6kPEO-OH complex (A) and the triphosphonate 3kPPO-b-3kPEO-OH complex over time in PBS at 25°C.

By contrast, no aggregation was observed for the triphosphonate complexes, even with a reduction in polymer loading. The differences in size for the triphosphonate complexes are not very significant considering the intensity weighting. The number average diameters of these three complexes are roughly the same. This stability correlates well with dialysis data, which shows very little polymer desorption after dialysis in PBS for the triphosphonate complexes, but significant desorption for the triammonium complexes for varying molecular weights (Table 6.4.2.1).

Table 6.4.2.1. Polymer desorption before and after PBS dialysis for the polymer-magnetite complexes.

PPO Molecular Weight ($g\ mol^{-1}$)	PEO Molecular Weight ($g\ mol^{-1}$)	Anchor Group	Initial Polymer Loading after Dialysis against H_2O (Wt %)	Polymer Loading after Dialysis against PBS (Wt %)
3,000	3,000	Triphosphonate	64	64
3,000	5,000	Triphosphonate	65	64
3,300	2,600	Triammonium	62	51
5,600	3,800	Triammonium	64	44
5,600	7,200	Triammonium	64	46

Slight aggregation can be measured by measuring the rate at which the size increases over time. The triphosphonate-anchored 3kPPO-5kPEO did show small amounts of aggregation in PBS (between 0.2 – 0.7 nm h^{-1}). However, because no there was no detectable level of polymer desorption, we believe that this aggregation may be due to an attractive force between the phosphonate anchor groups of one complex with the magnetite of another complex, as discussed in detail in Chapter 5.

6.4.3. Solvation of the hydrophobic poly(propylene oxide) (PPO) Layer

As described in previous chapters, the existing extension of the density distribution model can predict the primary particle size of various polymer-magnetite complexes to within 8% over a wide range of magnetite loadings for PEO homopolymers. Additionally, the calculated half-life for doublet formation ($t_{1/2}$) can be used to predict, in some cases, particle aggregation and thus correlations between the particle size and magnetite loading can be made. This predictive tool makes it possible to compare complexes with different polymer molecular weights, loadings, and even different types of polymers.

For studies involving a hydrophobic polymer block, the modeling strategy has been to incorporate the PPO layer as a non-solvated shell while the PEO chains extend out into solution.[28, 29] Typically, hydrophobic layers have been treated as essentially melts completely covering the surface.[30] However, a growing body of evidence indicates that this may not be the case, particularly at elevated temperatures or in mixed solvents.[31-33] SANS is a powerful technique for probing the solvation of polymer layers attached to colloidal particles.

6.4.4. Small Angle Neutron Scattering to Determine PPO Solvation

Neutron scattering is analogous to light scattering, especially in the calculation of structure factors and scattering vectors. While light scattering relies on interactions in the electron cloud, neutron scattering relies on interactions between the neutrons and the atomic nucleus. These nuclear interactions are more short-range than interactions with electrons. This means neutron scattering has the main advantage of an increased penetration depth due to the small interaction range. However, this also means that neutrons are only weakly scattered. Weak scattering combined with the fact that neutron beams typically have much lower flux compared to electron beams means that neutron scattering is a signal-limited technique. This means that no one instrument can be used to study all neutron scattering and so a large array of instruments have been developed to study neutron scattering.[34, 35]

Small angle neutron scattering (SANS) is one of these techniques and is used to probe molecular structures at the nanoscale. The angles in SANS typically vary from 0.2º-20º which corresponds to a scattering vector (q) range of 0.001 $Å^{-1}$ to 0.45$Å^{-1}$ and d-spacings of 14Å – 6,300Å. A principal advantage of SANS is the ability to use deuterium-labeled samples to increase contrast.[35]

Neutron scattering is based on the scattering length densities of the material, which is the ratio of the scattering length per molecule and the molecular volume of the material.[35] Table 6.4.4.1 shows scattering length densities for some relevant materials for this study.[36]

Table 6.4.4.1. Neutron scattering length densities for relevant materials.[36]

Material	SLD (_10^{-6} Å^{-2})
Magnetite	6.97
H_2O	-5.58
D_2O	6.38
DPPO-PEO	5.06
PPO-PEO	1.51

Water and deuterated water are on opposite ends of the scattering length density spectrum. Also, the deuterated and non-deuterated polymers also show significant differences. Thus, through mixing the solvents in different ratios, different scattering patterns can be obtained.

For this study, magnetite complexes were made with two different diblock copolymers, each with triammonium anchor blocks: a 3.3kPPO-*b*-2.6kPEO-OH block copolymer and a 3.1kDPPO-*b*-3.4kPEO-OH block copolymer, where again DPPO is used to describe a deuterated PPO block. The details of the synthesis and characterization of the 3.3kPPO-*b*-2.6kPEO-OH block copolymer were given in previous chapters, and the synthesis of the deuterated diblock copolymer follows the same general procedure using a deuterated PO monomer. Due to differences in the scattering length density of the polymers, different scattering patterns should emerge. Figure 6.4.4.1 depicts the scattering that would be expected from each polymer coating in 100 % water.

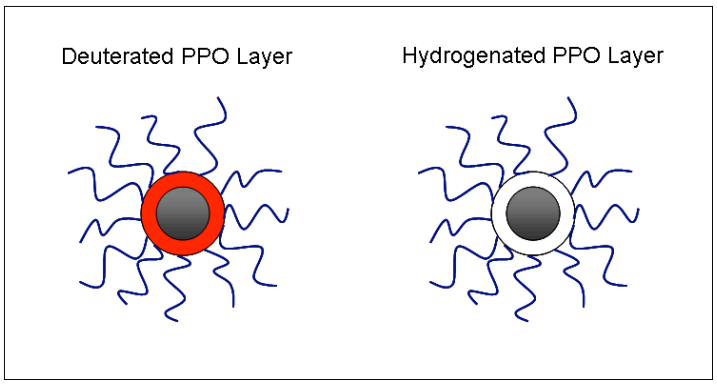

Figure 6.4.4.1. The difference in scattering in 100% H_2O between a magnetite complex with an attached non-solvated, deuterated PPO layer and a complex with a nonsolvated, hydrogenated PPO layer.

Because the deuterated polymer has such a high scattering length density compared to the hydrogenated polymer, there is much more contrast between the solvent (water) and the deuterated polymer. Also, there is a high level of scattering from the magnetite. Thus, the scattered intensity for the hydrogenated polymer should be significantly less than for the deuterated polymer. In this case, the PEO layer is so solvated that the effective scattering length density is very close to the solvent. By mixing H_2O and D_2O, the scattering intensities of each component change based on the match between the component scattering length density and the solvent scattering length density. This is analogous to light scattering in that no scattering occurs if the refractive index of the solvent matches that of the material.

SANS was performed at the National Institute for Standards and Technology in Gaithersburg, Maryland using the neutron guide 7 (NG-7), a 30 m SANS instrument that measures artifacts ranging from 1-500 nm. The measurements were carried out at a polymer-magnetite complex concentration of approximately 10 mg mL^{-1} while varying the D_2O:H_2O ratio from 0 to 100 in 20% increments. Measurements were taken at three

scattering distances (1, 4, and 13 meters) and a composite figure was assembled using IGOR Pro 5 software.

Figure 6.4.4.2 shows the SANS results for both diblock copolymer-magnetite complexes. The target composition for each complex was 35% magnetite - TGA determined the deuterated complex was 35% and the hydrogenated complex was 37% magnetite.

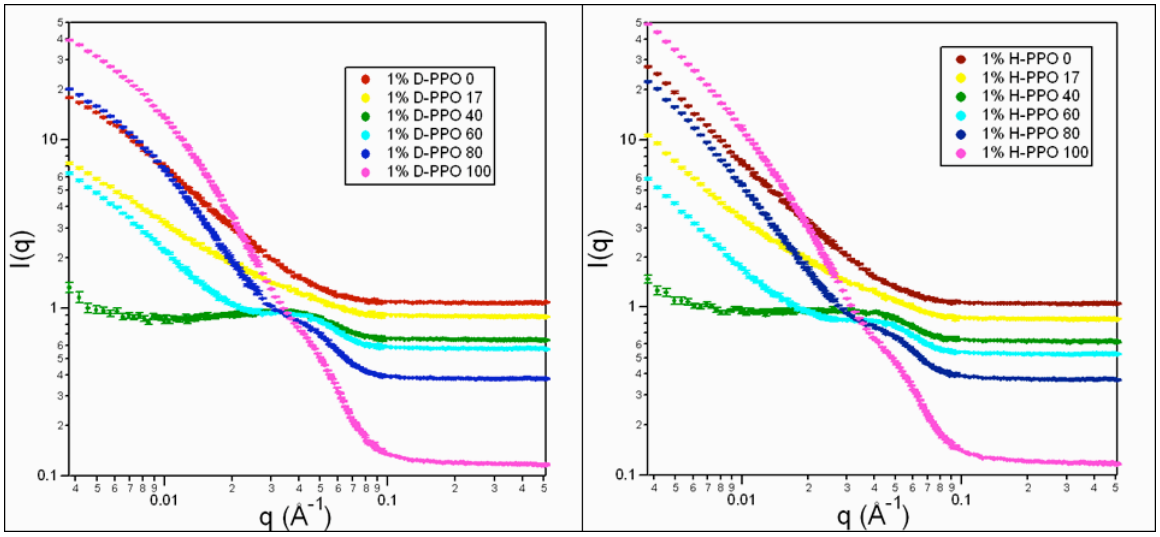

Figure 6.4.4.2. SANS data for magnetite complexes stabilized with the 3.1kDPPO-b-3.4kPEO-OH (left) and 3.3kPPO-b-2.6kPEO-OH (right) block copolymers at the indicated H_2O/D_2O ratios.

The most striking result from Figure 6.4.4.2 is that there are practically no significant differences between the scattering patterns. This indicates that the only significant scattering taking place is from the magnetite nanoparticles. The only way that both the hydrogenated and deuterated PPO could exhibit the same scattering pattern is if they are heavily solvated. The solvation of the PPO layers would cause the average

scattering length density of the PPO layer to approach that of the solvent. That appears to have happened as the scattering patterns from each complex are virtually identical.

The most significant difference in the scattering patterns in Figure 6.4.4.2 occurs at low values of the scattering vector q, where, for some of the H_2O/D_2O ratios, the slopes of the complexes made with the deuterated diblock are less than those of the complex made with the hydrogenated diblock. At low q values, the scattering intensity I(q) typically levels off at values corresponding to the size of the largest aggregate in solution. The lower slopes of the I(q) vs q plots for the complexes made with the deuterated diblock suggest that they are less aggregated than those made with the hydrogenated diblock. This would be consistent with the trend discussed earlier, where for the same molecular weight PPO block, an increase in the PEO molecular weight decreased the equilibrium cluster size.

To probe the aggregation effect further, the hydrodynamic diameters of the complexes were measured using dynamic light scattering at 0.05 mg/mL after filtration with a 100 nm Whatman Anotop aluminum oxide filter, and these results are shown in Table .

Table 6.4.4.2. DLS of SANS samples shows similar results to other diblock copolymer complexes.

Sample	% Magnetite	Solvent	D_i (nm)	D_v (nm)	D_n (nm)
3.1kDPPO- *b*-3.4kPEO-OH	35	H_2O	64.6	39.6	30.7
3.1kDPPO- *b*-3.4kPEO-OH	35	D_2O	49.3	32.5	24.7
3.3kPPO- *b*-2.6kPEO-OH	37	H_2O	51.8	34.6	26.0
3.3kPPO- *b*-2.6kPEO-OH	37	D_2O	48.2	32.4	25.0

As illustrated in Table 6.4.4.2, the value of D_n of the complex made with the deuterated diblock is essentially the same as the size of the hydrogenated diblock, which is

the same result as shown in Table 6.4.2.1 and Table 6.4.2.2. This latter comparison provides a useful consistency check. There is a slightly larger size for the deuterated polymer in H_2O, but the number average diameter is not much larger, indicating that the flocculation observed is rather minimal. Thus, it appears that the differences observed in the slopes of the SANS data are either not a function of the aggregation behavior of the samples or that the SANS is more sensitive to aggregation than the DLS.

To probe the solvation of the PPO block further, the sizes of selected complexes made with fully hydrogenated diblocks described in Tables 6.4.2.1 and 6.4.2.2 were measured by DLS as a function of temperature. Since PPO becomes more hydrophobic (less solvated by water) as the temperature is increased, it was hypothesized that a change in the solvation of the PPO layer could affect the particle size as the temperature is increased (Figure 6.4.4.3).

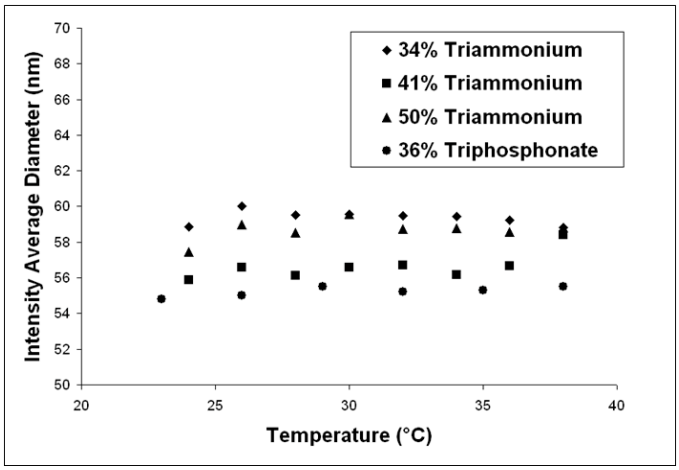

Figure 6.4.4.3. DLS measurements of magnetite complexes made with hydrogenated diblocks with triammonium and triphosphonate anchors at various wt% polymer loadings in 100% H_2O.

No change in diameter was observed for temperatures ranging from 22-38 °C. While this is not a definitive test of PPO solvation, it does indicate that whatever changes occur in the degree of solvation of the PPO layer are not sufficient to appreciably alter the complex diameter.

6.4.5 QCM-D to Compare Adsorption of Various Polymer Brushes

In order to further probe the issue of the solvation of the PPO block, the adsorption of PPO-PEO diblocks was compared to that of PEO homopolymers that were adsorbed onto magnetite-coated crystals in a quartz crystal microbalance with dissipation monitoring (QCM-D). QCM-D is advantageous over QCM in that the dissipation of the film can be measured with the former, but not with the latter. The dissipation factor is determined by the damping effect of the film on the quartz crystal that slows the oscillation after the voltage is cut off. In essence, the dissipation factor is the energy dissipated per oscillation per the total energy stored in the system. Thus, direct comparison of the dissipation of two different materials does not require any viscoelastic modeling. This dissipation can be related to the rigidity (in terms of the viscoelasticity and elastic modulus) of the adsorbed polymer film.[37, 38] It was hypothesized that, if a PPO-*b*-PEO-OH diblock copolymer is completely solvated, that should be observable using QCM-D technology as a similar change in dissipation to a PEO-OH homopolymer with a similar molecular weight to that of the total diblock. This was done using a Q-Sense E-4 system in conjunction with an Ismatec IPC centrifugal pump flowing the polymer solution through titanium flow cells containing iron oxide coated quartz crystals at 25 ± 0.1° C.

This experiment compared the adsorption of a triammonium-terminated 5kPEO-OH homopolymer (D.P. ~ 113) and a triammonium-terminated 3.3kPPO-*b*-2.6kPEO-OH

diblock copolymer (D.P. ~ 116) by adsorption of the polymer from solutions flowed past the crystals in the E-4 flow cell. The 5kPEO-OH homopolymer was synthesized as described in previous chapters had a molecular weight distribution of approximately 1.1. Figure 6.4.5.1 shows the adsorption characteristics of each polymer on a quartz crystal sputter coated with Fe_3O_4 and cleaned with oxygen plasma. Each polymer was introduced to the QCM crystal in the E-4 flow cell at a concentration of 30 μg mL^{-1} and a flow rate of 500 μL min^{-1}.

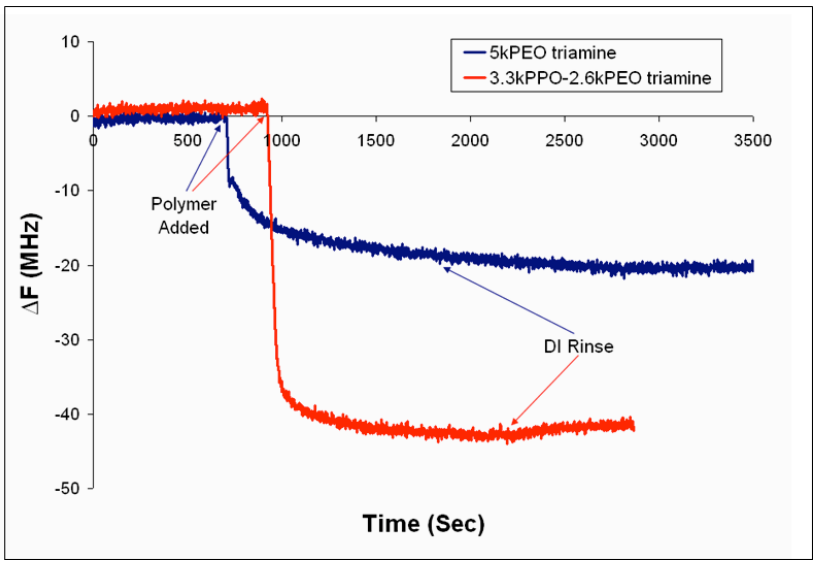

Figure 6.4.5.1. Adsorption of the triammonium-terminated 5kPEO-OH homopolymer and 3.3kPPO-b-2.6kPEO-OH diblock copolymer from DI water at 25°C onto an Fe_3O_4-coated quartz crystal. The level of the adsorption of the diblock is about twice that of the homopolymer.

Note that far more diblock copolymer adsorbed to the iron oxide surface than the homopolymer (0.25 and 0.14 chains nm^{-2} and 2.5 and 1.2 mg m^{-2}, respectively) and that the adsorption kinetics are significantly quicker for the diblock also. This is most likely due to the affinity of the PPO layer to the iron oxide surface compared to the thermodynamics of staying in solution. The higher adsorbed amount for the diblock means

that there should be more steric repulsion between polymer chains for the diblock than for the homopolymer, very likely producing a more rigid film and a smaller change in the dissipation factor. However, because the thickness was not independently measured, this may not be the case. Additionally, a non-solvated layer at the iron oxide surface should also generate a more rigid film and a smaller change in dissipation factor. However, Figure 6.4.5.2 shows that the dissipation factors for both the 5kPEO-OH homopolymer and 3.3kPPO-*b*-2.6kPEO-OH diblock copolymer are virtually the same.

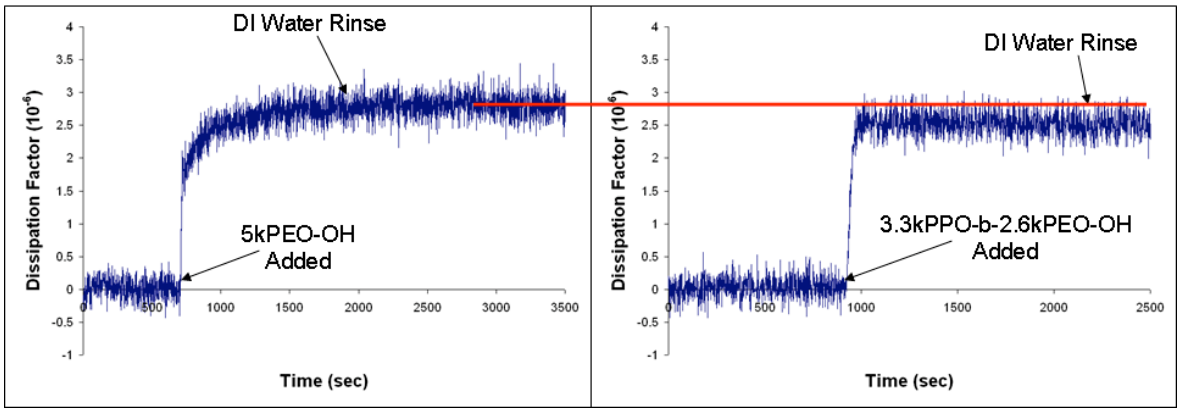

Figure 6.4.5.2. Adsorption of the triammonium-terminated 5kPEO-OH homopolymer and 5.6kPPO-*b*-3.8kPEO-OH diblock copolymer from DI water at 25°C onto an Fe3O4-coated quartz crystal. The dissipation factor of both polymers is nearly the same.

This is consistent with the hypothesis that the PPO layer is at least somewhat solvated. Otherwise, the dissipation factor would be considerably less with such a small hydrophilic block extending out from a non-solvated layer. Each polymer has approximately the same degree of polymerization, and so there should be a difference in the rigidity of the film were the PPO layer not somewhat solvated.

To probe the effect of diblock composition, the change in frequency and dissipation for a 5.6kPPO-*b*-3.8kPEO-OH diblock copolymer (D.P. ~ 183) was also measured (Figure 6.4.5.2).

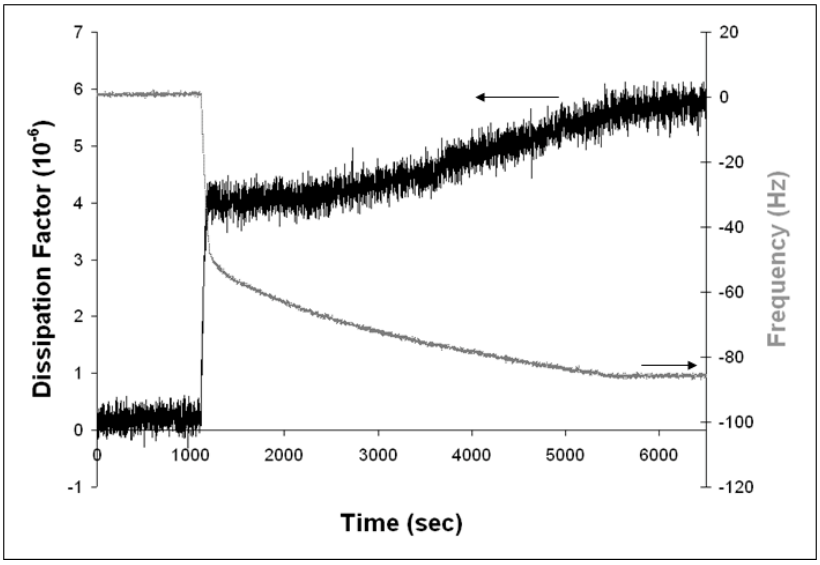

Figure 6.4.5.3. Adsorption of the triammonium-terminated 5.6kPPO-b-3.8kPEO-OH diblock copolymer from DI water at 25°C onto an Fe_3O_4-coated quartz crystal. The dissipation factor is much higher than the dissipation for the polymers shown in Figure 6.4.5.1.

Note that the dissipation factor is more than twice that for the polymers shown in Figure 6.4.5.1, indicating a much softer film. Note also the adsorbed amount is about twice that of the 5.6kPPO-b-3.8kPEO-OH diblock copolymer. Since the PEO block is fairly short (DP = 86), it appears that the PPO block is also solvated for this polymer. While the QCM-D is sensitive enough to detect differences in the dissipation, it should be noted that these measurements do not confirm solvation of the layer, but merely point towards that possibility. Use of a technique such as neutron reflectivity would likely be a more definitive measure of the solvation of the PPO layer on a flat surface. Additionally, these polymers were adsorbed onto the iron oxide crystals from water while the polyethers are

adsorbed onto the magnetite nanoparticles in chloroform. This most likely affects the brush density, as there may be significant electrostatic interactions between the charged anchor groups in water that would not be significant in a low dielectric constant medium such as chloroform. This is illustrated by the typical magnetite nanoparticle, which for 30% magnetite loading has approximately 10 mg of polymer per square meter, compared to 2.5 mg m^{-2} and 1.2 mg m^{-2} for the 3.3kPPO-*b*-2.6kPEO-OH complex and 5kPEO-OH complex, respectively.

6.4.6 Relaxation behavior of diblock copolymer complexes

A major advantage of magnetite clusters as opposed to larger particles of magnetite is that the clusters should retain their superparamagnetic behavior, but be affected much more strongly by an applied magnetic field. Thus, the cluster can be manipulated in ways that a 10 or 20 nm superparamagnetic particle cannot, but does not exhibit ferromagnetic behavior below the Curie temperature. A magnetic component can be incorporated into the extended DLVO theory as an attractive term and is calculated as shown in equation 6.4.6.1.

$$V_M = \frac{8\pi\mu_o a^3 M^2}{9\left(\frac{h}{a}+2\right)^3} \qquad (6.4.6.1)$$

Here, a is the particle radius, M is the magnetization (saturation value of 345,000 A/m), μ_o is the magnetite permeability in vacuum (1.26e-6 Tm/A), and h is the surface to surface separation of two particles.[39, 40] Equations 6.4.6.2 and 6.4.6.3 adjust the magnetic potential for systems of clusters where there is space between the particles where x_{mag} is

the mass fraction of magnetite, x_{in} is the mass fraction of interstitial space, and ρ_{in} is the density of the interstitial space.

$$V_M = -\frac{8\pi\mu_o (x_{mag} a)^3 M^2}{9\left(h/(x_{mag} a) + 2\right)^3} \qquad (6.4.6.2)$$

$$\rho_{cluster} = x_{mag}\rho_{mag} + x_{in}\rho_{in} \qquad (6.4.6.3)$$

For this particular treatment, the cluster was assumed to be hexagonal close packed and 74% of the interior cluster volume, with the other 26% attributed to the polymer. Using the methodology for the modified DLVO theory, Figure 6.4.6.1 illustrates how the range of the van der Waal's potential and magnetic potential change as the number of particles in the cluster increase as the number of magnetite particles in the cluster, n, increases.

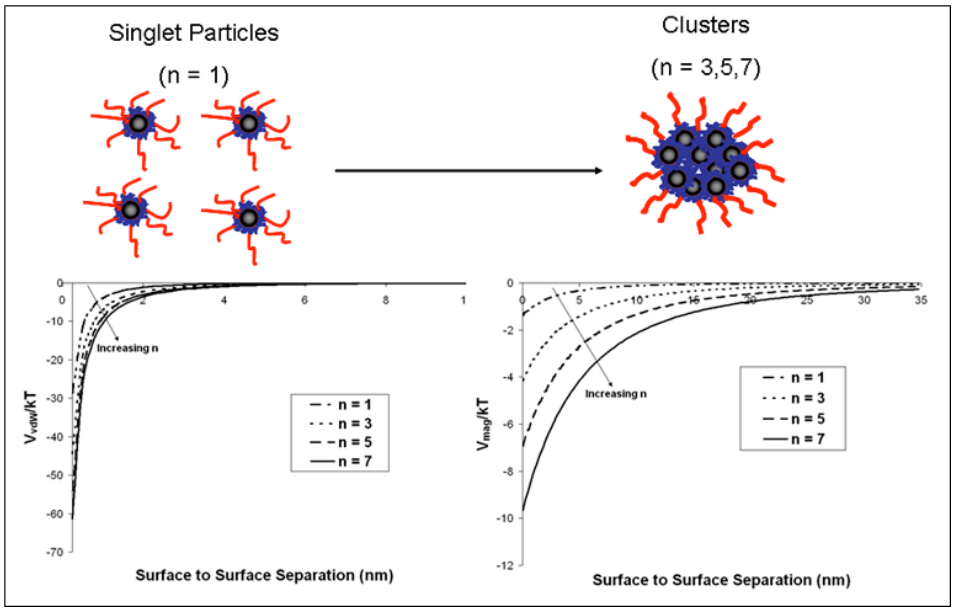

Figure 6.4.6.1. Modified DLVO potential energy diagrams for polymer-stabilized magnetite particles and clusters. In the latter, the number of magnetite particles per cluster, n, is varied. The range of the magnetic potential increases (right) but the range of the van der Waal's potential does not (left) as n increases.

While the assumption of hexagonal close packing may overestimate the volume fraction of magnetite in a cluster, the principle remains that the *range* of the magnetic force *increases* while the range of the van der Waal's force does not. This means that formation of a magnetite cluster of a particular size allows for tuning of the colloidal stability with an external field, as shown in Figure 6.4.6.1. A secondary potential energy minimum can be induced when a magnetic field is applied. However, this potential energy diagram also indicates that when the magnetic field is removed, the particles should redisperse in solution due to Brownian motion.

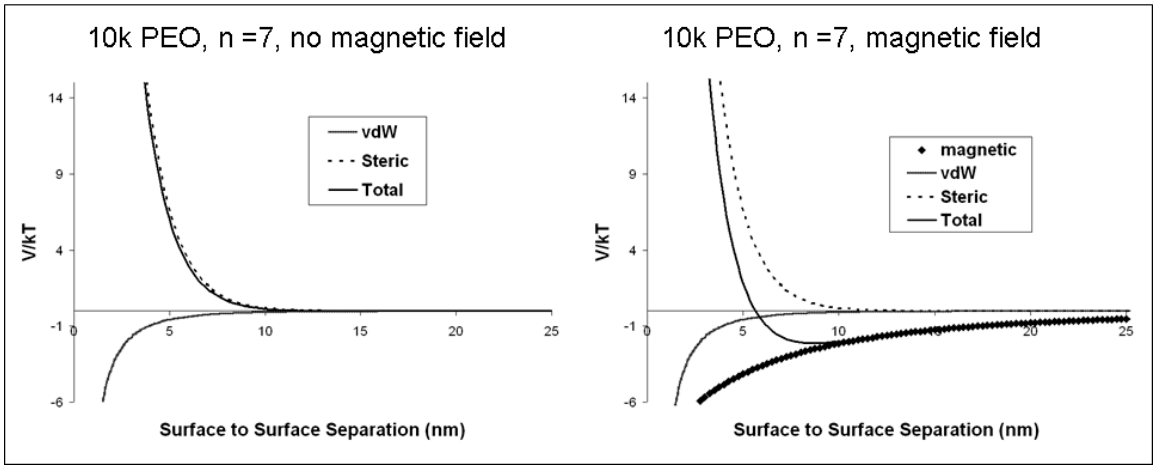

Figure 6.4.6.2. A secondary potential energy minimum can be induced by a magnetic field when the cluster size gets large enough (assumes 10kPEO with a surface coverage of 1 chain nm^{-2})

Additionally, the T_2 relaxation can be affected by aggregation of the magnetic particles. Roch et al. studied the effect of aggregation on the T_2 relaxation and found that the relaxation rate increases with the radius as shown in equation 6.4.6.4.

$$\frac{1}{T_2} = \frac{16 f_a \Delta\omega R_a^{\ 2}}{45D} \qquad (6.4.6.4)$$

Here, f_a is the volume fraction occupied by the clusters, $\Delta\omega$ is the difference in angular frequency between the local field and the bulk, R_a is the cluster radius, and D is the diffusion coefficient of water.[41]

However, when the size of the magnetic sphere gets too large and the translational diffusion time is longer than a diffusion time denoted $\tau_L=(1.49/\Delta\omega)x^{1/2}(1.52+f_a x)^{5/3}$, the relaxation rate then decreases with the particle radius as shown in equation 6.4.6.5, where $x = \Delta\omega(TE/2)$ and TE is the repetition time of the 90° radio frequency pulse .[41]

$$\frac{1}{T_2} = \frac{1.8 f_a x^{1/3}(1.52 + f_a x)^{5/3} D}{R_a^{\ 2}} \qquad (6.4.6.5)$$

T_2 relaxation can also be increased through inhomogeneities in a magnetic field.[42, 43] Figure 6.4.6.2 illustrates how a magnetite particle can significantly alter the local magnetic field and how even just a small cluster ensures that the magnetic field is extremely inhomogeneous, speeding up dephasing of the protons' angular momentum.

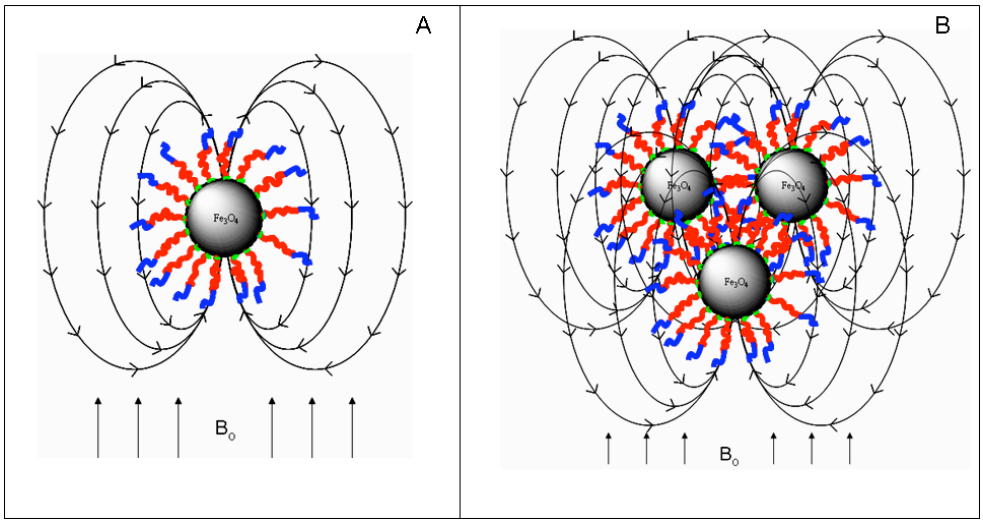

Figure 6.4.6.3. The local magnetic field becomes extremely homogeneous even for small magnetic clusters.

At this point, only the relaxation behavior of the ammonium diblock complexes has been measured. However, it is worth looking at the colloidal stability and size of a homopolymer complex first, this one with tri-zwitterionic phosphonate anchors (Figure 6.4.6.2).

Figure 6.4.6.4A shows potential energy diagrams for each of the three polymer loadings and Figure 6.4.6.4B shows the relaxation data in conjunction with DLS measurements. Typical commercial relaxation agents exhibit R_2 relaxivities far below those shown by these complexes (107, 53, and 72 (s-mM Fe)$^{-1}$ for ferrumoxides, ferrumoxtran, and ferumoxsil, respectively).[11]

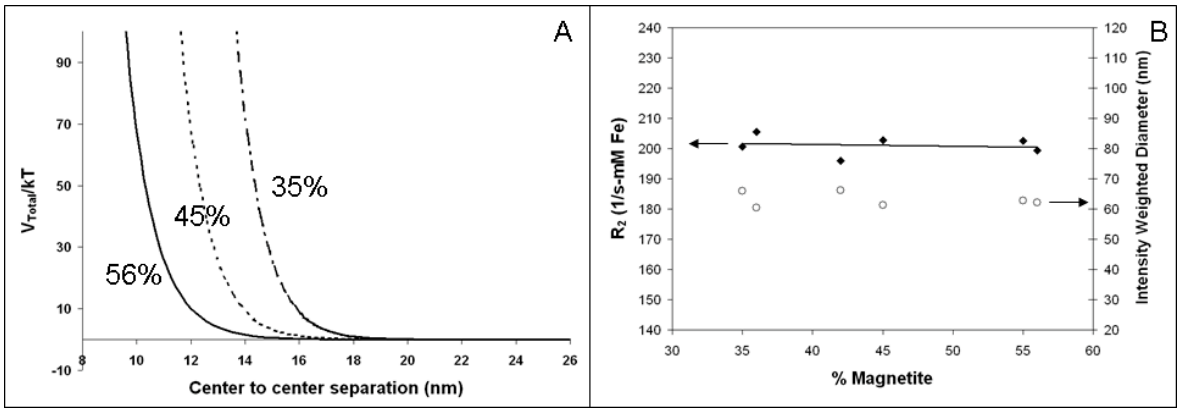

Figure 6.4.6.4. Tri-zwitterionic phosphonate-anchored 3.4kPEO-OH complexes in DI water at 25°C – modified DLVO energy diagram as a function of wt% polymer loading (A) and relaxivities and DLS intensity weighted hydrodynamic diameters (B).

The potential energy diagram predicts that none of the materials should aggregate at all, and this is observed with very little change in diameter with reduction in polymer loading. The DLS measurements are in good agreement with the model and indicate that the complexes are primary particles. Additionally, there is almost no change in relaxivity of the materials (note that this measurement is per mM iron) with a reduction in polymer loading. This is not the case for the diblock complexes, whose relaxation behavior is illustrated in Figure 6.4.6.4.

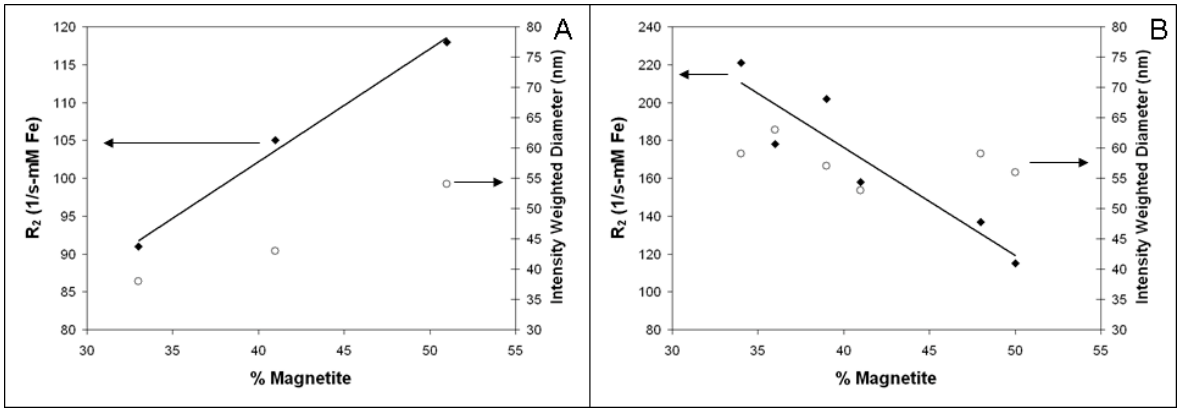

Figure 6.4.6.5. Relaxation behavior for triammonium 3.3kPPO-b-4.8kPEO-OH (A) and 3.3kPPO-b-2.6kPEO-OH (B) complexes.

Opposite trends are observed here - the 3.3kPPO-*b*-4.8kPEO-OH complex shows an increase in relaxation with a decrease in polymer loading while the 3.3kPPO-*b*-2.6kPEO-OH complex shows an increase in relaxation with an *increase* in polymer loading. Again, the relaxivity of 220 is more than twice that reported in the literature for commercially available materials.[11] From the light scattering data for the 3.3kPPO-b-4.8kPEO-OH complexes, it appears that reducing the polymer loading causes an increase in particle size, i.e. clustering occurs, and most likely the increase in relaxivity. There also appears to be a slight increase in size with an increase in polymer loading for the 3.3kPPO-b-2.6kPEO-OH complex. Thus, it appears that aggregation is a primary cause of the observed increases in relaxivity, but that the aggregation must occur due to two mechanisms. The first mechanism (for the 3.3kPPO-*b*-4.8kPEO-OH complex, i.e. the complex with the longer PEO brush) is the same as presented in chapter 4 where a reduction in polymer loading reduces the steric repulsion, thus causing aggregation. The second mechanism (for the 3.3kPPO-*b*-2.6kPEO-OH complex) must be due to the polymer because the size stays relatively constant with an increase in polymer loading, meaning that the complex is not becoming more dispersed with an increase in steric repulsion. In this case, it is hypothesized that a hydrophobic interaction between the PPO layers of neighboring magnetite particles causes aggregation thus causing the relaxivity to increase. Additionally, none of these DLS measurements were done in the presence of an applied magnetic field. It is distinctly possible that the behavior of both complexes is significantly different in a magnetic field, particularly for complexes that are already aggregating.

Future work will need to utilize light scattering that is coupled with the ability to apply a magnetic field of significant strength.

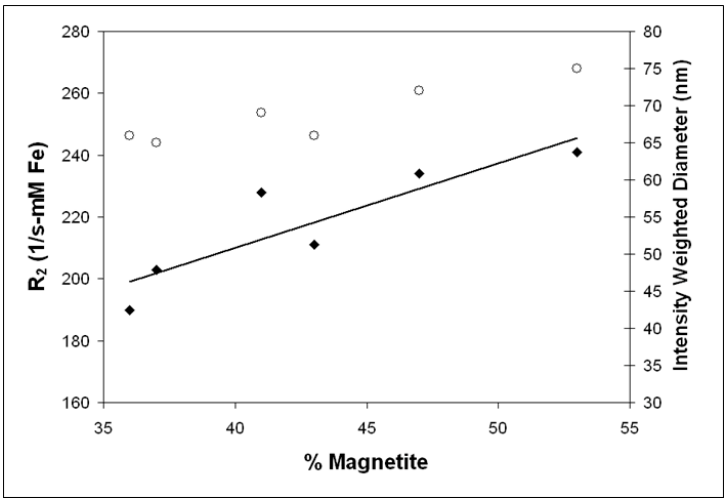

Figure 6.4.6.6. Relaxation data vs. magnetite loading for the tri-zwitterionic phosphonate 3kPPO-*b*-5kPEO-OH complexes.

The same phenomenon as observed for the triammonium 3.3kPPO-*b*-4.8kPEO-OH complex was also observed for the tri-zwitterionic phosphonate 3kPPO-*b*-5kPEO-OH as shown in Figure 6.4.6.6. Aggregation of the complexes is observed with an increase in magnetite loading as is an increase in relaxivity. However, these complexes have significantly larger relaxivities than their ammonium counterparts, which may be attributable to the strong interaction of phosphonate groups between complexes.

The presence of a hydrophobic interaction for the triammonium 3.3kPPO-*b*-2.6kPEO-OH complex is further bolstered by cell culture experiments measuring rhodamine R123 accumulation of multi-drug resistant cancer cells (MCF7/ADR) after exposure to the magnetite complexes (Figure 6.4.6.7). This technique has been used to determine cellular uptake due to exposure of these same cells to Pluronics®.[17, 18] In these

experiments, the hydrophobic to hydrophilic ratio affects the cellular uptake, as has been seen with Pluronics®.

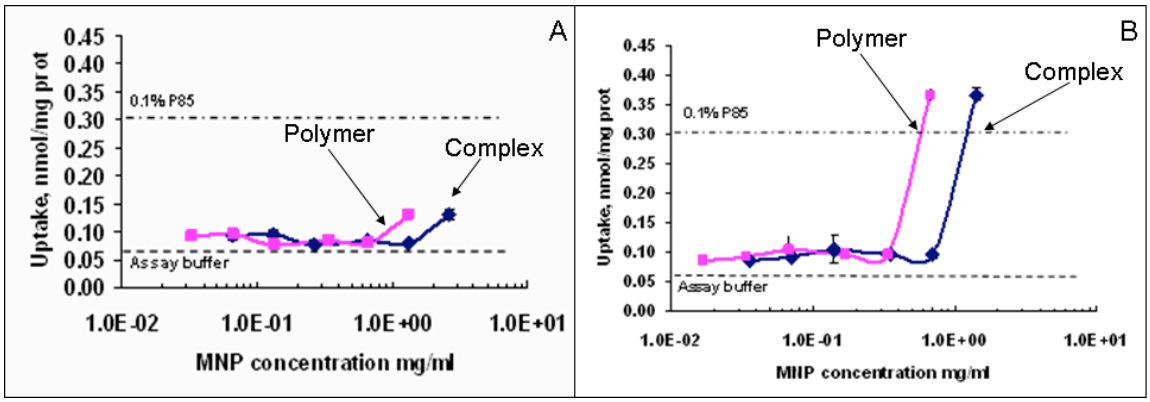

Figure 6.4.6.7. Measure of R123 accumulation of 51% magnetite 3.3kPPO-*b*-4.8kPEO-OH (A) and 48% magnetite 3.3kPPO-*b*-2.6kPEO-OH (B) complexes in MCF7/ADR cells.

While it is not clear whether this increased cellular uptake is due to hydrophobic interactions between the complex and the cell membrane, clustering of the complexes, or possibly both, it does indicate that the hydrophobic to hydrophilic ratio of the diblock copolymer is critical to uptake.

6.5 Conclusions

Amphiphilic diblock copolymer-stabilized magnetite nanoparticle complexes were synthesized and characterized for two different molecular weights and two different anchor groups. Both the triammonium and triphosphonate-anchored complexes exhibited the same trends in size with changes in magnetite loading. However, the brush model fit the triphosphonate data considerably better. It is hypothesized that the PPO layer in these complexes is less solvated than that in the triammonium complexes but this has not been proven yet.

However, both SANS and QCM-D data indicate a degree of solvation of the PPO layer that is fairly unexpected. This solvation is in stark contrast with an assumption in the brush model that the PPO layer is a non-solvated shell surrounding the magnetite core. The differences in size between anchor groups may be due to their affect on PPO solvation. There is no increase in size with a change in temperature which means that the degree of solvation is not so large to appreciably affect the mean polymer-particle distribution appreciably (i.e. the change is less than 1-2 nm).

Varying the block copolymer composition leads to considerably different behavior in both relaxivity measurements and in cell uptake experiments. For both experiments, the presence of a smaller hydrophilic PEO brush - while keeping the PPO molecular weight constant – led to what is likely an attractive hydrophobic interaction between complexes that, in the case of relaxivity, leads to enhanced relaxivity due to cluster formation. Further characterization of this hydrophobic interaction will be critical to control cell uptake and contrast enhancement.

Both the triammonium and triphosphonate-anchored complexes were stable in DI water. However, as the polymer loading was reduced for the 3.3kPPO-b-2.6kPEO-OH triammonium complex, flocculation was observed in phosphate buffered saline (PBS). This behavior was not observed for the 3kPPO-b-3kPEO-OH triphosphonate complex. This is in agreement with comparisons in Chapter 4 and 5 of the anchor groups.

6.6 References

1 T. N. Bronich, H.; Eisenberg, A.; Kabanov, A., *Journal of the American Chemical Society* **122:**8339-8343 (2000).

2 C. J. Jung, P., *Magnetic Resonance Imaging* **13:**661-674 (1995).

3 O. T. Mefford, M. R. J. Carroll, M. L. Vadala, J. D. Goff, R. Mejia-Ariza, M. Saunders, R. C. Woodward, T. G. S. Pierre, R. M. Davis and J. S. Riffle, *Chemistry of Materials* **20:**2184-2191 (2008).

4 O. T. Mefford, M. L. Vadala, J. D. Goff, M. R. J. Carroll, R. Mejia-Ariza, B. L. Caba, T. G. S. Pierre, R. C. Woodward, R. M. Davis and J. S. Riffle, *Langmuir* **24:**5060-5069 (2008).

5 A. S. Thunemann, D.; Kaufner, L.; Pison, U.; Mohwald, H., *Langmuir* **22:**(2006).

6 K. S. Wilson, J. D. Goff, J. S. Riffle, L. A. Harris and T. G. St Pierre, *Polymers for Advanced Technologies* **16:**200-211 (2005).

7 J. A. Dagata, N. Farkas, C. L. Dennis, R. D. Shull, V. A. Hackley, C. Yang, K. F. Pirollo and E. H. Chang, *Nanotechnology* **19:**(2008).

8 H. W. Duan, M. Kuang, X. X. Wang, Y. A. Wang, H. Mao and S. M. Nie, *Journal of Physical Chemistry C* **112:**8127-8131 (2008).

9 J. D. G. Duran, J. L. Arias, V. Gallardo and A. V. Delgado, *Journal of Pharmaceutical Sciences* **97:**2948-2983 (2008).

10 M. Hoehn, U. Himmelreich, K. Kruttwig and D. Wiedermann, *Journal of Magnetic Resonance Imaging* **27:**941-954 (2008).

11 C. W. Jung and P. Jacobs, *Magnetic Resonance Imaging* **13:**661-674 (1995).

12 S. J. Kim, S. H. Kim, J. M. Lee, S. Chang, Y. S. Kim, S. H. Kim, Y. H. Jeon and D. Choi, *Journal of Computer Assisted Tomography* **32:**379-385 (2008).

13 H. L. Ma, Y. F. Xu, X. R. Qi, Y. Maitani and T. Nagai, *International Journal of Pharmaceutics* **354:**217-226 (2008).

14 A. Tanimoto, K. Oshio, M. Suematsu, D. Pouliquen and D. D. Stark, *Journal of Magnetic Resonance Imaging* **14:**72-77 (2001).

15 A. B. Kabanov, T.; Kabanov, V.; Yu, K.; Eisenberg, A., *Advancers in Genetics* **53:**231-261 (2005).

16 L. A. Harris, J. D. Goff, A. Y. Carmichael, J. S. Riffle, J. J. Harburn, T. G. St. Pierre and M. Saunders, *Chemistry of Materials* **15:**1367-1377 (2003).

17 Z. Yang, G. Sahay, S. Sriadibhatla and A. V. Kabanov, *Bioconjugate Chemistry* **19:**1987-1994 (2008).

18 E. V. Batrakova and A. V. Kabanov, *Journal of Controlled Release* **130:**98-106 (2008).

19 E. V. Batrakova, S. Li, V. Y. Alakhov, D. W. Miller and A. V. Kabanov, *Journal of Pharmacology and Experimental Therapeutics* **304:**845-854 (2003).

20 B. Lee and M. A. Firestone, *Biomacromolecules* **9:**1541-1550 (2008).

21 L. J. M. Vagberg, K. A. Cogan and A. P. Gast, *Macromolecules* **24:**1670-1677 (1991).

22 J. D. Goff, P. P. Huffstetler, W. C. Miles, N. Pothayee, C. M. Reinholz, S. Ball, R. M. Davis and J. S. Riffle, *Chemistry of Materials* **Accepted:**(2009).

23 P. P. Huffstetler, W. C. Miles, J. D. Goff, C. M. Reinholz, M. R. J. Carroll, R. C. Woodward, T. G. St. Pierre, R. M. Davis and J. S. Riffle, *Polymer Preprint* **49:**1103-1104 (2008).

24 W. C. Miles, J. D. Goff, P. P. Huffstetler, O. T. Mefford, J. S. Riffle and R. M. Davis, *Polymer* **Submitted:**(2009).

25 W. C. Miles, J. D. Goff, P. P. Huffstetler, C. M. Reinholz, N. Pothayee, B. L. Caba, J. S. Boyd, R. A. Davis and J. S. Riffle, *Langmuir* **25:**803-813 (2009).

26 B. B. Yellen, Z. G. Forbes, D. S. Halverson, G. Fridman, K. A. Barbee, M. Chorny, R. Levy and G. Friedman, *Journal of Magnetism and Magnetic Materials* **293:**647-654 (2005).

27 CRC Handbook of Chemistry and Physics. CRC Press, Boca Raton, FL (2006-2007).

28 Q. A. Zhang, M. S. Thompson, A. Y. Carmichael-Baranauskas, B. L. Caba, M. A. Zalich, Y. N. Lin, O. T. Mefford, R. M. Davis and J. S. Riffle, *Langmuir* **23:**6927-6936 (2007).

29 W. C. Miles, J. D. Goff, P. P. Huffstetler, C. M. Reinholz, N. Pothayee, B. L. Caba, J. S. Boyd, R. M. Davis and J. S. Riffle, *Langmuir* **Submitted:**(2008).

30 G. J. Fleer, M. A. Cohen Stuart, J. Scheutjens, T. Cosgrove and B. Vincent, *Polymers at Interfaces*, Chapman and Hall, London (1993).

31 B. Foster, T. Cosgrove and B. Hammouda, *Langmuir* **25:**6760-6766 (2009).

32 P. Alexandridis and L. Yang, *Macromolecules* **33:**5574-5587 (2000).

33 L. Yang and P. Alexandridis, *Langmuir* **16:**4819-4829 (2000).

34 R. Pynn, *Los Alamos Neutron Science Center* 1-31 (1990).

35 B. Hammouda, *Probing Nanoscale Structures: The SANS Toolbox*, National Institute of Standards and Technology, Gaithersburg (2008).

36 NIST, Scattering Length Density Calculator. National Institute of Standards and Technology: NIST Center for Neutron Research, Gaithersburg.

37 L. Palmqvist and K. Holmberg, *Langmuir* **24:**9989-9996 (2008).

38 I. Reviakine, F. F. Rossetti, A. N. Morozov and M. Textor, *J Chem Phys* **122:**8 (2005).

39 R. C. Plaza, J. de Vicente, S. Gomez-Lopera and A. V. Delgado, *Journal of Colloid and Interface Science* **242:**306-313 (2001).

40 R. E. Rozenzweig, *Ferrohydrodynamics*, Cambridge University Press, Cambridge, U.K. (1985).

41 A. Roch, Y. Gossuin, R. N. Muller and P. Gillis, *Journal of Magnetism and Magnetic Materials* **293:**532-539 (2005).

42 J. P. Hornak, The Basics of MRI (2008).

43 D. Weishaupt, V. Kochli and B. Marincek, *How Does MRI Work?*, Springer, Berlin (2006).

Chapter 7: Effects of Polyether Coatings on the Stabilities and Transverse Relaxivities of Potential MRI Contrast Agents

P. P. Huffstetler,[1] M. R. J. Carroll,[3] W. C. Miles,[2] J. D. Goff,[1] A. Y. Chen,[1] R. Woodward,[3] T. G. St. Pierre,[3] R. M. Davis,[2] and J. S. Riffle[1]

[1]Department of Macromolecular Science and Engineering, Virginia Tech Blacksburg, VA 24061, [2]Department of Chemical Engineering, Virginia Tech Blacksburg, VA 24061, [3]School of Physics, University of Western Australia, Crawley, WA

7.1 Abstract

A series of polyether magnetite complexes coated with well-defined tri-zwitterionic phosphonate-PEO-OH and tri-zwitterionic phosphonate-PPO-*b*-PEO-OH oligomers were synthesized and characterized via ^{1}H NMR, GPC, TEM, SQuID, and DLS. The stabilities of the complexes in phosphate buffered saline as a simulated physiological medium were demonstrated. The polymer loading on the magnetite nanoparticles was varied to determine effects of chemical composition on transverse relaxivities. These properties were correlated with sizes of the complexes in solution via dynamic light scattering (DLS). Comparison of the particle sizes in solution was shown to have a profound effect on the relaxivity, r_2, of the complexes. As the hydrodynamic radius of the complexes increased, the r_2 increased. An indepth study revealed that polymer loading, chemical composition, and molecular weight have profound effects towards the clustering of the magnetic nanoparticles. Relaxivites, r_2, of these complexes were also shown to have much higher relaxation rates than that of a commercial magnetite contrast agent with a dextran coating.

7.2 Introduction

Magnetic resonance imaging (MRI) has been one of the most prominent non-invasive imaging tools for detecting various diseased tissues over the past few decades.[1-6] The

enhancement of contrast in this imaging technique comes from the use of contrast agents. The most common contrast agents are gadolinium-based chelates, but there is significant interest in the development of iron oxide nanoparticles due to their capacity to generate larger contrast enhancement.[7-13] Superparamagnetic magnetite-based contrast agents are already used for a variety of applications, particularly for image enhancement of the liver, spleen and lymphatic system.[5, 6, 14-17] However, there is increased interest in developing cell-specific or "smart" contrast agents for early diagnosis and detection of disease for various forms of cancer as well as contrast agents that can manipulate the cell membrane.[7, 9, 18-20] The basis for contrast enhancement is the high magnetic susceptibility of iron oxide nanoparticles. Localized field gradients generated by these particles in applied magnetic fields result in rapid dephasing of the proton spins, thus increasing transverse relaxivities (r_2).[5, 6, 21, 22] A number of factors can affect the contrast including magnetite size and distribution of size, the structure of the polymer coating as well as thickness of the polymer coating, and the aggregation characteristics of the magnetite-polymer complexes in physiological media.[23-29] Many polymer coatings have been used to stabilize magnetite in physiological and aqueous media.

Because of their high transverse relaxivities, colloidal suspensions of superparamagnetic nanoparticles are good candidates for the development of new "smart" contrast agents, allowing early detection of several pathologies.[2, 9, 11, 23, 30-35] The development and optimization of these "smart" or site specific contrast agents requires in-depth knowledge of relationships between proton relaxation, physical, and morphological properties of the particles and their coatings. In the present work, magnetite nanoparticles were synthesized and coated with a series of hydrophilic PEO and amphiphilic PPO-*b*-

PEO block copolymers with systematically varied compositions. The complexes consisted of an inner magnetite core surrounded by a relatively hydrophobic PPO sheath, and an outer hydrophilic PEO brush. The sizes and aggregation characteristics of the complexes in water were measured by DLS and compared to the transverse relaxivities in order to understand how the polymer loading and block length affect the rate of relaxation.

7.3 Experimental

7.3.1 Materials

Tetrahydrofuran (THF, Optima Grade, EMD Chemicals, 99.5%) was refluxed over sodium metal with benzophenone until the solution reached a deep purple, fractionally distilled, and deoxygenated just prior to use. Azobisisobutyronitrile (AIBN), benzyl alcohol (>98%), ethylene oxide (EO, 99.5+%), cysteamine hydrochloride, potassium (98%), hexanes (HPLC grade), propylene oxide (PO, ≥99%), oleic acid, sodium iodide (>98%), iron (III) acetylacetonate ($Fe(acac)_3$) and 1.0 M vinyl magnesium bromide were purchased from Aldrich and used as received. 3-Chloropropyltrichlorosilane (Gelest) was used as received. Dichloromethane and sodium bicarbonate (Fisher Scientific) were used as received. Naphthalene (Aldrich, 99%) was sublimed prior to use. Glacial acetic acid (Aldrich) was diluted with THF to yield a 2.5 M solution. N,N-Dimethylformamide (DMF, EMD Chemicals) was dried over CaH_2, fractionally distilled under vacuum and stored under nitrogen at 25 °C. A double-metal catalyst, ($Zn_3[Co(CN)_6]_2$), graciously donated by Bayer Materials Science was dried at room temperature for 24 h under vacuum and diluted with distilled THF to yield a 4.1 mg mL^{-1} dispersion. Dulbecco's PBS (10X,

Aldrich) without calcium or magnesium was diluted to a concentration of 1X. Dialysis tubing (1,000-, 25,000- and 50,000 g mol^{-1} MWCO) was obtained from Spectra/Por.

7.3.2 Characterization

Spectroscopic analyses of block copolymers were performed using a Varian Inova 400 NMR and a Varian Unity 400 NMR. Gel permeation chromatography (GPC) was conducted with an Alliance Waters 2690 Separations Module with a Viscotek T60A dual viscosity detector and laser refractometer equipped with a Waters HR 0.5 + HR 2 + HR 3 + HR 4 styragel column set at 30 °C. A Universal calibration was utilized to obtain absolute molecular weights.

Thermogravimetric analysis (TGA) was carried out on the PEO- and PPO-*b*-PEO/magnetite complexes using a TA Instruments TGA Q500. Each sample was dried at 120 ºC for 15 min to drive off any excess moisture prior to determination of polymer loss. The sample was subsequently equilibrated at 50 ºC and the temperature was ramped at 10 °C min^{-1} to a maximum of 650 ºC in a nitrogen atmosphere. The mass remaining was recorded throughout the experiment. The remaining mass at 600 ^{o}C was taken as the fraction of magnetite in the complexes.

TEM was conducted with a Philips EM-420 field-emission-gun transmission electron microscope. The microscope was equipped with a 2000x3000 pixel digital imaging system. Dry samples of the magnetite complexes were dispersed in water and cast onto amorphous carbon-coated copper grids for analysis. Images were acquired at a magnification of 96 kx, corresponding to a resolution of 3.7 pixels nm^{-1}. Particle distribution analyses were performed using Reindeer Graphics' Fovea Pro 4 plug-in for Adobe Photoshop 7.0.

Proton transverse relaxation rate measurements were performed using a Bruker mq60 Minispec NMR Analyzer with a magnetic field strength of 1.4 T and a measuring frequency of 60 MHz. Samples were diluted to specific concentrations between 0.01 and 0.001 wt%. Iron concentrations were measured by inductively coupled plasma atomic emission spectroscopy (ICP-AES) following acid digestion. These concentrations were in good agreement with TGA values. Each sample (0.6 μL) was transferred to a 7.5-mm glass NMR tube and sealed with an airtight cap. The sample tubes were placed in an aluminum block enclosed in a water bath at 25 °C for 15 min prior to relaxometry measurements. A Carl-Purcell-Meiboom-Gill (CPMG) spin echo sequence (1000 echoes, 4 averages, 2 ms echo spacing and 5 s repetition time) was used to measure relaxation rates.

DLS measurements were conducted with a Malvern Zetasizer NanoZS particle analyzer (Malvern Instruments Ltd, Malvern, UK) at a wavelength of 633 nm from a 4.0 mW, solid-state He-Ne laser at a scattering angle of 173° at 25 ± 0.1 ˚C. Intensity, volume, and number average diameters were calculated with Malvern's Zetasizer Nano 4.2 software.

A 7T MPMS SQuID magnetometer (Quantum Design) was used to determine magnetic properties. Hysteresis loops were generated for the magnetite nanoparticles at 300K and 5K.

7.3.3 Synthesis of 3-hydroxypropyltrivinylsilane (3-HPTVS)

3-HPTVS was prepared utilizing a modified procedure originally developed by Vadala *et al.*[36-38] 3-Chloropropyltrichlorosilane (10.0 g, 0.05 mol) was syringed into a clean, flame-dried, two-neck, round-bottom flask equipped with a stir bar under a N_2

purge. The reaction flask was placed in an ice bath and cooled to 0 ºC. A 1.0 M solution of vinylmagnesium bromide (142.0 mL, 0.142 mol) in THF was slowly added to the flask over 30 min. The flask was allowed to warm to room temperature, and the mixture was stirred for 24 h. The reaction mixture was diluted with dichloromethane (100 mL), transferred to a separatory funnel and washed with a saturated aqueous ammonium chloride solution (150 mL), then the organic layer was further washed with aqueous sodium chloride (3 X 150 mL). Magnesium sulfate was added to the organic layer to remove any residual water, followed by vacuum filtration. Dichloromethane was removed under vacuum and the product was distilled at 100 ºC, 0.8 Torr, yielding 3-chloropropyldimethylvinylsilane (8.60 g, 0.047 mol, 97% yield) (3-CPTVS). ^{1}H NMR was used to confirm the quantitative addition of vinyl groups.

3-CPMVS (8.60 g, 0.047 mol) was placed in a 250-mL round-bottom flask equipped with a stir bar and condenser. In a separate round-bottom flask, sodium iodide (16.4 g, 0.11 mol) was dissolved in acetone (60 mL) and the solution was syringed into the flask. The mixture was heated at 56 ºC for 24 h. Acetone was removed under vacuum and the product was dissolved in dichloromethane (100 mL) and vacuum filtered to remove the salt by-products. Dichloromethane was removed under vacuum and the product was distilled at 100 ºC, 0.8 Torr, yielding 3-iodopropyldimethylvinylsilane (3-IPTVS, 13.4 g, 0.05 mol). ^{1}H NMR confirmed the expected structure.

3-IPTVS (13.4 g, 0.05 mol) was placed in a 250-mL round-bottom flask equipped with a stir bar and condenser. DMF (20 mL) was added to the reaction flask followed by sodium bicarbonate (8.8 g, 0.10 mol) and DI water (5 mL). The mixture was heated to 100 ºC for 24 h and conversion of the alkyl iodide to an alcohol was monitored via ^{1}H NMR.

The reaction mixture was transferred to a separatory funnel and washed 3X with DI water to remove the excess sodium bicarbonate and DMF. The product was fractionally distilled at 90 °C, 0.8 Torr, yielding 3-hydroxypropyldimethylvinylsilane (3-HPTVS, 7.4 g, 0.048 mol, 95% yield). ^{1}H NMR confirmed the expected chemical structure.

7.3.4 Synthesis of trivinylsilylpoly(ethylene oxide) (TV-PEO-OH)

An exemplary procedure for the synthesis of PEO homopolymers is provided. A 9,100 g mol^{-1} PEO was initiated with 3-hydroxypropyltrivinylsilane (3-HPTVS). EO (10 g, 0.23 mol) was charged to a 300-mL pressure reactor under vacuum that was cooled with an isopropanol-dry ice bath, then it was pressurized to 30 psi with ultra high purity nitrogen. An initiator solution was prepared by adding 3-HPTVS (0.21 g, 0.11 mmol), THF (5 mL), and potassium naphthalide (1.07 mL of a 0.95 M solution, 1.07 mmol) to a flame-dried 100-mL round-bottom flask. The alkoxide solution was added to the reactor via syringe and the reactor was warmed to room temperature and stirred for 24 h. The polymer was terminated by adding acetic acid (how much?) to the reaction mixture (before exposing the mixture to oxygen), then the mixture was purged (into what?) with nitrogen for one h to evolve any residual EO. The reaction mixture was transferred to a 250-mL round-bottom flask, then the solvent was removed via roto-evaporation. The polymer was dissolved in methylene chloride (~200 mL) and washed with water (200 mL) three times to remove salt by-products. The solution was concentrated by removing most of the methylene chloride and the polymer was precipitated in cold diethyl ether and dried under vacuum at room temperature to afford 9.4 g of TV-PEO-OH.

7.3.5 Synthesis of trivinylsilylpoly(propylene oxide-b-ethylene oxide) (TV-PPO-b-PEO-OH)

An exemplary procedure for synthesizing a 3,000 g mol^{-1} TV-PPO-OH oligomer utilizing 3-hydroxypropyltrivinylsilane as the initiator is provided. 3-HPTVS (1.12 g, 6.7 mmol) was syringed into a clean, flame-dried round-bottom flask followed by THF (5 mL) and ARCOL 3 catalyst solution (0.72 mL, 3.0 mg). The mixture was stirred at 25 °C for 20 hours. Propylene oxide (PO, 20 g, 0.34 mol) was syringed into a 300-mL, high-pressure Series 4561 Parr reactor filled with 30 psi of ultra high purity nitrogen. The initiator mixture was syringed into the reactor and the mixture was heated to 105 ^{o}C and a pressure of 170 psi was noted. An increase in temperature (47 ^{o}C) followed by a pressure decrease (100 psi) was noted. The pressure decrease was observed over 52 minutes following the initial temperature increase. The reaction was cooled to room temperature and diluted with chloroform (250 mL). The polymer solution was filtered through celite in order to remove the catalyst followed by roto-evaporation of the chloroform. The resulting polymer was dried at 60 ^{o}C under vacuum for 24 h. ^{1}H NMR analysis revealed a M_n of 3,010 g mol^{-1} and GPC showed a M_n of 3,100 g mol^{-1} with a MWD of 1.09.

Naphthalene (14.1 g, 0.11 mol) was sublimed and transferred to a 250-mL round-bottom flask and dissolved in THF (100 mL). Potassium metal (3.91 g, 0.10 mol) was added to the naphthalene solution and the mixture was stirred at 25 °C overnight. The potassium naphthalide solution was titrated with standardized 1.0 N HCl containing bromophenol blue as an indicator and yielded a 0.95 M potassium naphthalide solution. TV-PPO-OH (5 g, 0.9 mmol) was used to form a macroinitiator for the polymerization of EO. An alkoxide macroinitiator was formed by reaction with the potassium naphthalide solution (0.9 mL) in THF (5 mL) in a 50-mL round-bottom flask. A 300-mL Parr pressure

reactor was evacuated and cooled with an isopropanol-dry ice bath. EO (8.5 g, 0.19 mol) was distilled into the reactor, then THF (10 mL) was added via syringe. The macroinitiator mixture was added to the stirring, cold, 300-mL pressure reactor, then the reactor was pressurized with 30 psi of ultrahigh purity nitrogen. The reactor was allowed to warm to room temperature and the mixture was stirred overnight at 25 ^{o}C. A stoichiometric amount of a 2.5 M acetic acid solution (aq., 0.36 mL, 0.9 mmol) was added to the reaction via syringe to terminate the polymer prior to its exposure to oxygen. The block copolymer was precipitated into cold diethyl ether and dried under vacuum at room temperature overnight yielding 12.9 g of polymer. Characterization of the material by ^{1}H NMR yielded a M_n of 8,000 g mol^{-1} and GPC revealed a M_n of 8,300 g mol^{-1} with a MWD of 1.07.

7.3.6 Functionalization of trivinylsilyl(PPO-b-PEO) and trivinylsilyl(PEO)with 2-mercaptoethylamine hydrochloride

The trivinylsilyl termini of the amphiphilic diblock copolymers and homopolymers were functionalized with amino groups via ene-thiol reactions. An exemplary procedure for an 8,000 g mol^{-1} TV-PPO-*b*-PEO-OH oligomer is given. TV-PPO-*b*-PEO-OH (2 g, 0.25 mmol, 0.75 meq vinylsilane) was dissolved in deoxygenated DMF (3 mL) at 60 ^{o}C in a 50-mL, round-bottom flask. In a separate flask, cysteamine hydrochloride (127 mg, 1.13 mmol) was dissolved in DMF (1 mL) and added to the polymer. AIBN (26 mg, 0.15 mmol) was dissolved in DMF (0.5 mL) and added to the reaction and the mixture was deoxygenated for 20 min with N_2. The mixture was reacted at 70 ^{o}C for 24 h. The mixture was dissolved in water (200 mL) and the block copolymer was extracted into methylene chloride to separate it from the excess cysteamine hydrochloride. This extraction process was repeated 3x to ensure that the polymer was completely extracted from the water and

the excess cysteamine hydrochloride was removed. Methylene chloride was removed via roto-evaporation and the polymer was precipitated into cold diethyl ether followed by drying under vacuum for 24 h at 25 ^{o}C yielding 1.86 g of tri-ammonium-PPO-*b*-PEO-OH.

7.3.7 Michael addition of tri- ammonium-PEO-OH onto diethyl vinyl phosphonate

A characteristic procedure for adding phosphonate groups to an 8,000 g mol^{-} tri-ammonium-PEO-OH is provided. A tri-ammonium-PEO-OH oligomer (1.0 g, 0.12 mmol, 0.375 meq amine) was charged to a clean, flame-dried, 100-mL, round-bottom flask equipped with a stir bar, and dissolved in ethanol (9 mL). TEA (0.10 mL, 0.45 mmol) was added to the reaction, followed by diethyl vinyl phosphonate (0.24 mL, 0.45 mmol). The reaction was carried out at 70 ^{o}C for 24 h. The reaction mixture was diluted with DI water to obtain a 75:25 water:ethanol composition and placed in a 1,000 g mol^{-1} MWCO cellulose acetate dialysis bag and dialyzed against 4 L of DI water for 24 h to remove excess diethyl vinyl phosphonate. The contents of the dialysis bag were transferred to a 100-mL round-bottom flask and lyophilized, yielding 0.91 g of tri(diethyl phosphonate)-functionalized PPO-*b*-PEO.

7.3.8 De-esterification of tri(diethylphosphonate)-PPO-b-PEO-OH yielding trizwitterionic phosphonate-PPO-b-PEO-OH

Tri-zwitterionic phosphonate-PPO-*b*-PEO-OH was prepared from tri(diethyl phosphonate)-PPO-*b*-PEO-OH using a hydrolysis procedure adapted from Caplan *et al.*[39] In a representative procedure, an 8,000 g mol^{-1} tri(diethyl phosphonate)-PPO-*b*-PEO-OH (1.0 g, 0.13 mmol) was charged to a clean, 100-mL round-bottom flask equipped with a stir bar and dissolved in 5 mL of dichloromethane. Trimethylsilyl bromide (0.07 mL, 0.45

mmol) was syringed into the reaction flask and stirred at room temperature for 24 h. Methanol (0.02 mL, 0.45 mmol) was added and the mixture was stirred for 2 h to cleave the trimethylsilylester groups. Dichloromethane (50 mL) was added, and the mixture was washed 3X with DI water (100 mL each) in a separatory funnel. The dichloromethane layer was concentrated, then the oligomer was precipitated by pouring the mixture into cold diethyl ether. The polymer was vacuum-dried at 25 ºC for 24 h yielding 0.89 g of phosphonic acid-PEO-OH.

7.3.9 Synthesis and Stabilization of Magnetite Nanoparticles with Trizwitterionic phosphonate-(PPO-b-PEO)

Magnetite nanoparticles were synthesized using a thermal decomposition method adapted from Pinna *et al.*[40] A procedure for preparing a magnetite-copolymer complex containing 33 wt% magnetite is provided. Fe(III) acetylacetonate (2.14 g) was added to benzyl alcohol (45 mL) in a 250-mL, three-neck round-bottom flask equipped with a water condenser and placed in a Belmont metal bath with an overhead stirrer with both thermostatic (+/- 1 ^{o}C) and revolution per minute control. The mixture was sparged with N_2 for 1 h. The solution was stirred and reacted at 100 ^{o}C for 15 minutes and the temperature was increased to 205 ^{o}C over 4 h, and held at 205 ^{o}C for 40 h. The mixture was cooled to room temperature, centrifuged and the supernatant was discarded. The resulting magnetite nanoparticles were washed with acetone (200 mL) 3x, then collected with a magnet and dried under N_2 for 1 h. The particles were diluted with chloroform (25 mL) and oleic acid (0.3 mL) was added to disperse the particles. The solvent was removed under vacuum at room temperature, and the oleic acid-stabilized magnetite nanoparticles were washed 3X with acetone (100 mL each). The particles were dried under vacuum for

24 h at 25 ˚C. Magnetite nanoparticles stabilized with oleic acid (50 mg) were dispersed in chloroform (10 mL) in a 50-mL round-bottom flask. Trizwitterionic phosphonate-PPO-*b*-PEO-OH (100 mg) dissolved in chloroform (10 mL) was pipetted into the magnetite dispersion and the mixture was sonicated in a VWR 75T sonicator for 16 h. The resulting dispersion of the magnetite-copolymer complexes solution was precipitated into hexane (300 mL) to remove free oleic acid and the particles were collected with a magnet. The complexes were dried under N_2 for 30 minutes at 25 °C, dispersed in DI water (50 mL) and dialyzed against water with a 25,000 g mol^{-1} MWCO cellulose acetate dialysis bag.

7.4 Results and Discussion

The major goal of this research deals with determining the effects of specific polyether coatings towards the stability and transverse relaxivities of superparamagnetic nanoparticles. A series of tri-zwitterionic phosphonate PEO's and PPO-*b*-PEO's were used in the stabilization of well-defined magnetite nanoparticles. Previous work in the field of magnetite-based contrast agents have shown that increasing the amount of magnetite in the sample yields higher transverse relaxation rates.[5, 6, 28] Jung and Josephson *et al.* demonstrated that complexes with low polymer loadings (ie. containing the highest amount of magnetite) should have the highest relaxivity.[5, 6] However, the exact relationship between the transverse relaxivity and the polymer coating has yet to be determined. Herein, we discuss the synthesis of well-defined heterobifunctional polyethers and their effects on the transverse relaxivities of magnetite nanoparticles.

7.4.1 Synthesis of well-defined heterobifunctional polyether oligomers for magnetite stabilization

In order to synthesize tri(zwitterionic phosphonate) polyethers, a specific initiating species, 3-hydroxypropyltrivinylsilane, was utilized[36, 37] for the living anionic polymerization of ethylene oxide (Scheme 7.4.1.1). These heterobifunctional oligomers were post-functionalized to adsorb onto magnetite nanoparticles.

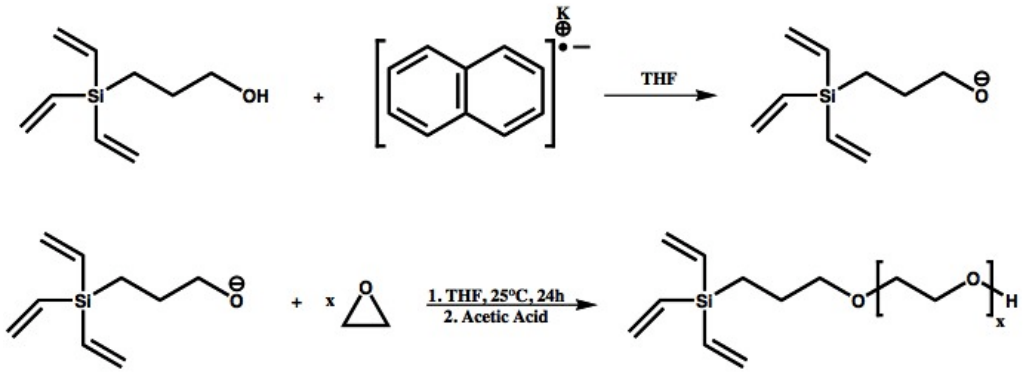

Scheme 7.4.1.1. Synthesis of a trivinylsilyl-PEO-OH oligomer via living anionic ring-opening polymerization techniques

Potassium naphthalide was reacted with 3-HPTVS forming an alkoxide for initiating EO. The number of moles of 3-HPTVS relative to EO controlled the molecular weight of the oligomer. A small deficiency of base (naphthalide) relative to 3-HPTVS ensured that only the alkoxide initiated the chains, and the remaining alcohol chains transferred with the growing PEO chains throughout the reaction. The polymerizations were terminated with acetic acid prior to opening the reactor to avoid any unwanted oxidative side reactions.

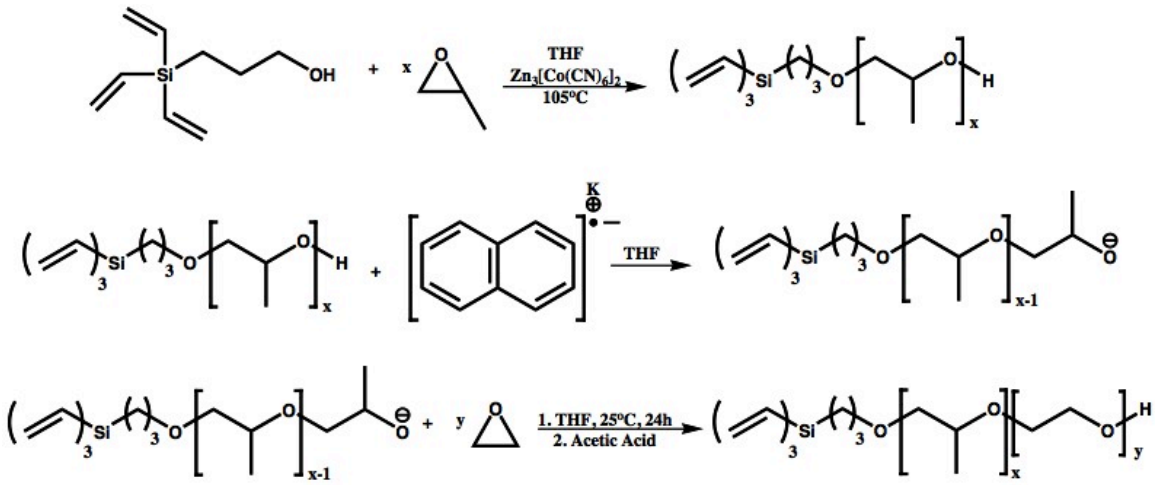

Scheme 7.4.1.2. Synthesis of trivinylsilyl-PPO-*b*-PEO-OH oligomers via coordination polymerization followed by living anionic ring-opening polymerization

In order to add a hydrophobic component for possible biological applications, a double metal coordination catalyst was utilized in synthesizing a well-defined PPO homopolymer (Scheme 7.4.1.2). Utilization of the coordination catalyst was instrumental in the polymerization of the hydrophobic component due to side reactions associated with base catalyzed ring-opening of propylene oxide. The initiating species (3-HPTVS) and coordination catalyst ($Zn_3[Co(CN)_6]_2$) were mixed together in the presence of THF for 24 hours prior to the polymerization. This "aging" technique yielded molecular weight distributions of 1.1 or less. Molecular weight was controlled by stoichiometrically varying the amount of initiator relative to monomer. Polymerization of PO occurred by heating the catalyst to its activation temperature (105 ^{o}C) in the presence of the initiating species (3-HPTVS). Once the catalyst was activated, a temperature spike was noted associated with the rapid ring-opening of the epoxy rings followed by a pressure decrease. The polymerization was deemed complete after the pressure and temperature reached equilibrium. Addition of the hydrophilic component involved using the trivinylsilyl-PPO-

OH oligomer as a macroinitiator for the living anionic polymerization of EO as discussed above (Scheme 7.4.1.2).

GPC and ^{1}H NMR were used to characterize both trivinylsilyl-polyether oligomers (Table 7.4.1.1). GPC of the trivinylsilyl-PPO-*b*-PEO-OH oligomers revealed symmetric monomodal peaks with molecular weight distributions of less than 1.1.

Table 7.4.1.1. Characterization of trivinylsilyl-polyethers via ^{1}H NMR and GPC

Sample (PPO-PEO)	Target MW (g mol^{-1})	^{1}H NMR M_n (g mol^{-1})		GPC M_n (g mol^{-1})	MWD
		PPO	PEO		
3.4k	3,000	-	3,400	3,400	1.04
3k-5k	8,000	3,000	5,000	8,300	1.07
3k-3k	6,000	3,000	2,900	6,200	1.11

Specific chemistries were used to introduce zwittierionic phosphonate functionality for the stabilization of magnetite. The first step towards this goal is through the use of free-radical ene-thiol chemistries as previously reported. The vinylsilyl functionality is unusual among vinyl groups in that it does not readily polymerize via free radical reactions, making it an ideal substrate for ene-thiol additions. During the addtion, an excess of 2-mercaptoethylamine hydrochloride (1.5:1 mol ratio) to vinylsilane was used to ensure quantitative addition (Scheme 7.4.1.3).

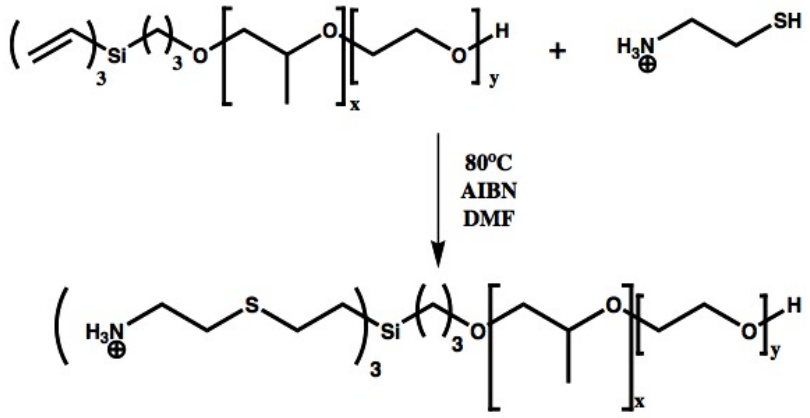

Scheme 7.4.1.3. Addition of 2-mercaptoethylamine hydrochloride via ene-thiol chemistries to the amphiphilic polyethers

Addition of 2-mercaptoethylamine hydrochloride to a trivinylsilyl-PPO-*b*-PEO-OH oligomer was monitored by ^{1}H NMR. Stoichiometric conversion to ammonium groups were determined by the complete disappearance of vinyl groups between 5.8-6.2 ppm (Figure 7.4.1.1). Appearance of new methylene protons, peaks A-D, indicated addition of the ammonium functionality. Comparison of the resonance integrals corresponding to the methylene peaks of the thiol to the silyl methylene protons, peak E, confirmed quantative addition across the vinylsilyl groups.

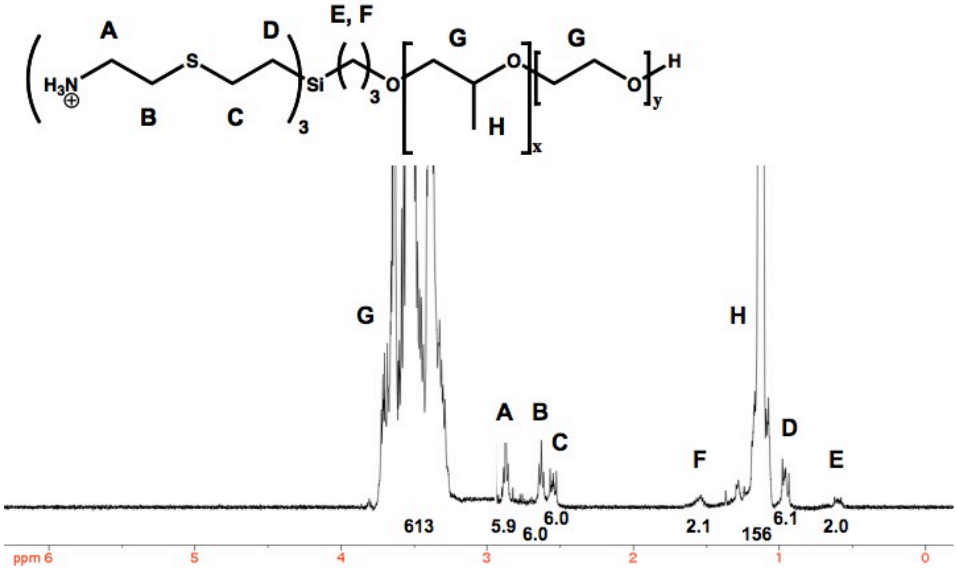

Figure 7.4.1.1. ^{1}H NMR of triammonium-PPO-*b*-PEO-OH oligomer

These triammonium-polyether oligomers were used as precursors to the formation of the tri(zwitterionic phosphonate)-polyethers. The ammonium endgroups were neutralized by addition of triethylamine yielding free amines. A slight excess of triethylamine was added to maintain basic conditions, aiding in the nucleophilic addition to diethyl vinyl phosphonate via Michael addition (Scheme 7.4.1.4).

Utilization of the phosphonate functionality towards the binding of magnetite involved cleaving the ethyl phosphonate groups using trimethylsilyl bromide (TMS-Br). Introduction of TMS-Br yielded an intermediate bis-trimethylsilyl ester and an alkyl halide by-product. Through methanolysis, the alcohol cleaved the silyl ester yielding phosphonic acid (Scheme 7.4.1.4). A zwitterionic endgroup was afforded at a pH of less than 10, due to the negative charge of the phosphonate and the protonated secondary amine.

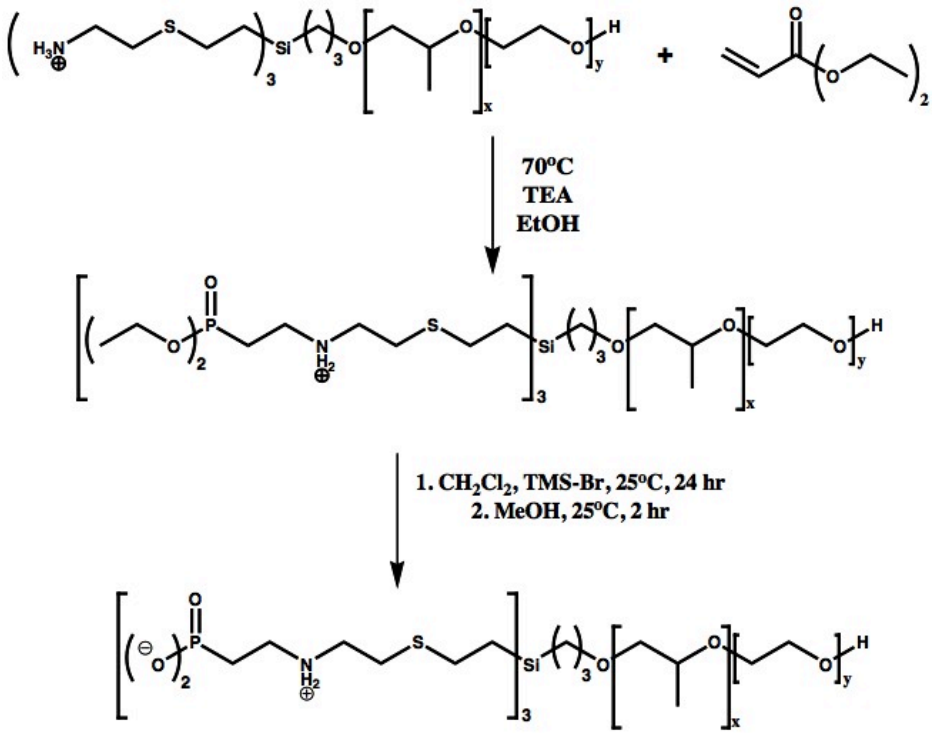

Scheme 7.4.1.4. Michael addition of diethyl vinyl phosphonate followed by de-esterification yielding a tri-zwitterionic phosphonate-PPO-*b*-PEO-OH oligomer

^{1}H NMR spectra (Figures 7.4.1.2A and B) confirmed the addition of diethyl vinyl phosphonate followed by the de-esterification yielding zwitterionic phosphonate functionality. Figure 7.4.1.2A shows quantitative addition to diethyl vinyl phosphonate was determined by comparing the integrals of peaks A-D to the methylene peak I. ^{1}H NMR (Figure 7.4.1.2B) confirmed the de-esterification of the ethyl groups yielding a

zwitterionic phosphonate polyether species. In addition to the disappearance of the ethyl ester groups in the spectrum, an upfield shift from 2.0 ppm to 1.6 ppm of the methylene group adjacent to the phosphorus atom was noted due to the increased resonance.

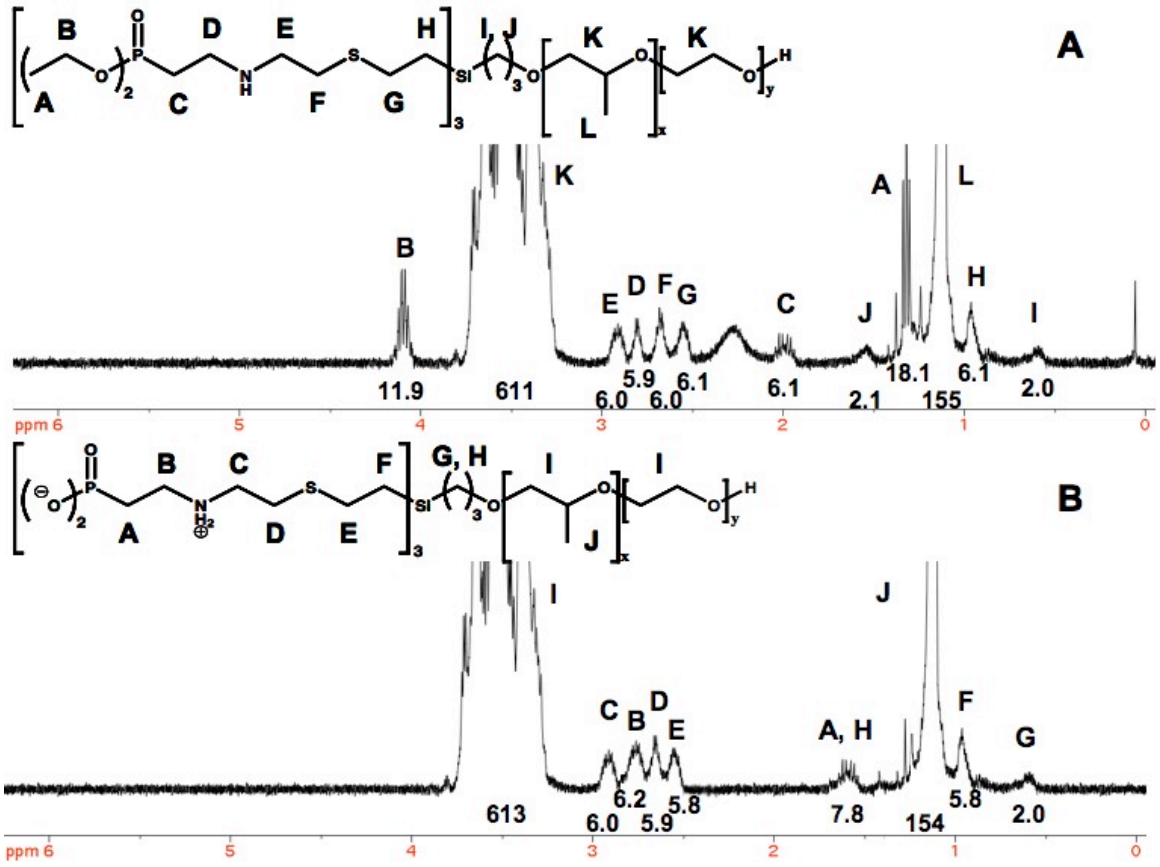

Figure 7.4.1.2. ^{1}H NMR characterization of (A) tri(diethyl phosphonate)-PPO-*b*-PEO-OH and (B) de-esterification of the ethyl groups yielding tri(zwitterionic phosphonate)-PPO-*b*-PEO-OH.

7.4.2 Synthesis and stabilization of magnetite nanoparticles with well-defined polyethers

Pinna *et al.* have described high-temperature reactions of iron(III) acetylacetonate with high boiling point solvents capable of reduction of iron(III) to iron(II) in the presence of oleic acid forming fairly monodisperse nanoparticles.[40] An adapted procedure using benzyl alcohol as both solvent and reducing agent was used for the formation of magnetite nanoparticles, as shown in Figure 7.4.2.1. The particles were then coated with a tri-

zwitterionic phosphonate polyether via ligand exchange and the particles were dried with nitrogen followed by dispersion of the nanoparticles in DI H_2O.

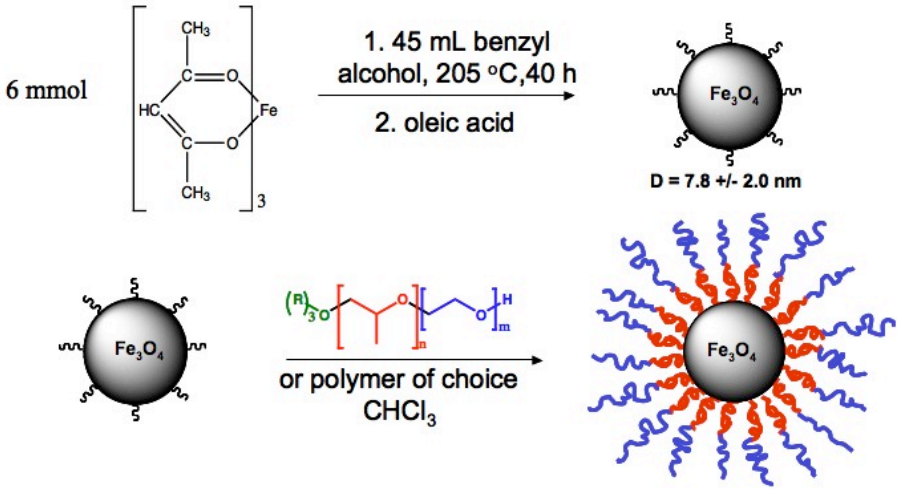

Figure 7.4.2.1. Synthesis via thermal decomposition and stabilization of magnetite nanoparticles with well-defined polyethers

Characterization of the polyether-magnetite nanoparticles was performed using transmission electron microscopy (TEM) and superconducting quantum interference device (SQuID) to determine the particle size distribution and magnetic properties. TEM (Figure 7.4.2.2) revealed fairly monodisperse magnetite nanoparticles. At least 2000 particles per sample were analyzed using Reindeer Graphis' Fovea Pro 4 plug-in for Adobe Photoshop 7.0 yielding a particle distribution diameter of 7.8 ± 2.0 nm.

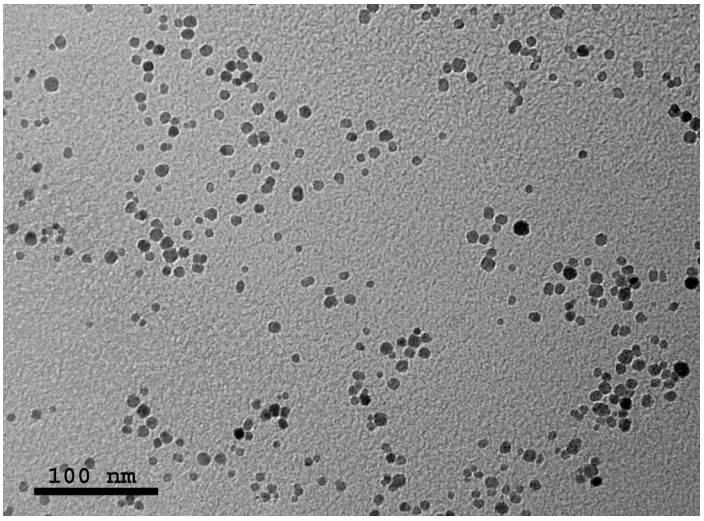

Figure 7.4.2.2. TEM of the copolymer/magnetite complexes dispersed in aqueous media yielding a particle distribution diameter of 7.8 ± 2.0 nm

The magnetic properties of the magnetite nanoparticles were characterized via SQuID. Hysteresis loops revealed superparamagnetic behavior and a saturation magnetization of 80 emu g^{-1} of magnetite (Figure 7.4.2.3).

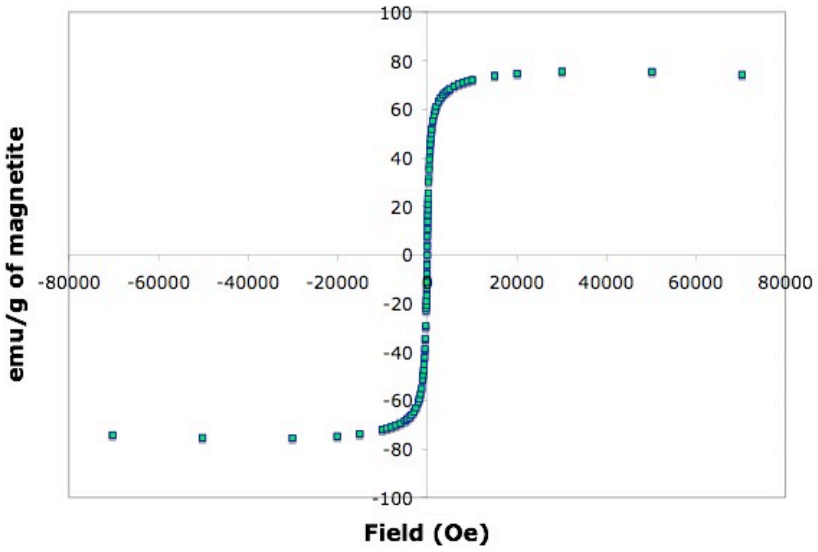

Figure 7.4.2.3. Hysteresis loop of the polyether-magnetite nanoparticles via SQuID yielding a saturation magnetization of ~80 emu/g of magnetite

7.4.3 Determining the polyether-magnetite bond stability in physiological conditions

Determining the stability of the complexes in physiological media is important for biological applications. The polyether-magnetite nanoparticles were dialyzed against water for 24 hours followed by TGA analysis determining the amount of polymer bound to the surface. The samples were further dialyzed against phosphate buffered saline (PBS) solution for 24 hours followed by water dialysis (24 hours) in order to remove residual PBS salts. PBS was used due to its ability to mimic physiological salt conditions encountered in the body. Extensive TGA-dialysis studies were performed at various polymer loadings to determine the stability of the tri-zwitterionic phosphonate/magnetite bond. Tables 7.4.3.1 and 7.4.3.2 show the stability of the polymer-magnetite interaction. Table 7.4.3.2 contains an abbreviated list of polyether-magnetite complexes. As shown in the data, no loss in polymer loading was observed for the PEO and PPO-*b*-PEO magnetite complexes after PBS dialysis. The complexes have also shown no sedimentation in PBS over a period of 30 days. Dialysis studies of a commercially available iron oxide contrast agent revealed coating desorption from the magnetite surface as shown in Table 7.4.3.2. A significant amount of sedimentation was noted for the material in PBS solution indicating a need for a better coating such as the tri(zwitterionic phosphonate) polyethers.

Table 7.4.3.1. 3.4k PEO complexes before and after PBS dialysis

Sample (g mol^{-1})	Anchor Group	% Polymer After H_2O Dialysis (wt%)	% Polymer After PBS Dialysis (wt%)
3,400	Tri-zwitterionic Phosphonate	65.4 ± 0.5	65.1 ± 0.4
3,400	Tri-zwitterionic Phosphonate	64.0 ± 0.1	64.0 ± 0.1
3,400	Tri-zwitterionic Phosphonate	57.6 ± 0.4	57.9 ± 0.3
3,400	Tri-zwitterionic Phosphonate	55.0 ± 0.9	54.7 ± 0.8
3,400	Tri-zwitterionic Phosphonate	44.0 ± 0.6	44.8 ± 0.5
3,400	Tri-zwitterionic Phosphonate	45.3 ± 0.8	44.7 ± 0.1
3,400	Tri-zwitterionic Phosphonate	34.5 ± 0.9	35.4 ± 0.5

Table 7.4.3.2. Anchor-group/magnetite bond stability against PBS

Sample (PPO-PEO) (g mol^{-1})	Anchor Group	% Polymer After H_2O Dialysis (wt%)	% Polymer After PBS Dialysis (wt%)
3,000-5,000	Tri-zwitterionic Phosphonate	64.5 ± 0.5	64.0 ± 0.1
3,000-5,000	Tri-zwitterionic Phosphonate	59.5 ± 0.7	59.2 ± 0.7
3,000-5,000	Tri-zwitterionic Phosphonate	52.9 ± 0.8	52.7 ± 0.3
3,000-2,900	Tri-zwitterionic Phosphonate	64.4 ± 0.4	64.1 ± 0.3
3,000-2,900	Tri-zwitterionic Phosphonate	59.3 ± 0.5	41.6 ± 0.6
3,000-2,900	Tri-zwitterionic Phosphonate	45.2 ± 0.7	44.9 ± 0.4
40,000*	Dextran	47.4 ± 1.2	27.7 ± 2.1

*Dialysis was conducted using a 50,000 g mol^{-1} MWCO dialysis bag

Based on this study, it was reasoned that polyether-magnetite nanoparticles with the tri-zwitterionic phosphonate anchor groups would have superior stability in physiological media compared to the commercially available materials shown in this study.

7.4.4 Transverse relaxations of polyether-magnetite complexes

Many studies involving the effects of polymer and small molecule coatings of magnetite on transverse relaxation have been investigated. However, few have looked into probing the transverse relaxation as a function of polymer loading and colloidal size. The study of transverse relaxation presents two main interests. The first step in characterization of a new superparamagnetic nanoparticle complex involves the evaluation of its relaxometric properties determining its potential application for MRI. Secondly, relating the transverse data to the morphological and physical properties of the polyether-magnetite complexes can be performed in order to develop new parameters for the development of new contrast agents. Well-defined heterobifunctional polyether stabilizers were utilized to determine the effect of block length, chemical composition, and colloidal size on the transverse relaxivities, r_2, of the polyether-magnetite complexes.

According to the literature, particles less than 100 nm in diameter have a better chance of longer blood circulation making these materials useful for the imaging of other areas.[41] Polyether coatings also allow the nanoparticles to stay in the body longer due to PEO's ability to mask itself from the immune system. Incorporation of a hydrophobic segment into the polymer coating may transfect the polyether-magnetite complexes across a cellular membrane as well as aid in the particles ability to slightly cluster. A series of amphiphilic polyethers were used in which the hydrophobic segment was the same for both samples and the hydrophilic portion was varied from 5,000 g mol^{-1} to 2,900 g mol^{-1} yielding a DP ratio (EO:PO) of 2.2 and 1.2, respectively.

In order to investigate the relaxation properties of well-defined polymer-magnetite complexes, one must look into what is actually causing the behavior. Figure 7.4.4.1 shows

the comparison of the static dephasing model against the motional average model. Comparison of these two models may yield some insight into the behavior of the complexes. When a magnetic field, B_o, is applied to the particles in both models, the superparamagnetic particles align with the field and thus field lines indicative of a permanent magnet, as denoted by the + and – charges on the particles in Figure 7.4.4.1. Therefore, the poles of the particles experience an enhanced magnetic moment of B_o plus the magnetic moment of the nanoparticle (B_{pole}) and a decreased magnetic moment of B_o minus the magnetic moment of the nanoparticle at the equator (B_{eq}) for both models (Figure 7.4.4.1). Looking at the behavior of water molecules as a function of time placed at various locations in both models potentially yield valuable insight into the r_2 phenomenon.

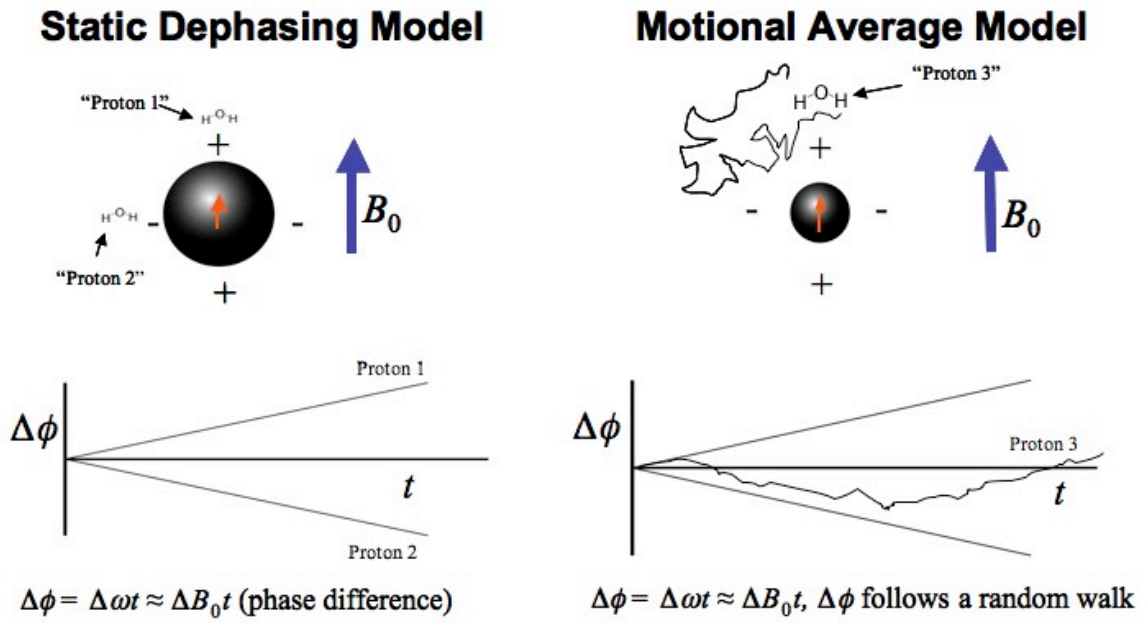

Figure 7.4.4.1. Significance of particle size and its possible effect on the relaxation rate

The static dephasing model suggests that if the particle size is large, the water molecules, labeled proton 1 and 2 are unable to move around the particle in a given amount of time. This leads to the protons experiencing homogeneous magnetic fields. As the protons continue to experience homogeneous fields, the protons begin to dephase at the rates of $B_o + B_{pole}$ for proton 1 and $B_o - B_{eq}$ for proton 2 (Figure 7.4.4.1). Therefore the protons experience a greater dephasing as a function of time and thus a greater relaxation rate. Comparison of a larger particle to a smaller particle is shown in the motional average model (Figure 7.4.4.1). Placing a water molecule on a smaller particle (proton 3 in Figure 7.4.4.1) allows the proton to move around in a given time frame experiencing a variety of magnetic moments ranging from $B_o + B_{pole}$ to $B_o - B_{eq}$. This shows the particle experiencing a inhomogeneous magnetic moment as a function of time thus the dephasing of the proton mimics a 'random walk' leading to small relaxation rates.

Investigation of the relaxivities, r_2, of the polyether-magnetite complexes as a function of particle size in water yields an interesting trend. Figure 7.4.4.2 shows the r_2 of a series of polyether-magnetite complexes as a function of number average diameter in H_2O. The most notable trend shown in Figure 7.4.4.2 shows that as the complexes become larger in diameter the relaxivity increases. This data indicates that transverse relaxivity, r_2, is dependent on particle size. Further investigation of the trend yields important information regarding the polymer coatings. As the coating is broken down into the three specific coatings, it is shown that the 3kPPO-5kPEO coating yields the highest r_2 as well as the largest particle size followed by the 3.4kPEO then the 3kPPO-5kPEO coating.

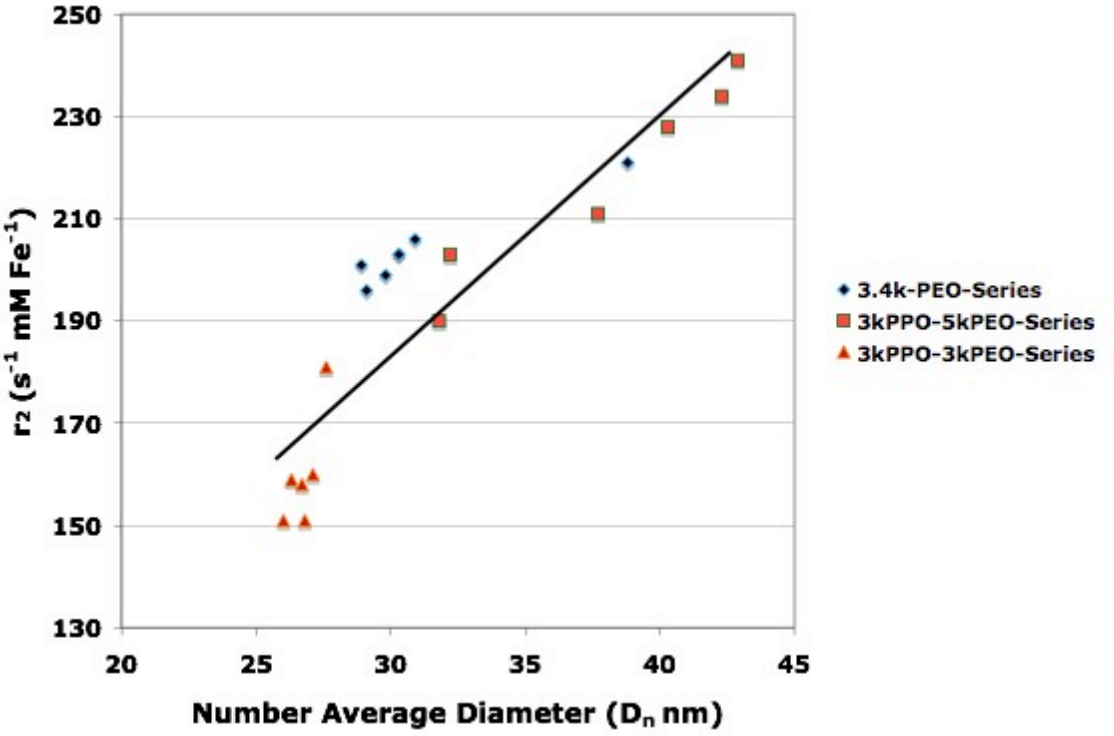

Figure 7.4.4.2. Determination of the transverse relaxivity (r_2) and comparison of the colloidal sizes in H_2O

Furthermore, comparison of the hydrodynamic intensity weighted diameters as a function of r_2 yielded a strikingly similar trend (Figure 7.4.4.3). As shown before in Figure 7.4.4.2, the coating yields these specific sizes and relaxivities which can be directly linked to the chemical composition of the complexes. Comparing the intensity weighted diameters to the number weighted diameters show a better linear fit of $R^2 = 0.93$ for D_i versus an $R^2 = 0.88$ for D_n. This phenomenon reveals an interesting point in that the D_i is a weighted average, radius to the sixth power, in comparison to D_n, radius to the first power, therefore the fit for D_i should be better due to its account of aggregated or clustered particles.

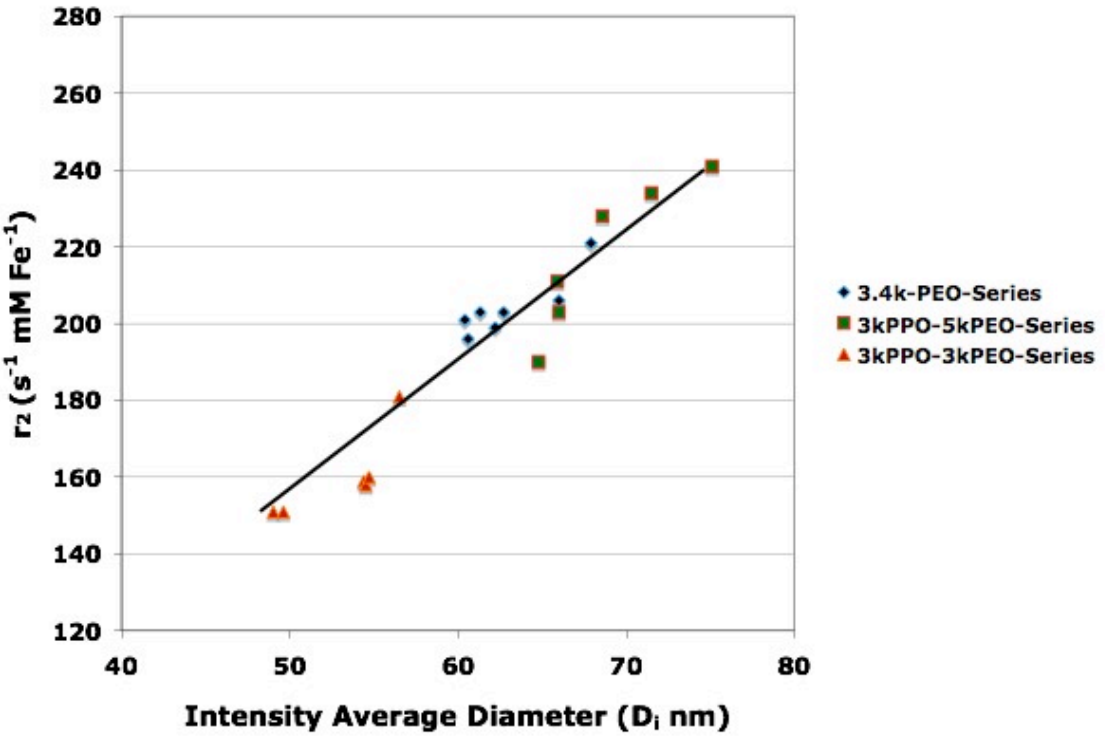

Figure 7.4.4.3. Relaxivity, r_2, as a function of intensity average diameter reveals particle size plays an integral role

In order to understand this data more clearly, the individual polyether coatings were broken down with the r_2 and number average diameter as a function of polymer loading. These variables were utilized to gain vital information followed by comparison of the experimental D_n to the theoretical D_n obtained from the modified density distribution model developed by Miles and Mefford.[16, 42]

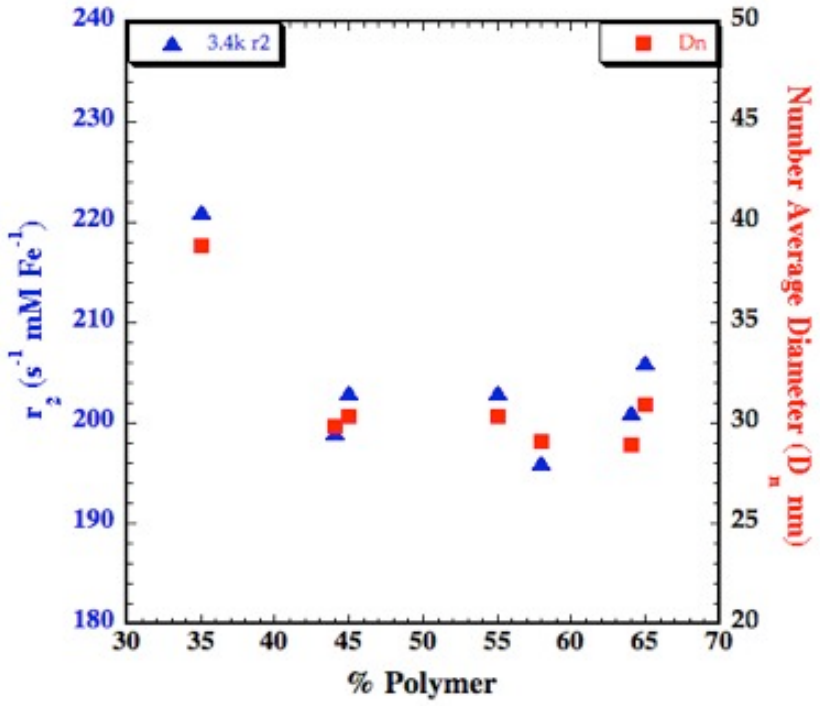

Figure 7.4.4.4. Relaxivity and number average diameters as a function of polymer loading reveals aggregation of particles

Table 7.4.4.1. Comparison of Experimental and Model number average diameters

Anchor Group	Molecular Weight (g/mol)	% Magnetite	DLS D_n (nm)	Model D_n (nm)	% Deviation
Triphosphonate	3,400	35	30.9	30.0	3%
Triphosphonate	3,400	36	28.4	29.8	5%
Triphosphonate	3,400	42	31.2	28.4	9%
Triphosphonate	3,400	45	29.2	27.8	5%
Triphosphonate	3,400	55	29.8	25.8	13%
Triphosphonate	3,400	56	27.3	25.7	6%
Triphosphonate	3,400	65	38.8	24.0	38%

Figure 7.4.4.4 shows the r_2 and number average diameter as a function of polymer loading for a series of 3,400 g mol^{-1} tri(zwitterionic phosphonate)-PEO-OH coated magnetite complexes with polymer loadings ranging from ~65- to 35 wt % polymer. Comparison of r_2 to the polymer loading reveals that as the polymer loading changes, r_2 does not change (Figure 7.4.4.4) with the exception of 35% polymer loading. The r_2 is only different for the lowest polymer loading of 34.5 wt %. The same trend is also

observed in comparison of the D_n to the polymer loading. Based on modeling methods done previously,[16, 42] the number average diameters indicate that the complexes are mostly single sterically-stabilized magnetite particles as opposed to aggregates with the exception of the 35 wt % polymer loading. Comparing the model prediction to the experimental D_n reveals clustering as shown in Table 7.4.4.1 for the 34.5 wt% polymer loading.

Transverse relaxation and D_n as a function of polymer loading for the 3kPPO-5kPEO polyether-magnetite complexes are shown in Figure 7.4.4.5. In contrast to the 3.4k PEO series, the 3k-5k series shows an increasing relaxivity from 190 to 241 s^{-1} mM Fe^{-1} as the wt % polymer is decreased. Comparison of the transverse relaxivities to the intensity average diameters of each complex shows that as the particle size increases, the transverse relaxation rate increases. Incorporation of the PPO block significantly decreases the number of chains adsorbed onto the magnetite surface compared to the 3.4kPEO complexes (1.0 vs. 3.4 chains nm^{-2} for 70 wt % polymer loading, respectively). Thus, the steric stabilization provided by the polymer stabilizer is significantly less for the diblock complex than for the homopolymer complex. Table 7.4.4.2 shows comparison of the experimental D_n to the theoretical D_n for the 3kPPO-5kPEO series. Comparison reveals a large deviation between the values as the polymer loading is decreased revealing clustering of the nanoparticles. This clustering allows the protons to experience a homogeneous magnetic field yielding faster dephasing of the proton spin vectors yielding high r_2 values.

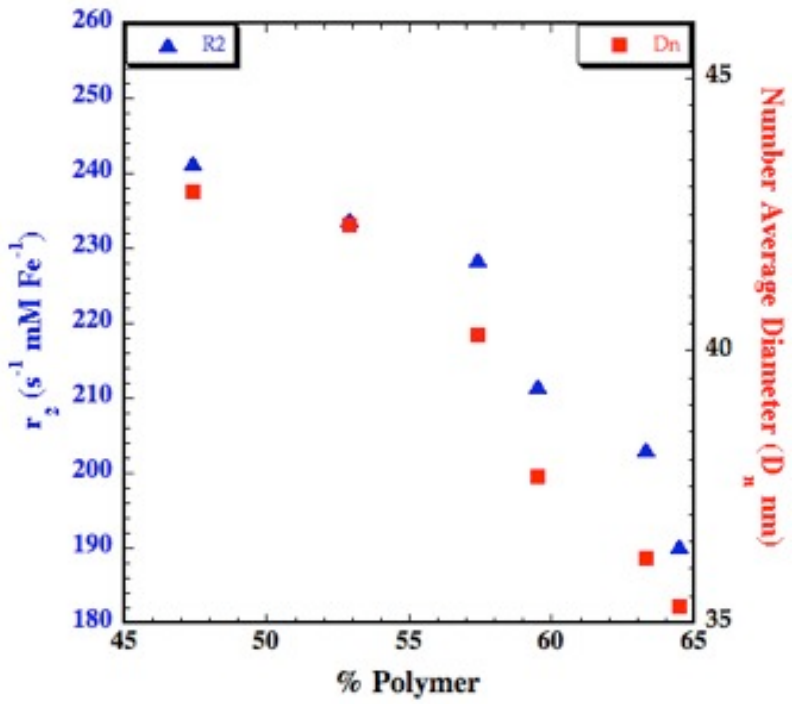

Figure 7.4.4.5. Determination of the transverse relaxivity (r_2) as a function of polymer loading for the 3kPPO-5kPEO complexes and comparison of the colloidal sizes in H_2O

Figure 7.4.4.6 shows the transverse relaxation and D_n as a function of polymer loading for the 3kPPO-3kPEO polyether-magnetite complexes with various polymer loadings. For these complexes there is no increase in the number-weighted diameter with decreasing polymer loading as there was for the 3kPPO-5kPEO series. Just as for the 3.4kPEO complexes where there was no difference in diameter with decreasing polymer loading, no appreciable difference in r_2 was noted for the 3kPPO-3kPEO polyether-magnetite complexes was observed. Again, comparison of the number average diameters of the complexes to predicted sizes from a previously developed model (Table 7.4.4.2) indicate that these complexes are primary particles with little to no clustering. The increased stability of the 3kPPO-3kPEO complexes in comparison to the 3kPPO-5kPEO

complexes may be due to an increased surface chain density and thus, an increased steric repulsion.

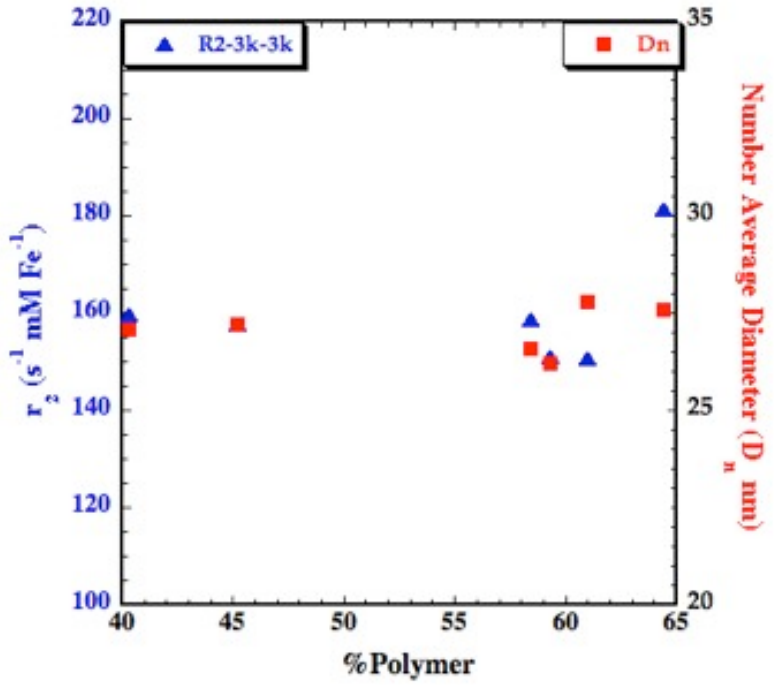

Figure 7.4.4.6. Determination of the transverse relaxivity, r_2, of the 3kPPO-3kPEO complexes and their comparison to intensity weighted diameter

Thus, it appears that the size of the polyether-magnetite complexes is the determining factor on r_2. The polymer composition, molecular weight, and polymer loading directly affect the clustering of the complexes as can be determined from the data given. Thus, the r_2 could be indirectly controlled by varying the polymer coating and loading with a given composition yielding a controlled cluster.

Table 7.4.4.2. Comparison of experimental D_n to model reveals the ability to form controlled clusters based on polymer composition and loading

Anchor Group	PPO Molecular Weight (g/mol)	PEO Molecular Weight (g/mol)	Magnetite Loading (%)*	DLS D_n (nm)	Model D_n (nm)	% Difference
Triphosphonate	3,000	2,900	35	27.6	26.7	3%
Triphosphonate	3,000	2,900	39	27.8	25.5	8%
Triphosphonate	3,000	2,900	41	26.2	25.1	4%
Triphosphonate	3,000	2,900	42	26.6	24.8	7%
Triphosphonate	3,000	2,900	51	27.2	22.9	16%
Triphosphonate	3,000	2,900	54	27.1	22.3	18%
Triphosphonate	3,000	5,000	36	35.3	31.4	11%
Triphosphonate	3,000	5,000	37	36.2	31.1	14%
Triphosphonate	3,000	5,000	43	40.3	30.0	26%
Triphosphonate	3,000	5,000	41	37.7	29.4	22%
Triphosphonate	3,000	5,000	47	42.3	28.4	33%
Triphosphonate	3,000	5,000	53	42.9	27.0	37%

Further comparison of the r_2 values of the polyether-magnetite complexes to dextran-coated magnetite complexes (r_2 = 80 s^{-1} mM^{-1})[5, 6, 14] show roughly a 2 to 3-fold increase in r_2 and the intensity weighted diameters reveal an aggregated system, ~227 nm diameter,[5, 6] in the case of the dextran coated magnetite. Thus, not only does the polyether-magnetite complexes provide larger r_2 values, but the complexes are relatively dispersed, which should allow them to be used in applications that require longer blood circulation or site specific binding due to its smaller size and greater relaxivity.

7.5 Conclusions

These results have important implications for the design of future polymer stabilized superparamagnetic MRI contrast agents. The relaxivity of the complexes were shown to be dependent on a variety of variables such as polymer length, composition, and polymer loading that leads to aggregation and indirectly an increase in relaxation, r_2. With this information future MRI contrast agents can be designed to either remain completely

dispersed (for applications such as molecular imaging) or purposefully aggregated to maximize contrast.

7.6 References

1. *Magnetic Resonance Imaging: Method and Biologic Applications*. Humana Press: Totowa, NJ, 2006.

2. Chan, D., Kirpotin, DB, Bunn, PA. , Synthesis and evaluation of colloidal magnetic iron oxides for the site-specific radiofrequency- induced hyperthermia of cancer. *J. Magn. Magn. Mater.* **1993,** 122, 374-378.

3. Hafeli, U. S., W.; Teller, J.; Zbrorowski, M., Scientific and Clinical Applications of Magnetic Carriers. *Plenum Press: New York* **1997**.

4. Hahn, P., Gastrointentinal contrast agents. *AJR* **1991,** 156, 252-254.

5. Josephson, L., Lewis, J., Jacobs, P., Hahn, P., Stark, D., The effects of iron oxide on proton relaxivity. *Magnetic Resonance Imaging* **1988,** 6, 647-653.

6. Jung, C. W.; Jacobs, P., Physical and Chemical-Properties of Superparamagnetic Iron-Oxide MR Contrast Agents - Ferumoxides, Ferumoxtran, Ferumoxsil. *Magnetic Resonance Imaging* **1995,** 13, (5), 661-674.

7. Nitin, N., LaConte, L. E., Zurkiya, O., Hu, X., and Bao, G. , Functionalization and Peptide-Based Delivery of Magnetic Nano-particles As an Intracellular MRI Contrast Agent. *J. Biol. Inorg. Chem.* **2004,** 9, (706-712).

8. Olsson, M., Persson, B., Salford, L., Schroder, U., Ferrormagnetic particles as contrast agents in T2 imaging. *Magnetic Resonance Imaging* **1986,** 4, (437-440).

9. Tilborg, G., Mulder, W., Deckers, N., Storm, G., Annexin A5-Functionalized Bimodal Lipid-Based Contrast Agents for the Detection of Apoptosis. *Bioconjugate Chem* **2006,** 17, 741-749.

10. Yeh, T., Zhang, W., Ildstad, S. T., and Ho, C. , Intracellular labeling of T-cells with superparamagnetic contrast agents. *Magn. Reson. Med.* **1993,** 30, 617-625.

11. Yeh, T., Zhang, W., Ildstad, S. T., and Ho, C. , Dynamic MRI tracking of rat T-cells labeled with superparamagnetic iron-oxide particles. *Magn. Reson. Med.* **1995,** 33, (200-208).

12. Yurt, A. K., Nadide, Investigation of magnetic properties of various complexes prepared as contrast agents for MRI. *Journal of Molecualr Structure* **2008,** 892, 392-397.

13. Zhang, Y., Kohler, N, Zhang, M. , Surface modification of super- paramagnetic magnetite nanoparticles and their intracellular uptake. *Biomaterials* **2002,** 23, 1553-1561.

14. Josephson, L. T., C. H.; Moore, A.; Weissleder, R. , *Bioconjungate Chem.* **1999,** 10, 186-191.

15. Lutz, J., Stiller, S., Hoth, A., Kaufner, L., Pison, U., Cartier, R., One-Pot Synthesis of PEGylated Ultrasmall Iron-Oxide Nanoparticles and Their in Vivo Evaluation as Magnetic Resonance Imaging Contrast Agents *Biomacromolecules* **2006,** 7, 3132-3138.

16. Mefford, O. T.; Carroll, M. R. J.; Vadala, M. L.; Goff, J. D.; Mejia-Ariza, R.; Saunders, M.; Woodward, R. C.; Pierre, T. G. S.; Davis, R. M.; Riffle, J. S., Size analysis of PDMS-magnetite nanoparticle complexes: Experiment and theory. *Chemistry of Materials* **2008,** 20, (6), 2184-2191.

17. Morris, P., *Nuclear Magnetic Resonance Imaging in medicine and Biology*. Oxford University Press: Oxford, 1986.

18. Hogemann, D. J., L.; Weissleder, R.; Basillion, J., Improvement of MRI Probes To Allow Efficient Detection of Gene Expression. *Bioconjugate Chem.* **2000,** 11, 941-946.

19. Horak, D. B., M.; Jendelova, P.; Herynek, V.; Trchova, M.; Pientka, Z.; Pollert, E.; Hajek, M.; Sykova, E., D-Mannose-Modified Iron Oxide Nanoparticles for Stem Cell Labeling. *Bioconjugate Chemistry* **2007,** 18, 635-644.

20. Huh, Y. J., Y.; Song, H.; Kim, S.; Choi, J.; Lee, J.; Yoon, S.; Kim, K.; Shin, J.; Suh, J.; Cheon, J., In Vivo Magnetic Resonance Detection of Cancer by Using Multifunctional Magnetic Nanocrystals. *J. Am. Chem. Soc.* **2005,** 127, 12387-12391.

21. Jain, T. M., M.; Sahoo, S.; Leslie-Pelecky, D.; Labhasetwar, V., *Molecular Pharmaceuticals* **2005,** 2, (3).

22. NessAiver, M., *All You Really Need to Know about MRI Physics*. SImply Physics: Baltimore, MD, 1997.

23. Brown, J. M., and Attardi, L. D. , The Role of Apoptosis in Cancer Development and Treatment Response. *Nat. Rev. Cancer* **2005,** 5, 231-237.

24. Chen, R. L., J.; Chou, C.; Chang, T.; Chen, W.; Li, C.; Tu, H., T2-weighted and T1-weighted Dynamic Superparamagnetic Iron Oxide (Ferucarbotran) Enhanced MRI of Hepatocellular Carcinoma and Hyperplastic Nodules. *J Formos Med Assoc* **2008,** 107, (10), 8.

25. Cormode, D. C., R.; Delshad, A.; Briley-Saebo, K.; Calcagno, C.; Barazza, A.; Mulder, W.; Fisher, E.; Fayad, Z., Comparison of Synthetic High Density Lipoprotien

(HDL) Contrast Agents for MR Imaging of Atherosclerosis. *Bioconjugate Chemistry* **2009,** 20, 937-943.

26. Duan, H. K., M/; Wang, X.; Wang, Y.; Mao, H.; Nie, S., Reexamining the Effecs of Particle Size and Surface Chemistry on the Magnetic Properties of Iron Oxide Nanocrystals: New Insights into Spin Disorder and Proton Relaxivity. *J. Phys. Chem. C Letters* **2008,** 112, 5.

27. Glasel, J., Lee, K., On the interpretation of water NMR relaxation times in heterogeneous systems. *J. Am. Chem. Soc.* **1974,** 96, 970-978.

28. Kean, D., Smith, M., *Magnetic Resonance Imaging: Principles and Applications*. William Heinemann Medical Books: Bedford Square, London, 1986.

29. Kim, D. K., Mikhaylova, M., Zhang, Y., Muhammed, M., Protective Coating of Superparamagnetic Iron Oxide Nanoparticles. *Chemistry of Materials* **2003,** 15, (1617-1627).

30. Chanana, M. J., S.; Georgieva, R.; Lutz, J.; Baumler, H.; Wang, D., Fabrication of Colloidal Stable, Thermosensitive, and Biocompatible Magnetite Nanoparticles and Study of Their Reversible Agglomeration in Aqueous Milieu. *Chemisty of Materials* **2009,** 21, 9.

31. Lee, H., Lee, E., Kim, D., Jang, N., Jeong, Y., Antibiofouling Polymer-Coated Superparamagnetic Iron Oxide Nanoparticles as Potential Magnetic Resonance Contrast Agents for in Vivo Cancer Imaging *J. Am. Chem. Soc.* **2006,** 128, 7383-7389.

32. Martina, M. F., J.; Menager, C.; Clement, O.; Barratt, G.; Grabielle-Madelmont, C.; Gazeau, F.; Cabuil, V.; Lesieur, S., Generation of Superparamagnetic Liposomes Revealed as Highly Efficient MRI Contrast Agents for in Vivo Imaging. *J. Am. Chem. Soc.* **2005,** 127, 10.

33. Veiseh, O. S., C.; Gunn, J.; Kohler, N.; Gabikian, P.; lee, D.; Bhattarai, N.; Ellenbogen, R.; Sze, R.; Hallahan, A.; Olson, J.; Zhang, M., Optical and MRI Multifunctional Nanoprobe for Targeting Gliomas. *Nano Letters* **2005,** 5, (6), 1003-1008.

34. Venditto, V. R., C.; Brechbiel, M., PAMAM Dendrimer Based Macromolecules as Improved Contrast Agents. *Molecular Pharmaceutics* **2005,** 2, (4), 302-311.

35. Yellen, B. B.; Forbes, Z. G.; Halverson, D. S.; Fridman, G.; Barbee, K. A.; Chorny, M.; Levy, R.; Friedman, G., Targeted drug delivery to magnetic implants for therapeutic applications. *Journal of Magnetism and Magnetic Materials* **2005,** 293, (1), 647-654.

36. Vadala, M. L.; Thompson, M. S.; Ashworth, M. A.; Lin, Y.; Vadala, T. P.; Ragheb, R.; Riffle, J. S., Heterobifunctional poly(ethylene oxide) oligomers containing carboxylic acids. *Biomacromolecules* **2008,** 9, (3), 1035-1043.

37. Huffstetler, P. P.; Miles, W. C.; Goff, J. D., et al. , Synthesis, Modeling, and Relaxivities of Contrast Agents for MRI. *Polymer Preprints* **2008,** 49, (2), 1103-1104.

38. Thompson, M. S.; Vadala, T. P.; Vadala, M. L.; Lin, Y.; Riffle, J. S., Synthesis and applications of heterobifunctional poly(ethylene oxide) oligomers. *Polymer* **2008,** 49, (2), 345-373.

39. Caplan, N. P., C.; Hayes, D.; Blackburn, M., The synthesis of novel bisphosphonates as inhibitors of phosphoglycerate kinase (3-PGK). *The Royal Society of Chemistry* **2000,** 1, 421-437.

40. Pinna, N., Grancharov, S., Beato, P., Bonville, P., Antonietti, M., Niederberger, M, *Chem. Mater.* **2005,** 17, 3044.

41. Laurent, S. F., D.; Port, M.; Roch, A.; Robic, C.; Elst, L.; Muller, R., magnetic Iron Oxide Nanoparticles: Synthesis, Stabilization, Vectorization, Physicochemical Charactgerizations, and Biological Applications. *Chem. Rev.* **2008,** 108, 2064-2110.

42. Miles, W. C.; Goff, J. D.; Huffstetler, P. P.; Reinholz, C. M.; Pothayee, N.; Caba, B. L.; Boyd, J. S.; Davis, R. M.; Riffle, J. S., Synthesis and Colloidal Properties of Polyether Magnetite Complexes in Water and Phosphate-Buffered Saline. *Langmuir* **2008**.

Chapter 8: Conclusions

8.1 Conclusions

The main goal achieved in this work includes novel synthetic techniques for well-defined heterobifunctional polyethers for multiple applications. In this work the polyethers were utilized for the stabilization of magnetite nanoparticles for use as negative contrast agents in magnetic resonance imaging.

Chapter 3 discussed in detail the synthetic techniques of using zinc(II) hexacyanocobaltate as a coordination catalyst for the ring-opening polymerization of a variety of epoxy rings yielding novel polyethers.

Chapters 4 and 5 address the issue of anchoring the polymer to the magnetite surface. Three different anchor group chemistries were explored, resulting in PEOs with carboxylic acid, ammonium, or zwitterionic phosphonate functionality. Both monofunctional and trifunctional PEOs were synthesized. For the monofunctional anchor groups, both the carboxylate and ammonium-anchored complexes were stable in DI water but not in PBS. The monophosphonate-anchored complexes showed far greater stability in PBS but were not stable in DI water, particularly at lower polymer loadings. For the trifunctional anchor groups, again the carboxylate and ammonium-anchored complexes were stable in DI water but not in PBS. However, the triphosphonate-anchored complexes were stable in both DI water and in PBS. Two main conclusions could be drawn from this work: 1) the aggregation of the monophosphonate complexes was caused by the attraction of the anchor group to magnetite of another complex and 2) the triphosphonate anchors are the most-likely candidate for success *in vivo*. Additionally, the instability observed in the carboxylate and ammonium-anchored complexes in PBS gives clues as to the accessibility

of the magnetite surface to small molecules. This may be important for the design of delivery vehicles where access to the surface must be carefully controlled.

Chapter 6 consists of an analysis of PPO-b-PEO-OH block copolymer-magnetite complexes with varying molecular weight and both a triammonium anchor and a triphosphonate anchor. Dynamic light scattering measurements were compared to the density distribution model. While the comparisons do not deviate by a large percentage (?? %), they do deviate more for the diblock complexes than for the homopolymer complexes discussed in the previous chapters. Small Angle Neutron Scattering (SANS) and Quartz Crystal Microbalance with Dissipation (QCM-D) data both seem to indicate a significant amount of solvation of the PPO layer rather than the assumed non-solvated shell. However, there was also no noticeable change in diameter when the complexes were heated from 20°C to 40° C. Current relaxation data indicates that for homopolymer complexes that appear stable, no change is observed in relaxation. However, for the triammonium complexes, significant (and opposite) trends exist depending upon the molecular weight of the polymer stabilizer. Thus, it appears as though the hydrophobic force detailed in Chapter 4 as a reason for deviation from model predictions plays a significant role. This is evidenced by an increase in diameter (and relaxivity) with reduced polymer loading for a 3.3kPPO-b-4.8kPEO-OH complex and an increase in diameter (and relaxivity) for a 3.3kPPO-b-2.6kPEO-OH complex with increased polymer loading. Additionally, the smaller diblock shows increased cellular uptake. This indicates that the hydrophobic to hydrophilic ratio is both a critical variable and extremely sensitive to small variations in polymer molecular weight.

Chapter 7 addressed the use of these polyether-magnetite complexes as negative contrast agents for MRI. It was shown that the design of polymer coating is essential to future development of MRI contrast agents. The lack of dependence of relaxivity on the polymer loading for the PEO homopolymer and 3k-3k series indicates that variations in the polymer loadings, block lengths and polymer morphologies had no effect of the r_2 unless the hydrophobic component of the complex is sufficient enough to cause aggregation as shown by the 3k-5k series.